

SAND85-0598 • UC-70
Unlimited Release
Printed February 1988

DRAFT

Nevada Nuclear Waste Storage Investigations Project

Analyses to Evaluate the Effect of the Exploratory Shafts on Repository Performance at Yucca Mountain

Joseph A. Fernandez, Thomas E. Hinkebein, John B. Case

Prepared by
Sandia National Laboratories
Albuquerque, New Mexico 87185 and Livermore, California 94550
for the United States Department of Energy
under Contract DE-AC04-76DP00789

8809210239
PDR WASTE
WM-11

PDC

102.2

**ANALYSES TO EVALUATE THE EFFECT OF THE EXPLORATORY SHAFTS ON
REPOSITORY PERFORMANCE AT YUCCA MOUNTAIN**

**Joseph A. Fernandez
Thomas E. Hinkabein
NNWSI Geotechnical Design Division
Sandia National Laboratories
Albuquerque, NM 87185**

**John B. Case
IT Corporation
2340 Alamo SE
Albuquerque, NM 87106**

ABSTRACT

This report presents a number of analyses to determine whether the construction of two shafts associated with the Exploratory Shaft Facility could influence significantly the long-term isolation capabilities of a high-level nuclear waste repository at Yucca Mountain, on and adjacent to the Nevada Test Site. The calculational effort, using analytical solutions, focuses primarily on the potential influence of the shaft liner and the zone of increased rock damage around the shaft (due to shaft construction). The potential impact of the shaft penetrating into the Calico Hills unit on the sorptivity of zeolites of this unit is also evaluated. Two mechanisms are considered in determining whether the rock damage zone (or the modified permeability zone, MPZ) can significantly enhance radionuclide releases. These mechanisms include water flow down the shaft fill and MPZ from a highly improbable scenario occurring at the surface, and air flow up the shaft due to convective and barometric forces. The influence of the liner on the performance of the repository is determined by evaluating the potential chemical interaction between ground water and the concrete liner and the subsequent potential for precipitates to deposit within the MPZ and the shaft fill. The sorption capability of the Calico Hills unit is evaluated by calculating the changes in ground-water temperature as water migrates down the shaft and MPZ. It is concluded from these calculations and the current knowledge of the hydrology of the unsaturated zone at Yucca Mountain that the presence of the shafts and the associated MPZ and shaft liner does not significantly impact the long-term isolation capability of the repository. This conclusion is reached because (1) highly improbable amounts of water postulated to enter the shaft can be dissipated effectively at the base of the shaft (these postulated amounts of water are much greater than the amounts anticipated to enter the shafts), (2) air flow out of the shaft can be controlled effectively by emplacement of shaft fill, (3) deposition of solids from the interaction of the shaft liner with the ground water is a localized phenomenon and should not significantly decrease the drainage capability of the rock at the base of the shaft, and (4) the elevation of the temperature of ground-water reaching the base of the shaft does not significantly impact the sorptivity of the Calico Hills zeolites. This report also describes methods to remove the liner, to restore the MPZ and to emplace a seal, in the event that future analyses suggest that these actions are necessary.

ACKNOWLEDGMENTS

The authors wish to acknowledge the assistance of other individuals who contributed to this study. Mr. John G. S. Hynd, an engineering consultant, provided information on the techniques associated with seal and backfill emplacement, liner removal and their associated costs. Messrs. Joe Tyburski and Bernard Lauctes, International Technology Corporation, performed selected calculations. Messrs. Joe Tillerson, Ralph Peters, and Andy Peterson, SNL, provided review comments to the authors. We also thank those individuals at Creative Computer Services for providing general support services to prepare this report.

BACKGROUND OF REPORT

The original version of this report was prepared as a letter report in response to the question: Do the shaft liner, the shaft internals, and the increased rock damage around the shaft (due to shaft construction) significantly influence the release of radionuclides from the repository? The letter report was submitted to U.S. Department of Energy - Nevada Operations Office, Waste Management Project Office (U.S. DOE-NVO, WMPO) in July 1985. The contents of this letter report were subsequently discussed during a NRC/DOE workshop titled "NNWSI Exploratory Shaft Facility Design and Construction Workshop" in August 1985.

During the workshop additional concerns were raised by the workshop participants on details associated with the approach used to resolve the original question and the level of detail contained in the original letter report. To address the original question and the additional concerns raised during the August 1985 meeting, Sandia National Laboratories (SNL) decided to prepare three reports. These reports were:

- (1) "Technical Basis for Performance Goals, Design Requirements and Material Recommendations for the NNWSI Repository Sealing Program," SAND84-1895, by J. A. Fernandez, P. C. Kelsall, J. B. Case, and Dann Meyer (published),
- (2) "Modification of Rock Mass Permeability in the Zone Surrounding a Shaft in Fractured, Welded Tuff," SAND86-7001, by J. B. Case and P. C. Kelsall (published), and
- (3) "Analyses to Evaluate the Effect of the Exploratory Shafts on Repository Performance at Yucca Mountain," SAND85-0598, by J. A. Fernandez, T. E. Hinkebein, and J. B. Case.

During the preparation of this report, the designs and surface locations of the exploratory shafts changed. These changes necessitated performing additional calculations to address, among other things, the impact of flooding and erosion at the new shaft locations. The impact

of flooding and erosion at the new exploratory shaft locations were raised during another NRC/DOE meeting in April 1987.

This report, therefore, addresses:

- (1) the original question defined before July 1985.
- (2) the concerns raised during the August 1985 workshop between NRC, and DOE.
- (3) the concerns raised during the April 1987 meeting between NRC and DOE, and
- (4) additional concerns raised by the authors during the development of this report.

CONTENTS

	<u>Page</u>
EXECUTIVE SUMMARY	15
1.0 PURPOSE OF REPORT	23
2.0 SHAFT DESIGN INFORMATION	27
2.1 Location of the Exploratory Shafts	29
2.2 Construction of the Exploratory Shafts	29
2.3 Shaft Sealing Concepts	31
2.4 Preferred Options for Shaft Seals	32
3.0 INFLUENCE OF THE EXPLORATORY SHAFTS INCLUDING THE MODIFIED PERMEABILITY ZONE AND SHAFT FILL ON THE PERFORMANCE OF THE YMGDS	35
3.1 Modified Permeability Zone Characteristics	35
3.2 Potential for Enhancing Radionuclide Release Due to Water Entering the Exploratory Shaft	43
3.2.1 Scenario Description	44
3.2.2 Model Used for Water Flow Into the Shaft	45
3.2.2.1 Model Description	46
3.2.2.2 Input Values Used	54
3.2.2.3 Inflow Volumes	55
3.2.2.4 Duration and Rate of Flow Into Shaft	55
3.2.3 Model Used for Water Flow Out of the Shaft	62
3.2.3.1 Model Description	63
3.2.3.2 Input Values Used	68
3.2.4 Water Balance in the Exploratory Shaft	69
3.2.5 Impact of Relocating the Exploratory Shafts	74
3.2.5.1 Erosion Potential at the New Exploratory Shaft Locations	74
3.2.5.2 Flooding Potential at the New Exploratory Shaft Locations	76
3.2.5.3 Scenario Describing Uniform Dispersion of Surface Water at Depth	77
3.2.5.4 Analysis of the Drainage Capacity of the New Exploratory Shafts and Associated Facility	82
3.2.5.5 Conclusions	83
3.3 Potential for Enhancing Radionuclide Release From Air Movement Due to Convective Forces	85
3.3.1 Air Flow Mechanisms	85
3.3.2 Method of Analysis	87
3.3.3 Model Description	88

	<u>Page</u>
3.3.3.1 Temperature and Pressure Distributions	88
3.3.3.2 Flow Path Resistances	89
3.3.4 Model Results	92
3.3.5 Conclusions	97
3.4 Potential for Enhancing Radionuclide Release From Air Movement Due to Barometric Forces	98
3.4.1 Model Description	99
3.4.1.1 Physical Model	100
3.4.1.2 Mathematical Model and Assumptions	100
3.4.2 Input to the Mathematical Model	105
3.4.3 Model Results	107
3.4.4 Conclusions	116
3.5 Remedial Measures to Restore the Modified Permeability Zone	117
3.5.1 Restoration of the MPZ by Grouting	119
3.5.2 Restoration of the MPZ Using Expansive Concrete	120
3.5.3 Conclusions	122
4.0 INFLUENCE OF THE SHAFT LINER ON THE PERFORMANCE OF YMGDS	125
4.1 Changes in the Hydraulic Conductivity of the Liner	125
4.2 Effect of Ground-Water Chemistry on the Hydraulic Conductivity of the Exploratory Shaft Fill and Modified Permeability Zone	127
4.2.1 Leaching of Alkaline Species From the Concrete Liner	128
4.2.2 Chemical Equilibrium Model of Ground- Water Reactions	131
4.2.2.1 Migration of Precipitates	135
4.2.2.2 Model for Precipitate Deposition	137
4.2.3 Results	138
4.2.4 Conclusions	139
4.3 Remedial Measures to Remove the Liners From the Exploratory Shafts	139
4.3.1 Liner Removal	141
4.3.2 Muck Removal	145
4.3.3 Conclusions	150
5.0 INFLUENCE OF THE ES PENETRATION INTO THE CALICO HILLS UNIT	153
5.1 Changes in the Sorptivity of the Calico Hills Unit Due to Elevated Ground-Water Temperature	153

	<u>Page</u>
5.1.1 Temperature Elevation of Water Entering the Shaft	153
5.1.2 Impact of Increased Ground-Water Temperature on the Sorptivity of the Calico Hills Unit	154
5.2 Changes in the Thickness of the Calico Hills Unit Above the Ground-Water Table	155
5.3 Conclusions	156
6.0 CONCLUSIONS AND RECOMMENDATIONS	159
 APPENDICES	
A. Perspective into Radionuclide Transport	163
B. Explanation of Water Inflows to ES-1	175
C. The Density Method as Applied to Flow Through a Porous Media	183
D. Estimated Construction Schedule and Costs	189
E. Calculation of Temperature of Water From the Base of the Exploratory Shafts	193
F. Comparison of Data Used in This Report With the Reference Information Base (RIB)	201
G. Data Recommended for Inclusion Into the Site and Engineering Properties Data Base (SEPDB) and Information Proposed for the Inclusion Into the Reference Information Base (RIB)	211
REFERENCES	213

FIGURES

		<u>Page</u>
2-1.	Schematic of Exploratory Shafts and Corresponding Geologic Stratigraphy	28
2-2.	Surficial Geology of the Exploratory Shaft Area	30
2-3.	General Arrangement for Shaft Seals Showing Optional Components	33
3-1.	Cross Section Through a Shaft in Welded Tuff Showing Fracture Spacing Relative to Shaft Radius	38
3-2.	Modified Permeability Zone Model for Topopah Spring Welded Tuff for Expected Conditions at 310-m Depth	42
3-3.	Geometry of Model Used to Estimate Flow Into a Shaft From Saturated Alluvium	47
3-4.	Phases of Flow for Flow Into a Shaft From Saturated Alluvium	49
3-5.	Types of Flow Considered in Estimating Flow Into a Shaft	51
3-6.	Capture Zone Near a Shaft	52
3-7.	Estimated Volumes of Water Entering ES-1 (PMF, Shaft Fill Conductivity = 10^{-2} cm/s, Excavated Shaft Diameter = 4.42 m)	56
3-8.	Estimated Duration of Flows Into ES-1 (PMF, Hydraulic Conductivity of Alluvium - 100 and 10 cm/s)	57
3-9.	Estimated Duration of Flows Into ES-1 (PMF, Hydraulic Conductivity of Alluvium - 1 and 0.1 cm/s)	58
3-10.	Estimated Duration of Flow Into ES-1 (PMF, Hydraulic Conductivity of Alluvium - 10^{-2} cm/s and 10^{-3} cm/s)	59
3-11.	Estimated Duration of Flow Into ES-1 (PMF, Hydraulic Conductivity of Alluvium - 10^{-4} and 10^{-5} cm/s)	60
3-12.	Schematic of Model Used to Compute Water Balance in the Exploratory Shaft	64
3-13.	Comparison of Methods Used to Compute Drainage From Shaft	67
3-14.	Estimated Buildup of Water in Sump of ES-1 (Hydraulic Conductivity of Alluvium - 100 cm/s and 10 cm/s)	70

	<u>Page</u>
3-15. Estimated Buildup of Water in Sump of ES-1 (Hydraulic Conductivity of Alluvium - 1 cm/s and 0.1 cm/s)	71
3-16. Estimated Buildup of Water in Sump of ES-1 (Hydraulic Conductivity of Alluvium - 10^{-2} cm/s and 10^{-3} cm/s)	72
3-17. Estimated High-Water Locations Associated With a PMF in the Exploratory Shaft Area	75
3-18. Topographic Cross Section in the Vicinity of the New ES-1 and ES-2 Locations	78
3-19. Topography, Drainage Basin Outline, and Grid Used in Developing the Uniform Dispersion Scenario	79
3-20. Illustration of the Water Flow That Enters the Exploratory Shaft and the MPZ From a Single Surface Element	81
3-21. Drift Drainage Pattern Proposed in the Vicinity of the Exploratory Shafts	84
3-22. Mechanisms for Convective Air Flow - (A) Flow Through Shafts Only and (B) Flow Through Shafts and Rock	86
3-23. Total Flow Rate as a Function of Shaft Fill, Air Conductivity (Vertical Emplacement and Low Conductivity MPZ Model)	93
3-24. Total Flow Rate as a Function of Shaft Fill, Air Conductivity (Vertical Emplacement and High Conductivity MPZ Model)	93
3-25. Total Flow Rate as a Function of Shaft Fill, Air Conductivity (Horizontal Emplacement and Low Conductivity MPZ Model)	94
3-26. Total Flow Rate as a Function of Shaft Fill, Air Conductivity (Horizontal Emplacement and High Conductivity MPZ Model)	94
3-27. Air Flow Through ES-1 and ES-2 (Shaft Fill and MPZ Flows Included) as a Percentage of Flow Through the Rock Over Repository Area (Vertical Emplacement and Low Conductivity MPZ Model)	95
3-28. Air Flow Through ES-1 and ES-2 (Shaft Fill and MPZ Flows Included) as a Percentage of Flow Through the Rock Over Repository Area (Vertical Emplacement and High Conductivity MPZ Model)	95

	<u>Page</u>
3-29. Air Flow Through ES-1 and ES-2 (Shaft Fill and MPZ Flows Included) as a Percentage of Flow Through the Rock Over Repository Area (Horizontal Emplacement and Low Conductivity MPZ Model)	96
3-30. Air Flow Through ES-1 and ES-2 (Shaft Fill and MPZ Flows Included) as a Percentage of Flow Through the Rock Over Repository Area (Horizontal Emplacement and High Conductivity MPZ Model)	96
3-31. Schematic of Repository Used in Barometric Pressure Model	101
3-32. Barometric Pressure Events	106
3-33. Ratio of Displaced Air Volume to Void Volume for ES-1 (Vertical Emplacement and Low Conductivity MPZ Model) for a Severe Thunderstorm Event	109
3-34. Ratio of Displaced Air Volume to Void Volume for ES-1 (Vertical Emplacement and High Conductivity MPZ Model) for a Severe Thunderstorm Event	109
3-35. Ratio of Displaced Air Volume to Void Volume for ES-1 (Vertical Emplacement and Low Conductivity MPZ Model) for a Tornado Event	110
3-36. Ratio of Displaced Air Volume to Void Volume for ES-1 (Vertical Emplacement and High Conductivity MPZ Model) for a Tornado Event	110
3-37. Ratio of Displaced Air Volume to Void Volume for ES-1 (Vertical Emplacement and Low Conductivity MPZ Model) for a Seasonal Event	111
3-38. Ratio of Displaced Air Volume to Void Volume for ES-1 (Vertical Emplacement and High Conductivity MPZ Model) for a Seasonal Event	111
3-39. Ratio of Displaced Air Volume to Void Volume for ES-1 (Horizontal Emplacement and Low Conductivity MPZ Model) for a Severe Thunderstorm Event	112
3-40. Ratio of Displaced Air Volume to Void Volume for ES-1 (Horizontal Emplacement and High Conductivity MPZ Model) for a Severe Thunderstorm Event	112
3-41. Ratio of Displaced Air Volume to Void Volume for ES-1 (Horizontal Emplacement and Low Conductivity MPZ Model) for a Tornado Event	113
3-42. Ratio of Displaced Air Volume to Void Volume for ES-1 (Horizontal Emplacement and High Conductivity MPZ Model) for a Tornado Event	113

	<u>Page</u>
3-43. Ratio of Displaced Air Volume to Void Volume for ES-1 (Horizontal Emplacement and Low Conductivity MPZ Model) for a Seasonal Event	114
3-44. Ratio of Displaced Air Volume to Void Volume for ES-1 (Horizontal Emplacement and High Conductivity MPZ Model) for a Seasonal Event	114
3-45. Schematic of MPZ Restoration and Shaft Seal Emplacement . . .	118
3-46. Minimum Conductivity for Grouting	121
4-1. Plot of pH of Water From Below the Shaft Liner as a Function of the Volumetric Flow Rate of Water Through the Shaft or MPZ	132
4-2. Schematic of Deposition of Precipitate	136
4-3. Frontal Advance of the Precipitation Front in the MPZ . . .	140
4-4. Production Cycle for Breaking and Removing the Liner and Placement of Backfill	142
4-5. Conceptual Illustration of Liner Breakage by the Roadheader Method	143
4-6. Removal of Concrete Using the Orange Peel Grab	151
5-1. Contours of the Thickness of the Unsaturated Portion of the Calico Hills Unit Beneath the Repository	157

TABLES

	<u>Page</u>
3-1. Relative Permeability Factors Associated With the Modified Permeability Zone	43
3-2. Summary of Areas and Lengths - Vertical Emplacement	90
3-3. Summary of Areas and Lengths - Horizontal Emplacement	90
4-1. Chemical Analyses of Water Before and After Contact With PSU 82-022 Cement	130
4-2. Summary of Advantages, Disadvantages, and Cost of Liner Removal Methods	146
4-3. Comparison of Production Cycle Times for Various Methods Used to Remove Concrete Liners	148
4-4. Comparison of Costs for Breaking Out the Concrete Lining and Rock	149

EXECUTIVE SUMMARY

One aspect of the Nevada Nuclear Waste Storage Investigations (NNWSI) Project is the development of the Exploratory Shaft (ES) testing program. The purpose of the ES testing program is to obtain at-depth site information on the hydrology and geology at the site. The results from these tests will be used to determine the effectiveness of the geologic setting at Yucca Mountain to isolate high-level radioactive waste. Before initiating the construction of the exploratory shafts (ES-1 and ES-2), it is necessary to determine the quality assurance levels to be applied to the ES design and construction. The purpose of this report is to provide a portion of the technical basis for use by the U.S. Department of Energy-Nevada Operations Office (U.S. DOE-NVO) in establishing the appropriate quality assurance levels for the design and construction of the exploratory shafts. This technical basis is developed through the use of analytical solutions that address the primary concern in this report: Do the shaft liner, the shaft internals, and the increased rock damage around the shaft (due to shaft construction) significantly influence the release of radionuclides from the repository? The approach taken to resolve this concern is to evaluate selected physical processes and bounding scenarios which, in our judgment, answer the most important concerns brought up by the DOE, U.S. Nuclear Regulatory Commission (NRC) and by ourselves. Therefore, this report is not intended to provide an exhaustive analysis of all possible scenarios and physical processes which could occur and may impact the future repository performance but is considered sufficient to initiate construction of the exploratory shafts.

Rather than performing a total systems analysis, the significance of the rock damage zone or the modified permeability zone (MPZ)* and the shaft liner on the long-term performance of the repository are considered. A secondary concern addressed in this report is the potential effect of one

*The modified permeability zone is the zone immediately surrounding an underground excavation in which the permeability of the rock mass has been altered due to stress redistribution and blast damage effects.

shaft penetrating the Calico Hills unit. Because the shaft penetrates the zeolitic portion of the Calico Hills unit, the potential effect of elevated temperature of ground waters on the zeolites at the base of the shaft is evaluated. The thickness of the Calico Hills unit at the ES-1 is also discussed in this report. Because the shaft internals will be removed to accommodate emplacement of shaft fill, there is no impact of the shaft internals on the postclosure performance of the repository.

Because release and transport of radionuclides from the underground facility can be due to several mechanisms, scoping calculations are presented in the beginning of the report to provide a perspective on the more important mechanisms that should be considered when assessing the significance of the MPZ. From these calculations, release of radionuclides due to downward water transport is considered to be the most realistic and dominant mechanism. Air transport of gases by convective and barometric forces through the drifts and/or shafts was also determined as important to evaluate because of the thermal energy differences within the repository. The calculations, therefore, focus primarily on conditions that would enhance the downward transport of radionuclides in the aqueous phase and air transport of gases due to convection.

In the first mechanism (downward water transport), it is assumed that water can enter the upper portion of the shaft, infiltrate to the base of the shaft, potentially build up at the base of the ES, and drain into the surrounding rock mass. The calculation presented in this report first defined a broad range of inflows into the shaft. These inflows are dependent on the hydrologic conditions assumed at the surface. Of particular concern is the influence of the MPZ on the inflow into the shaft. These inflows, in turn, are assumed to be transported to the base of the shaft where buildup of waters can occur as well as drainage.

Because, in general, water entering the shaft is predicted to be contained within the exploratory shaft sump and subsequently drained, it is concluded that the MPZ is not expected to influence the radionuclide release performance of the Yucca Mountain Mined Geologic Disposal System (YMMGDS). In two cases (using the new ESF design) where limited water

entry through seals at the repository station* is computed, the transport of radionuclides is not influenced. This is because the maximum computed flow through the repository station seals is 40 m^3 , which can be isolated from the waste disposal drifts by repository passive design features. These features can include constructing a sump capable of storing and draining this volume of water near the exploratory shaft or within the Exploratory Shaft Facility (ESF).** In addition, with proper repository drift grading, the water can be directed to the low point in the repository, so that the water would not enter the waste disposal area.

The authors conclude that for water inflow the MPZ does not influence the performance of the YMGDS because (1) the occurrence of the scenario*** selected to develop a source of water that could enter the shaft is highly improbable or incredible, (2) even if this highly improbable scenario occurs, the volume of water entering the shaft can be contained within the shaft sump and/or the ESF, and (3) both the ES-1 and ES-2 have been relocated to more favorable locations outside the flood plain of existing arroyos and in an area where the bedrock is exposed.

An additional concern about the water inflow in the MPZ and out of the base of the shaft is the potential to form precipitates in the MPZ and the shaft fill. Precipitation could occur because the concrete liner will cause some modifications to the chemistry of the ground water. These water chemistry changes may cause the ground water to become supersaturated with respect to some minerals and precipitation could then occur. If precipitation occurs above the repository station, lower water flows would be

*The repository station is a location in the underground facility that corresponds to the drift area that is adjacent to a repository shaft at the repository level.

**The ESF is the exploratory shaft, any associated surface structure and underground openings constructed for the purpose of site characterization.

***The scenario used to compute the unanticipated volume of water ($\sim 20,000 \text{ m}^3$) is considered highly improbable because it couples a probable maximum flood event with an obstruction in the drainage basin that can retain the flood waters above the exploratory shaft locations.

expected to enter the base of the shaft. If precipitates form at the base of the shaft, the drainage capacity at the base of the shaft could be decreased.

From the models of precipitate deposition in this report, precipitates are predicted to form and quickly deposit at nucleation sites in void spaces. This deposition is controlled by diffusional processes where the diffusional path length (i.e., 1/2 of the pore diameter or 1/2 of the fracture aperture) is small and travel times are short. Hence, forward migration of precipitates in the porous medium is expected to be limited. As this process continues, a buildup of precipitates occurs in a frontal advance. This precipitation front is projected to start at the top of the liner and progress downward in both the shaft fill and the MPZ. It is concluded that if anticipated volumes of water ($-44 \text{ m}^3/\text{year}$) enter the shafts, no significant formation of precipitates occurs. If unanticipated volumes ($-20,000 \text{ m}^3/\text{event}$) enter the shaft, precipitates could advance as much as 60 m radially out from the liner in the MPZ where fracture porosity is small. However, once the front advances beyond the base of the liner, the maximum frontal advance will be 0.016 m/event due to the increased porosity of the shaft fill. Hence, the deposition of solids from the interaction of the shaft liner with ground water is expected to be a localized phenomenon. We can, therefore, conclude that the fractures in the MPZ above the repository horizon will tend to fill with precipitate, thereby reducing the permeability of the MPZ where deposition occurs. Because deposition is a localized phenomenon, the drainage capacity of the rock at the base of the shaft should not be detrimentally reduced, assuming that the shaft liner in the base of the shaft is removed during decommissioning.

As mentioned earlier, the MPZ may be significant if it can substantially enhance the release of gaseous radionuclides by increasing the air flow through the MPZ. Because the emplaced waste in the repository will release heat, temperature gradients will develop in the rock mass. The temperature differential will tend to cause air to rise in the exploratory shafts. The convective air flow analyses presented in this report consider potential airflow in and near the shafts and also consider the potential flow through the rock above the waste disposal areas.

For several combinations of host rock air conductivity above the repository the percentage of flow through the shaft (including the MPZ) to the total flow (including shaft, the MPZ, and the rock mass above the waste disposal area) was plotted as a function of shaft fill, air conductivity. It was concluded from the analysis that shafts and ramps are not preferential pathways for gaseous radionuclide releases if the air conductivity of the shaft fill is less than about 3×10^{-4} m/min or an equivalent hydraulic conductivity of 10^{-2} cm/s. When the air conductivity of the shaft fill is greater than 3×10^{-4} m/min the air flow through the shaft fill and MPZ is predominantly through the shaft fill. It is only when the conductivity of the shaft fill is low that flow through the MPZ is proportionally greater than flow through the shaft fill. However, when flow through the MPZ is proportionally greater than flow through the shaft fill, the total air flow through the MPZ and shaft fill, as compared to the flow through the rock over the repository, is extremely low, i.e., less than 2.5%. Therefore, it can also be concluded that the MPZ is not likely to detrimentally influence the performance of the YMGDS by enhancing the release of gaseous radionuclides.

A second mechanism was considered in assessing the influence of the shaft fill and the MPZ on increasing the release of gaseous radionuclides from the repository. This second mechanism involves the displacement of air out of ES-1 or ES-2 due to barometric forces. The purpose of the analysis associated with the mechanism is to predict what volume of air contained in the shaft fill and the MPZ under unsaturated conditions can be displaced due to several meteorological events. If only a portion of the shaft fill and MPZ air volume is displaced when the pressure drop occurs at the surface, the surface air will be forced into the shaft fill and MPZ when the pressure reversal occurs at the surface.

It is concluded from these analyses that the volume of air in the exploratory shafts is not fully displaced during the occurrence of a broad range of meteorological conditions if the shaft fill, air conductivity is less than about 10^{-1} m/min.

A final area of evaluation mentioned above was the penetration of the ES into the Calico Hills unit. From the analyses presented in this report,

the impact of this penetration on the sorptivity of the Calico Hills unit was found to be negligible. This conclusion was reached for the following reasons:

- (1) Water passing through the ES will be separated from waste stored in the repository. Therefore, the likelihood of water containing radionuclides reaching the ES is diminished.
- (2) The minimum thickness (70 m) of the Calico Hills unit at the eastern edge of the repository will be preserved while allowing much valuable information to be gained by sinking the ES into the upper margin of the Calico Hills.
- (3) The temperature of water passing through the ES was calculated to closely approach the global formation temperature for all considered water flow rates, including the maximum flooding event defined in this report. This calculated temperature increase will be far less than that required to have any significant impact on the sorptivity of the Calico Hills zeolites. Therefore if any radionuclides do reach the base of ES-1, radionuclides would still be effectively retained at the base of the shaft.

The discussion and results presented above were focused on determining if the design and construction of the ESs could significantly influence the performance of the YMMGDS. Should future analyses indicate that either the shaft liner or the MPZ could significantly influence the performance of the YMMGDS, we have provided a description of the preferred methods for restoration of the MPZ, liner removal, and seal emplacement. In this report, the following conclusions were reached on the preferred methods for restoration of the MPZ, liner removal and seal emplacement.

- o Grouting in the welded tuff is feasible and is the preferred method for restoring the MPZ because drilling smooth-walled, grout holes allows an examination of fractures in the modified permeability zone through the use of a borescope. Also, at present, it is not certain how large an interface stress can be developed through the use of only an expansive concrete (one of the alternatives) or how effective such stress

development would be in reducing the potential for flow in closing fractures. Grouting the MPZ, however, does incur a greater cost than constructing an expansive concrete plug.

- o Evaluation of the advantages and disadvantages suggests that the hydraulic splitter method is the favored approach for liner removal, although the other approaches are technically feasible. Conventional equipment with the slight modification of suspending the splitters from chains may be used. The costs are somewhat less than for other methods evaluated. The method does not leave potentially undesirable chemical residue. While supplemental hand methods may be required, this is not considered a significant disadvantage.
- o The construction sequence for emplacing a shaft plug entails making saw cuts at the top and bottom of the plug, removing the liner, excavating the keyway, backfilling to the underside of the plug, placement of concrete, and contact grouting.

This page is for page number only

1.0 PURPOSE OF REPORT

The Nevada Nuclear Waste Storage Investigations (NNWSI) Project, managed by the Nevada Operations Office of the U. S. Department of Energy (U.S. DOE-NVO), is examining the feasibility of developing a nuclear waste repository in an unsaturated tuff formation beneath Yucca Mountain. Yucca Mountain is located on and adjacent to the Nevada Test Site, Nye County, Nevada. One aspect of the NNWSI Project is the development of the Exploratory Shaft (ES) testing program. The purpose of the ES testing program is to obtain at-depth site information on the hydrology and geology of the site. The testing will be performed in the unsaturated tuff at Yucca Mountain. The results from many of these tests will be used to determine the effectiveness of the geologic setting at Yucca Mountain to isolate high-level radioactive waste.

Before initiating the construction of the exploratory shafts (ES-1 and ES-2), it is necessary to determine the quality assurance levels to be applied to the ES design and construction. The DOE-NVO is responsible for assigning the quality assurance levels. This report provides analyses to establish part of the technical basis for the appropriate quality assurance levels. This basis is established by evaluating whether the design and construction of ES-1 and ES-2 could compromise long-term isolation capabilities of the repository. The concern raised was: Do the shaft liner, the shaft internals, and the increased rock damage around the shaft (due to shaft construction) significantly influence the release of radionuclides from the repository? Because the shaft internals, including instrument conduits, utility piping, ventilation ducts, and conveyances hardware, will potentially be removed for repository operations (i.e., development, waste emplacement, monitoring, and, if necessary, retrieval) and will certainly be removed to accommodate emplacement (during decommissioning) of shaft fill, shaft internals will have no impact on the long-term performance of the repository. Therefore, only the significance of the rock damage zone or the modified permeability zone (MPZ) and the shaft liner on the long-term performance of the repository is considered. The approach taken to determine the significance of the MPZ and shaft liner on the long-term performance of the repository is to evaluate selected physical processes and bounding scenarios which have been raised by the DOE, the NRC or by ourselves. Therefore, this report is not intended

to provide an exhaustive analysis of all possible scenarios and physical processes which could occur and may impact the future repository performance, but is considered sufficient to initiate construction of the exploratory shaft.

An integral part of the overall repository system in the long-term performance of the repository is the closure of the Exploratory Shafts (ES-1 and ES-2). Therefore, it is necessary to determine the desired performance of these sealed shafts and, for completeness, the entire sealing system. Additionally, the development of a model for the MPZ is required. In Fernandez et al. (1987), performance goals and design requirements for the sealing system are presented. The need for sealing is also assessed by evaluating the water flow into and out of the underground facility, shafts, and ramps for anticipated conditions. In Case and Kelsall (1987), a model for the MPZ in welded tuff is presented. Development of the MPZ is due to the blast damage effects and stress relaxation. In this report, selected results from both of the previous reports are restated. These results are supplemented by additional analyses that establish a perspective into the potential mechanisms of most concern to radionuclide release, and potential geochemical modification of ground-water chemistry due to the presence of the liner. This report also describes contingency plans to remove the liner, to restore the MPZ, and to emplace a seal. This information is presented in case future analyses suggest that removal of the liner and restoration of the MPZ are required. It is not the intent of this report to present a total systems analysis.

Appendix A presents analyses used to establish a perspective on the most likely mechanisms for radionuclide transport. Reference conditions considered in this report are given in Chapter 2. Chapter 3 presents the analyses used to assess the influence of the MPZ on the performance of the Yucca Mountain Mined Geologic Disposal System (YMMGDS). The analyses described in Chapter 3 assess the potential of water to enter the waste disposal area after entering the shaft and the potential for air flow (and indirectly radionuclide release) out of the repository due to convective and barometric forces. The assessment of the amount of water that could

enter waste disposal areas from shafts is made by considering a range of shaft inflows that vary in time as well as in total flow. These inflows are then coupled with the drainage capacity of the ES sump to determine if these could cause water buildup in the sump.* Where the buildup of water exceeds the sump storage capacity, water flow into the underground facility and duration of flow are noted. Both water flow volumes and duration of flow contribute to determining the potential for enhancing radionuclide releases. The assessment of potential air flow out of the repository is made by considering the convective circulation of air in response to thermal gradients and the movement of air in response to changes in barometric pressures. The significance of this air movement is determined by considering how much air might flow preferentially through the shafts and ramps. For the barometric analysis the volume of air that can exit from shafts and ramps due to several, surface, weather conditions is also evaluated.

The potential influence of the liner on the performance of the YMMGDS is evaluated in Chapter 4, and the interaction of water entering the shaft with the shaft liner is evaluated. Once the potential changes in water chemistry are predicted, the likelihood and location of mineral precipitation is assessed. Remedial measures to restore the MPZ and remove the liner are presented in Chapters 3 and 4, respectively. Also, in Chapter 4 the procedure for emplacing a shaft seal is presented together with the schedule and cost estimate for removing the shaft liner, emplacing backfill and emplacing a shaft seal if this becomes necessary. Chapter 5 addresses the potential influence of ES-1 penetration into the Tuffaceous Beds of Calico Hills. Specifically, the potential change of the sorptivity of the Calico Hills unit is evaluated. This potential sorptivity change may result from elevating the temperature of water potentially passing through the ES. The thickness of the Calico Hills unit below the bottom of the shaft is also discussed.

*The ES sump is that volume within the shaft between the repository station and the base of the shaft.

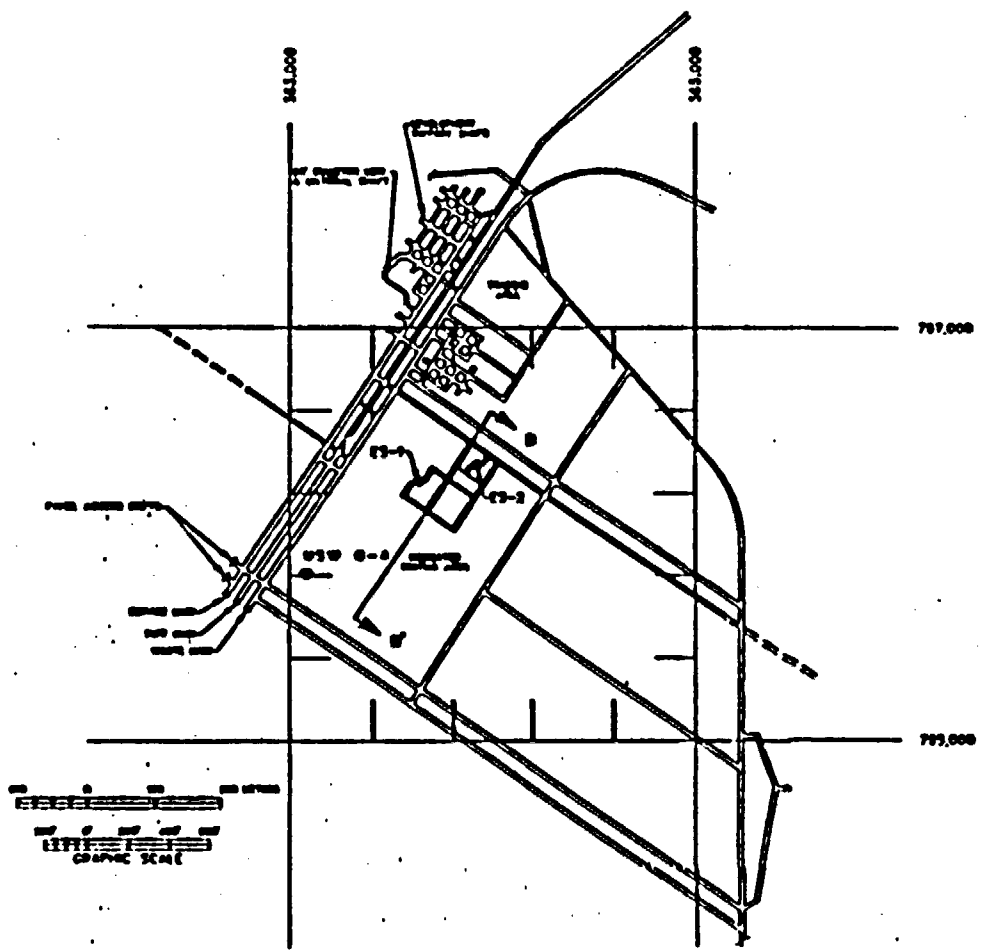
This page is for page number only

2.0 SHAFT DESIGN INFORMATION

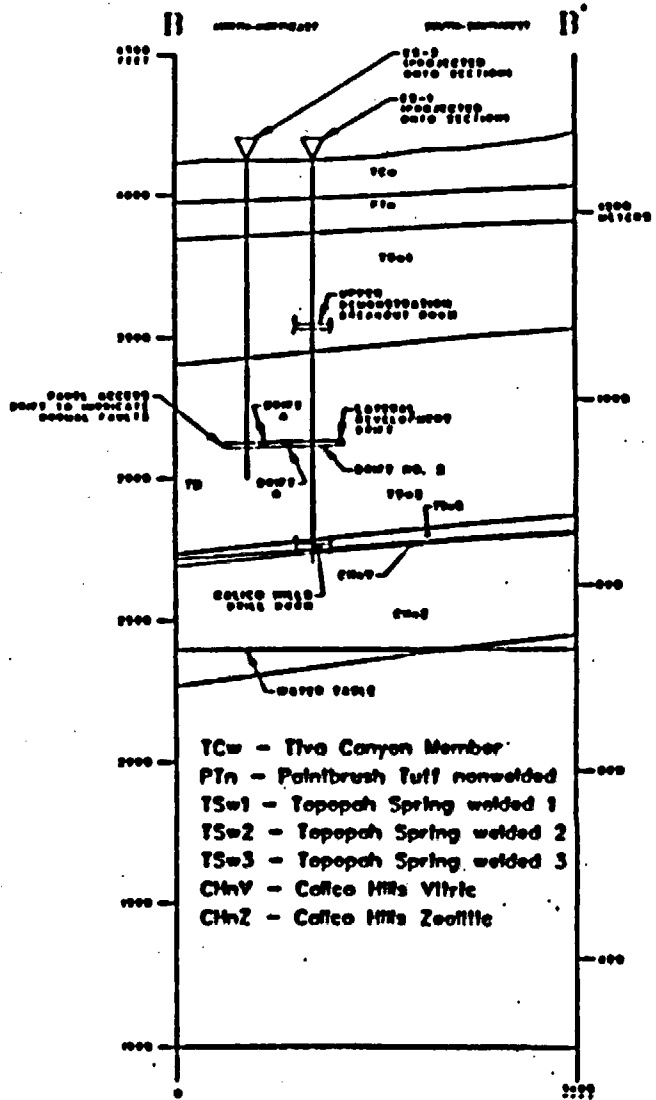
This chapter contains information primarily on the design of the exploratory shafts. Limited information on the repository design is also presented to better understand how the ESs are integrated into the design of the repository. In general, the repository in the underground facility is comprised of interconnecting access and emplacement drifts. The underground facility is planned to be located in the unsaturated portion of the Topopah Spring Member approximately 200 to 400 m above the ground-water table. The Topopah Spring Member is predominantly a densely welded, highly fractured tuff having a low matrix hydraulic conductivity.

Access to the underground facility is provided by ramps and shafts. The current, repository design (MacDougall et al., 1987, pp. 4-10 to 4-12) incorporates six openings to the underground facility, including four vertical shafts and two inclined ramps. Both types of excavation will penetrate several stratigraphic units, including the alluvium and welded and nonwelded tuff units. The ramps connect directly into the main access drifts at the northern end of the repository. The shafts are located in the northeastern portion of the repository. The men-and-materials and emplacement exhaust shafts have shallow sumps extending 24 and 3 m below the repository, respectively. The bottoms of both of these shafts are within the Topopah Spring Member. The sump for the ES-1 as originally analyzed was 140 m* below the repository station. ES-1 will penetrate part of the unsaturated portion of the tuffaceous beds of Calico Hills. The bottom of the ES-2 will only slightly extend below the repository level (MacDougall et al., 1987, pp. 4-10 to 4-12).* Figure 2-1 shows profiles of the shafts superimposed on the geologic stratigraphy at each location.

*The sump depth in the current ES-1 design is 110 m. The sump depth in the current ES-2 design is 30 m.



Reference: SNL No. F07048a/1



Reference: SNL No. F07048a/13

Figure 2-1. Schematic of Exploratory Shafts and Corresponding Geologic Stratigraphy

2.1 Location of the Exploratory Shafts

After this study was concluded, new locations for ES-1 and ES-2 (DOE-NWO, 1987, p. 1-3) were selected. The old locations of ES-1 and ES-2 (DOE, 1986) are located in a wide valley through which the north and south forks of Coyote Wash flow at the northern and southern margins (Figure 2-2). The valley floor is underlain by coarse alluvium and mud/debris flow deposits, with surficial fine-grained sand, probably of eolian origin. Bedrock (Tiva Canyon Member) is exposed in the steep valley walls to the north and south and to the west. Bedrock is exposed in the washes upstream of the ES-1 location.

The originally proposed location of ES-1 is within the alluvial-filled valley. The ES-2 site is located out of the alluvium and in a southwest direction from ES-1. The new locations are also shown on Figure 2-2. These new locations for ES-1 and ES-2 will be approximately 107 m and 93 m north of and above the confluence of two small ephemeral streams that are tributaries of the Coyote Wash drainage system. The new locations for both shafts will be out of the alluvium.

2.2 Construction of the Exploratory Shafts

Before the underground facility is constructed, an exploratory shaft facility (ESF) will be developed. The ESF primarily includes (1) the main shaft (ES-1), which will transport people, materials, and equipment from the surface to the subsurface test area and will provide ventilation to the ESF, (2) an underground testing area, and (3) a secondary shaft (ES-2) which will provide secondary emergency egress, transport people and materials, provide for muck removal, and provide additional ventilation capacity. It is the current intent of the NNWSI Project to incorporate ES-1 and ES-2 into the underground facility design.

In the SCP-CDR, (MacDougall et al., 1987, p. 3-107 and p. 4-85) it is planned that the exploratory shafts and the waste ramp will supply intake air for the waste emplacement area including the shops and decommissioning facility. In the SCP-CDR design hoisting equipment and fixtures would be removed prior to waste emplacement, but the concrete liners will be left in place.

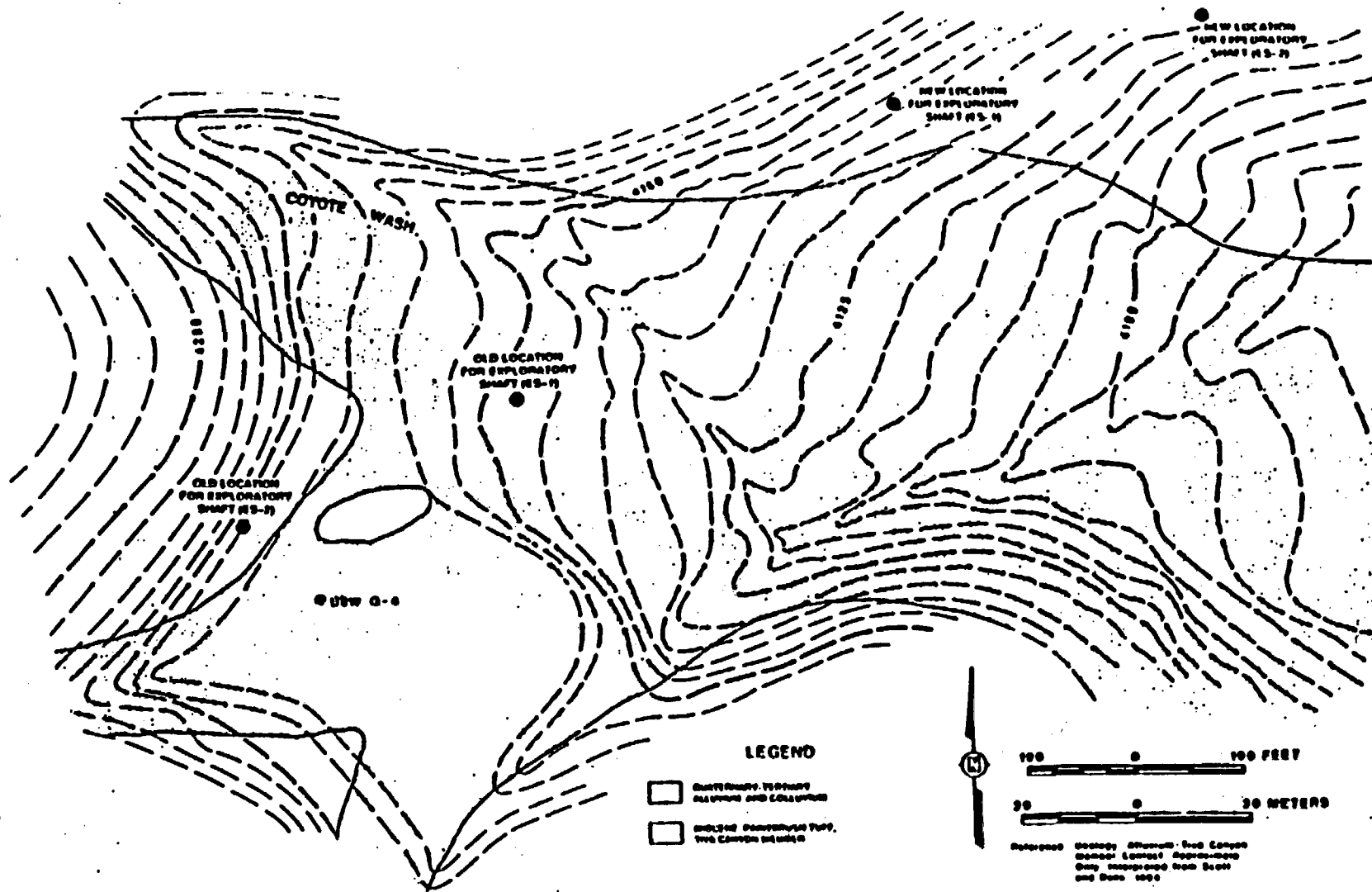


Figure 2-2. Surficial Geology of Exploratory Shaft Area

The current design details for ES-1 and ES-2 follow. The excavated diameter for ES-1 and ES-2 will be approximately 4.3 m with a finished diameter of 3.7 m. Both shafts are planned to be lined with an unreinforced concrete liner at least 0.3 m thick. Some reinforcement is planned in the shaft collar and in the brow* at each breakout (DOE, 1988, pp. 8.4-12 and 8.4-33). The collars for the new locations of ES-1 and ES-2 will be in bedrock. Most of the concrete liner will not be reinforced but will contain some steel rods to hold the forms used to construct the liner.

Both shafts will be mined using a conventional drill-blast-muck mining sequence. During the mucking operation, minimal amounts of water will be used to suppress the dust in the shaft so that tests characterizing the unsaturated zone will not be affected. Because the excavation of the shafts involves blasting, some additional fracturing of the rock mass into the shaft wall may occur. The blasting will be controlled (i.e., to enhance the vertical advance, limit damage in the rock surrounding the shaft, and produce acceptable-sized rock fragments (DOE, 1988, Section 8.4.2.1.1).

2.3 Shaft Sealing Concepts

The primary functions of shaft seals are to:

- o Reduce the potential for surface water or ground water to enter the waste emplacement areas via the shafts
- o Deter human entry to the repository via the shafts.

These functional requirements may be satisfied by one or more seal components. For example, human entry will be discouraged by backfill or seals placed below the ground surface.

*The portion of the shaft liner that is located at the upper portion of the shaft and is generally reinforced concrete is the shaft collar. The shaft brow refers to the roof rock in the shaft station where the shaft opens up into the shaft station. The shaft station refers to the location where the drift intersects the shaft.

Flow through the shaft can be reduced by backfill placed along the length of the shaft or by one or more seals (plugs) placed at intervals. Backfill alone may not be a satisfactory option if there is the potential for significant flow through an MPZ adjacent to the shaft wall. In such a case, it might be necessary to form a cutoff through the damaged zone, possibly by keying a plug into the walls. Another alternative to reducing the potential of water flow into the waste disposal area is the emplacement of a repository station seal in the drift connected to the exploratory shaft. Figure 2-3 illustrates the general arrangement for shaft seals.

2.4 Preferred Options for Shaft Seals

Currently, the preferred option for reducing water flow and deterring human entry is the anchor-to-bedrock plug/seal because:

- o The anchor-to-bedrock plug/seal can be located in a relatively benign environment protected from surficial temperature extremes, surficial geologic processes, and heat generated by the waste. Station plugs, located at the intersection of the shafts and repository station drifts, are isolated from the waste emplacement areas by barrier pillars.* The maximum temperatures at the station plug location are estimated to be 40°C (Richardson, in preparation, Appendix B). The in situ stress would also be greater than that associated with a plug/seal closer to the surface.
- o The design requirement for the anchor-to-bedrock plug/seal is less stringent than that for a seal at the base of the shaft because of the lower maximum head (Fernandez et al., 1987).
- o Only one seal is required for each shaft, making a total of four, whereas eight total seals might be required if seals are placed in the shaft stations.

*The barrier pillar refers to the rock zone surrounding the shaft that isolates the shaft from subsidence effects of underground rooms. For a nuclear waste repository, the barrier pillar also isolates the shaft from a high temperature environment.

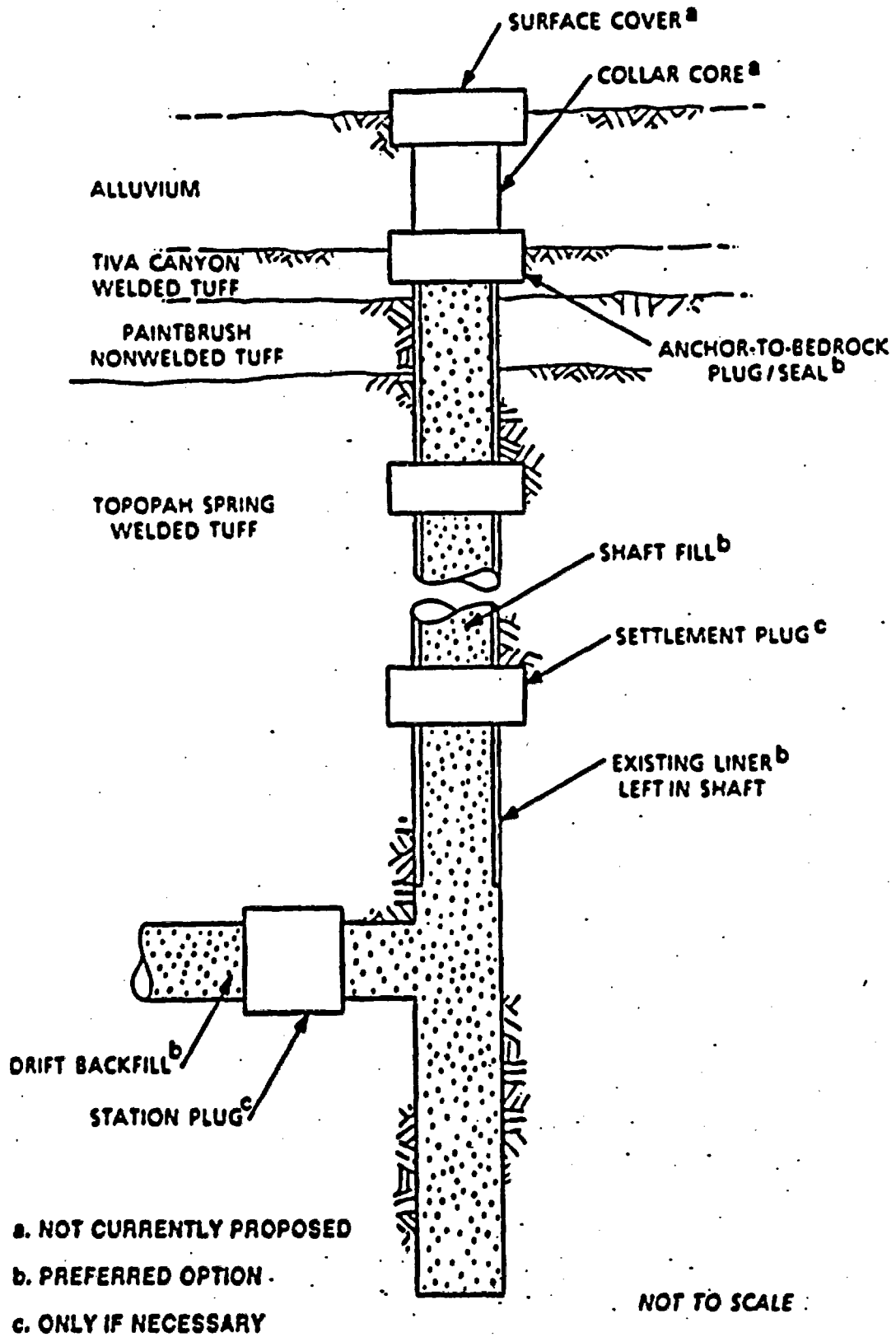


Figure 2-3. General Arrangement for Shaft Seals Showing Optional Components

- o Construction of a seal at shallow depth in a shaft (about 10 m) should be easier and cheaper than construction at the base of the shaft. If necessary, the alluvium can be stripped away to facilitate construction of the anchor-to-bedrock plug/seal.

- o The anchor-to-bedrock plug can be designed to reduce the potential for flow through the MPZ, whereas simple placement of shaft backfill would have no influence on the MPZ. Moreover, development of the MPZ at the shallow depth of the anchor-to-bedrock plug should be less than that at the station plug location where inelastic deformation is more likely to occur (Case and Kelsall, 1987).

3.0 INFLUENCE OF THE EXPLORATORY SHAFTS INCLUDING THE MODIFIED PERMEABILITY ZONE AND THE SHAFT FILL ON THE PERFORMANCE OF THE YMGDS

Shafts represent potential pathways that could compromise the ability of the geologic repository to meet the performance objectives for the period following permanent closure. As analyzed in this report, performance can be compromised in two ways. First, water could enter the underground facility through the shafts and contact waste packages in waste disposal areas, potentially accelerating the radionuclide release. Second, release of gaseous radionuclides could occur through the shafts.

Two zones associated with shafts can affect the water entry and air-borne release--the shaft interior and the MPZ behind the shaft liner. The intent of this chapter is to determine if the MPZ and the shafts could significantly affect repository performance. This is accomplished by assuming that the shaft is filled by a simple granular material and by using an MPZ model. Using this information, potential water flow into the underground facility from the shafts and air flow out of the shafts is computed.

3.1 Modified Permeability Zone Characteristics

This section presents a brief description of a model of the MPZ that considers modification due to stress redistribution and blasting. A more complete description of the model and the site-specific parameters at Yucca Mountain that were used in the development of the model is presented by Case and Kelsall (1987) and is described briefly below.

It is postulated that the significant mechanisms for modifying permeability in fractured, welded tuff are 1) the opening or closing of fractures in response to stress changes, and 2) creating new fractures or the opening of old fractures by blasting. The approach for developing the modified permeability zone model includes the following five steps which are described in detail in Case and Kelsall:

1. Calculate stress changes around a shaft by using an appropriate closed-form solution for elastic or elastoplastic analysis of a circular shaft located in a uniform stress field.
2. Obtain relationships from published laboratory and field testing results which describe the effects of stress on the permeability of single fractures and fractured rock.
3. Calculate rock mass permeability as a function of radius away from the shaft based on the calculated stresses and the stress-permeability relationships obtained from testing.
4. Estimate permeability changes due to blasting from evaluation of case histories which indicate the depth of damage and estimate the probable increase in fracture frequency in the damaged zone.
5. Combine the results derived from performing steps 3 and 4 to estimate the combined effects of stress redistribution and blasting.

In the interest of simplification, three assumptions form the basis for the modified permeability zone analysis:

1. Prior to excavation, the in situ stress state is isotropic and the normal stress acting across each fracture is equal to the average far-field value.
2. Stresses existing around the opening after excavation are calculated by using closed-form solutions as normal principal stresses acting in the radial and tangential (or hoop) directions; shear stresses are ignored.
3. The stress acting across each fracture after excavation is the calculated radial stress at the appropriate location relative to the shaft wall. (Note that the radial stress is always less than the tangential stress in an isotropic stress field.)

These assumptions are conservative for the isotropic state of stress (i.e., they tend to over-predict increases in permeability) in that stress increases across some fractures are ignored and each fracture is, in effect, assumed to be perpendicular to the direction of maximum stress relief. Conversely, the simplified analysis does not account for the effects of shearing along fractures. On balance, it is the authors' judgment that the model is a reasonable representation of permeability changes in fractured, welded tuff.

As excavation occurs, stresses are relieved and blast induced fracturing may occur. Considering a representative volume of rock adjacent to the shaft, it is to be expected that the geomechanical response to excavation will be most influenced by rock mass properties (which take into account the effect of fractures) rather than by the properties of the intact rock since the range of fracture spacing is small relative to the shaft diameter (Figure 3-1). Similarly, the permeability of the rock mass will be influenced by fractures as well as by the rock matrix. [This discussion applies specifically to welded tuff and may be less applicable to nonwelded units in which the typical fracture spacing is 80 cm to 200 cm (Langkopf and Gnirk, 1986, p. 66).] The fracture orientations shown in Figure 3-1 are schematic; actual fracture patterns in welded tuff are expected to range from two oriented sets plus a random set to three oriented sets plus a random set (Langkopf and Gnirk, 1986, p. 48). Also, Langkopf and Gnirk (1986, p. 66) estimate a fracture frequency of 2 to 16 corresponding to a spacing of 50 cm and 6 cm (see Figure 3-1).

The redistribution of stresses around an opening in fractured tuff might affect the permeability of the rock mass in two ways: (1) by the fracturing of originally intact rock due to excessive compressive or tensile stresses and (2) by the opening or closing of preexisting fractures due to changes in the normal stresses acting across the fractures or shearing along the fractures. The potential for fracturing of intact rock was evaluated by simple elastic analysis by Case and Kelsall (1987) for the case of a circular shaft excavated in a homogeneous, isotropic and linearly elastic medium. This analysis showed that the maximum tensile or compressive stresses at the shaft wall at repository depth are approximately 10% of the reported mean values for tensile and unconfined compressive strength

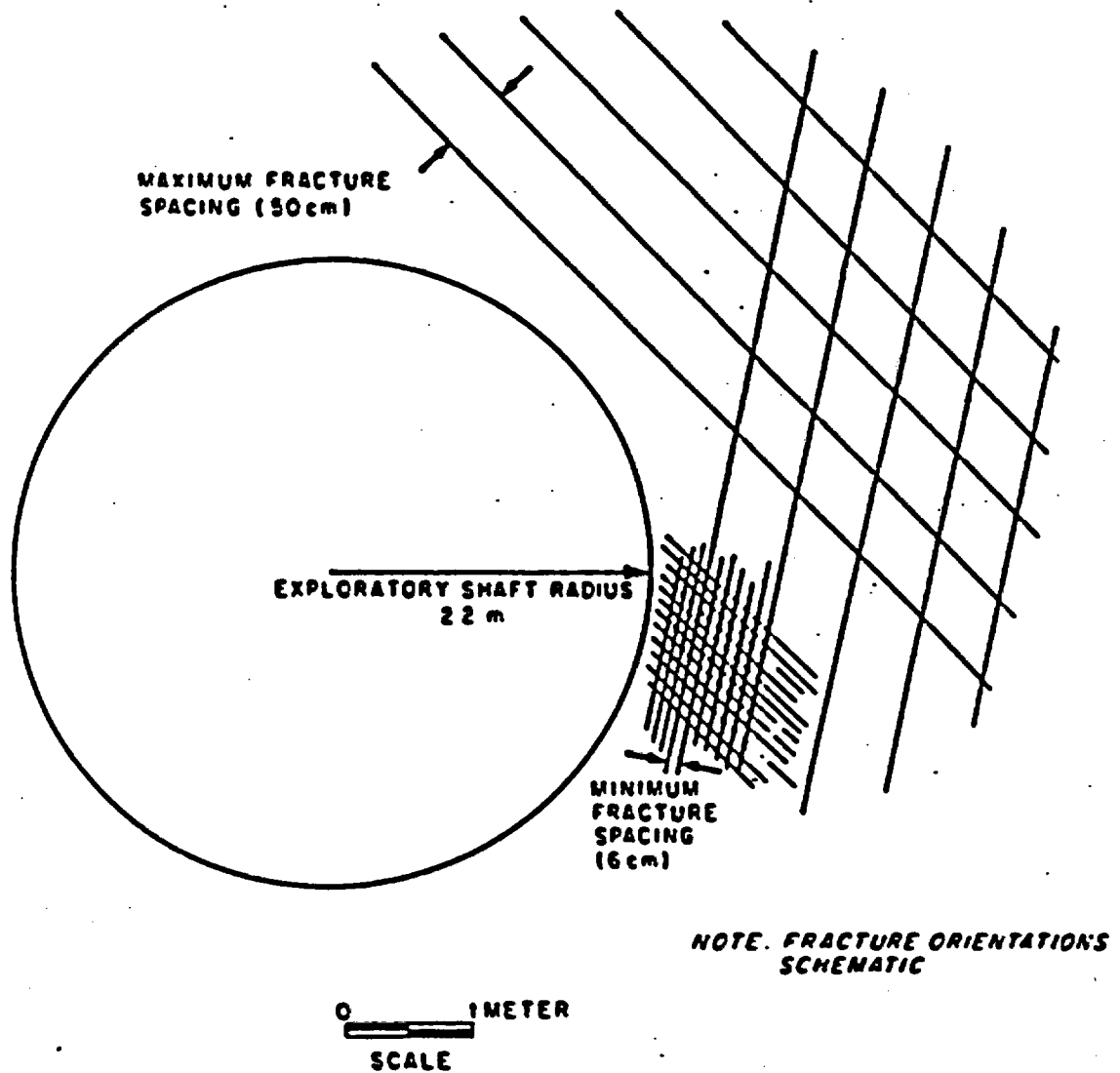


Figure 3-1. Cross Section Through a Shaft in Welded Tuff Showing Fracture Spacing Relative to Shaft Radius

of intact rock. The analysis showed that fracturing of intact rock due to stress concentrations around a repository at depth is unlikely, even allowing for variation from the mean reported strength values and potential anisotropy in the stress field.

Whereas stress redistribution around a shaft is unlikely to lead to fracturing of intact rock (which could in turn lead to increased permeability), the effects of stress changes across fractures may have a significant effect on permeability. This arises because the rock mass is densely fractured and because the aperture of the fracture is sensitive to the stress applied across the fractures. Conceptually, permeability should be increased where normal stresses are reduced across fractures, while permeability should be reduced where normal stresses are increased. Furthermore, the opening or closing of fractures is dependent on the relative orientation of fractures with respect to the shaft wall and the orientation of the stress field.

Elastic and elastoplastic stress analysis for a shaft excavated in tuff were performed by Case and Kelsall (1987). Their results indicate that a wide variation in rock mass behavior might be observed, depending on depth, in situ stress, and rock properties. Because rock mass strength* may vary with depth (due to variations in porosity and fracture spacing), rock mass behavior may vary even within a lithologic unit. For the welded units, the expected response is elastic in nonlithophysal zones, but plastic response may occur in lithophysal zones or in intensely fractured zones where strength is lower. Plastic behavior is expected for the nonwelded Calico Hills tuff near the base of the shaft because of the relatively low strength and the higher in situ stresses due to depth. For the nonwelded Paintbrush unit overlying the Topopah Spring the behavior may be elastic or plastic depending on rock mass strength and in situ stresses. Formation

*Rock mass strength is defined as the maximum stress that can be carried by the rock mass (Hoek and Brown, 1980, p. 150). The maximum stress level is found to be dependent on the strength properties of intact rock, and discontinuities, and is dependent on confining stress.

of a plastic zone surrounding the shaft may be limited to less than one shaft radius from the shaft boundary; however, if rock support is provided after excavation, this plastic zone can be potentially reduced. However, the effects of rock support in limiting inelastic deformation were not considered in this analysis.

Fractures may also be introduced by blasting. Several investigators have described the mechanics of blasting in rock (Langefors and Kihlstrom, 1978, Chapter 1; Hoek and Brown, 1980, Chapter 10; Brady and Brown, 1985, Chapter 17). Fracturing may occur in several ways after blast detonation. Fracturing may be induced near the blasthole due to quasi-static gas pressure that sets up tensile tangential stress or by crack propagation where gas pressure enters existing fractures and extends them. Fracturing may also occur further from blast detonation holes as seismic compressive waves are partially reflected off free surfaces (voids or open joints).

In actual rock masses, the extent and pattern of fracturing will be influenced by rock properties such as strength, anisotropy, pre-existing fractures in the rock mass and in situ stress. Fracturing is also influenced by the blasting method and by the charge weight of explosives, which are expected to be reduced near the excavation perimeter. Because relatively low charge weights can be used in the perimeter holes, the damage to the rock beyond the perimeter can be limited.

In this report, the blast-damaged zone is a zone extending from either 0.5 m to 1.0 m from the rock wall where blast-induced fracturing may occur. The extent of the zone is derived from a general relationship between blast damage and charge density for tunnel blasting conditions (Holmberg and Persson, 1980) where some measures for controlling blasting are utilized. Blasting is assumed to increase the fracture frequency by a factor of three in the blast-damaged zone. It is further assumed that the newly created fractures have similar characteristics to existing fractures. In this preliminary model, the permeability in the blast-damaged zone would increase by a factor of three due to an increase in fracture frequency over the increase that occurs due to stress relief.

The increase in permeability due to stress relief and blast effects for the exploratory shaft for the expected case is illustrated in Figure 3-2 and summarized for expected and upper-bound cases at two depths in Table 3-1. The analyses were conducted for depths of 100 m and 310 m, corresponding to depths near the top of the Topopah Spring and at the repository horizon. The results in Table 3-1 are reported as a relative, rock-mass permeability factor, which is expressed as a ratio of increased permeability to undisturbed permeability in the modified permeability zone, and which is expressed for convenience in subsequent calculations as a uniform factor over an annulus extending one radius from the shaft wall.*

The expected case is based upon an elastic analysis with expected strength, in situ stress, sensitivity of permeability to stress, and a 0.5-m-wide, blast-damaged zone. The upper-bound case is based upon an elastoplastic analysis with lower-bound strength, upper-bound, in situ stress, greatest sensitivity of permeability to stress, and a 1.0-m-wide, blast-damaged zone.

For the expected conditions at 310-m depth (i.e., considering mean values for rock mass strength, in situ stress, and stress permeability sensitivity, and a 0.5-m-wide, blast-damaged zone), the relative, rock mass permeability factor is 20 times the permeability of the undamaged rock mass. For the upper-bound condition at 310-m depth, the relative, rock mass permeability factor is 80 times the undisturbed permeability.

*The relative, rock mass permeability factor for the expected case is calculated by first performing the radial integration of relative, rock mass permeability from the shaft radius (2.2 m) to approximately a radius of 10 m and then calculating a factor by dividing by the area of the annulus extending from 2.2 m to 10 m from the shaft.

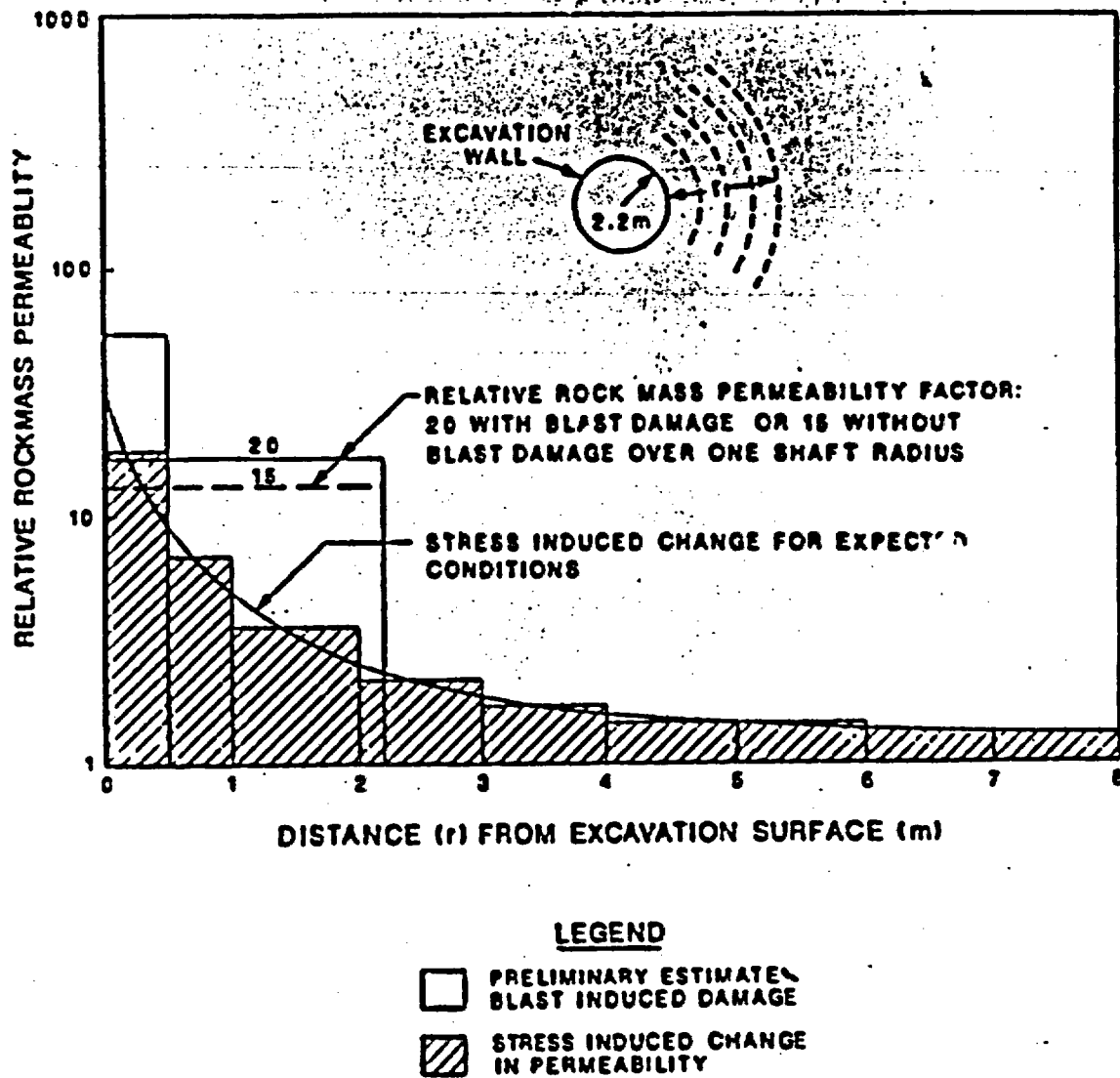


Figure 3-2. Modified Permeability Zone Model for Topopah Spring Welded Tuff for Expected Conditions at 310-m Depth

Table J-1. Relative Permeability Factors Associated With the Modified Permeability Zone^(a) (After Case and Kelsall, 1987)

Depth	Stress Redistribution Without Blast Damage		Expected ^(b) Case	Upper Bound ^(c) Case
	Elastic	Elastoplastic		
100	15	20	20	40
310	15	40	20	80

(a) Relative permeability factors are averaged over an annulus one radius wide around the 4.4-m diameter ES.

(b) This is based upon an elastic analysis with expected strength, in situ stress, sensitivity of permeability to stress, and a 0.5-m wide, blast damage zone.

(c) This is based upon an elastoplastic analysis with lower-bound strength, upper-bound, in situ stress, greatest sensitivity of permeability to stress, and a 1.0-m-wide, blast damage zone.

3.2 Potential for Enhancing Radionuclide Releases Due to Water Entering the Exploratory Shaft

The purpose of this section is to determine whether the presence of the exploratory shafts and the rock damage surrounding a shaft, caused by excavation of the shaft, can significantly enhance the release of radionuclides. The release mechanism considered here is water entering the waste disposal areas through the ES and contacting the waste. Therefore, it is necessary to establish the hydrologic properties of the zone through which water can be transmitted to the base of the shaft. This zone includes the shaft interior and the MPZ. Therefore, it is important to define the MPZ and establish a scenario of water entry into the shaft and potentially into the waste disposal area. Relative permeability factors for the MPZ are given for the expected and the upper bound cases (Section 3.1). Both MPZ models include a blast-damaged zone and are evaluated to provide a range of water flows through the MPZ. The scenario of water entry postulated in this section includes two major events occurring at the ground surface (see Section 3.2.1) which establish hydrologic conditions that could lead to water flow into the upper portion of the shaft (see

Section 3.2.2). This water then migrates to the base of the shaft where buildup of the water occurs if water entry into the shaft is greater than water drainage. This portion of the overall model is described in Section 3.2.3. If the water height in the shaft is greater than the floor of the repository station, water entry into the underground facility through the connecting repository drift is possible. This scenario and the hydrologic model used are described below respectively in Sections 3.2.1, 3.2.2, and 3.2.3.

3.2.1 Scenario Description

In arriving at a reasonable, upper-bound estimate of water flow into the ES-1, the scenario developed here assumes the occurrence of two events. The first event is surface, earth movement downgradient from the exploratory shaft which blocks the natural drainage course. Following this event, a probable maximum flood (PMF) occurs, the waters of which are fully retained in that portion of the drainage basin upgradient of the blockage. These waters are then assumed to flow into the underlying bedrock, horizontally in the alluvium, and into the shaft and MPZ. No evapotranspiration is assumed to occur.

While it is reasonable to assume that a PMF can occur at the exploratory shaft location, it is highly unlikely that earth movement sufficient to retain all the waters from a PMF would occur because:

1. A landslide large enough to completely block the valley down-gradient is not credible given the thin cover of alluvium and weathered rock on the adjacent slopes. To impound a volume of water approximately half of the volume of 159,000 m³ computed for a PMF (Bullard, 1986, Table 10) would require a dam across the entire drainage course having a height of about 12 m. Further, at Yucca Mountain there is at present no evidence of surface impoundments formed by landslides (DOE, 1986, p. 6-232) and of the size needed to contain this flood volume. As indicated in Fernandez et al. (1987, p. 4-2 to 4-4), the occurrence of small obstructions blocking portions of the wash and slowing down the flow, is a more probable and realistic scenario.

2. Four areas where slide blocks occur have been identified in the Yucca Mountain area. These slide blocks can be described as rock-slumps that are gravitationally driven. Three rock slumps which are very small, i.e., 0.01 to 0.03 km² in area, are located on the steep west-facing scarp of Yucca Mountain. A larger rock slump, about 0.13 km² in area, is located in midslope on the ridge routh of Yucca Wash (DOE, 1988, p. 1-32, 33). The common characteristic between these rock slumps is that they occur on steep slopes, estimated to be about 25°. The slope near the exploratory shafts is about 15° to 20°. Because (a) the slope in the vicinity of the exploratory shafts is less than that occurring in the areas where slumps do occur, and (b) massive lateral movement sufficient to block Coyote Wash is not characteristic of these rock slumps, blockage of the drainage basin associated with the exploratory shafts by massive rock slumps is not considered to be credible.

Nevertheless while this scenario is considered to be highly improbable at the new locations for the exploratory shafts which are out of the flood area, we have decided to model the scenario to obtain a larger than expected inflow potentially into the underground facility.

3.2.2 Model Used for Water Flow Into the Shaft

In Figure 2-2 the upper portion of the ES-1* is located in the alluvial-filled portion of the drainage basin; whereas, the upper portion of the ES-2 is located in bedrock upgradient from the location of ES-1. Because the upper portion of the ES-1 is located in alluvium and at the confluence of two washes, Coyote Wash and the wash to the south, a greater potential exists for surface-water entry into ES-1 than into ES-2. The mechanism modelled in this section is water flow from saturated alluvium to the shaft. Because the upper portion of ES-2 is not surrounded by alluvium, this mechanism does not exist. It is, therefore, assumed that water from a major flooding event that saturates the alluvium can enter the

*The ES-1 and ES-2 locations used in the analysis are the locations presented in the final EA (DOE, 1986, p. 4-11).

ES-1 only. Using this logic, a hydrologic flow model was developed (Fernandez et al., 1987) to estimate the amount of water that could enter the upper portion of the ES. This model, discussed below, assumes that the alluvium surrounding the ES becomes saturated and water can enter the shaft. This scenario is evaluated to arrive at a realistic, upper bound of water flow into ES-1. In reality, alluvium in an initially, unsaturated state can provide an effective barrier to downward water infiltration, thereby limiting flow into the shaft.

At the conclusion of this study, new locations of ES-1 and ES-2 were proposed by U.S. DOE/NVO (Figure 2-2) further north and east of the original locations. Because the proposed locations for the exploratory shafts are out of the alluvial-filled portion of the drainage basin, which has a potentially high capacity to retain water, and is farther removed from the drainage channel, the potential for surface-water entry has been reduced substantially. Therefore, we feel that the estimates of water flow entering the shaft provided in this chapter do represent conservative, upper-bound values to water flow into the exploratory shafts.

3.2.2.1 Model Description

The model used to compute the flow into the upper portion of the shaft is illustrated by Figure 3-3. Alluvium overlies the welded, highly fractured Tiva Canyon Member. For the purpose of the present analysis, the upper portion of the shaft through the alluvium is assumed to be filled with a coarse fill to minimize restriction of flow into the shaft. The lower portion of the shaft is modeled as containing a fill having a saturated hydraulic conductivity of 10^{-2} cm/s, extending to the outside diameter of the shaft. (In reality, a shaft liner, having a lower hydraulic conductivity than the shaft fill, remains in place. By ignoring the presence of the shaft liner in the analysis, a higher flow through the shaft is computed.) The MPZ is modeled as extending one radius from the shaft wall. Two cases for the MPZ are considered in which the MPZ is either 20 or 60 times the undisturbed, rock mass hydraulic conductivity.

*The Probable Maximum Flood (PMF) is the greatest flood that may reasonably be expected taking into account all pertinent conditions of location, meteorology, hydrology and terrain (Chow, V. T., 1964, p. 25 to 72).

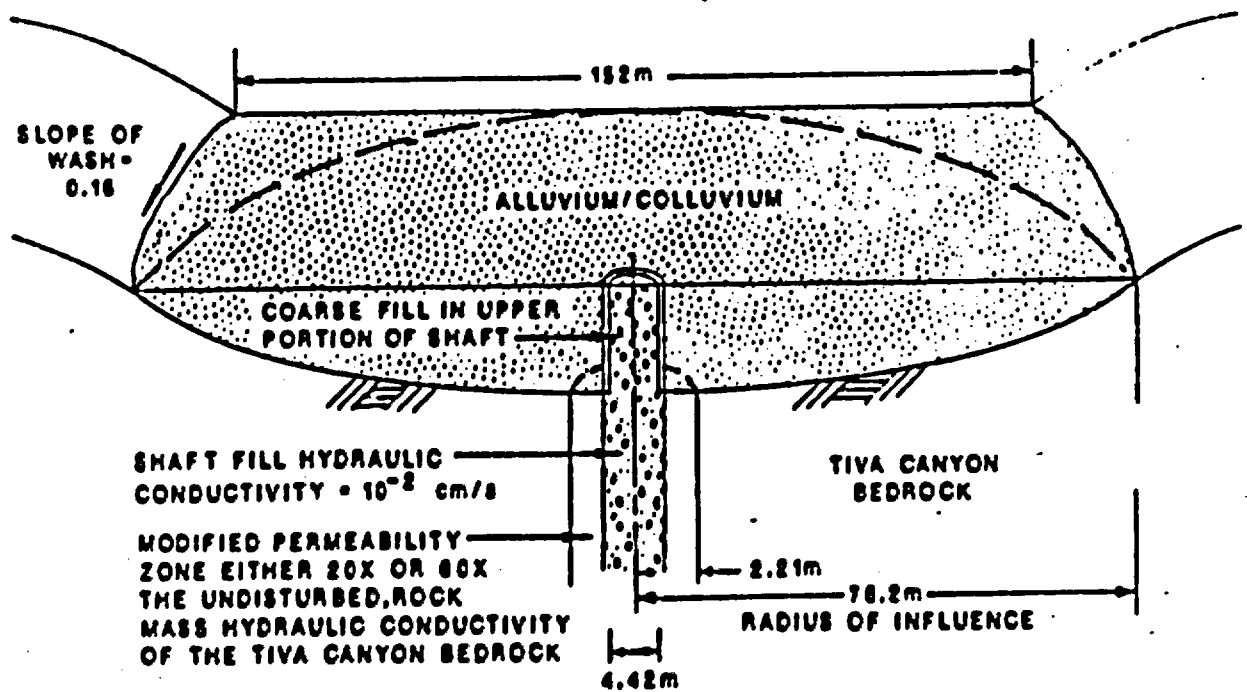


Figure 3-3. Geometry of Model Used to Estimate Flow Into a Shaft From Saturated Alluvium

This value of 60 is the average of two values, 40 and 80 (see Table 3-1), associated with MPZ models at 100- and 310-m depths. This is believed to be a conservative assumption because it implies the permeability of the MPZ is 60 times the undisturbed, rock-mass permeability over the entire length of the shaft, including the MPZ down to a depth of 100 m. For more detail of the MPZ model used see Case and Kelsall (1987).

Flow progresses in three phases: an initial desaturation phase, a steady-state phase, and a final desaturation phase (Figure 3-4). Before initiation of Phase I, it is assumed that the alluvium becomes fully saturated, and the water in the shaft above the alluvium-Tiva Canyon contact enters the upper portion of the shaft. Desaturation of the alluvium occurs first at curve "1" and progressively to curve "n" (Figure 3-4a). As the radius of influence is changed in response to desaturation, the radius of influence associated with curve "n" represents quasi-steady-state conditions that are held constant until the supply of water replenishing the alluvium no longer exists (Figure 3-4b). As Phase III begins, the only water remaining is that contained under curve "n." Desaturation then proceeds from curve "n" to curve "m."

During each phase of drainage, four types of flow are considered: unconfined radial flow under the Dupuit flow assumption, alluvial flow, Tiva Canyon flow, and flow through the MPZ and the shaft fill. Each of the flows are discussed below.

Radial flow is computed using the following equation:

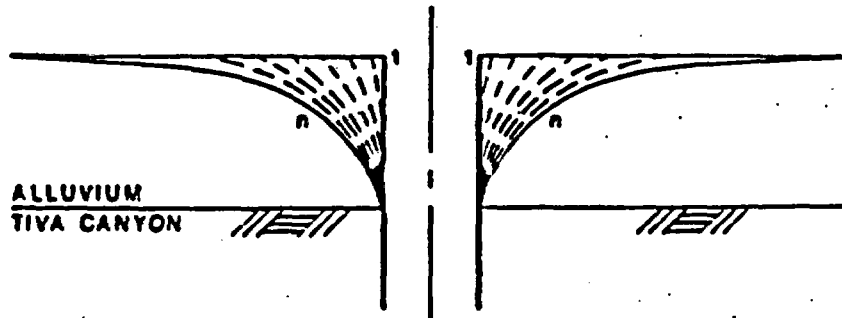
$$Q_s = \frac{\pi K (H^2 - H_0^2)}{\ln\left(\frac{R}{r_0}\right)} \quad (3-1)$$

where R = radius of influence,

Q_s = flow rate into the shaft,

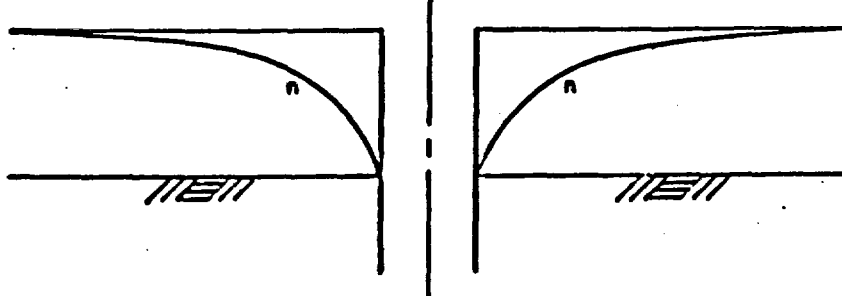
K = hydraulic conductivity,

A. PHASE I: INITIAL DESATURATION



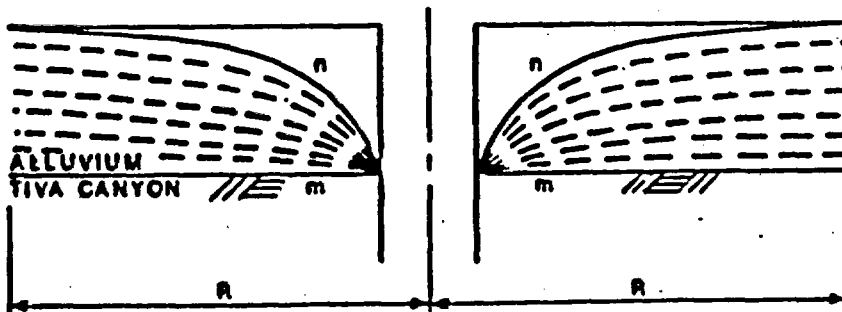
Radius of Influence moves to outer radius of model under full saturation height.

B. PHASE II: STEADY-STATE DRAINAGE



Radius of Influence is maintained at outer radius, and under full saturation height during the steady state period.

C. PHASE III: DESATURATION OF ALLUVIUM



R - RADIUS OF INFLUENCE
Saturation height declines with time.

Figure 3-4. Phases of Flow for Flow Into a Shaft From Saturated Alluvium

H - piezometric level at radius R ,
 H_0 - piezometric level at radius r_0 , and
 r_0 - shaft radius.

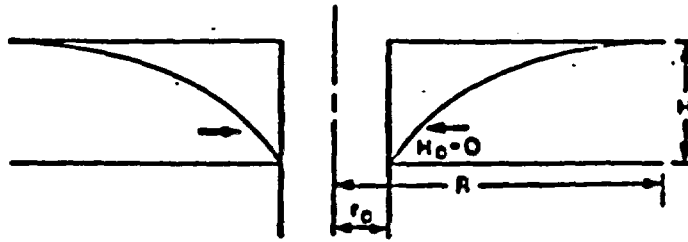
This equation, taken from Terzaghi and Peck (1967, p. 167), assumes steady-state flow in the horizontal direction under unconfined conditions. Radial flow is illustrated in Figure 3-5a.

Alluvial flow is assumed to occur through the shaded area as shown in Figure 3-5b, under a hydraulic gradient that coincides with the average alluvial grade. This approach was adopted to simplify the calculations and was compared to an alternate calculation that involved uniform flow above the shaft and a "zone of capture" near the shaft (Fernandez et al., 1987, Appendix A-4). In the "zone of capture" calculation (Figure 3-6), all water flowing down the wash that lies within the capture zone is predicted to eventually flow down the shaft. In this zone, the radial flow velocity induced by the drawdown of the water surface near the shaft is sufficiently strong to overcome the tendency for flow to occur laterally down the alluvium in the wash. The more detailed calculation indicated that the simplified approach of computing the alluvial flow as the product of the shaded area times the alluvial grade was reasonable.

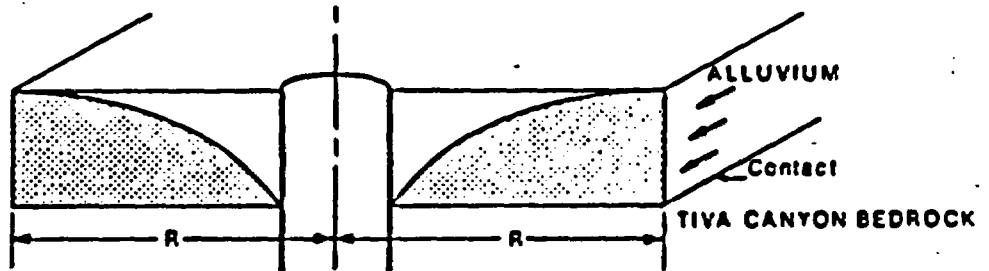
Tiva Canyon flow is the assumed vertical infiltration of water through the Tiva Canyon unit. It is assumed to occur through the shaded area under a unit gradient as might occur for fractured rock that is nearly saturated. It is recognized that the bedrock is unsaturated and that infiltration rates are likely to be higher; nevertheless, the flow calculation is conservative in underestimating this component of flow (greater proportion of flow is directed to the shaft).

MPZ and shaft flow is the vertical infiltration through the MPZ and the shaft fill and the shaft liner. In this analysis, it is assumed that the hydraulic conductivity of the shaft liner is equivalent to the hydraulic conductivity of the shaft fill. It is also assumed that the shaft fill is near saturation, and is exposed to atmospheric conditions. Accordingly, flow occurs under unit gradient. It is noted that the degree to which infiltration would occur at unit gradient depends on the level of

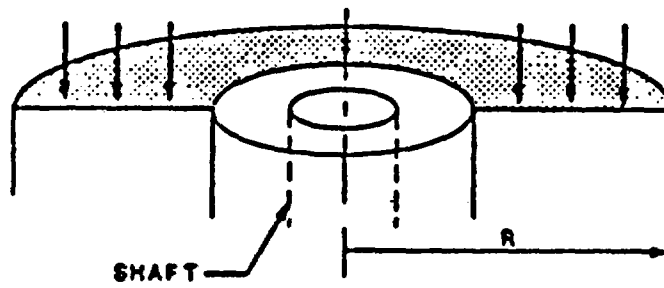
A. DUPUIT (RADIAL) FLOW



B. ALLUVIAL FLOW



C. TIVA CANYON FLOW



D. MPZ AND SHAFT FLOW

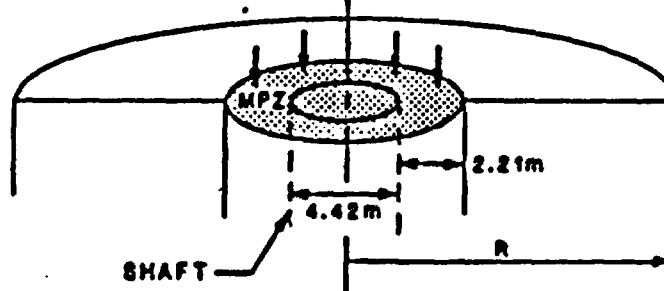
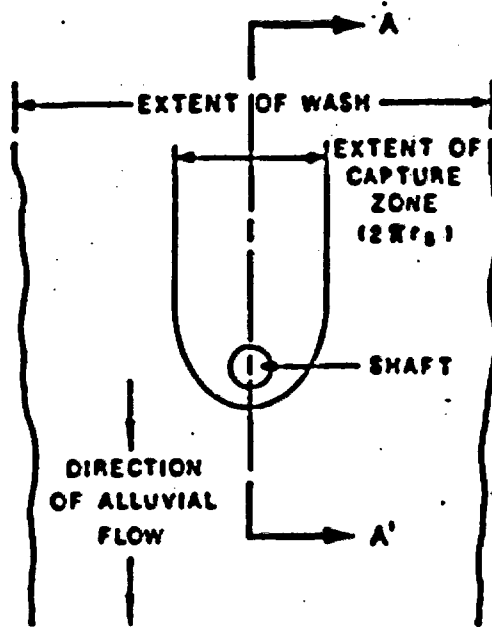
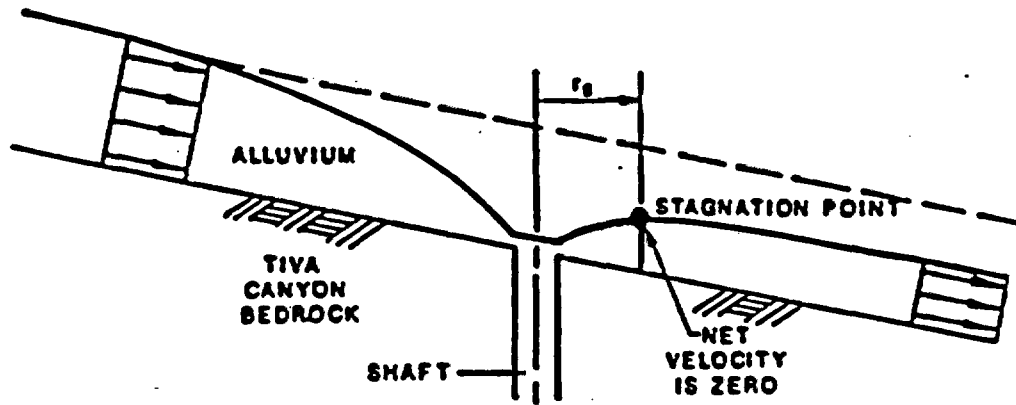


Figure 3-5. Types of Flow Considered in Estimating Flow Into a Shaft (Flows Occur Concurrently During Phases I, II, and III)



(a) PLAN VIEW
(Not to Scale)



(b) ELEVATION VIEW A-A'

Figure 3-6. Capture Zone Near a Shaft

saturation and that initially the hydraulic gradient could exceed unity. These high infiltration rates would be associated with the saturation of voids due to capillarity and not transmission of water to the base of the shaft. As the infiltration front reaches the base of the shaft, at which point water could potentially enter the repository, the hydraulic gradient would be approximately one.*

These flows are superimposed such that flow can occur as Tiva Canyon flow, alluvial flow, or shaft flow. Therefore, as a volume of water is computed for each portion of each phase, flow occurs proportionately through the Tiva Canyon Member, alluvium, and the shaft, as determined by the flow rate computed for each. Flow through the shaft is either the amount computed using the radial formula or the amount computed by the MPZ and shaft fill model, whichever amount is lower. The entire process of desaturation continues until the water supply is depleted. The potential water supply is assumed to be the waters associated with specific flooding events. The input values and assumptions used for this model are discussed below in Section 3.2.2.2.

To arrive at the maximum inflow to the shaft, it is assumed that retainment of all the water associated with a flooding event occurs above each shaft location. This implies that the alluvium has a sufficient storage volume to retain all the water from the flood event, an overly conservative assumption that involves no losses by evapotranspiration or sheet flow downgradient from the shaft locations. In reality, a high percentage of the precipitation is expected to exit the drainage basin, with only a small part percolating into the alluvium or exposed bedrock. Further, it is assumed that water flow is directed vertically downward

*This can be shown by the Green and Ampt solution for vertical infiltration (Hillel, 1971, p. 142). At the base of the shaft, the hydraulic gradient

is given by $1 + \frac{H_0 - H_f}{L_f}$ where H_0 equals the pressure head at the surface.

H_f equals suction head at wetting front, and L_f equals the length over which the wetting front has moved. If we assume the pressure head at the surface is 9.1 m (height of saturated alluvium above bedrock), the suction head for the backfill is -1.0 m (a typical value for coarse material) and the length over which the wetting front has moved (311 m), then the calculated hydraulic gradient is nearly one.

inside the shaft liner or in the shaft fill as the water percolates to the base of the shaft. It is further assumed that flow occurs through fractures within the MPZ and that water is not absorbed within the tuff matrix.

To verify the numerical results obtained from the model presented in this section, an alternate calculation was performed to check major assumptions, analyses methods, and input (materials properties and geometry). This alternate calculation incorporates the concept of the "capture zone", illustrated in Figure 3-6. A comparison of the results from the model presented above and the "capture zone" model are in good agreement as discussed in Fernandez et al. (1987).

3.2.2.2 Input Values Used

In applying this model, it was necessary to develop assumptions and evaluate specific conditions for water flow. The following assumptions were used in applying the model.

- o PMF occurs at the ES location. The volume of water used for the PMF is 159,000 m³ (Bullard, 1985).
- o No sheet flow or evapotranspiration occurs and all of the flood waters are retained in the alluvium upgradient from the shaft location.
- o ES-1 has an inside diameter of 3.7 m.
- o Both ES-1 and ES-2 in the Tiva Canyon have an outside diameter of 4.3 m. In this analysis an overbreak of 0.08 m on each side of the shaft is assumed giving an excavated diameter of 4.4 m.
- o MPZ in Tiva Canyon Member extends from shaft wall to a radius of 4.4 m from the centerline of the shaft.
- o Hydraulic conductivity of the alluvium varies from 10⁻⁵ to 100 cm/s (Freeze and Cherry, 1979, pp. 29, 147).
- o Hydraulic conductivity of the Tiva Canyon Member varies from 10⁻⁵ to 10⁻² cm/s (Fernandez et al., 1987).
- o Alluvial grade of the water course is 0.16 (based on average water course grade in Coyote Wash).
- o Radius of influence is 76.2 m (based on the approximate width of alluvium at ES-1 location).

- o Depth of alluvium is 9.1 m (based on depth of alluvium at borehole USW G-4).
- o Porosity of alluvium is 0.30 (Fernandez et al., 1987, Appendix D).

3.2.2.3 Inflow Volumes

Applying the model described above, the maximum, yearly inflow into the ES-1 is computed following a PMF event. Because no evapotranspiration and sheet flow out of the drainage basin are assumed, flow into the shaft will continue until the initial water volume associated with the PMF is depleted. For the majority of cases evaluated, the initial flood volume is depleted within the first year following the flooding event. Figure 3-7 illustrates the flow into the shaft for a broad range of conditions predicted by the model described in Section 3.2.2.1 and using the input volumes given in Section 3.2.2.2. The flow volumes can range from approximately 30 to 20,640 m³/year. By comparison, for anticipated conditions as defined in Fernandez et al. (1987), the computed, estimated volume of water entering ES-1 was approximately 44 m³/year. In some instances, differences are observed between the two models assumed for the MPZ. Differences occur for two reasons. First, flow occurs through the MPZ and the shaft fill. If the majority of the total flow occurs through the shaft fill, the difference between the flows associated with each MPZ model is negligible or small. Secondly, flow into the MPZ and shaft fill can be no greater than the rate at which the water is released from the alluvium using the Dupuit assumption of radial flow to the shaft. Thus, when the saturated, hydraulic conductivity of the alluvium is low, the volume of water entering the MPZ and shaft fill is less than the full capacity of the MPZ and shaft fill. Therefore, no discrimination between the models is observed. A more complete explanation of the shape of the curves, presented in Figure 3-7, is given in Appendix B.

3.2.2.4 Duration and Rate of Flow Into Shaft

In addition to knowing the total flow down the shaft, it is also important to understand the rate and duration of flow into the shaft. Figures 3-8 to 3-11 illustrate the rate and duration of flow into the upper

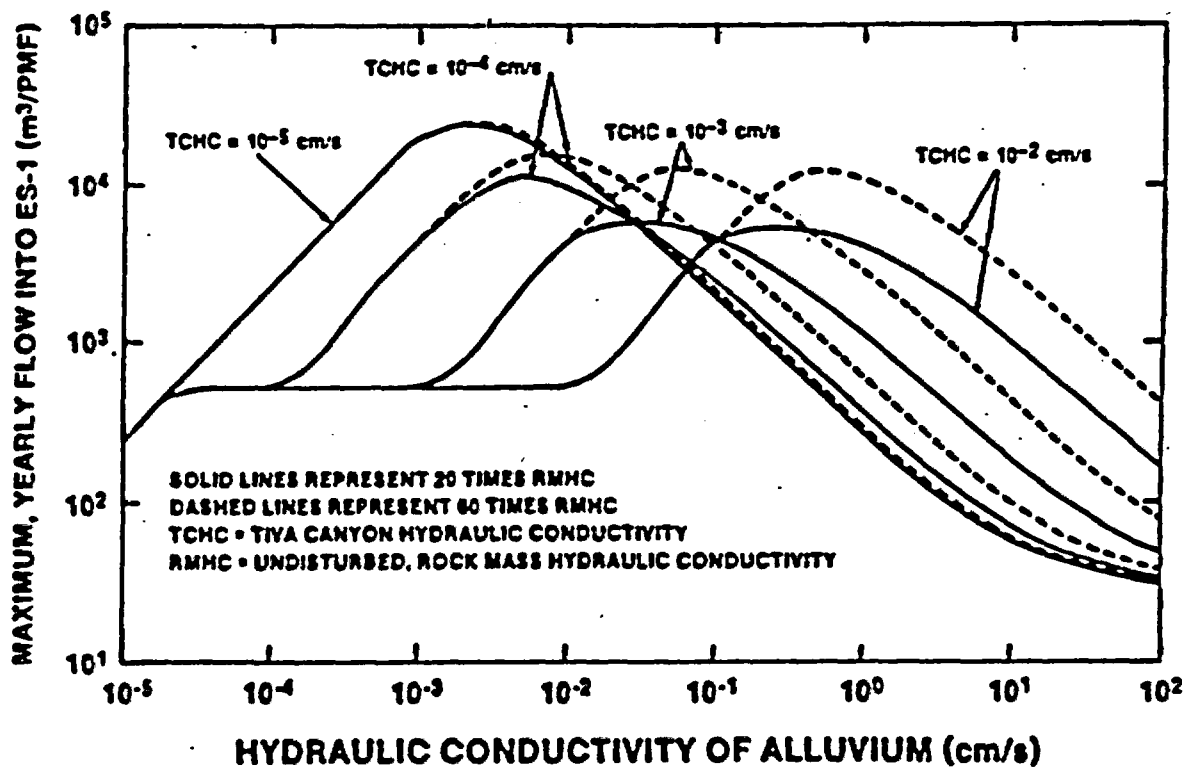


Figure 3-7. Estimated Volumes of Water Entering ES-1 (PMF, Shaft Fill Conductivity = 10⁻² cm/s, Excavated Shaft Diameter = 4.42 m)

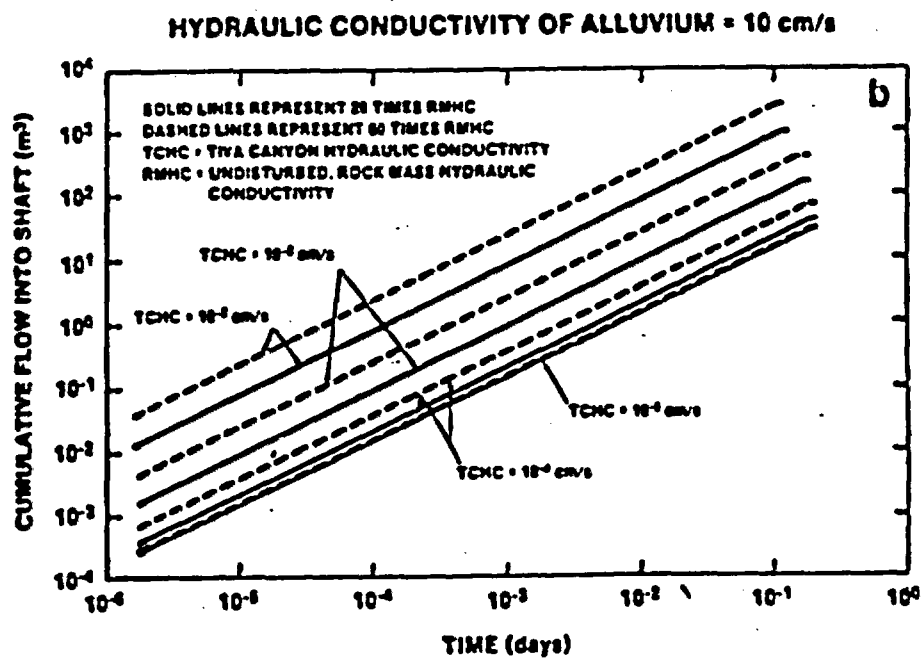
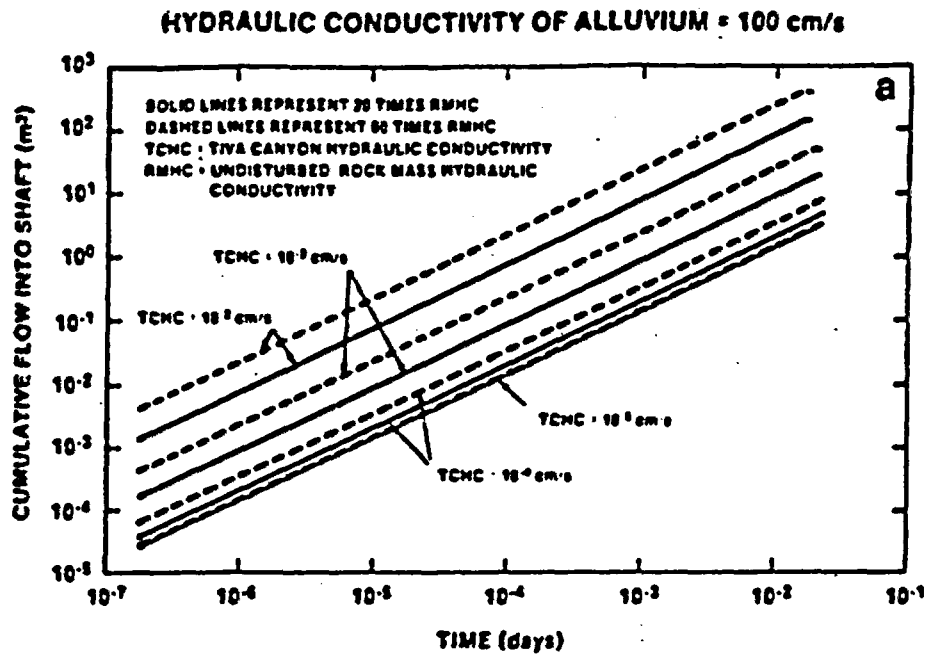


Figure 3-8. Estimated Duration of Flows Into ES-1 (PMF, Hydraulic Conductivity of Alluvium - 100 and 10 cm/s)

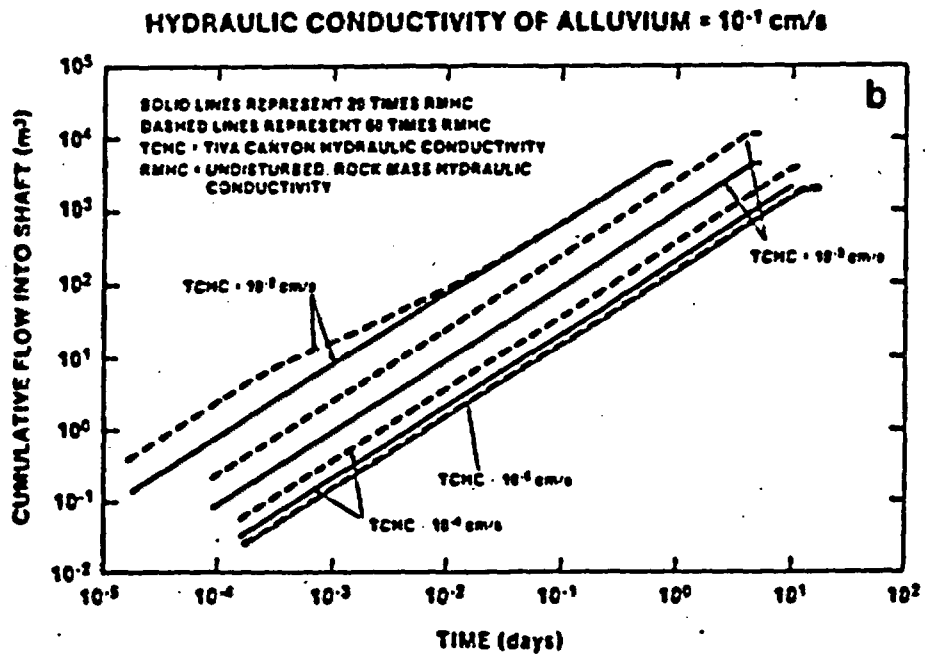
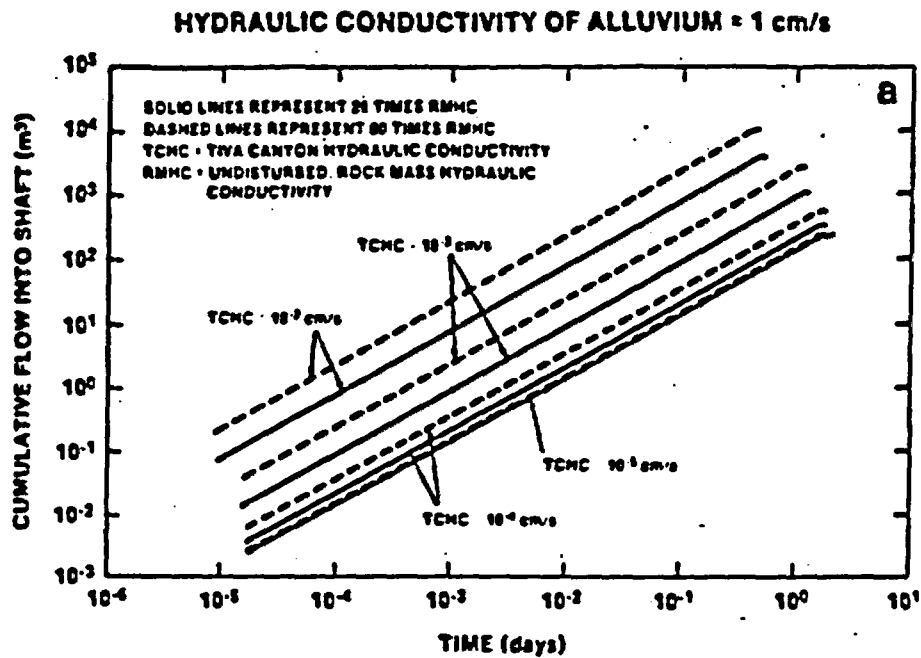


Figure 3-9. Estimated Duration of Flows Into ES-1 (PMF, Hydraulic Conductivity of Alluvium - 1 and 0.1 cm/s)

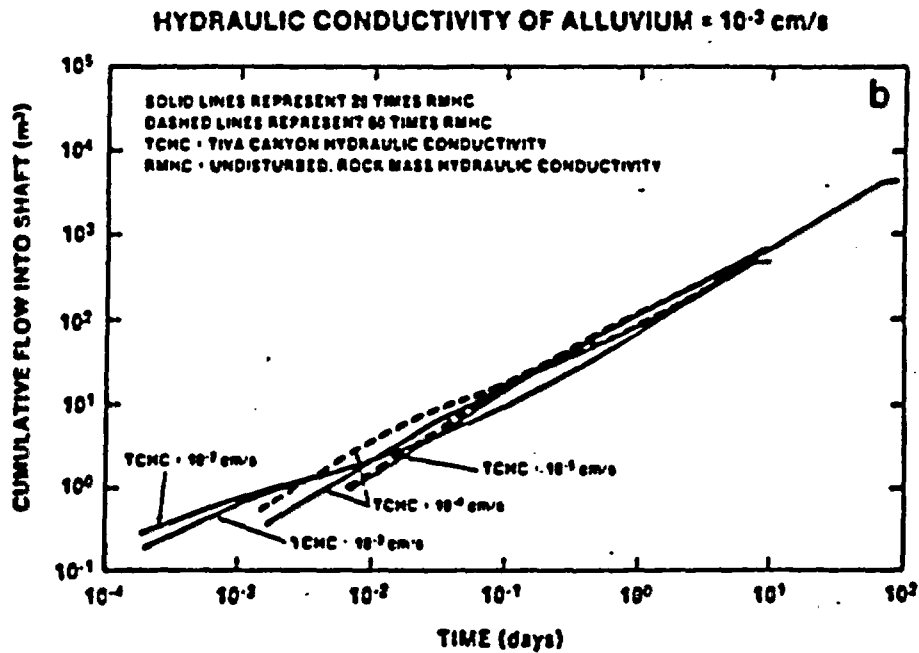
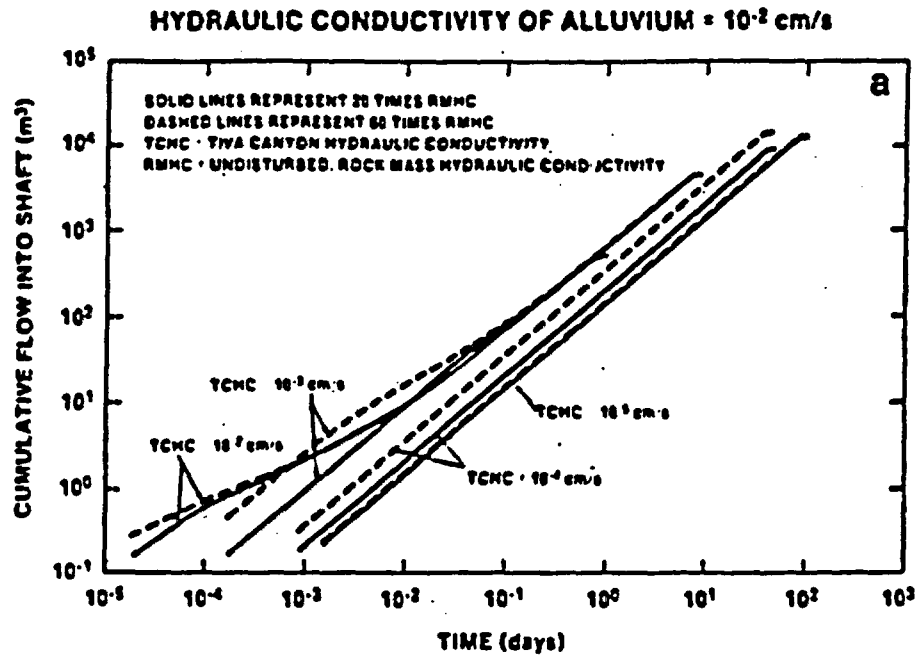


Figure 3-10. Estimated Duration of Flows Into ES-1. (PMF, Hydraulic Conductivity of Alluvium - 10^{-2} cm/s and 10^{-3} cm/s)

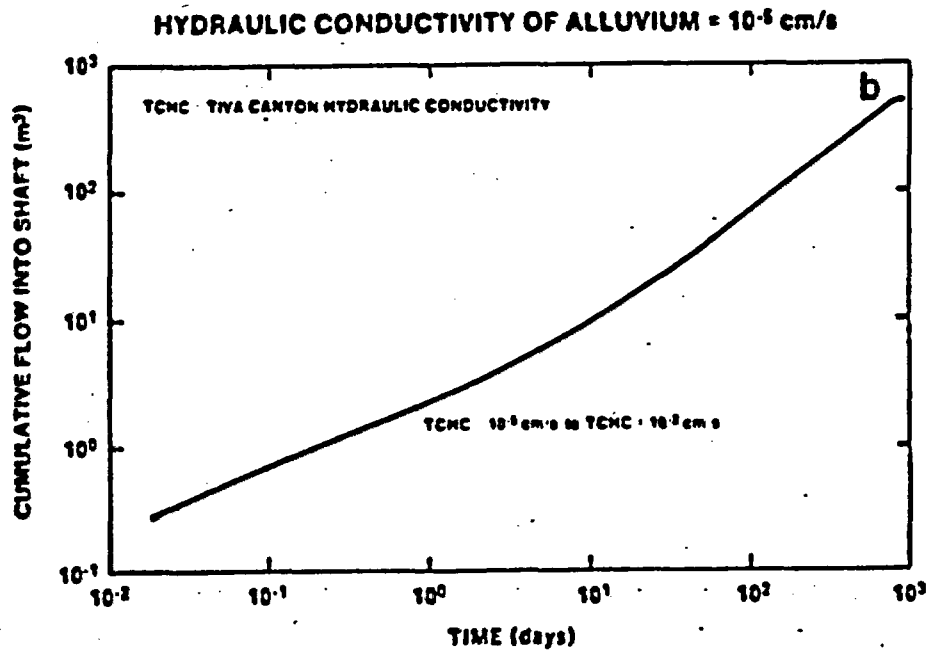
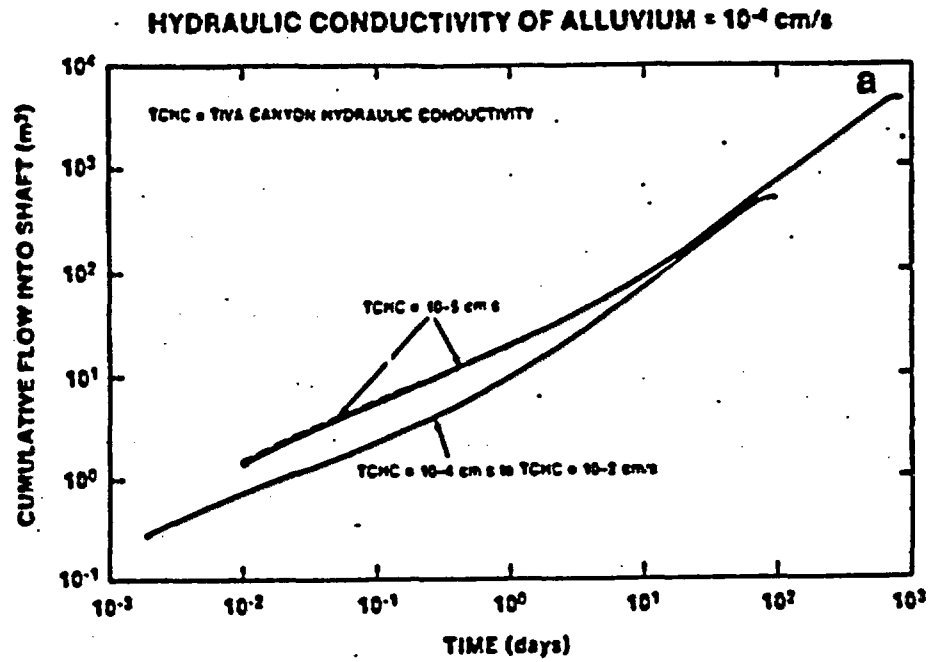


Figure 3-11. Estimated Duration of Flows Into ES-1 (PHF, Hydraulic Conductivity of Alluvium = 10^{-4} and 10^{-5} cm/s)

portion of the shaft. The data presented by these figures are used as the input functions of water flow into shaft to evaluate the potential for water buildup in the sump of the ES.

Each graph in Figures 3-8 through 3-11 illustrates water flows into the ES assuming a constant value of hydraulic conductivity of the alluvium. The range of hydraulic conductivity values for alluvium is 10^{-5} to 100 cm/s (Freeze and Cherry, 1979, p. 29). Each graph further illustrates the effect of altering the hydraulic conductivity of the Tiva Canyon Member, located immediately below the alluvium. Because the MPZ models are related to the undisturbed, rock-mass hydraulic conductivity of the Tiva Canyon, a distinction between the different MPZ models is also displayed.

As indicated earlier, duration of flow and rate of flow (Figures 3-8 to 3-11) are important considerations as to how water can potentially build up at the base of the shaft. Both considerations are discussed below. Duration of flow is dependent on the flow that occurs as described in Section 3.2.1.1, i.e., Tiva Canyon flow, alluvial flow, and radial or shaft flow. These flows are dependent on the selected hydraulic properties of the alluvium and the Tiva Canyon Member. If the selected hydraulic properties are low, the time to drain the waters retained in the alluvium can be long. Conversely, if the hydraulic conductivities are high, the duration of flow into the shaft is limited. This effect is clearly displayed in Figures 3-8 to 3-11. When the hydraulic conductivity of the alluvium is high, 100 cm/s, the duration of flow into the shaft is computed as approximately 10^{-2} days or less than 15 minutes (Figure 3-8a). When the alluvial hydraulic conductivity is low, 10^{-5} cm/s, drainage of flow into the shaft is computed to occur up to 1000 days (Figure 3-11b) following the PMF. The effects of changing duration is also noticed when the hydraulic conductivity of the Tiva Canyon Member changes. As the hydraulic conductivity of the Tiva Canyon Member decreases from 10^{-2} to 10^{-5} cm/s, the duration of flow into the shaft increases. This effect is noticed on the graphs in Figures 3-8 to 3-11a. However, the effect is more pronounced in total durations when the alluvial hydraulic conductivity decreases.

Another important consideration, aside from the duration of flow, is the rate of flow into the shaft. Flow into the upper portion of the shaft is controlled by the radial flow from the alluvium to the shaft or the flow

through the MPZ and the shaft fill. If the radial flow is greater than the potential for flow through the MPZ and shaft fill, the flow entering the MPZ and shaft fill will be controlled by hydrologic properties of the MPZ and shaft fill. This condition suggests that the more water flow that is restricted from entering the shaft and the MPZ due to the properties of the MPZ and the shaft fill, the greater will be the flow down the wash in the alluvium further reducing flow into the shaft. If the radial flow is less than the potential for flow through the MPZ and shaft fill, then the flow, entering the MPZ and shaft fill is limited by the radial flow toward the upper portion of the shaft (Figures 3-8 to 3-11). For example, when the alluvial hydraulic conductivity is 100 to 0.1 cm/s, radial flow to the shaft is greater than the capacity of flow through both the MPZ and shaft fill. Therefore, a distinction between the cumulative flows for both MPZ models is noticed. As the alluvial hydraulic conductivity decreases further, the radial flow into the shaft decreases until the radial flow into the upper portion of the shaft is less than full-flow capacity of the MPZ and shaft fill. This effect is first noticed (Figure 3-9b) when the flow model is 60 times the Tiva Canyon hydraulic conductivity of 10^{-2} cm/s. The flow rate into the upper portion of the shaft is further reduced as the alluvial hydraulic conductivity is reduced. When the alluvial hydraulic conductivity is extremely low, i.e., 10^{-5} cm/s, the flow through all MPZ and shaft models is controlled by the radial flow toward the shaft. In this case (Figure 3-11b), no distinction between any of the MPZ models is possible. It is also true that when flow through these MPZ models is less than their full flow capacity, the model is only partially saturated. As mentioned earlier, the data presented in Figures 3-8 to 3-11 are used as input to estimate the potential for water buildup at the base of the ES.

3.2.3 Model Used for Water Flow out of the Shaft

If water enters the shaft at a rate faster than it can be effectively drained, buildup of water in the shaft is possible. Further, if water buildup is greater than the sump capacity, then lateral migration through the repository station seal, into the underground facility, and ultimately toward the waste disposal areas is possible. The model and input used to

determine the potential for water buildup in the sump of the ES-1 are discussed below. As indicated in Section 3.2.2, because the upper portion of the old ES-2 location is not surrounded by alluvium and is out of the path of the PMF, the mechanism of water flow from the alluvium into the shaft as described in Section 3.2.2 does not exist.

3.2.3.1 Model Description

The purpose of this section is to describe the model used in assessing the potential for water buildup at the base of the ES. It is assumed that the concrete liner at the base of the shaft has been removed. This corresponds to an unlined portion of the shaft approximately 145.5 m from the base of the shaft to the crown of the repository station drift. The modeled sump depth is about 140 m, i.e., the distance from the invert* of the repository station drift to the base of the shaft. The excavated diameter of the sump is 4.42 m. The entire shaft is assumed to be backfilled with a shaft fill having a porosity of 0.3. Figure 3-12 illustrates the physical model described above.

To compute the maximum buildup of water at the base of the shaft the following conservative assumptions are made: (1) the amount of water entering the upper portion of the shaft (see Section 3.2.2.4) is transported immediately to the base of the shaft and (2) no leakage outside of the MPZ occurs above the buildup of water in the base of the shaft. In reality, leakage of water into the rock mass outside of the MPZ can occur as water migrates down the MPZ. The reason for restricting the downward flow of water to the MPZ and shaft fill is primarily to maximize the buildup of water at the base of the shaft. If water inflow to the shaft is dispersed into the undisturbed rock mass, the significance of the presence of the MPZ and shaft fill diminishes.

Once water reaches the base of the shaft, buildup of water occurs increasing the saturation levels in the bulk rock. As water buildup

*The invert is the lowest point in elevation of the drift. This sump depth of 140 m corresponds to that presented in MacDougall et al. (1987, p. 4-69).

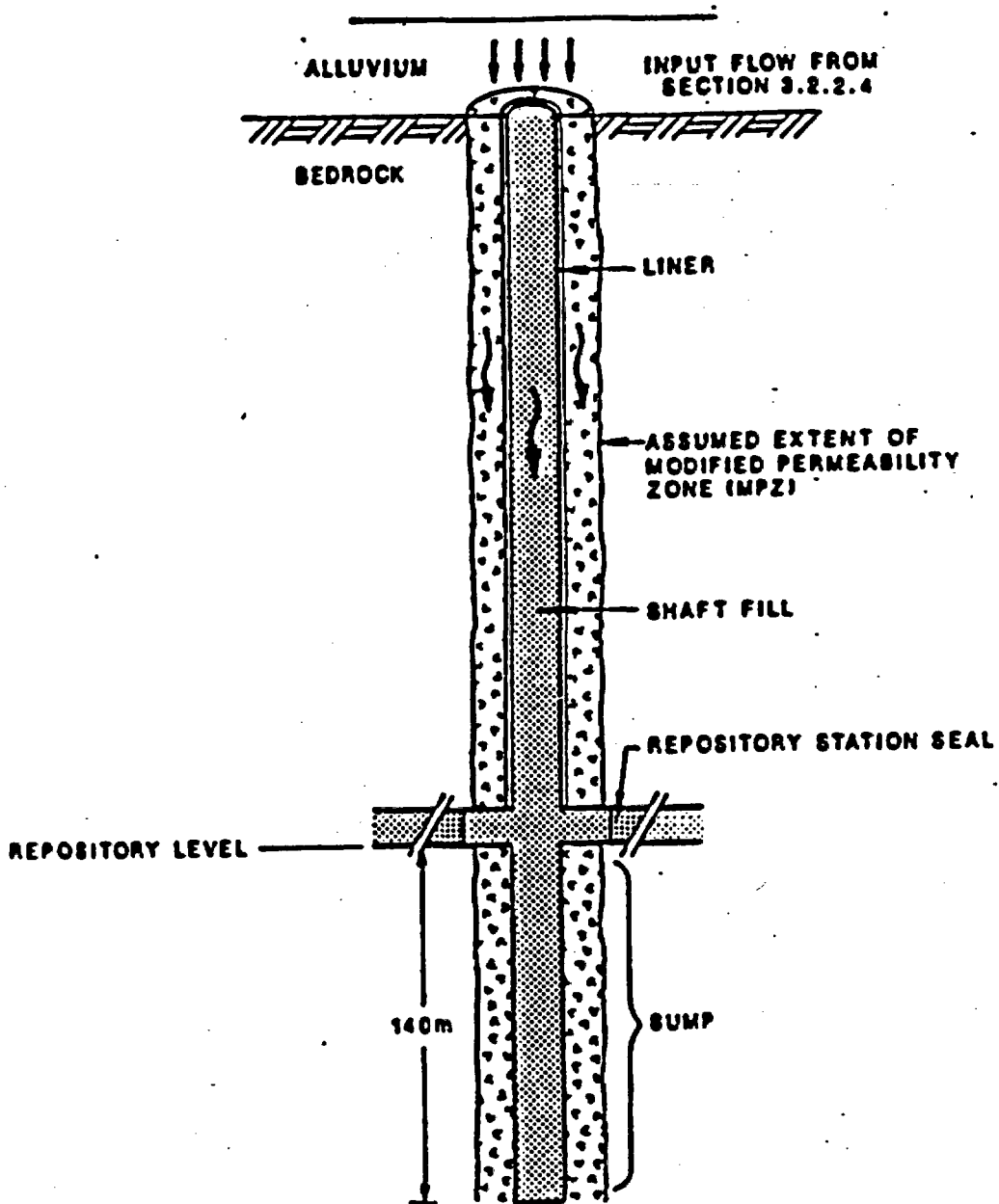


Figure 3-12. Schematic of Model Used to Compute Water Balance in the Exploratory Shaft

occurs, water can also drain through the bulk rock at the base of the shaft, predominantly through fractures. Only when the height of water in the shaft reaches the invert of the repository station drift does water have the potential to pass through the repository station seals. (Two repository station drifts extend from the exploratory shaft.)

Flow from the base of the shaft is predicted by analytical solutions used for calculating the saturated hydraulic conductivity above the water table using borehole infiltration tests. Flow through the repository station seals is described by Darcy's law.

Several analytical solutions described in Stephens and Neuman (1982, p. 642) were considered in computing the flow through the sump of the shaft. It should be noted that Stephens and Neuman evaluated the suitability of several analytical solutions to predict the saturated hydraulic conductivity of soils. The pressure head in the soils evaluated ranged from 0 to -1.6 m of water. (Stephens and Neuman, 1982, p. 644). The pressure head in the matrix of tuff can range from 0 to -1000 m of water (Peters et al., 1984, p. 2). However, because we are computing the drainage of water from a shaft sump that is located predominantly in a highly fractured welded tuff, drainage will occur primarily through the fractures. Because these fractures are closely spaced and because the range of pressure heads for fractures (0 to -1 m) (Wang and Narasimhan, 1985, p. 24; Klavetter and Peters, 1986, p. 20), is similar to that of coarse sand, we feel that selected analytical solutions presented by Stephens and Neuman can reasonably approximate the drainage from a shaft. Furthermore, a better understanding of the hydrologic characteristics and the drainage properties of fractured tuff will be obtained by field tests associated with the Exploratory Shaft testing.

The analytical solutions considered in this report included those developed by Glover, Nasberg-Terletska, and Zanger (Stephens and Newman, 1982, pp. 640-659). To evaluate the differences between these analytical solutions, Stephens and Neuman defined two dimensionless quantities, C_u and H_D , defined as

$$C_u = \frac{Q_s}{K_s r H} \quad \text{and}$$

$$H_D = \frac{H}{r}$$

where Q_s = infiltration or drainage rate at steady state, m^3/s .

K_s = saturated, hydraulic conductivity, m/s .

r = shaft radius, m , and

H = height of water column in shaft, m .

The dimensionless value, C_u , was defined as follows:

$$C_u = \frac{2\pi H_D}{\sinh^{-1}(H_D) \cdot 1} \quad (\text{Glover})$$

$$C_u = \frac{2.364 H_D}{\log_{10}(2 H_D)} \quad (\text{Nasberg-Terletskata})$$

$$C_u = \frac{2\pi \frac{A}{H} H_D \left[2 - \frac{A}{H} \right]}{\sinh^{-1} \left[\frac{A}{H} H_D \right] - \frac{A}{H}} \quad (\text{Zanger})$$

The value of A in the Zanger equation represents the length of the shaft in hydraulic contact with the rock. Because the drainage rate is directly proportional to C_u , a relative comparison of C_u factors can illustrate a difference in the drainage rate out of the shaft. A comparison of the C_u factor, for the analytical solutions considered, is presented in Figure 3-13a. In Figure 3-13b, the flow rates from the shaft, as computed for each analytical solution, are displayed. To be conservative, the lowest drainage rate is selected in computing the drainage from the shaft sump. This suggests that the Nasberg-Terletskata formula is used for the majority of shaft, i.e., the lower 325 m of the shaft. In the upper part of the shaft, the Zanger formula provides a lower drainage rate.

When the height of water in the shaft is greater than the sump depth, drainage can also occur through the station seals. Flow through the station seals is defined by the following equation:

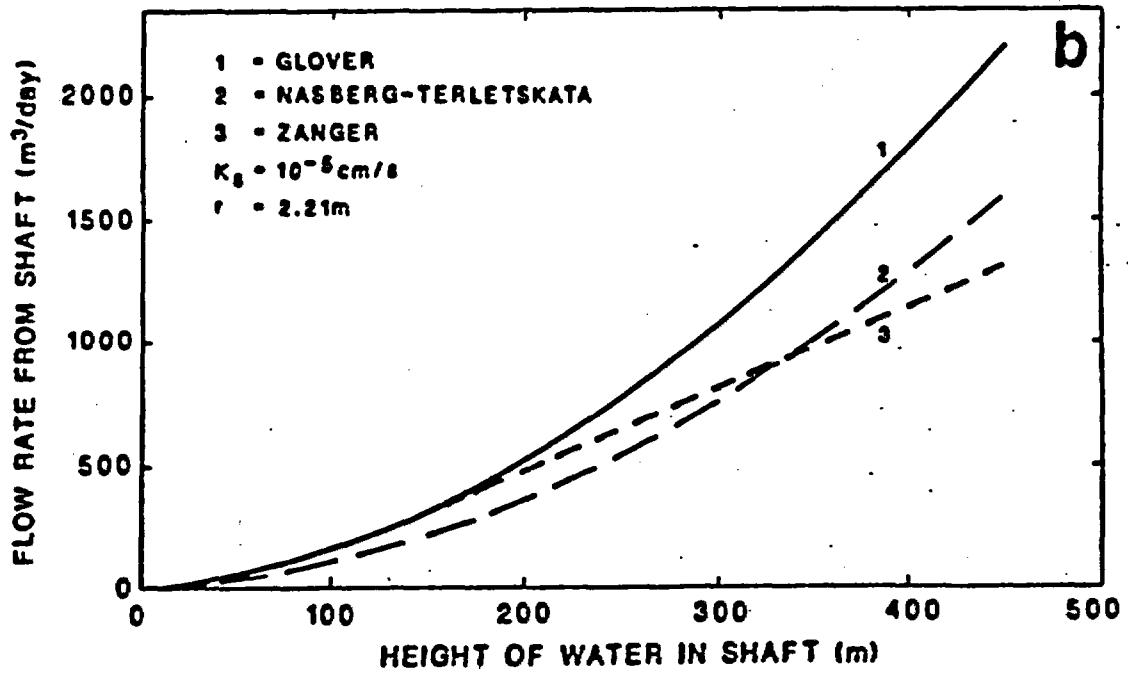
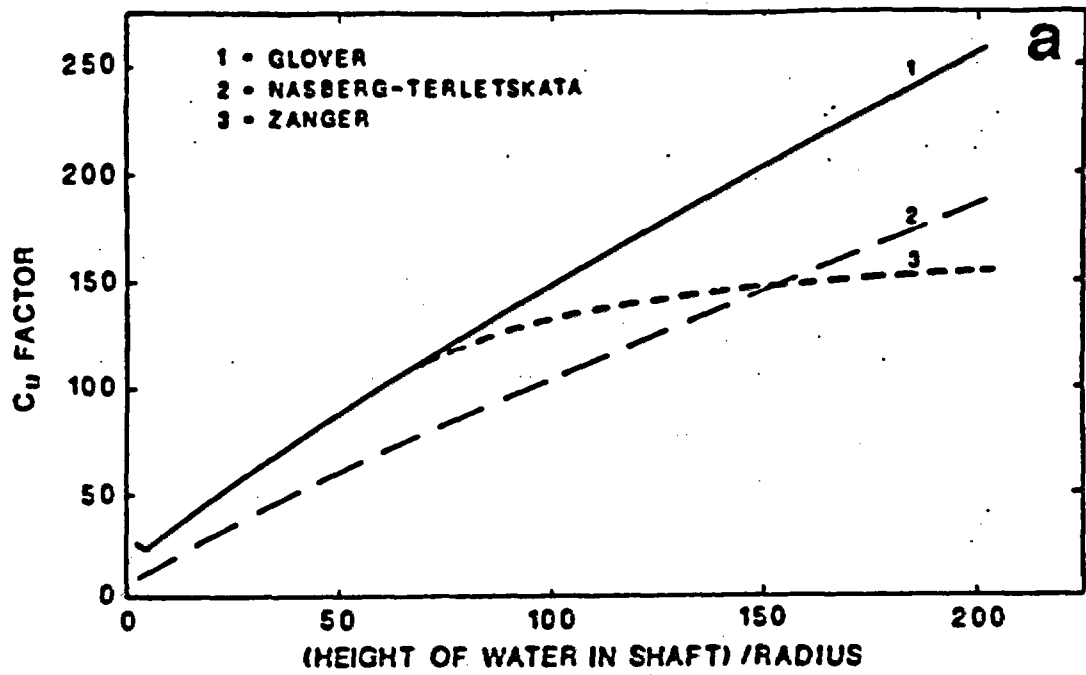


Figure 3-13. Comparison of Methods Used to Compute Drainage From Shaft

$$Q_p = K_s \frac{dh}{dl} A_p$$

where Q_p - drainage rate through the repository station plug;

$\frac{dh}{dl}$ - gradient of flow between the two faces of the repository station seal;

dh - change in hydraulic potential over the length of the seal;

dl - assumed length of the seal, i.e., twice the width of the drift cross-sectional; and,

A_p - cross-sectional area of the plug.

If it is assumed that the pressure head (equal to the height of water above) is dissipated by vertical flow, then as the height of water builds up in the shaft, the gradient across the plug increases. The following sections describe the input values of K_s used in formulas given above.

3.2.3.2 Input Values Used

The sump of the ES will be constructed predominantly in the densely welded portion of the Topopah Spring Member with approximately 15 m penetrating the nonwelded zeolitic portion of the tuffaceous beds of Calico Hills. The Topopah Spring Member is considered to be freely draining and has a high permeability because of its pervasive and abundant fractures. The nonwelded portion of the tuffaceous beds of Calico Hills, is not expected to be as intensely fractured. However, the saturated, bulk-rock hydraulic conductivity of either the densely welded portion of the Topopah Spring Member or the nonwelded Calico Hills vitric or zeolitic units is higher than their matrix hydraulic conductivity. Estimates for the bulk, saturated hydraulic conductivity are approximately 10^{-2} to 10^{-5} cm/s (Scott et al., 1983, p. 299) for the Topopah Spring Member and 2.4×10^{-4} or 10^{-3} cm/s for the tuffaceous beds of Calico Hills (Sinnock et al., 1984, pp. 11-12 and Scott et al., 1983, pp. 299). In calculating the drainage rate from the sump, the saturated, bulk-rock hydraulic conductivity is assumed to range from 10^{-5} to 10^{-2} cm/s. The selection of a specific value is dependent on and consistent with the undisturbed, rock-mass hydraulic conductivity assumed for the MPZ model. For example, if the undisturbed, rock-mass hydraulic conductivity is 10^{-4} cm/s, then the saturated,

hydraulic conductivity at the base of the shaft is also assumed to be 10^{-4} cm/s. Because the ES-1 is planned to penetrate slightly (approximately 23 m; DOE, 1988, p. 8.4-31) into the vitric and zeolitic portion of the Calico Hills nonwelded unit, the bulk, saturated hydraulic conductivity of the rock surrounding the sump has been restricted to the maximum value of 10^{-3} cm/s for the tuffaceous beds of Calico Hills when the undisturbed, rock-mass hydraulic conductivity is assumed to be 10^{-2} cm/s for the MPZ model. This restriction only slightly reduces the overall, bulk-rock, hydraulic conductivity of the sump because the majority of the sump (assumed to be 140 m in MacDougall et al., 1987, p. 4-69) potentially will be surrounded by welded and highly fractured tuff.

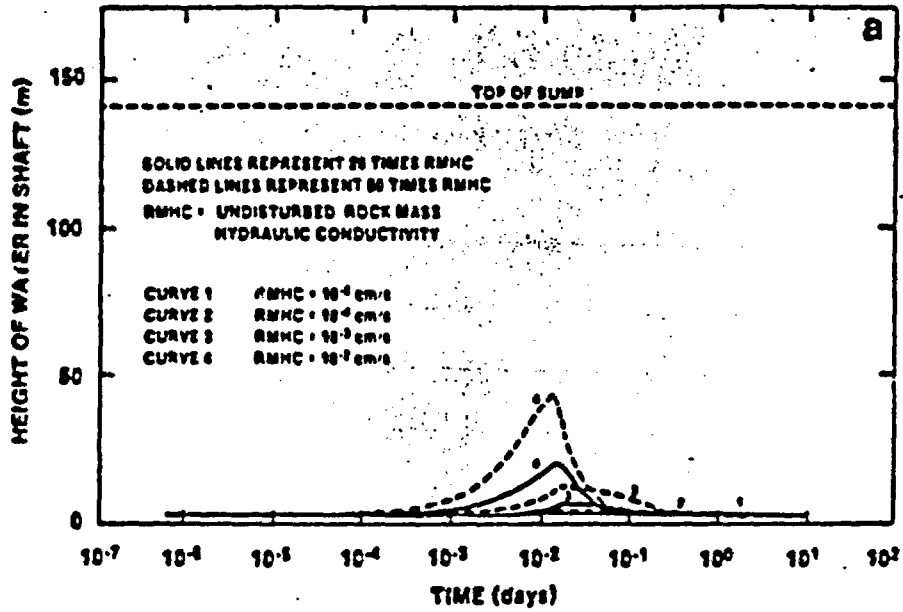
A similar logic is used in selecting the saturated, hydraulic conductivity of the repository station seal. In general, the repository station drift seal restores the surrounding rock mass to its original, undisturbed, rock-mass hydraulic conductivity. The repository station seal if needed will be located in the densely welded portion of the Topopah Spring Member.

3.2.4 Water Balance in the Exploratory Shaft

Using the inflow rates described by Figures 3-8 and 3-11 in Section 3.2.2 and the appropriate drainage rate from Section 3.2.3, the water balance in the ES is computed. In all cases, buildup of water is observed. However, in two cases, i.e., when the saturated hydraulic conductivity of the alluvium is 10^{-5} and 10^{-4} cm/s, the buildup is limited because the inflow into the shaft and MPZ is very low. Therefore, graphs of height of water in the shaft versus time are displayed for only six cases, i.e., when the hydraulic conductivity of the alluvium is between 100 to 10^{-3} cm/s.

The results displayed in Figures 3-14 to 3-16 show that the height of water buildup varies from essentially no water buildup to 126 m. In all cases when the MPZ model is 20 times or 60 times the undisturbed, rock-mass hydraulic conductivity, the maximum height of the water reached in the shaft is below the repository station invert. In all cases evaluated, no flow through the repository station seal is computed. Again, it should be stated that shaft inflows predicted here are unanticipated and highly

HYDRAULIC CONDUCTIVITY OF ALLUVIUM = 100 cm/s



HYDRAULIC CONDUCTIVITY OF ALLUVIUM = 10 cm/s

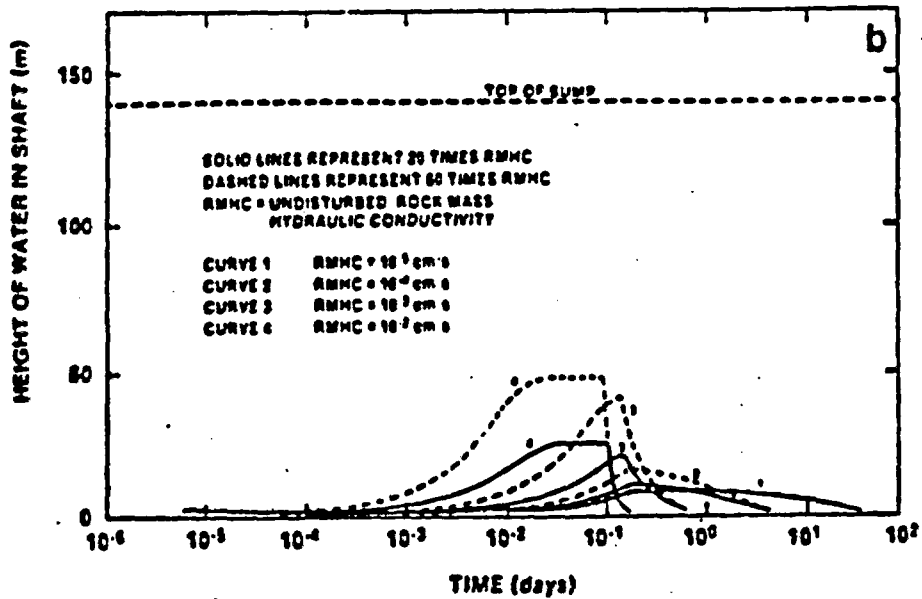
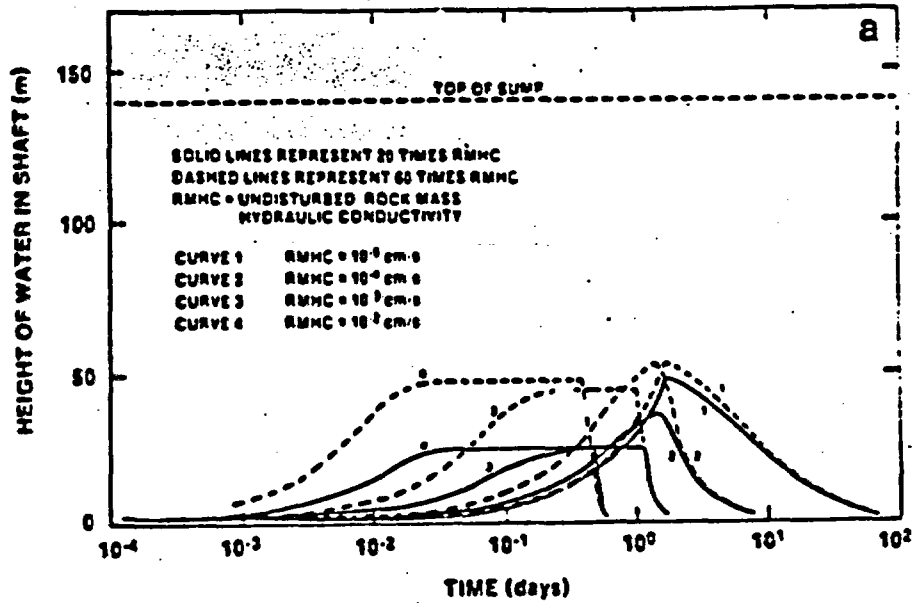


Figure 3-14. Estimated Buildup of Water in Sump of ES-1 (Hydraulic Conductivity of Alluvium = 100 cm/s and 10 cm/s)

HYDRAULIC CONDUCTIVITY OF ALLUVIUM = 1 cm/s



HYDRAULIC CONDUCTIVITY OF ALLUVIUM = 10⁻¹ cm/s

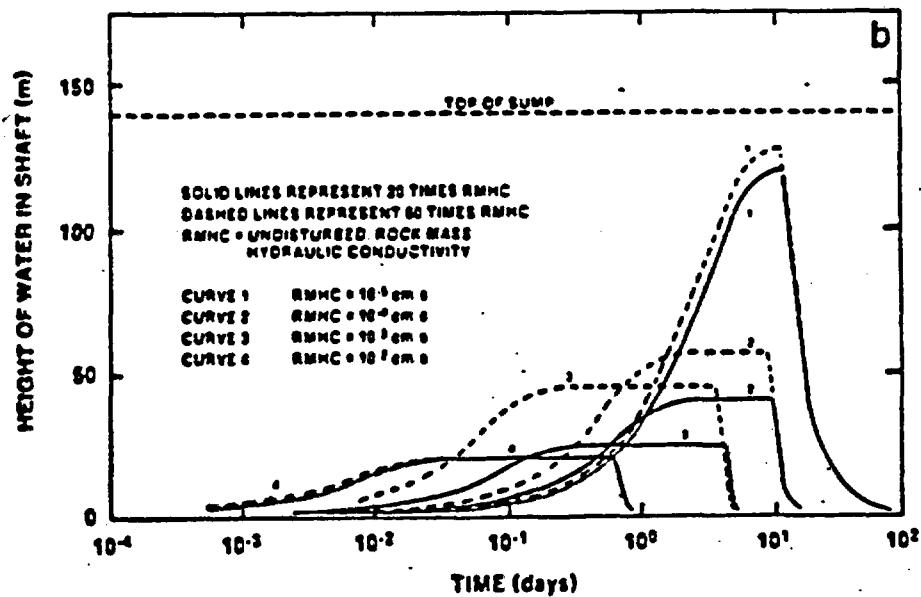
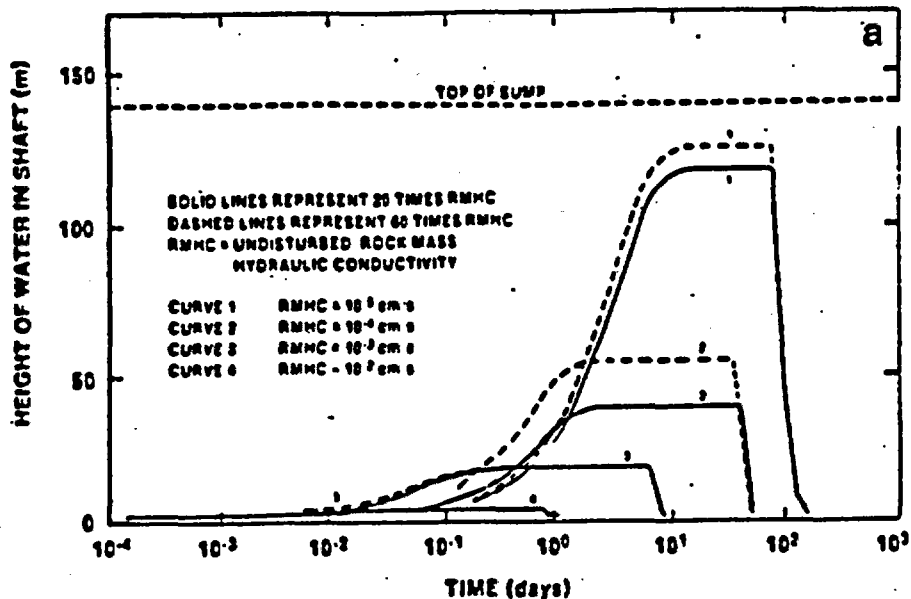


Figure 3-15. Estimated Buildup of Water in Sump of ES-1 (Hydraulic Conductivity of Alluvium = 1 cm/s and 0.1 cm/s)

HYDRAULIC CONDUCTIVITY OF ALLUVIUM = 10^{-2} cm/s



HYDRAULIC CONDUCTIVITY OF ALLUVIUM = 10^{-3} cm/s

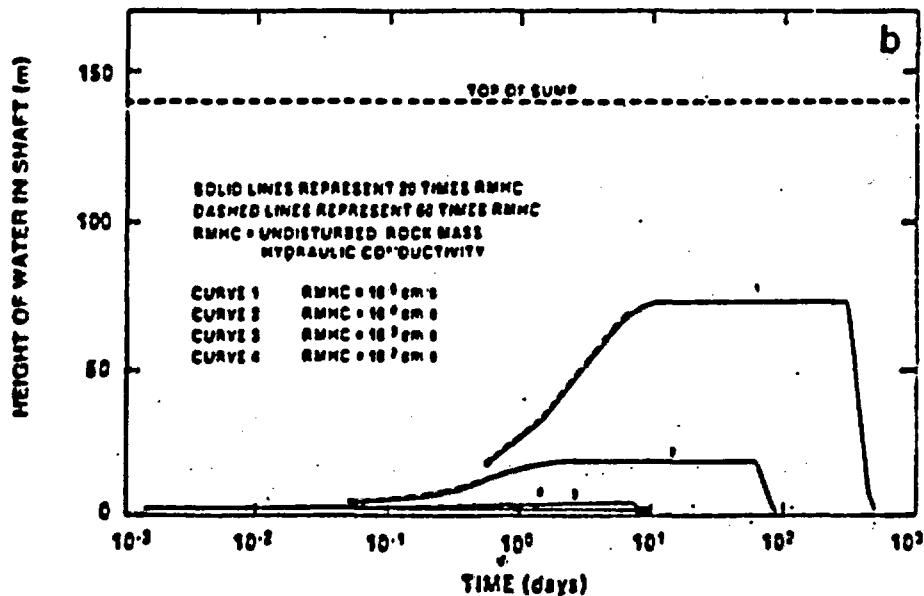


Figure 3-16. Estimated Buildup of Water in Sump of ES-1 (Hydraulic Conductivity of Alluvium = 10^{-2} cm/s and 10^{-3} cm/s)

improbable. The approach used in this report was to develop a water flow scenario that would develop a realistic, upper-bound water flow into the shafts.

Several general features are observed in curves in Figures 3-14, 3-15, and 3-16. The duration of inflow in all curves is greatest when the Tiva Canyon hydraulic conductivity is the lowest of the assumed range, i.e., 10^{-5} cm/s. This is to be expected as indicated by the duration of flows on Figures 3-8 to 3-11. The portion of the curves to the left of the peaks represent the period during which the drainage from the sump is less than the inflow into the upper portion of the shaft. The slopes of the curves beyond the peak are dependent on the hydraulic conductivity of the rock mass through which the water is draining and the height of water in the shaft. The greater the rock-mass hydraulic conductivity, the greater is the slope. The lower the height of water in the shaft the slower is the drainage and the longer it takes for the water in the shaft to fully drain from the shaft. In some cases plateaus are observed. These plateaus represent the condition when the inflow rate into the shaft is equal to the outflow rate from the base of the shaft. Also, when the inflows are greater for the 60 times undisturbed, rock-mass high conductivity, the height of water reached in the shaft is greater.

An additional observation is the point at which the peaks occur for a specific, undisturbed rock mass hydraulic conductivity. There are two factors that are important in noting where these peaks occurs, i.e., the magnitude of inflow and the duration of inflow. For example, when the alluvial hydraulic conductivity is 100 cm/s, the duration of inflow into the shaft is short. As the hydraulic conductivity of the alluvium decreases, the time for inflow and drainage from the base of the shaft are extended. This results in an increase in the height of water reached in the shaft. When the hydraulic conductivity of the alluvium is approximately 10^{-2} cm/s, this trend is reversed. The high-water level is reached when the hydraulic conductivity of alluvium is about 10^{-2} cm/s and the hydraulic conductivity of the rock mass is 10^{-5} cm/s. As the hydraulic conductivity of the alluvium decreases from 1 cm/s, the maximum height reached in the sump becomes comparatively lower for the case where the

rock-mass, hydraulic conductivity is 10^{-2} cm/s (see Figures 3-15 and 3-16). Conversely, a greater buildup of water in the shaft occurs for the case when the rock-mass, hydraulic conductivity is 10^{-5} cm/s. This greater buildup occurs when the rock-mass, hydraulic conductivity is 10^{-5} cm/s because inflow occurs over a long period of time (see Figures 3-10 and 3-11) and the drainage from the sump is lower than when the rock mass, hydraulic conductivity is 10^{-2} cm/s.

3.2.5 Impact of Relocating the Exploratory Shafts

After most of the analyses presented in this report were completed, the exploratory shaft locations were relocated to the northeast of the final EA locations as shown in Figure 2-2 and the design of the ES-1 and ES-2 were modified. The concern raised by this relocation and design change was the following: Does the influence of erosion and flooding at the new shaft locations adversely affect the long-term repository performance? To address this concern a comparison is made of comparative influence of (1) the erosion and flooding potential at the final EA location and the new locations and (2) the applicability of the flooding scenario for the new shaft locations. Section 3.2.5.1 briefly addresses the erosion potential at the new shaft locations. Section 3.2.5.2 includes the results from a flooding analysis which illustrates the potential to flood the exploratory shafts from the occurrence of a PMF. Section 3.2.5.3 includes a description of a scenario that is perhaps more applicable than the flooding scenario presented in Section 3.2.1. In Section 3.2.5.4 the impact of the flooding scenario (described in Section 3.2.1) on the repository performance using the most current ES-1 and ES-2 designs is discussed.

3.2.5.1 Erosion Potential at the New Exploratory Shaft Locations

Figure 3-17 shows the old and new locations for the exploratory shafts. The old location for ES-1 is located in the alluvial-filled portion of the wash. The old location for ES-2 is situated in bedrock slightly west of ES-1. Because the new locations of ES-1 and ES-2 will be collared in bedrock, the potential for eroding alluvium around the shaft collar is nonexistent. Furthermore, the shaft collars will be located in the Tiva Canyon Member that caps most of Yucca Mountain. In these caprock-

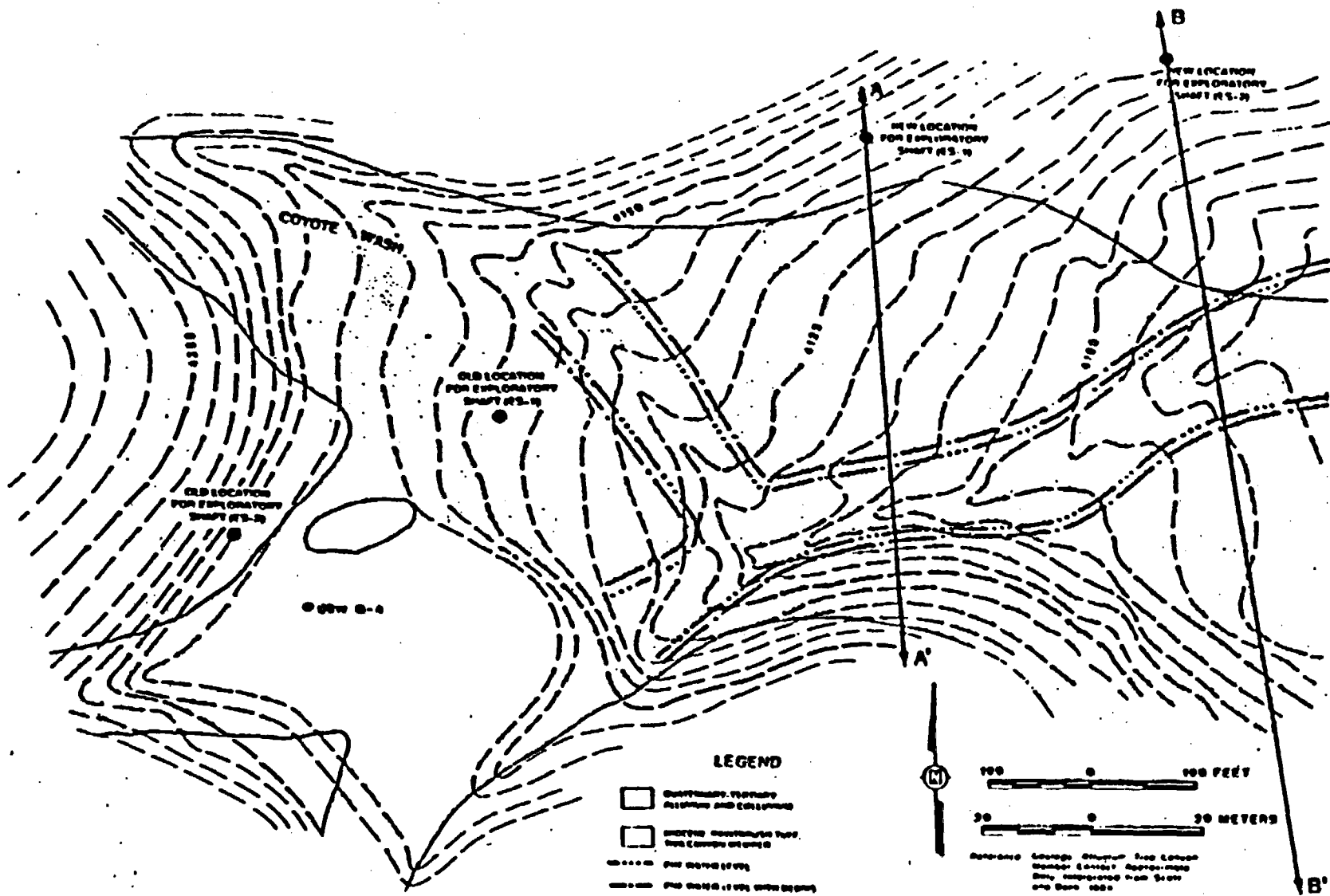


Figure 3-17. Estimated High-Water Locations Associated With a PHF in the Exploratory Shaft Area

protected areas, erosion is relatively slow providing a much greater resistance to downwasting than alluvium (DOE, 1988, p. 1-32). Therefore, the impact of the potential for focusing waters into the ES-1 due to erosion of rock at the new, exploratory shaft locations is considered to be negligible in comparison to the erosion of alluvium at the old exploratory shaft locations. From an erosional standpoint, the new locations are preferred over the old locations.

3.2.5.2 Flooding Potential at the New Exploratory Shaft Locations

To illustrate the comparative influence of flooding, a map defining the extent of the PMF was developed. In developing this map the existing topography and the Manning equation for open channel flow was used. Eight cross sections were used in developing the PMF high-water marks shown on Figure 3-17. In applying the Manning equation, the assumptions used were similar to those used by Squires and Young (1984, p. 24). Specifically, the values for slope of the energy-grade line used in Manning's equation was assumed to be equivalent to the slope of the water surface and the channel bottom. The value for the roughness coefficient, n , in Manning's equation was assumed to be 0.060. Roughness coefficients used by Squires and Young ranged from 0.030 to 0.055. Because we are estimating the high-level marks for the PMF and because ' n ' is proportional to the area of flow, a greater ' n ' value suggests a greater area of flow. This greater cross-sectional area of flow corresponds to a higher water-level during the occurrence of a PMF. Therefore selection of a greater ' n ' value (as used in this analysis) conservatively predicts a higher water-level rise.

Figure 3-17 shows the high-water locations for the PMF relative to the location of the exploratory shafts assuming two peak discharges. The inner lines represent the clear water flow only and the outer lines represent the clear water and debris flows. The peak discharge for the clear water flow is $95 \text{ m}^3/\text{s}$ (Bullard, 1986). To arrive at the peak discharge for the clear water plus debris flow, the debris flow is assumed to be 50% of the clear water flow. Figure 3-17 illustrates that some potential exists for the old ES-1 location to be inundated by a PMF. However, the potential for

inundating the shaft entry points of the new ES-1 and ES-2 locations is substantially reduced. The horizontal distance of the high-water mark from the ES-1 and ES-2, new locations is 90 m and 70 m, respectively. The ES-1 and ES-2 surface locations are 9 m and 11 m above the highest level of the PMF flows. Figure 3-18 presents the cross sectional diagrams of the topography and the water elevations of the PMF at the new locations of the ES-1 and ES-2. These cross sections are presented to illustrate the distance of the PMF flows from the new ES-1 and ES-2 locations.

From the preceding discussion, it can be concluded that relocation of the ESs to the northeast from the final EA locations has substantially reduced the impact that flooding could have on repository performance because the new shaft locations are at a greater distance from the water level of the PMF than the old shaft locations.

3.2.5.3 Scenario Describing Uniform Dispersion of Surface Water at Depth

Another concern raised by relocating the exploratory shafts is the applicability of the original flooding scenario presented in Section 3.2.1. As discussed earlier, the occurrence of the original scenario was considered to be highly improbable. Because the shafts at the new locations will not be in alluvium, the mechanism of water flow into the shaft assumed in the original flooding scenario is no longer present. Therefore, the probability of water flow into the shafts at the new location is even lower than the probability associated with the original shaft locations.

Another hypothetical scenario that may be more applicable at the new shaft locations is proposed below. This scenario was selected to depict the possibility of a variety of flows including fracture flow to intercept the shafts and associated MPZs anywhere below the surface. This scenario involves intense rainfall over the drainage basin associated with the exploratory shafts. This rainfall is equivalent to the volume associated with a PMF. Following the rainfall, it is assumed that all of the rainfall infiltrates into the ground surface either uniformly over the entire drainage area (Case 1) or only over a more restricted area defined by the existing water courses (Case 2). These two cases are depicted on Figure 3-19. In Case 1 the area considered is upgradient from the new,

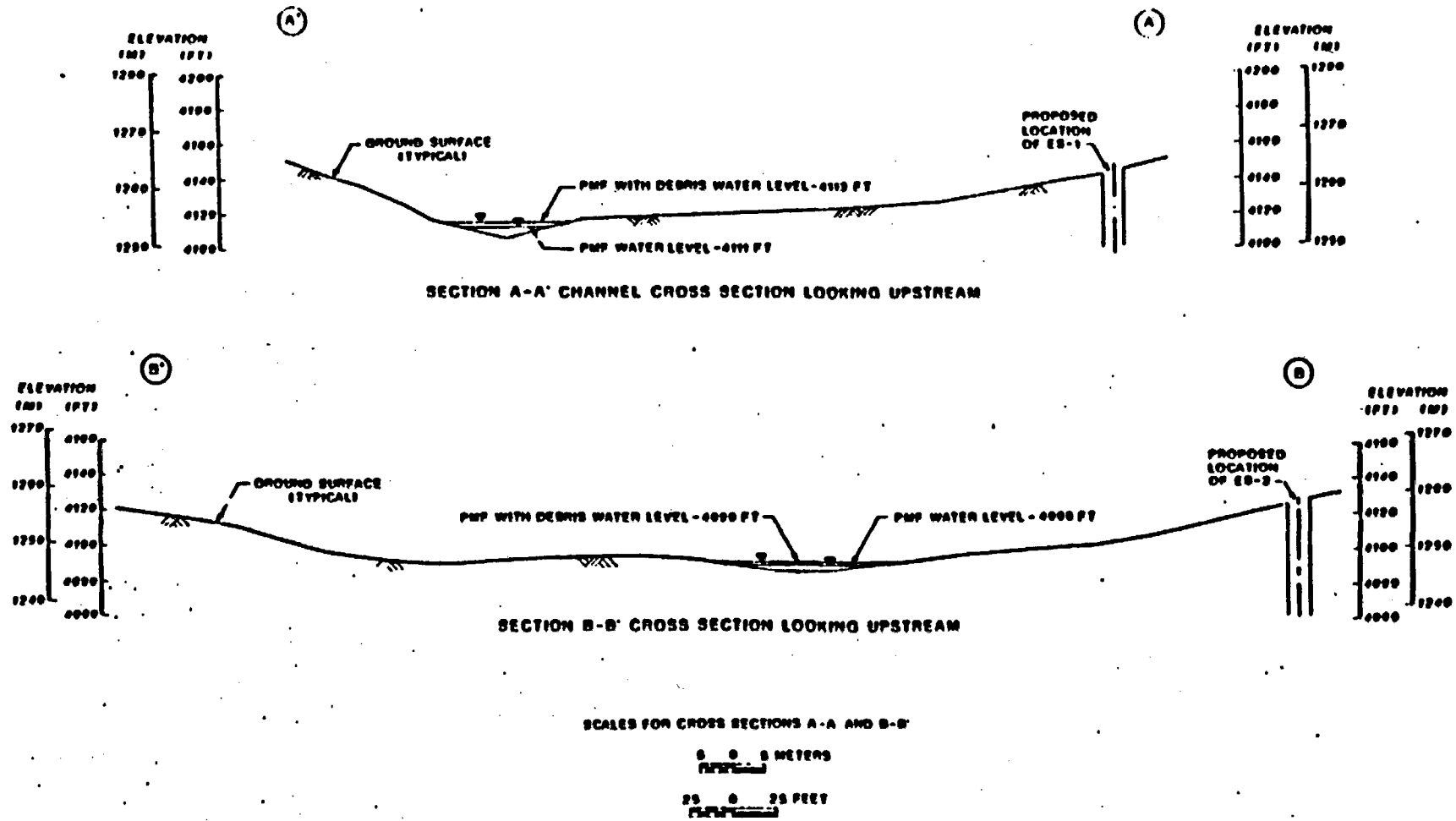
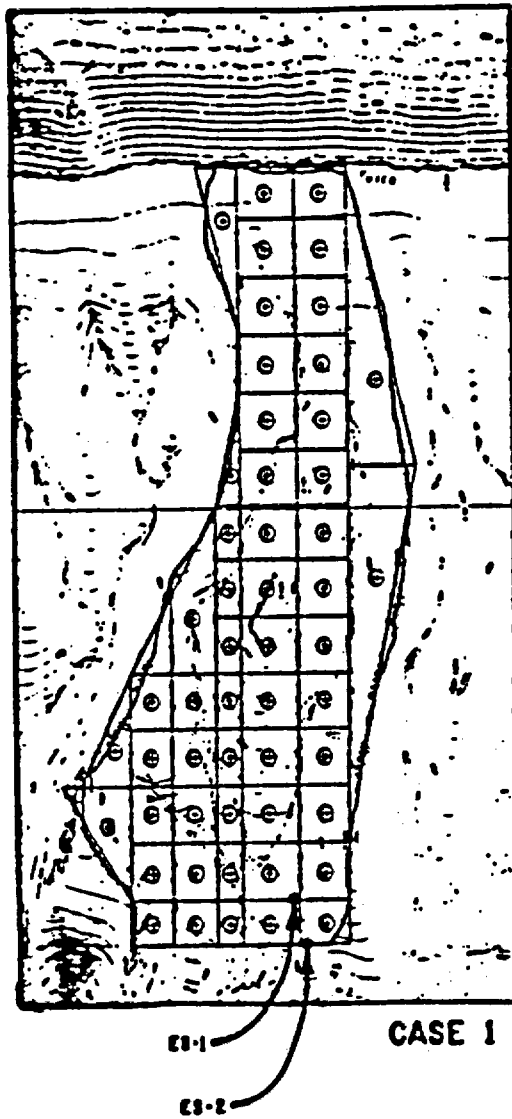


Figure 3-18. Topographic Cross Sections in the Vicinity of the New ES-1 and ES-2 Locations



CONTOUR INTERVAL 2 METERS

0 100 200 300 400 500

METERS

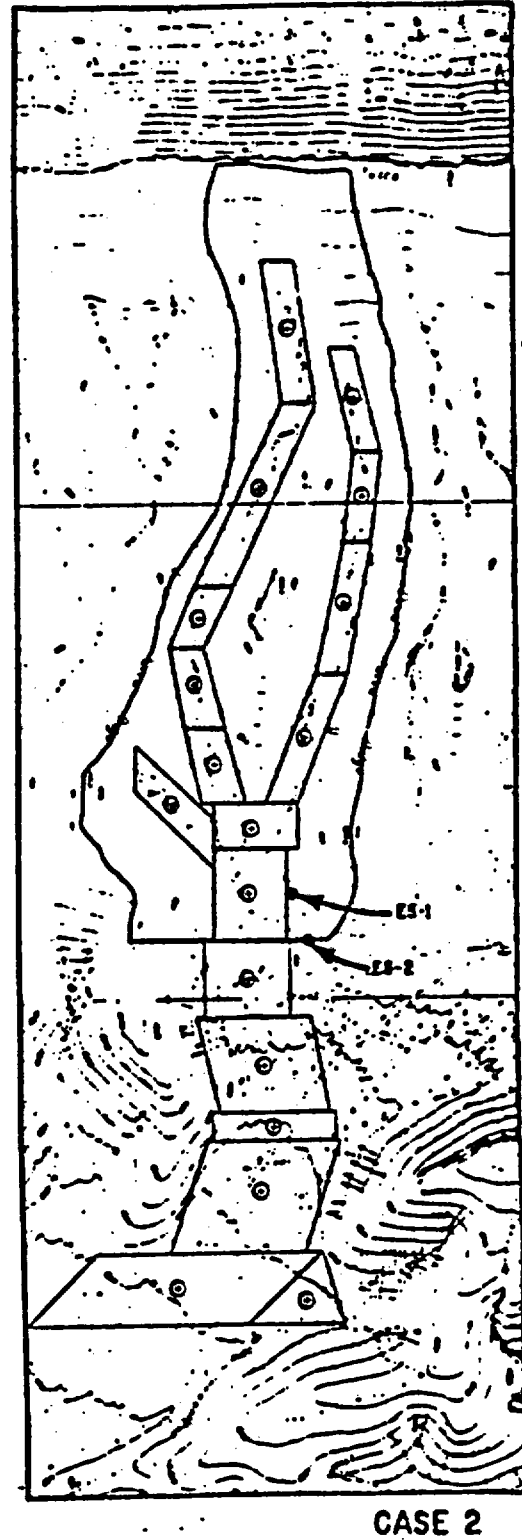


Figure 3-19. Topography, Drainage Basin Outline, and Grid Used in Developing the Uniform Dispersion Scenario

exploratory shaft location. In Case 2 the area considered is upgradient and downgradient from the new, exploratory shaft locations acknowledging the fact that flow into the shafts can occur from surface locations downgradient from the surface location of the shaft. Superimposed on the drainage basin is a network of discrete areas or elements that define the zones where infiltration occurs. The amount of water entering each element is proportional to its area compared with the entire area into which infiltration is assumed to occur. In Case 1, infiltration occurs over the entire drainage basin. In Case 2, infiltration occurs only in the areas, defined by the ephemeral stream locations.

In both cases it is assumed that all of the water from the rainfall is uniformly dispersed by the fractures in the stratigraphic column beneath each element. The portion of water that falls on each element and subsequently enters the ES-1 and ES-2 is schematically depicted on Figure 3-20. The portion of water entering the shafts from each element is defined by

$$V_i = \frac{2\theta}{360^\circ} \frac{A_i}{A_{\text{total}}} V_{\text{PMF}}$$

- where
- V_i = volume of water entering the exploratory shafts from rainfall occurring over element "i",
 - 2θ = angle formed by the center point of each element and the assumed extent of the MPZ around each shaft (in degrees),
 - A_i = the area of an element "i",
 - A_{total} = the total area of all the elements, and
 - V_{PMF} = volume associated with a PMF, 13.8 in. of rainfall over the entire basin.

The total amount of water, V_{shafts} , entering both ES-1 and ES-2 from "n" elements would be

$$V_{\text{shafts}} = \left[\sum_{i=1}^n V_i \right]_{\text{for ES-1}} + \left[\sum_{i=1}^n V_i \right]_{\text{for ES-2}}$$

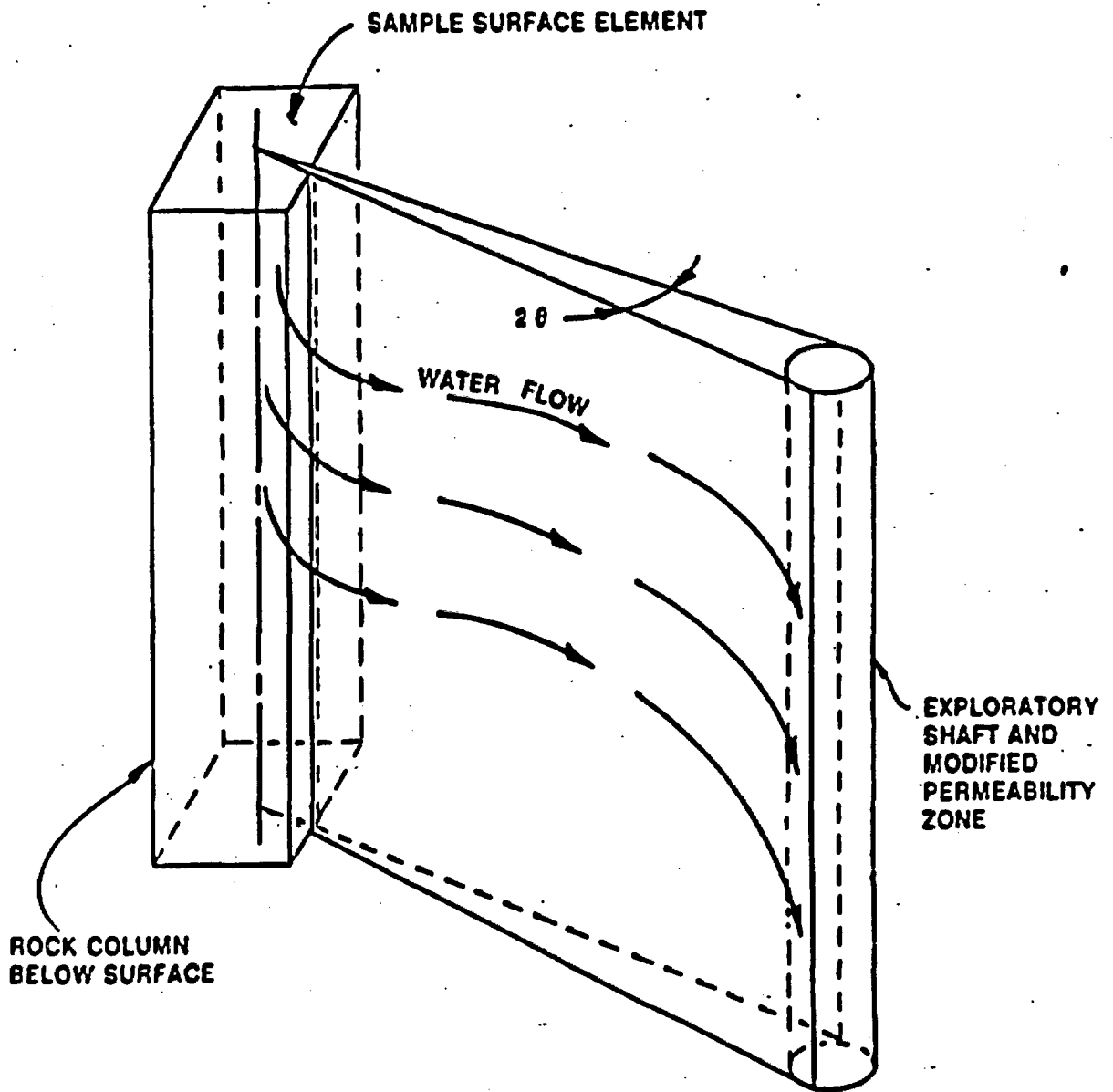


Figure 3-20. Illustration of the Water Flow That Enters the Exploratory Shaft and MPZ From a Single Surface Element

The farther an element is away from an exploratory shaft, the smaller will be the "20" term and the lower will be the flow of water from an element to the shaft.

Using the formulas above, the total amount of water entering both exploratory shafts for the scenario is 1250 m³ for Case 1 and 1320 m³ for Case 2. These values are considered to be upper bounds for the scenario because it is assumed that all of the rainfall, 13.8 in., falling over the entire basin, infiltrates down through the stratigraphic units and laterally to the exploratory shafts. In reality, 13.8 in. does not infiltrate downward into the stratigraphic column. The majority of rainfall would exit the drainage basin as a flood volume once the ground surface saturates to some threshold amount. If runoff occurs after 2 in. of rainfall, the upper bound of retention indicated by Bullard (1986), approximately 85%, would exit the drainage basin as runoff. Of the amount that saturates the soils, only a portion would percolate through the stratigraphic column. It is therefore reasonable to assume only a fraction of the 13.8 in. of rainfall would percolate through the stratigraphic column and migrate laterally to the exploratory shafts. A more realistic volume of water entering both shafts would therefore be an amount 1 to 2 orders of magnitude lower than the amount computed earlier. Therefore, volumes of approximately 10 m³ to 100 m³ are more realistic estimates of water entering the shafts during a PMF. These estimated volumes of shaft inflow are extremely small volumes when compared to the maximum volume computed from the original scenario described in Section 3.2.1. In fact, these small volumes could be contained within the ES-1 sump.

Nevertheless, to demonstrate the effectiveness of the new ES-1 and ES-2 designs, shaft inflows computed from the original flooding analyses are assumed to enter the ES-1.

3.2.5.4 Analysis of the Drainage Capacity of the New Exploratory Shafts and Associated Facility

The analysis performed in Section 3.2.4 were rerun assuming the new ES-1 and ES-2 designs. In the new ES-1 design the sump is 110 m rather than 140 m. The new ES-2 sump is approximately 30 m rather than 3 m. Thus, the total sump storage capacity for the new ES designs remains

approximately the same as that for the old ES designs. It is also important to note that the drifts between ES-1 and ES-2 provide additional storage and drainage capacity and slope towards the ES-1. The drainage pattern is illustrated in Figure 3-21. This drainage pattern suggests that water entering the ES-1 or ES-2 would first have to fill up the sumps of ES-1 and ES-2 as well as portions of the ESF drifts before water would exit the ESF into the connecting access drifts.

The results obtained from running the same analysis described in Section 3.2.4 using the current or new ES designs, are discussed below. Because the new ES-1 sump is approximately 30 m shallower than the old ES-1 design, the maximum height of water reached in the ES-1 exceeds the elevation of the repository station in two cases--first, when the hydraulic conductivities of the alluvium and the welded tuff units are assumed to be 10^{-2} cm/s and 10^{-5} cm/s, respectively, and second, when the hydraulic conductivities of the alluvium and the welded tuff units are assumed to be 10^{-1} cm/s and 10^{-5} cm/s, respectively. In the first case the maximum height of water reached in the shaft was computed to be approximately 125 m and the flow past the repository station seals at the ESF location was computed as 40 m^3 . For the second case, the maximum height of water reached in the shaft was also about 125 m but the duration of height above the repository station elevation was much less than for Case 1. The flow past the repository station seals was computed to be 3 m^3 for Case 2.

For the first case where the potential flow past the repository station seals was computed to be 40 m^3 , the storage capacity of the ESF and the ES-2 would easily contain this flow. The storage capacity of ESF between the ES-1 and ES-2, assuming the drifts are backfilled was computed as 650 m^3 . In addition, the storage capacity of the new ES-2 sump is about 100 m^3 .

3.2.5.5 Conclusions

From these computations it is concluded that the presence of the exploratory shafts, including their associated MPZ and shaft fill, does not compromise the performance of the repository because:

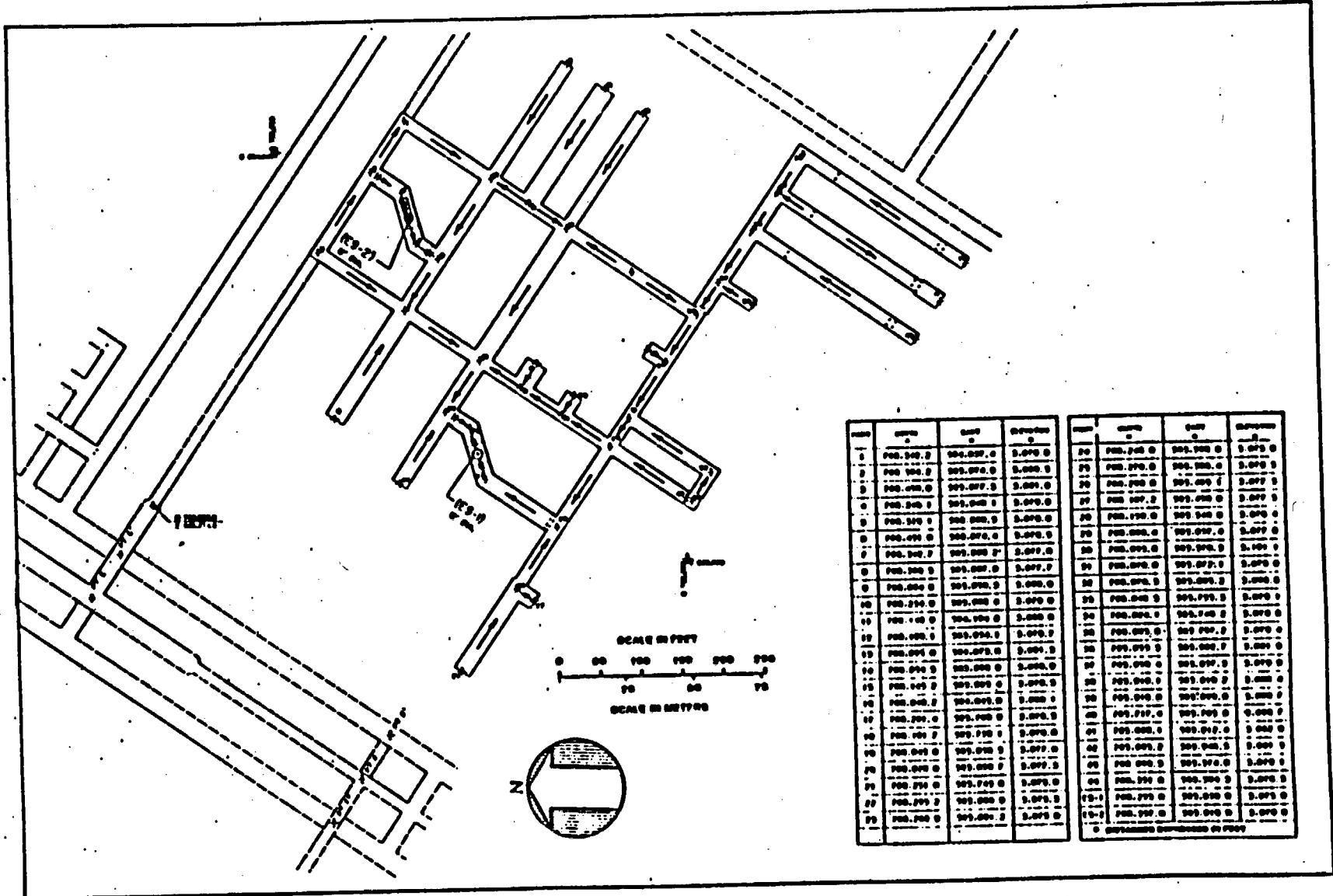


Figure 3-21. Drift Drainage Pattern Proposed in the Vicinity of the Exploratory Shafts

- o Even when a highly improbable flooding scenario (and possibly an incredible scenario at the new ES locations) is considered at the new ES locations, any water entry past the repository station seals is contained within the ESF.
- o The more realistic scenario presented in Section 3.2.5.3, postulated shaft inflows associated with a PMF to be 10 to 100 m³. These volumes can be contained within the sump of ES-1 even if no drainage from the sump is assumed.

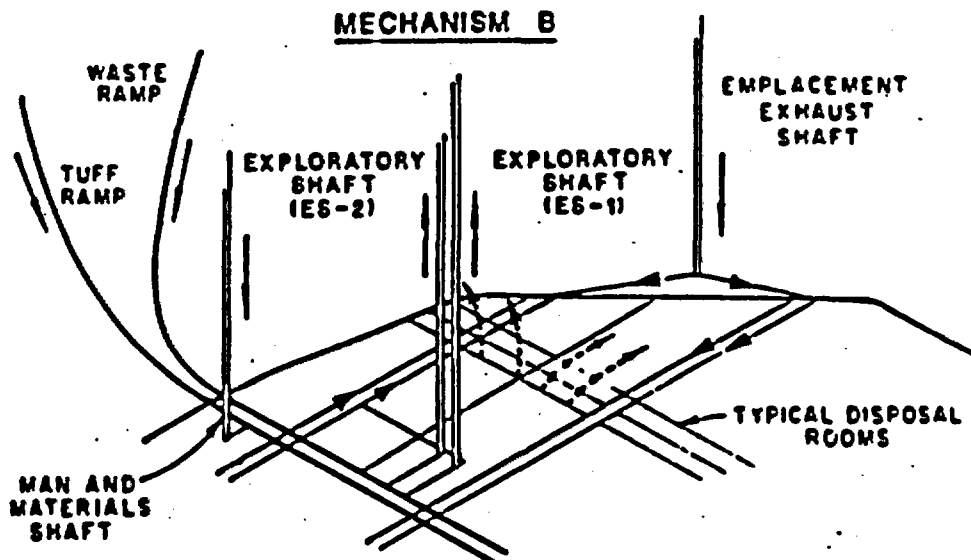
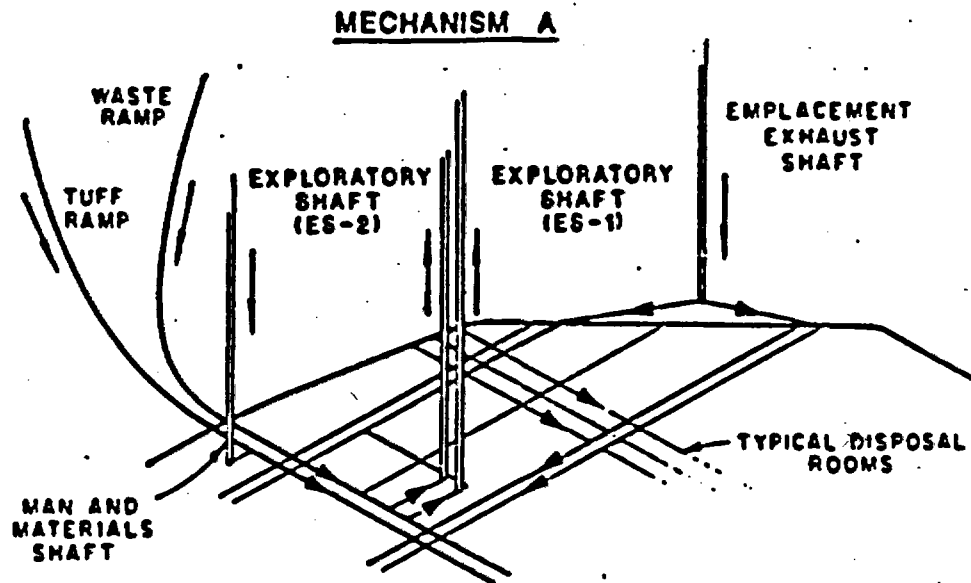
3.3 Potential for Enhancing Radionuclide Release From Air Movement Due to Convective Forces

For a repository located above the water table, there is the possibility of release of radionuclide by air flow out of the repository through the shafts or through the host rock. In Fernandez et al. (1987, p. 3-22) a performance goal for air flow out of the shafts and their associated MPZs was established considering the total gaseous releases that could potentially occur for C-14 and I-129. The performance goal established was that air flow through the shafts and their associated MPZs should be no greater than 25% of the total air flow. This section evaluates the potential magnitude of air flow rates from the repository and compares the relative influences of the shafts, ramps, and host rock in allowing air flow to occur. More specifically, the calculations examine the influence of the MPZ around the shafts and ramps and the degree to which flow can be limited by backfilling or sealing the shafts.

After emplacement of waste canisters, heat is initially transferred by conduction from the waste canisters to the surrounding rock. Vertical temperature gradients will develop from the repository horizon, and potentially affect air and water density. If sufficient energy in the form of heat is imparted to the air or water vapor, convective transport is established.

3.3.1 Air Flow Mechanisms

Two potential air flow mechanisms are illustrated in Figure 3-22. Mechanism A assumes that no upward flow occurs through the host rock



FLOW THROUGH ROCK MASS
FLOW THROUGH SHAFT

Figure 3-22. Mechanisms for Convective Air Flow (A) Flow Through Shafts Only and (B) Flow Through Shafts and Rock

relative to flow through the shafts, ramps, and drifts. ES-1 and ES-2 are within the repository area, and the temperature gradient is relatively high near the repository horizon due to the emplacement of thermally hot waste packages. The men-and-materials shaft, the emplacement exhaust shaft and the ramps are located outside or just inside the repository perimeter, and the temperature gradients are lower. In response to these temperature gradients, air will tend to rise in ES-1 and ES-2, and may be drawn in through the other entries. The mechanism may occur if the shafts and drifts are open, or if the backfill is relatively permeable so that the resistance to air flow through the backfill is less than that through the rock. In Mechanism B, convective air transport is assumed to occur through the host rock. The waste disposal areas are relatively hot and the heated air tends to rise vertically through the rock as well as through ES-1 and ES-2. Air is drawn in through the peripheral entries to maintain pressure in the rooms.

The analyses presented in this report consider Mechanism B in detail. As discussed subsequently for shafts filled with an engineered material (hydraulic conductivity less than 10^{-2} cm/s), the flow of air out of the repository would be dominantly through the rock. A detailed discussion of Mechanism A and a comparison between the two mechanisms is presented in Appendix C of Fernandez et al. (1987).

3.3.2 Method of Analysis

The mechanism of convective air flow through a heated repository is considered to be analogous to air flow through an underground mine resulting from natural ventilation. Draft air pressures are calculated by the density method. Air flows are assumed to be induced by the draft air pressure and are calculated using a network resistance model similar to that used in mine ventilation studies (Hartman, 1982, pp. 239-245). Flow is assumed to be governed by Darcy's law. In Appendix C, a relationship is derived for convective air transport through backfilled shafts and fractured rock from the assumptions mentioned above.

The principal input parameters are the resistance to air flow of the underground openings and the host rock, and the pressure gradient calculated from the difference in pressure between the inlet and outlet points

as derived by the air density profiles. A detailed discussion of the assumptions made in the analysis is presented in Appendix C. The assumptions may be summarized as follows: 1) Darcy's law is valid; 2) air temperatures in the shaft are the same as in the adjacent rock; 3) air flow is incompressible and the air is dry; and 4) air circulation occurs along specified paths.

3.3.3 Model Description

Air flows were calculated by assembling a "network stiffness matrix" (Zienkiewicz, 1977, pp. 12-13) of various resistances representing the network of underground openings and the rock mass, by applying pressure boundary conditions, and by solving a system of linear simultaneous equations to calculate nodal pressures. Air flows were then calculated through the network. The following sections describe the temperature and pressure boundary conditions, air conductivities (material properties), and model geometry (networks) used in the analyses.

3.3.3.1 Temperature and Pressure Distributions

Draft pressures were calculated using the accepted mine ventilation practice of computing pressure gradients (at the repository horizon) on the basis of differences in air density at the inlet and outlet points. The first step requires the temperature profiles at the potential repository inlet and outlet points. The inlet and outlet temperature at the ground surface were assumed to be 13°C. For purposes of calculating air densities, a peak temperature profile was estimated for the ES-1 based on a peak temperature of 115°C at the repository horizon. (The source of this temperature is the heat liberated from the radioactive waste contained in the waste packages.) At the time at which the peak temperature is attained, the temperature at the other entries outside the repository is assumed to be 23°C, indicative of the geothermal gradient. Using a value comparable to the geothermal gradient is conservative because the actual temperature at the repository horizon will be greater than 23°C. By assuming a value of 23°C the temperature difference between the inlet and outlet entries will be greater resulting in greater pressure gradients and subsequently greater air flows. In this way, this analysis is anticipated to be conservative.

The calculated draft pressure using the method described above was 0.35 kPa, which corresponds to 1.4 inches of water gage. By comparison, according to Hartman (1982, p. 240) the natural ventilation pressure generated by natural geothermal energy in mines is usually less than 0.5 inches water gage, and seldom exceeds three inches except in extreme cases. The calculated draft pressure falls within this range for this mechanism and would be expected to be higher than 0.5 inches, since the heat generation due to radioactive waste in an underground nuclear waste repository results in larger temperature contrasts than those experienced in a typical underground mine.

3.3.3.2 Flow Path Resistances

The resistance to air flow for incompressible fluid flow through shafts and drifts is dependent on the lengths and cross-sectional areas of the flow paths, and the air conductivities of the backfill, surrounding MPZ, and host rock. In the present analyses, MPZs were modeled around the shafts and ramps accessing the repository, but not around the drifts (see below). The cross-sectional areas and length for the flowpaths for vertical and horizontal emplacement are summarized in Tables 3-2 and 3-3 respectively. The cross sectional areas of the MPZ developed around the shafts were assumed to extend out one radius from the wall. For ramps which have a noncircular cross section, the MPZ area was calculated from the equivalent radius of a circle with the same area.

For flow through undisturbed rock it is necessary to know the cross-sectional area of the roof of the repository (waste rooms, submains and mains). This area is estimated to be 983,700 m² for vertical emplacement or 486,000 m² for horizontal emplacement. In these analyses, the roof areas above the mains and submains were included in the calculation since it is expected thermal convection would develop throughout the underground repository. The equivalent conductivity for flow through the rock to the ground surface was calculated according to the relation for flow in series (Freeze and Cherry, 1979, p. 34). In the present analyses, the thickness of the welded units (Tiva Canyon and Topopah Spring) is 260 m and the

Table 3-2. Summary of Areas and Lengths - Vertical Emplacement

Flowpath	Backfilled ^(a)	Modified Permeability	Length (m)
	Area (A) (m ²)	Zone ^(b) Area (m ²)	
Waste Ramp	34.2	115.8	2012
Tuff Ramp	42.8	136.8	1410
Men-and-Materials Shaft	29.2	105.9	314
EE Shaft	29.2	105.9	314
ES-1	10.5	42.9	311
ES-2	10.5	42.9	311

- (a) Backfilled area is based upon inside dimension of lined shaft or ramp.
 (b) MPZ based upon three times the excavated area of the shaft or ramp which corresponds to an MPZ extending one radius from the edge of the excavated, shaft wall.

Table 3-3. Summary of Areas and Lengths - Horizontal Emplacement

Flowpath	Backfilled ^(a)	Modified Permeability	Length (m)
	Area (A) (m ²)	Zone ^(b) Area (m ²)	
Waste Ramp	28.3	96.5	2012
Tuff Ramp	30.1	96.5	1410
Men-and-Materials Shaft	29.2	105.9	314
EE Shaft	29.2	105.9	314
ES-1	10.5	42.9	311
ES-2	10.5	42.9	311

- (a) Backfilled area is based upon inside dimension of lined shaft or ramp.
 (b) MPZ based upon three times the excavated area of the shaft or ramp which corresponds to an MPZ extending one radius from the edge of the excavated, shaft wall.

thickness of the nonwelded Paintbrush is 40 m. The air conductivity* of the nonwelded Paintbrush was assumed to be either 3×10^{-7} or 3×10^{-5} m/min. This corresponds to a range of hydraulic conductivity from 10^{-5} to 10^{-3} cm/s.** The welded tuff units (Tiva Canyon and Topopah Spring) were assumed to have either an air conductivity of 3×10^{-7} or 3×10^{-4} m/min. This corresponds to a range of hydraulic conductivities of from 10^{-5} to 10^{-2} cm/s (Scott et al., 1983, p. 299).

Three combinations of bulk rock hydraulic conductivity were evaluated in the analysis. These combinations were selected to cover a range of conductivities for welded and nonwelded tuff and to examine the influence of a thinner less permeable layer of nonwelded tuff on overall air flow rates if the welded tuff conductivity were high (10^{-2} cm/s).

	Nonwelded Hydraulic Conductivity (cm/s)	Welded Hydraulic Conductivity (cm/s)
Combination 1 (Low)	10^{-5}	10^{-5}
Combination 2 (Intermediate)	10^{-5}	10^{-2}
Combination 3 (High)	10^{-3}	10^{-2}

The equivalent air conductivity of the modified permeability zone was taken to be either 20 or 60 times higher than the conductivity of the undisturbed tuff averaged over an annulus one radius wide extending from the shaft wall. The equivalent conductivity factor of 20 corresponds to expected conditions at depth. The equivalent conductivity factor under worst case assumptions ranged from 40 to 80 times the undisturbed tuff conductivity. The average value of 60 was selected for analysis. The equivalent conductivity factor of the overlying rock was determined, as explained previously to take into account strata with varying conductivities, and the MPZ was assumed to be either 20 or 60 times more permeable than the undamaged rock in each stratigraphic unit.

*Air conductivity may be derived by calculating an intrinsic permeability from the hydraulic conductivity relationship presented by Freeze and Cherry (1979, p. 27) and then by calculating the air conductivity using the fluid properties of air.

**The range considered here bounds value for the bulk, saturated hydraulic conductivity of 2.4×10^{-4} cm/s given by Sinnock et al. (1984, p. 12) for the Paintbrush nonwelded unit.

Air conductivities in the backfill were varied over a range from 3.0×10^{-6} m/min to 3.0 m/min, equivalent to a range of hydraulic conductivity from 10^{-4} to 100 cm/s. The upper bound for air conductivity corresponds to a gravel, while the lower bound corresponds to a silty sand (Freeze and Cherry, 1979, p. 29). The lower bound might also correspond to a compacted backfill engineered for low permeability by adding silt or clay fines.

3.3.4 Model Results

The convective air flow analysis results are presented as a series of plots. The relationship of total flow rate out of the repository to the shaft fill, air conductivity for vertical and horizontal emplacement configurations, and low and high modified permeability zone models are presented in Figures 3-23 through 3-26. The flow rate through ES-1 and ES-2 expressed as a percentage of the total flow rate out of the repository are presented in Figures 3-27 through 3-30. The three curves on each plot represent the low, intermediate, and high rock conductivity combination presented previously.

The distribution of flow through the shaft fill, the MPZ, and the tuff roof rock was found to be dependent on the shaft fill, air conductivity. With high shaft fill, air conductivity of 1 m/min, the flow into and out of the repository is dominantly through the shaft fill with total flow ranging from approximately 1 to $10 \text{ m}^3/\text{min}$, depending on the conductivity of the roof rock. With low fill conductivities (less than 10^{-5} m/min), flow into the repository is primarily through the modified permeability zone, while flow out of the repository is dominantly through the tuff roof, and total flow rates are less than 0.1 m/min. The high conductivity MPZ model results in a somewhat higher flow rate than the low conductivity MPZ model under these circumstances. The conductivity of the tuff units in series influences the total air flow through the repository. For the high conductivity combination, the total flow begins to level off toward a constant value at a shaft fill, air conductivity of about 10^{-3} m/min. For the intermediate and low conductivity combinations, this stabilization of total flow occurs at shaft fill, air conductivity of approximately 10^{-5} m/min. At low, backfill air conductivity, the total flow rate varies over two orders of magnitude depending on the air conductivity of the rock.

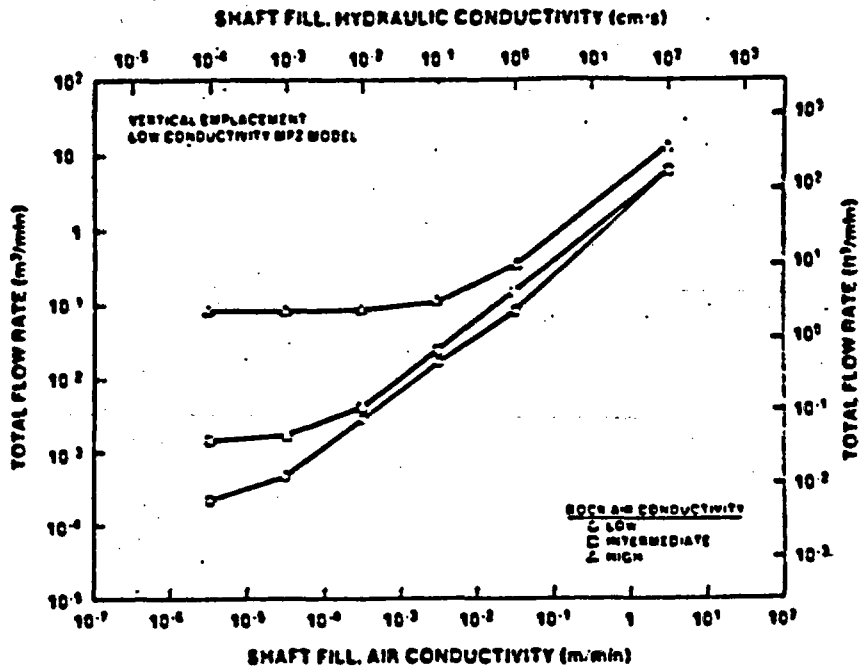


Figure 3-23. Total Flow Rate as a Function of Shaft Fill, Air Conductivity (Vertical Emplacement and Low Conductivity MPZ Model)

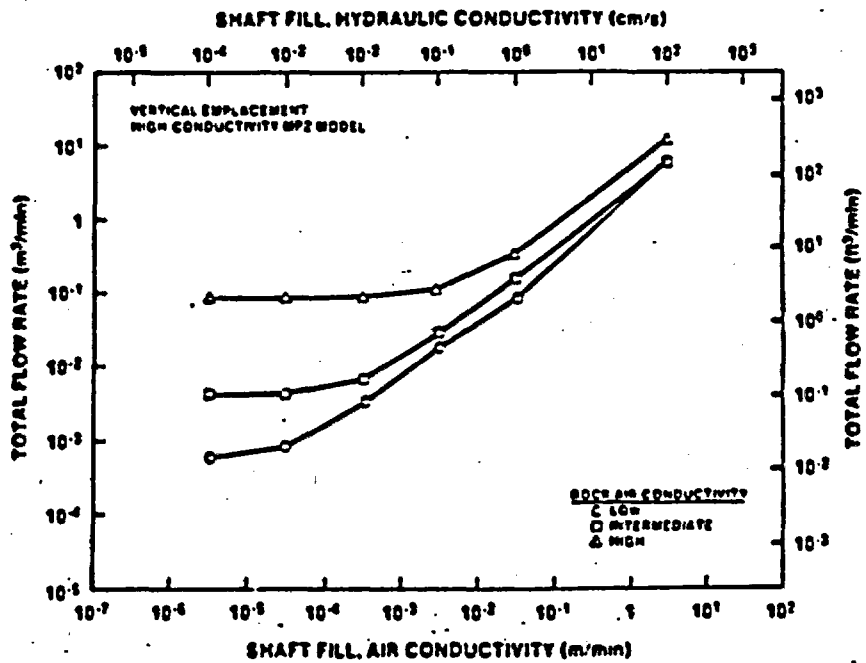


Figure 3-24. Total Flow Rate as a Function of Shaft Fill, Air Conductivity (Vertical Emplacement and High Conductivity MPZ Model)

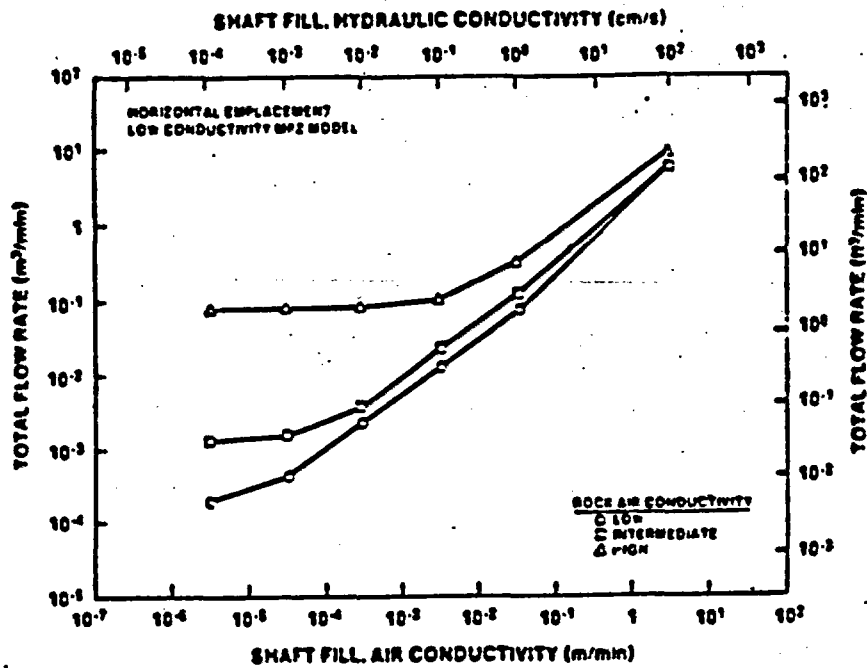


Figure 3-25. Total Flow Rate as a Function of Shaft Fill, Air Conductivity (Horizontal Emplacement and Low Conductivity MPZ Model)

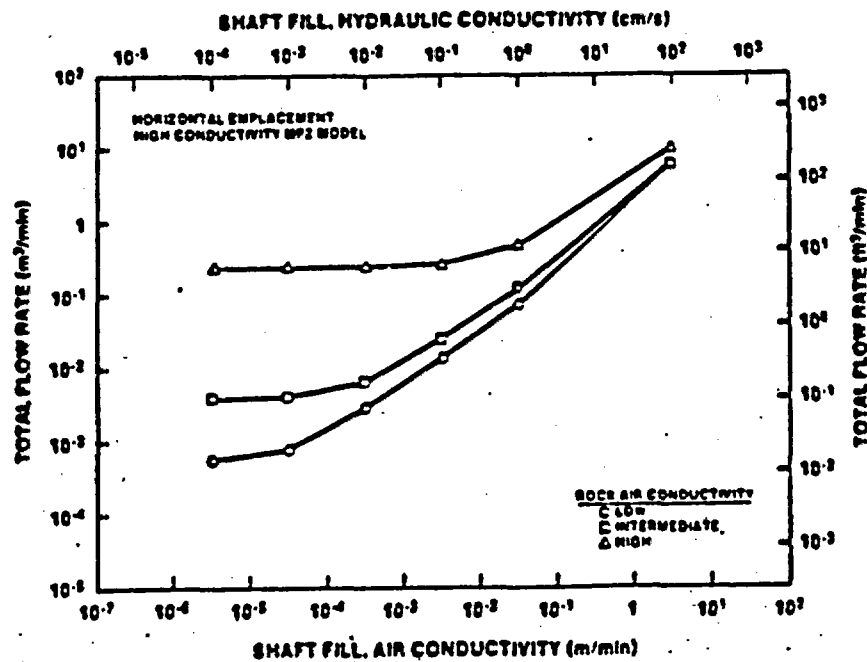


Figure 3-26. Total Flow Rate as a Function of Shaft Fill, Air Conductivity (Horizontal Emplacement and High Conductivity MPZ Model)

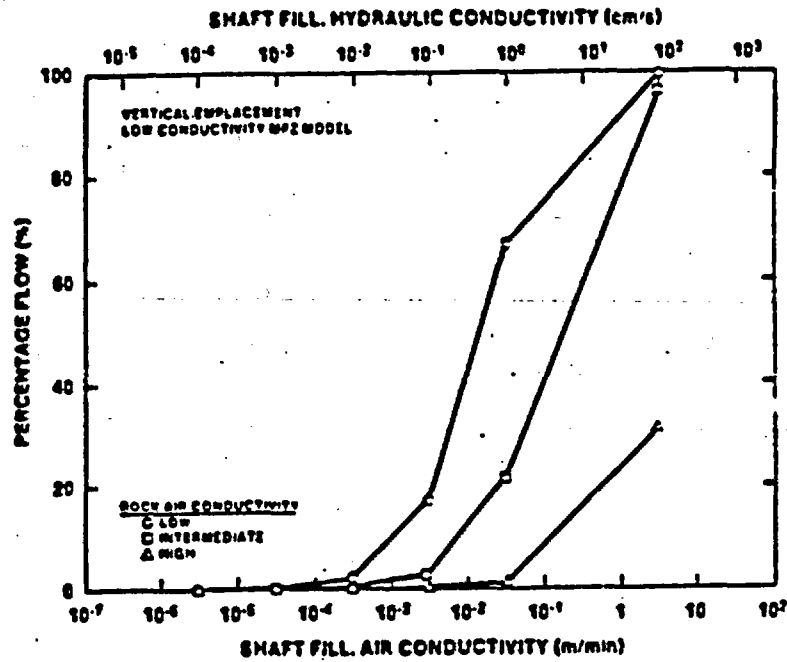


Figure 3-27. Air Flow Through ES-1 and ES-2 (Shaft Fill and MPZ Flows Included) as a Percentage of Flow Through the Rock Over Repository Area (Vertical Emplacement and Low Conductivity MPZ Model)

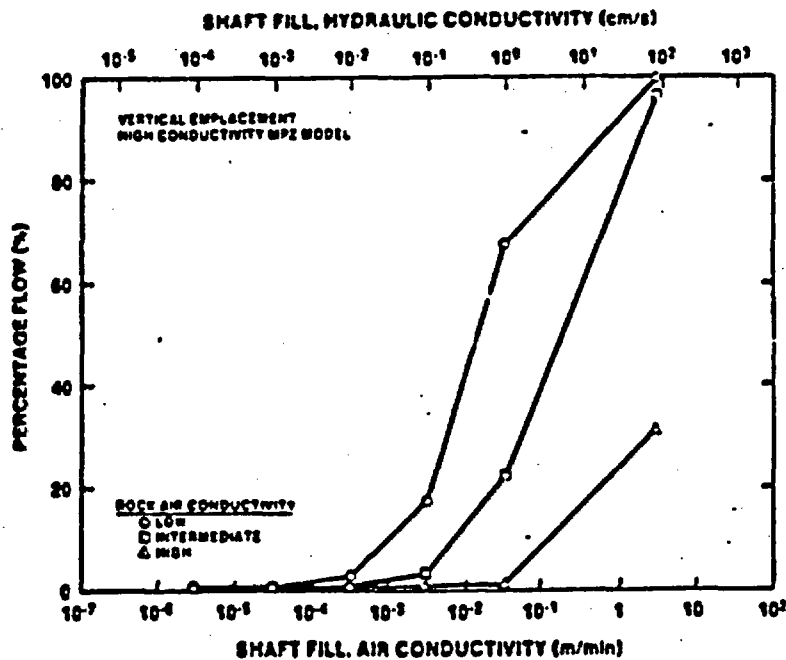


Figure 3-28. Air Flow Through ES-1 and ES-2 (Shaft the Fill and MPZ Flows Included) as a Percentage of Flow Through the Rock Over Repository Area (Vertical Emplacement and High Conductivity MPZ Model)

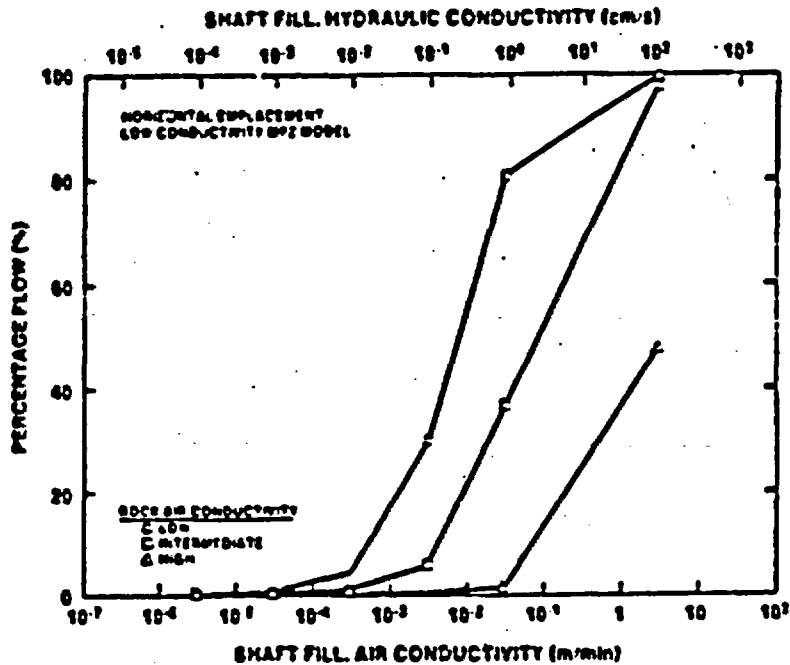


Figure 3-29. Air Flow Through ES-1 and ES-2 (Shaft Fill and MPZ Flows Included) as a Percentage of Flow Through the Rock Over Repository Area (Horizontal Emplacement and Low Conductivity MPZ Model)

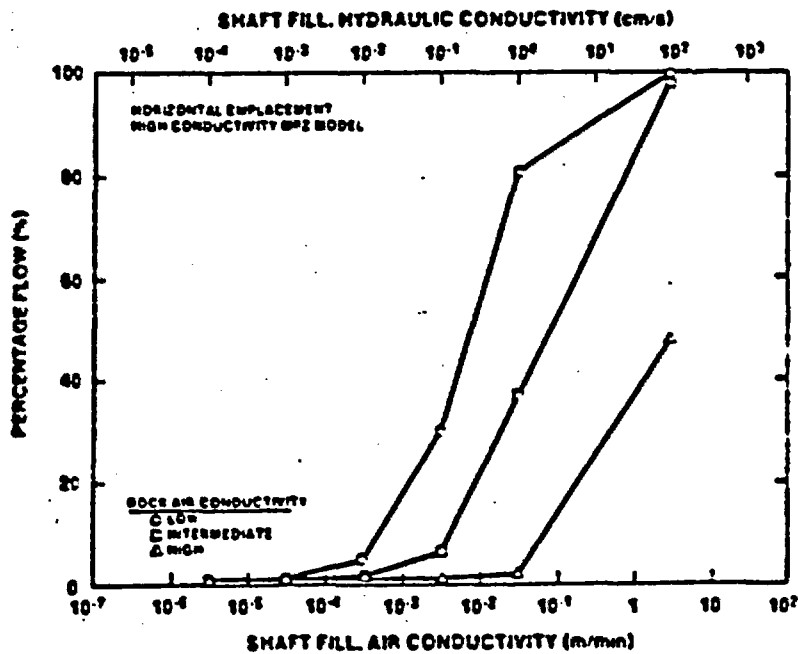


Figure 3-30. Air Flow Through ES-1 and ES-2 (Shaft Fill and MPZ Flows Included) as a Percentage of Flow Through the Rock Over Repository Area (Horizontal Emplacement and High Conductivity MPZ Model)

In comparing total flow for the vertical and horizontal emplacement modes, it is apparent that the results are very similar. This is because the geometry of the shafts and ramps accessing the repository are very similar. At high backfill air conductivity, flow is dominantly through the shafts and ramps. At low backfill conductivity, resistance to flow is dominantly through the MPZ of the inlet shafts and ramps. In this analysis, no attempt has been made to distinguish temperature fields between the two emplacement modes although this may have some influence on calculated upper-bound, convective air-flow rates. It is reiterated that the assumption of the inlet shafts/ramps being at geothermal temperature is conservative for both emplacement modes.

The analysis indicates that the percentage of flow through ES-1 and ES-2 to total flow is also dependent on shaft fill, air conductivity. When the backfill conductivity is low, the percentage of flow through the shafts and ramps is also low, regardless of the existence of either a low or high conductivity MPZ. For example, for vertical emplacement, with a shaft fill having an air conductivity less than 3×10^{-4} m/min (equivalent to a hydraulic conductivity of 10^{-2} cm/s) the contribution of ES-1 and ES-2 shaft to total flow is less than 2.5%. The percentage is somewhat higher for horizontal emplacement, and this is attributable to a smaller roof area which tends to increase the percentage flow through ES-1 and ES-2. Nevertheless, for either emplacement mode the percentage is smaller than 2.5% when the backfill air conductivity is less than 10^{-4} m/min. As indicated in Section 3.3, the performance goal established for air flow out of the exploratory shafts was that no more than 25% of the total flow out of the repository go through these shafts. The value of 2.5% given above therefore represents an even more conservative release of air through the shafts; i.e., one order of magnitude less than the performance goal.

3.3.5 Conclusions

From the preceding discussion, it is concluded that the exploratory shafts (including shaft fill and the MPZ) are not likely to be preferential pathways for gaseous radionuclide releases if the air conductivity of the shaft fill is less than about 3×10^{-4} m/min. This conclusion is reached because:

- o When the air conductivity is greater than this value, the air flow through the shaft fill and MPZ is predominantly through the shaft fill.
- o When the conductivity of the shaft fill is low, flow through the MPZ is proportionally greater than flow through the backfill. However, because the total air flow through the MPZ and the shaft fill as compared to flow through the roof rock over the repository, is extremely low, i.e., less than 2.5%, the potential release of air through the MPZ will also be low.
- o The temperatures used at the repository horizon in the convective air flow analysis are greater than those anticipated to occur at this location. Hence the driving force for this air flow scenario is larger than what would be expected under maximum thermal convections at the repository. Also, as the repository cools and before it heats up, thermally induced air flow is of lesser consequence.

Further, obtaining a shaft fill having a hydraulic conductivity of 10^{-2} cm/s is achievable. For example, for cohesionless materials (i.e., with no clay), values may range from as high as 100 cm/s for a clean, coarse gravel or rock fill to 10^{-5} cm/s for a fine silt. Specific values within this range can be engineered by crushing and screening crushed tuff. Lower values of hydraulic conductivity can be obtained by adding clay or crushed tuff. For example, a value of about 10^{-10} cm/s can be obtained from a mixture of crushed tuff with 30% Na-bentonite (Fernandez et al., 1987, Appendix D).

3.4 Potential for Enhancing Radionuclide Release From Air Movement Due to Barometric Forces

This section evaluates the potential volumes of air displaced out of ES-1 or ES-2 due to barometric forces. These barometric forces are created by pressure differences that are induced by postulated meteorological events occurring at the exploratory shaft locations. The purpose of the analyses in this section is to predict what volume of air contained in the shaft fill and MPZ under unsaturated conditions can be displaced due to

several meteorological events. If only a portion of the shaft fill and MPZ air volume is displaced when the pressure drop occurs at the surface, the surface air will be forced into the shaft fill and MPZ when the pressure reversal (pressure increase) occurs at the surface. As a result, contaminated air that reaches the shaft is not continuously displaced by barometric forces.

3.4.1 Model Description

Air pressure differences between the repository and the surface will cause air to move through shafts and ramps accessing the repository. Air movement may also be induced through the rock. The direction of air movement will be from areas of high pressure to those with low pressure. The magnitude of the flow rate will be proportional to the pressure difference, the air conductance, and the cross-sectional area through which air flows.

A one-dimensional, air flow model was developed to evaluate flow induced by barometric changes at the surface. Assumptions used in the development of the model include:

- o Darcy's law is valid for flow through the shafts and ramps; this assumption requires that air flow be laminar.
- o Atmospheric pressure follows a sinusoidal function. Individual pressure cycles occur within minutes to a year. The amplitude of the periodic functions are related to barometric pressure highs and lows found at Yucca Mountain for various events.
- o Air in the repository behaves according to the the Ideal Gas law. For this analysis, the temperature of the repository is constant, while the mass of the air in the repository is allowed to change in response to barometric pressure variations.
- o Compressive storage of the air in the backfilled shafts and ramps and rock is negligible compared to the compressive storage in the repository.

- o The MP2 model is the same as that used in the previous analyses of convective flow.

This model is structured to describe porous media flow between the repository and the surface air in response to a sinusoidal variation in barometric pressure. The pressure within the repository will also vary sinusoidally as air leaves and subsequently reenters the repository by way of thirteen parallel pathways. In this model, these pathways are the backfills and modified permeability zones associated with all six shafts and ramps and the host rock mass itself.

3.4.1.1 Physical Model

For purposes of model development, the repository is conceived of as an enclosed volume with parallel conduits to the surface such as shown in Figure 3-31. Gas within the repository may enter or leave by way of the parallel conduits and flow within each conduit is governed by Darcy's flow law. A pathway may consist of fill emplaced in a lined shaft or ramp, the surrounding modified permeability zone or the undisturbed rock. Because the fill and modified permeability zone associated with each shaft and ramp have different conductivities, flow areas, and lengths, they are treated as independent flow paths.

3.4.1.2 Mathematical Model and Assumptions

Flow through each conduit is described by Darcy's law:

$$Q_i = \frac{K_i A_i}{L_i \rho g} (P_r - P_a) \quad (3-2)$$

where K_i = air conductivity of the i^{th} flow path,
 A_i = cross sectional area of i^{th} flow path,
 L_i = length of i^{th} flow path,
 ρ = average density of air within the permeable conduit,
 g = acceleration due to gravity,
 Q_i = volumetric flow rate (positive for flow out of repository),
 $P_a = P_r - \rho g Z_a$.

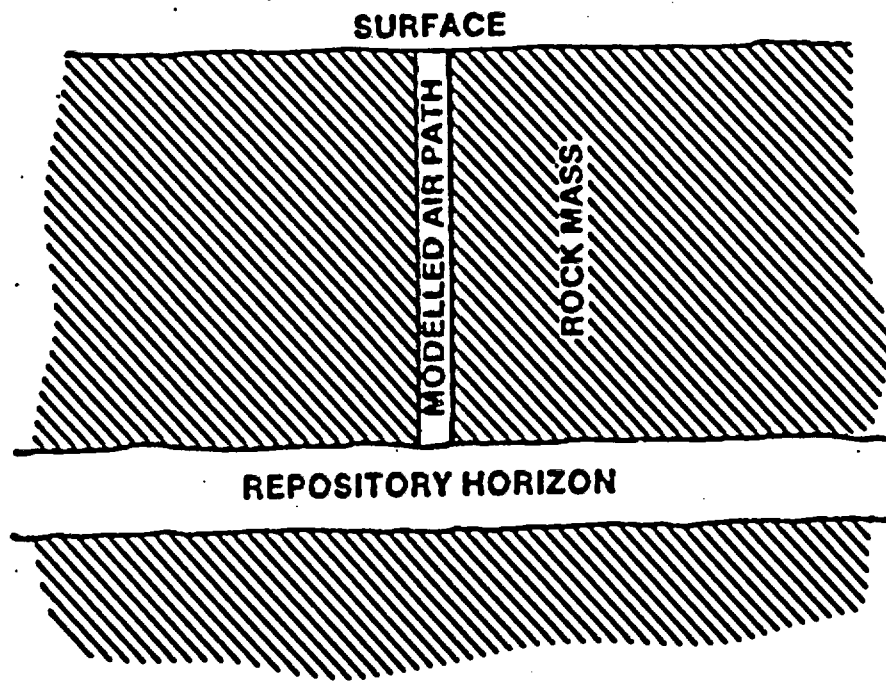


Figure 3-31. Schematic of Repository Used in Barometric Pressure Model

$$P_r = P_a + \rho g Z_r$$

P_r = repository pressure,

P_a = atmospheric pressure,

Z_r = repository elevation above a reference datum, and

Z_a = surface elevation above a reference datum.

The use of P in Equation 3-2 inherently allows for variation in the static head due to repository and surface elevation differences. Hence, the difference ($P_r - P_a$) is appropriate for all shafts and ramps.

The sum of the volumetric flow rates through all flow paths is also by a direct application of Darcy's law:

$$Q = \sum_i \frac{K_i A_i}{L_i \rho g} (P_r - P_a) \quad (3-3)$$

This volumetric flow rate may then be expressed as a molar flow rate,

$$\frac{dn_r}{dt} = -\frac{\rho Q}{M} \quad (3-4)$$

where M = the molecular weight of air,

n_r = moles of air contained within the repository, and

t = time.

The molar flow rate is also assumed to be related to the repository pressure through the ideal gas law so that

$$\frac{dn_r}{dt} = \frac{dp_r}{dt} \frac{V_r}{RT_r} \quad (3-5)$$

where V_r = repository volume,

R = ideal gas constant, and

T_r = repository temperature.

Noting that $\frac{n_r}{V_r} = \frac{\rho}{M}$ and combining Equations 3-3 through 3-5 yields an expression for the response of the repository pressure to atmospheric pressure variations:

$$\frac{dP_r}{dt} + c (P_r - P_a) = 0 \quad (3-6)$$

where

$$c = \frac{n_r RT_r}{\rho g V_r^2} \sum \frac{K_i A_i}{L_i} \quad (3-7)$$

The variation of atmospheric pressure with time is assumed to take the form of a sinusoid:

$$P_a = P_{a0} + m \sin \omega t \quad (3-8)$$

where P_{a0} = the average barometric pressure,
 m = amplitude, which is defined as $m = (P_H - P_L)/2$,
 ω = angular frequency = $2\pi/T$,
 T = period,
 P_H = average high pressure for a specific event, and
 P_L = average low pressure for a specific event.

The solution to this problem will be presented for various values of amplitude and frequency.

The significance of the constant c is that it is proportional to the ratio of the volumetric flow rate to the volume of the repository. It also influences the amplitude and phase relationships of the repository pressure under periodic conditions as described subsequently. The constant c is dependent on the air conductivity of all flow paths. The placement of shaft fill under certain circumstances affects the pressure response of the underground repository.

The solution to Equations 3-6 and 3-8 is

$$P_r = P_{a0} + \frac{m \sin(\omega t) - \frac{\omega m}{c} \cos(\omega t)}{1 + \frac{\omega^2}{c^2}} \quad (3-9)$$

The volumetric flow rate can be calculated by substituting the pressure relationships in Equations 3-8 and 3-9 into Darcy's law (Equation 3-3):

$$Q = \sum \frac{K_i A_i}{\rho E L_i} \left[m \sin(\omega t) \left(\frac{c^2}{c^2 + \omega^2} - 1 \right) - \frac{c \omega m}{c^2 + \omega^2} \cos(\omega t) \right] \quad (3-10)$$

or expressed as a sinusoid with a lagging phase angle

$$Q = \sum \frac{K_i A_i}{\rho E L_i} \frac{m \omega}{\sqrt{c^2 + \omega^2}} \sin \left[\omega t - \pi + \sin^{-1} \frac{c}{\sqrt{c^2 + \omega^2}} \right] \quad (3-11)$$

Equation 3-11 may be integrated over half of any cycle to give the amount of air entering or leaving a shaft as a consequence of the assumed barometric pressure variation. Hence, the cyclic volume of displaced air, V , is given by

$$V = \sum \frac{2K_i A_i}{\rho E L_i} \frac{m}{\sqrt{c^2 + \omega^2}} \quad (3-12)$$

Further, the cyclic volume of displaced air may be computed for any flow path, i :

$$V_i = \frac{2K_i A_i}{\rho E L_i} \frac{m}{\sqrt{c^2 + \omega^2}} \quad (3-13)$$

In Section 3.4.3 results are displayed in terms of the ratio of air displaced from a shaft, V_1 , to the volume of air in the shaft fill and MPZ. The void volume in the shaft fill was calculated from the total volume of ES-1 within the lined shaft with a porosity of 30% and a volume of the modified permeability zone and an effective, unsaturated rock porosity of 4.2%. The calculated volume of the voids in the exploratory shafts is 1,540 m³. It is assumed that the porosity of the shaft fill has a constant value of 30%. This value is at the lower range of porosities (i.e., 25 to 50%) for natural granular materials and artificial materials, indicated by standard texts (e.g., Winterkorn and Fang, 1979, p. 257, Davis and DeWeist, 1966, p. 375).

3.4.2 Input to the Mathematical Model

The cyclic volumetric displacement relationship developed in the previous section suggests that the displaced volume is proportional to the pressure amplitude and inversely proportional to the frequency of the weather event (proportional to the period). To cover a range of potential weather events, the following were considered:

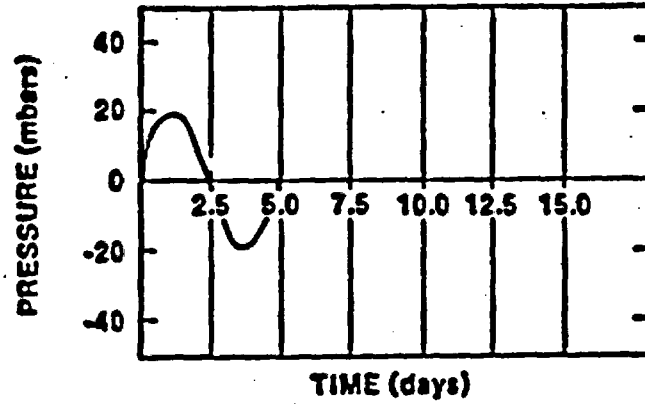
- o A severe thunderstorm event with a time period of five days
- o A tornado event with a time period of one minute.
- o A seasonal barometric pressure event with a time period of one year

These events are indicated schematically in Figure 3-32 and include a low frequency/low amplitude seasonal event, an intermediate frequency/intermediate amplitude event and a high frequency/high amplitude tornado event.

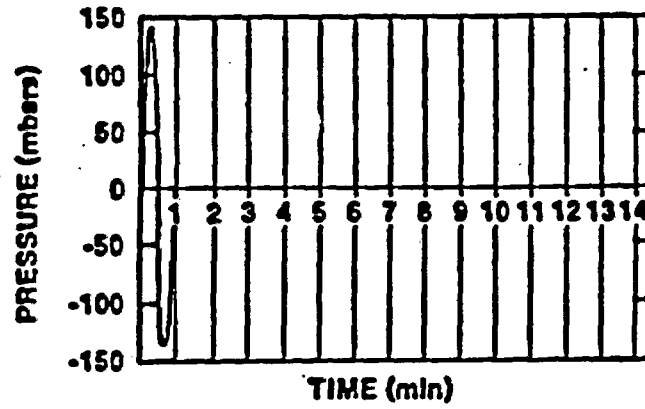
The severe thunderstorm event represents a bounding event to typical atmospheric pressure fluctuations (movement of weather fronts) that might occur at Yucca Mountain. The average high and low pressures for the months January through December have been compiled by the DOE (1986, p. 3-48) and indicate that the pressure amplitude ranges from 8.6 mbars to 19.0 mbars (0.25 to 0.56 in. Hg). Various strip charts at Yucca Mountain have been reviewed and indicate that a typical pressure variation for thunderstorm event occurs over approximately five days.

There are no published values for barometric pressure fluctuations for tornadoes which is due to pressure measurement difficulties during such events. An approximate value may be derived from the Bernoulli equation for conservation of energy for fluid flow and the equation of state for an adiabatic expansion of air. If it is assumed that the initial pressure is 850 mbars (25.1 in. Hg), and that the tornado event results in an air velocity of 200 mph (89.4 m/s), then the calculated drop in pressure is 132 mbars (3.9 in Hg). This calculated value may be compared to the difference between high and low pressure extremes recorded in the United States (Valley, 1986, p. 3-30). The high and low extremes are 1,063.3 and 954.8 mbars respectively with a difference of 108 mbars or an equivalent

EVENT 1 - THUNDERSTORM



EVENT 2 - TORNADO



EVENT 3 - SEASONAL FLUCTUATION

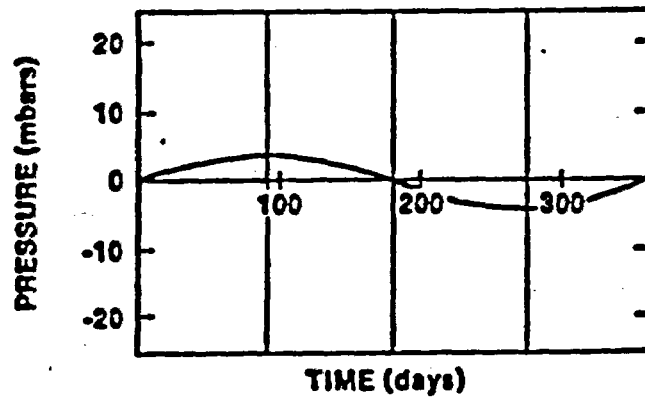


Figure 3-32. Barometric Pressure Events

pressure amplitude of 54 mbars. It is further assumed that the tornado pressure event would hover over the exploratory shaft for approximately one minute (Church, 1987).

The seasonal fluctuation in barometric pressure is derived from differences between average pressures in January and June (DOE, 1986, p. 3-48). The calculated difference is 3.0 mbars (0.09 in. Hg).

Other parameters are required for conducting analysis, these include: 1) the air conductivities of the shaft fill, the surrounding MPZ, and the undisturbed rock; 2) the lengths and areas of the parallel flow paths; 3) the volume of the repository; and 4) the repository temperature.

In these analyses, the same range of shaft fill, air conductivities, the same combination of rock conductivities, and the same modified permeability zone models were used as the convective air flow analyses. The analyses were conducted for both vertical and horizontal emplacement options as in the convective air flow analysis. Tables 3-2 and 3-3 summarize cross-sectional areas and lengths for each of the flow paths.

The cross-sectional area of rock flow path was again taken to be equal to the combined roof area of all underground mains, submains and rooms (983,700 m² for vertical emplacement or 486,000 m² for horizontal emplacement). The area of modified permeability zones surrounding either shafts or ramps was taken as three times the excavated area. In addition, the temperature of the air underground was taken as 115°C for determining the mass of air in the repository.

3.4.3 Model Results

The results of the analysis are presented as a series of plots relating the ratio of total flow or displaced volume out of ES-1 to void volume in ES-1*, and the surrounding MPZ versus backfill air conductivity. A

*While the discussion for these analyses focus on the ES-1, the results are equally applicable for the ES-2 because the size of the ES-2 and its MPZ are equal to ES-1.

series of six plots for vertical emplacement are presented in Figures 3-33 through 3-38 for the three pressure events and the two modified permeability zone models. The complementary set of six plots for horizontal emplacement are presented in Figures 3-39 through 3-44. Each plot presents three curves for the three cases of rock air conductivity presented previously.

For vertical or horizontal emplacement, the results indicate that the displaced volume out of ES-1 is dominantly affected by flow through the shaft fill at high shaft fill, air conductivities and by flow through the modified permeability zone (MPZ zone conductivities is dependent on rock air conductivity) at low, shaft fill, air conductivities. For example, in Figure 3-33 for Event 1 and the low conductivity MPZ model, the analysis indicates that one to 10 times the void volume might be displaced if the shaft fill, air conductivity were greater than 1 m/min. The displaced volume is independent of both the MPZ and rock conductivity. For shaft fill, air conductivities less than 10^{-2} m/min, the MPZ is more dominant, and the displaced air volume becomes independent of shaft fill, air conductivity for the high rock air conductivity combination. Similar trends are observed for the low and intermediate air conductivity combinations. The analysis indicates that 1/10,000 to 1/100 times the void volume would be displaced out of the shaft for frequently occurring weather events if a low conductivity backfill were emplaced in the shafts and ramps. Further for low conductivity backfill, flow through the shaft and MPZ is directly proportional to the MPZ conductivity because very little air escapes through the backfill. The analyses indicate that placement of a low conductivity backfill will be very effective in reducing the flow volume if the surrounding MPZ has low conductivity.

It is interesting to note that a lower rock air conductivity results in the displacement of somewhat greater amounts of air at higher shaft fill, air conductivities. The "cross over" phenomenon is related to the pressure phase relationship that develops between the surface and the underground repository. As seen from Equation 3-9, if the characteristic constant c is large, then the atmospheric and repository pressures are in phase, and the differential pressure inducing the flow rate is smaller resulting in a smaller displaced volume (Equation 3-11).

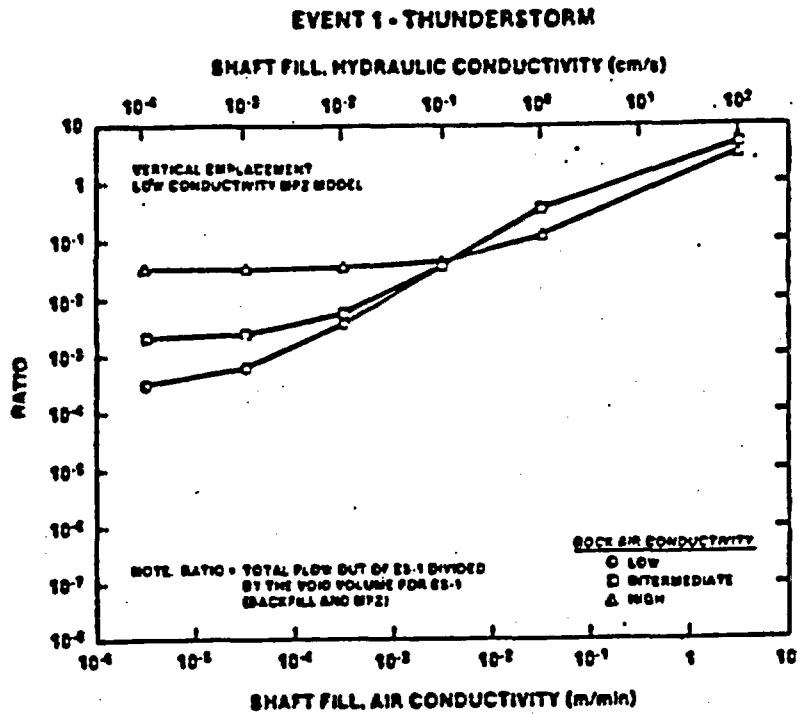


Figure 3-33. Ratio of Displaced Air Volume to Void Volume for ES-1 (Vertical Emplacement and Low Conductivity MPZ Model) for a Severe Thunderstorm Event

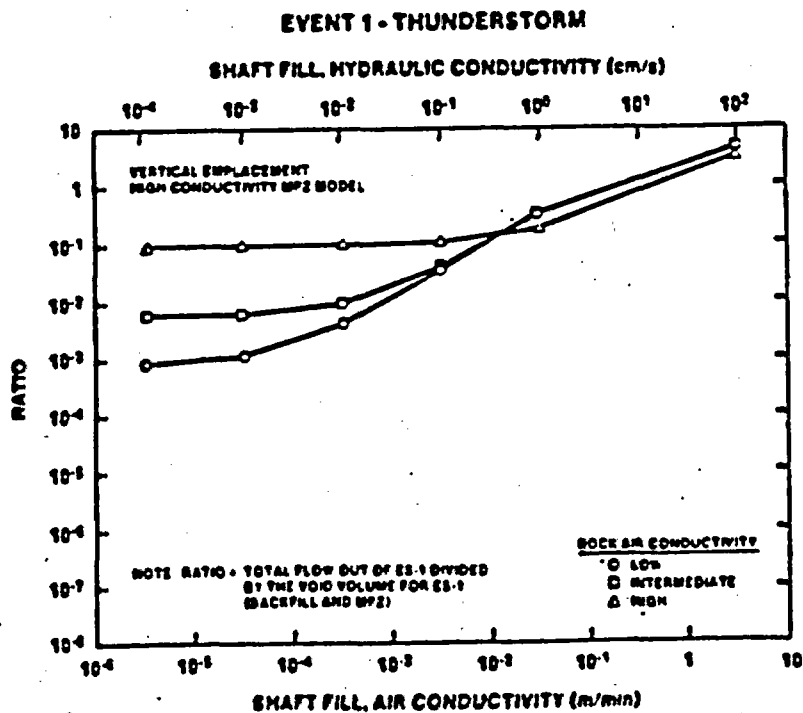


Figure 3-34. Ratio of Displaced Air Volume to Void Volume for ES-1 (Vertical Emplacement and High Conductivity MPZ Model) for a Severe Thunderstorm Event

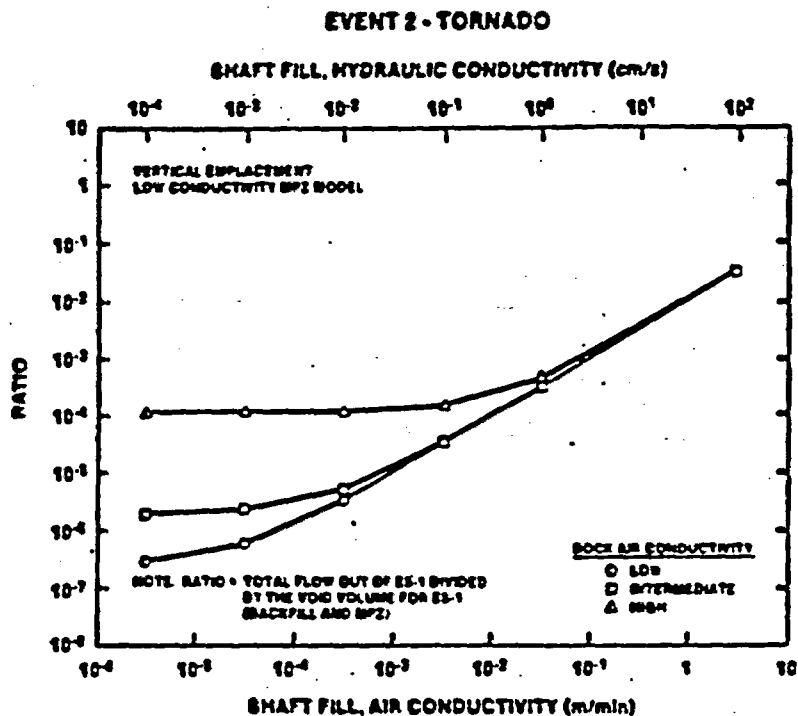


Figure 3-35. Ratio of Displaced Air Volume to Void Volume for ES-1 (Vertical Emplacement and Low Conductivity MPZ Model) for a Tornado Event

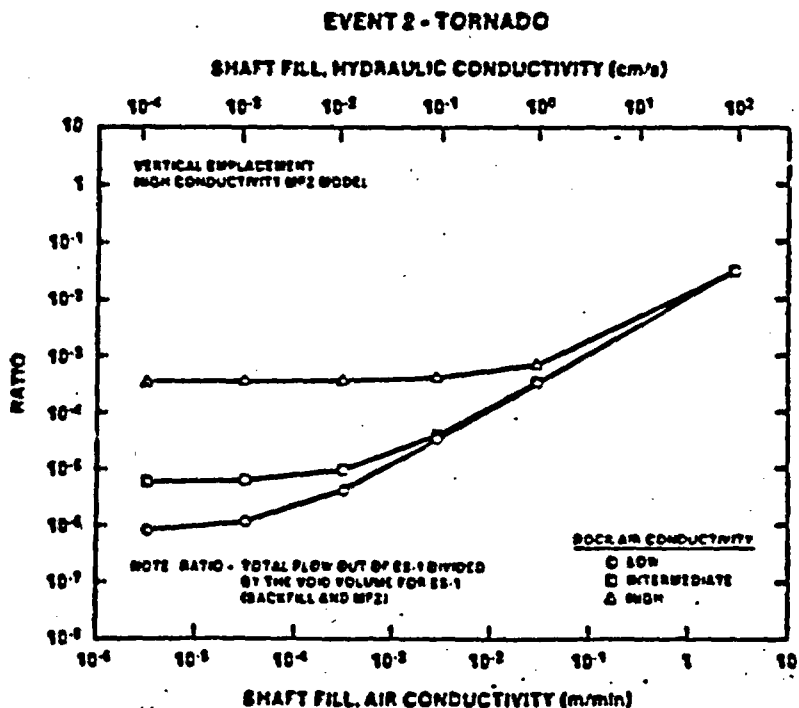


Figure 3-36. Ratio of Displaced Air Volume to Void Volume for ES-1 (Vertical Emplacement and High Conductivity MPZ Model) for a Tornado Event

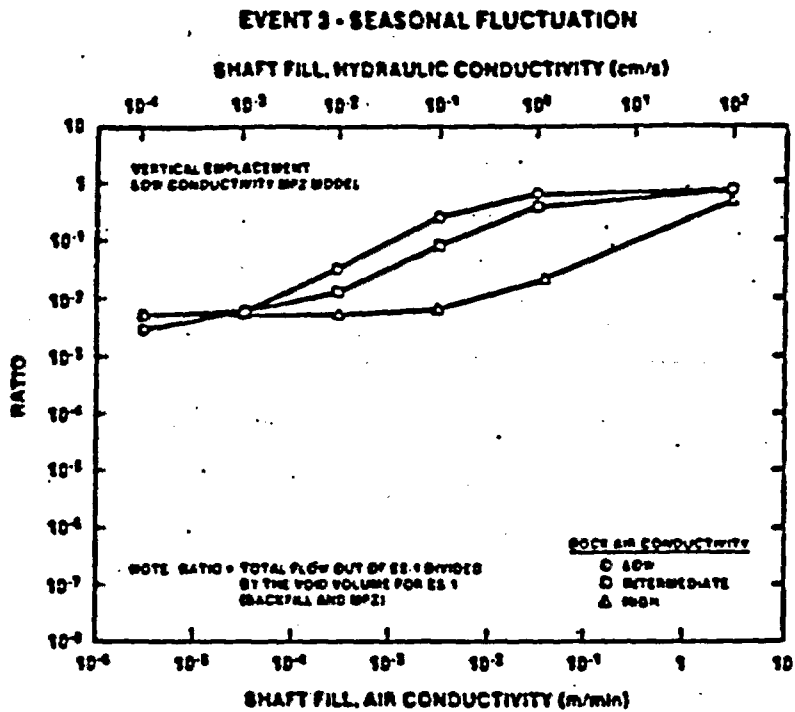


Figure 3-37. Ratio of Displaced Air Volume to Void Volume for ES-1 (Vertical Emplacement and Low Conductivity MPZ Model) for a Seasonal Event

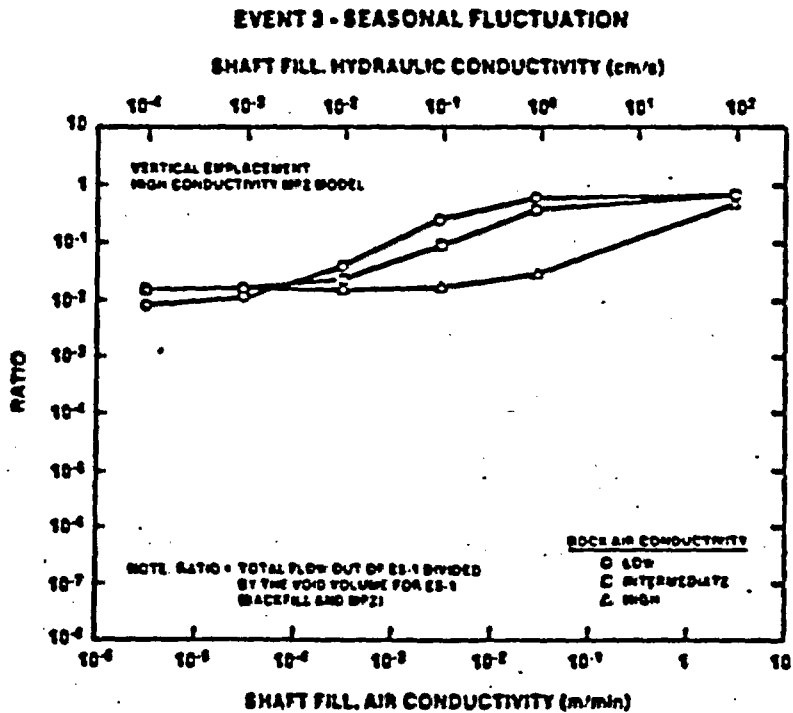


Figure 3-38. Ratio of Displaced Air Volume to Void Volume for ES-1 (Vertical Emplacement and High Conductivity MPZ Model) for a Seasonal Event

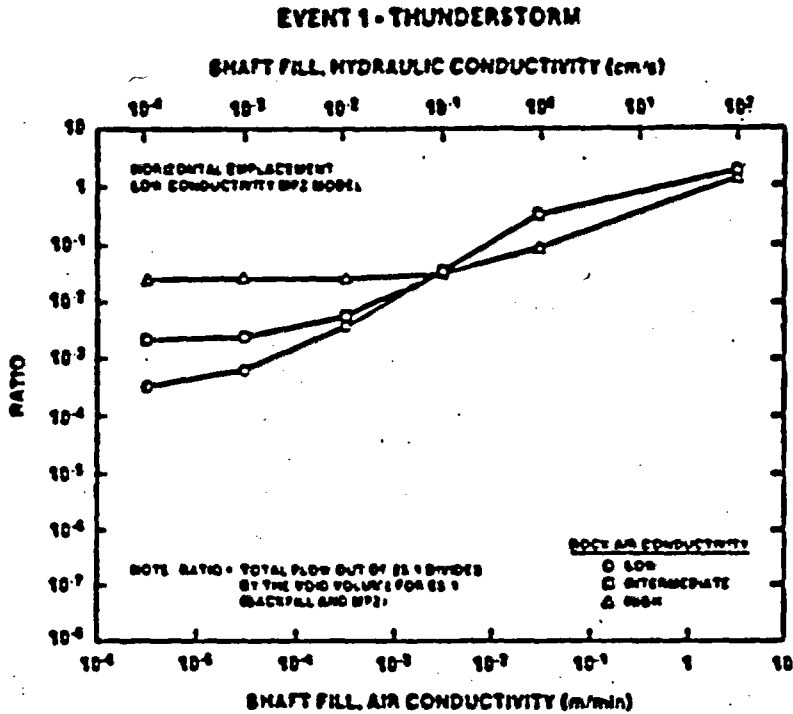


Figure 3-39. Ratio of Displaced Air Volume to Void Volume for ES-1 (Horizontal Emplacement and Low Conductivity MPZ Model) for a Severe Thunderstorm Event

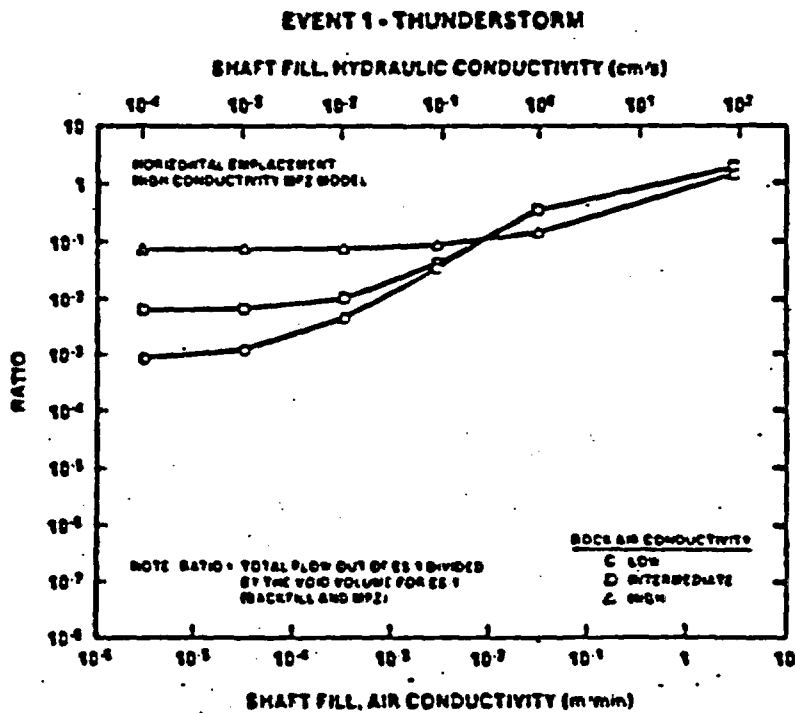


Figure 3-40. Ratio of Displaced Air Volume to Void Volume for ES-1 (Horizontal Emplacement and High Conductivity MPZ Model) for a Severe Thunderstorm Event

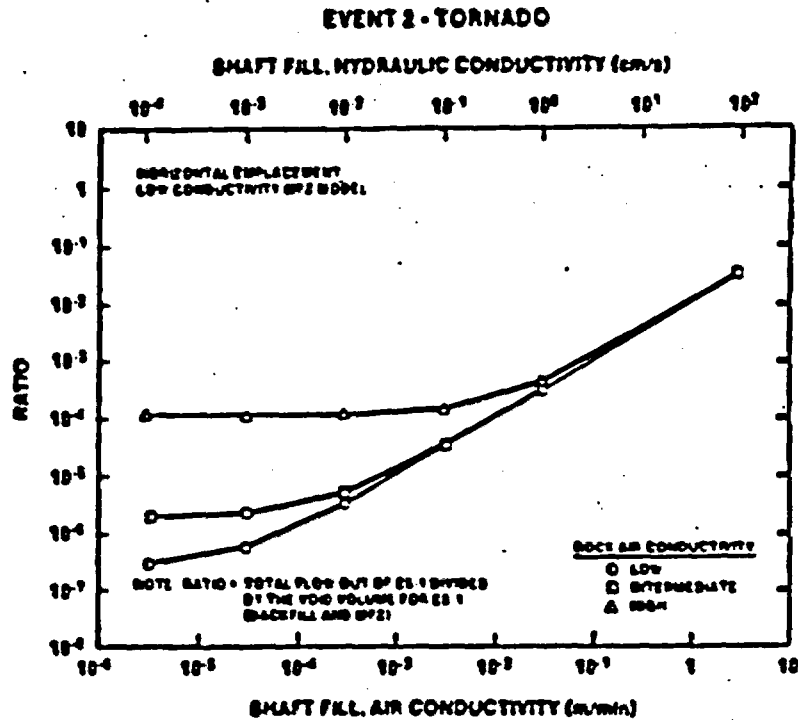


Figure 3-41. Ratio of Displaced Air Volume to Void Volume for ES-1 (Horizontal Emplacement and Low Conductivity MP2 Model) for a Tornado Event

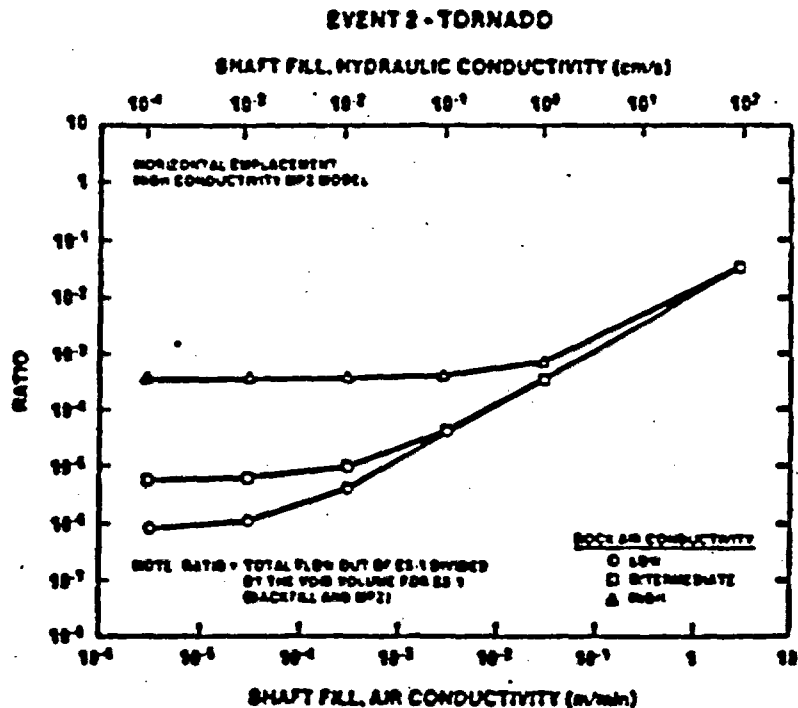


Figure 3-42. Ratio of Displaced Air Volume to Void Volume for ES-1 (Horizontal Emplacement and High Conductivity MP2 Model) for a Tornado Event

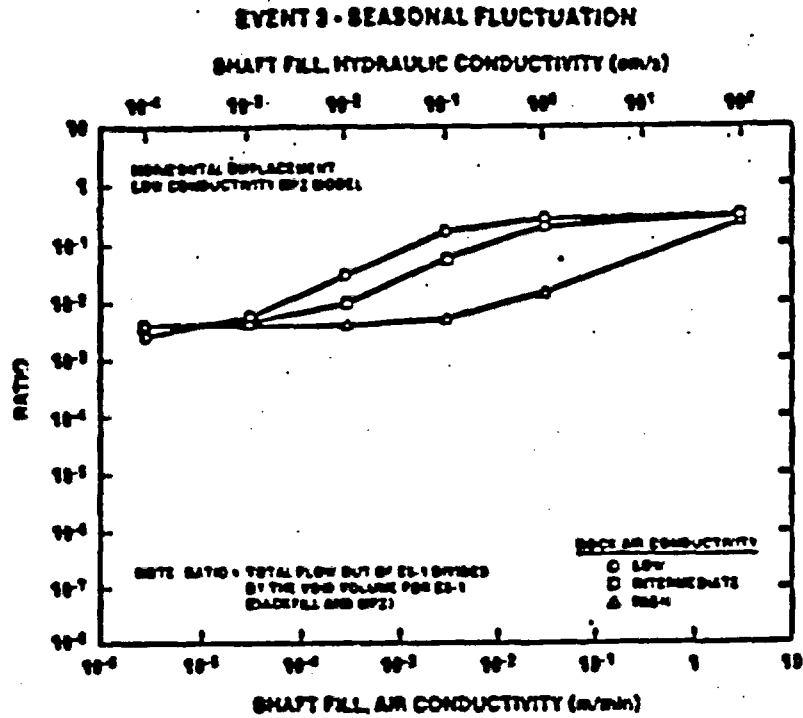


Figure 3-43. Ratio of Displaced Air Volume to Void Volume for ES-1 (Horizontal Emplacement and Low Conductivity MP2 Model) for a Seasonal Event

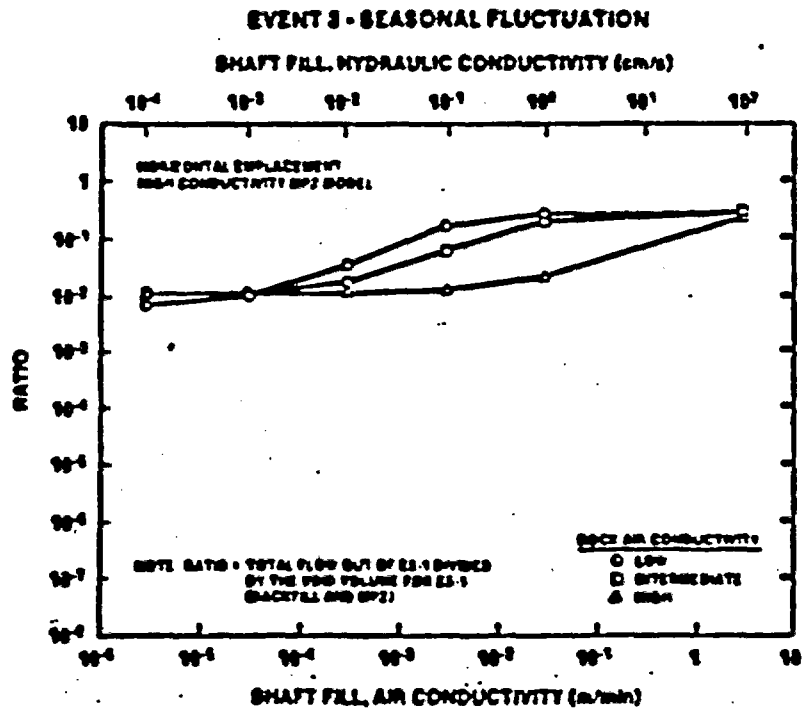


Figure 3-44. Ratio of Displaced Air Volume to Void Volume for ES-1 (Horizontal Emplacement and High Conductivity MP2 Model) for a Seasonal Event

In comparing displaced air volumes out of the exploratory shaft for various pressure events, it is apparent that the severe thunderstorm event is most significant, and the tornado event least significant. As seen from Equation 3-13, when the frequency of the event is high (equivalent to a small period), the displaced volume is inversely proportional to the frequency (proportional to the period), and the displaced volume is dominantly affected by the high frequency. The large pressure amplitude is of secondary importance for the tornado event. For the severe thunderstorm, the frequency is lower (by three orders of magnitude) and results in a higher displaced volume. The seasonal barometric pressure event is of intermediate significance. Because of the low frequency (equivalent to a large period) of this event, the ratio at large, shaft fill, air conductivities approaches a constant of 7/10 of the volume in the exploratory shaft. This may be seen from Equations 3-7 and 3-13 in which the frequency of the pressure event is much smaller than the c constant. The substitution of the relationship for the c constant (Equation 3-7) into the displaced volume relationship (Equation 3-13) results in the displaced air volume approaching a constant where the shaft fill, air conductivity is high, and flow is dominantly through the fill of shafts and ramps.*

The results of the analysis for the horizontal emplacement option are similar to the results for the vertical emplacement option at low backfill conductivities for the several events. This is because, at low, shaft fill, air conductivities, flow is dominantly through the modified permeability zone of the ES-1 which is identical for the two emplacement options. At high, shaft fill conductivities, the ratio of displaced air volume to void volume of the exploratory shaft is somewhat lower owing to the smaller mass of air in the underground repository for the horizontal emplacement option.

*The displaced air volume approaches an asymptote which is dependent on the initial air in the repository, the pressure amplitude, and the ratio of the conductance of the exploratory shaft (ES-1) flow path to the sum of the conductances of the other flow paths.

3.4.4 Conclusions

From the barometric, air flow analyses presented above, it is concluded that the exploratory shafts (including shaft fill and the MPZ) are not likely to be preferential pathways for gaseous radionuclide releases if the air conductivity of the shaft fill is less than about 10^{-1} m/min. This conclusion is reached because the volume of air in the exploratory shafts is not fully displaced during the occurrence of a broad range of meteorological conditions if the shaft fill, air conductivity is less than about 10^{-1} m/min.

Further, if the shaft fill, air conductivity is restricted to a value of 3×10^{-4} m/min, as recommended from the convective air flow analysis, the proportion of air displaced from the exploratory shafts is computed to be very low for the three meteorological conditions considered:

- o For a thunderstorm event, the displaced air volume from the exploratory shaft is always computed to be less than 1/10 of the total air volume in the shaft fill and the MPZ when the shaft fill, air conductivity is less than 3×10^{-4} m/min. Even when the shaft fill, air conductivity is high, less than approximately 0.1 m/min, the total volume of air in the shaft fill and the MPZ is not displaced.
- o For a tornado event, in all cases evaluated, the displaced volume of air from the shaft fill and the MPZ is always less than the total volume of air in the shaft fill and MPZ. When the shaft fill, air conductivity is 3×10^{-4} m/min the amount of air displaced is always less than 1/1000 of the total volume of all in the shaft fill and MPZ.
- o For a seasonal fluctuation event, in all cases evaluated, the displaced volume of air is always less than the total volume of air in the shaft fill and the MPZ. When the shaft fill, air conductivity is 3×10^{-4} m/min, the amount of air displaced is about 1/10 or less of the total volume of air in the shaft fill and the MPZ.

3.5 Remedial Measures to Restore the Modified Permeability Zone

When considering methods for the restoration of the MPZ, it is assumed that a plug would be constructed to reduce the flow of water down the shaft or the shaft/rock interface zone. It is further assumed that the plug would be keyed into the rock (Figure 3-45). This provides the most direct treatment or localized restoration of the MPZ, in that when a keyway is excavated, the more intensely fractured portion of the MPZ is removed. The structural performance of a plug keyed into the surrounding rock is also advantageous since overlying backfill loads would be transferred in bearing compression to the surrounding rock. A plug keyed into the rock should exhibit a higher rigidity when subjected to thermal or seismic loads than a simple, nonkeyed plug.

The construction sequence entails making saw cuts at the top and bottom of the plug, removing the liner, excavating the keyway, backfilling to the underside of the plug, placement of concrete, and contact grouting. Initial saw cuts -23 cm deep around the top and bottom of the plug are made. A series of holes is drilled horizontally at the top of the seal to the full depth of the keyway and perhaps loaded with an expansive agent. Because of the high strength of welded tuff, mechanical excavation of a keyway may not be feasible, and other methods similar to those employed in liner removal supplemented by hand methods could be used for rock excavation. The keyway is fragmented and excavated over a length of several meters to provide a larger working area. Excavation of the keyway then proceeds from the top to the bottom of the plug. To accomplish this excavation vertical holes on a precise pattern are drilled and loaded with an expansive agent from this working area to remove the rest of the keyway. The rock is removed to the surface. Fill is then emplaced to the base of the plug. The concrete is placed and allowed to mature for a period of time to achieve adequate strength and stiffness.

Methods for the treatment and restoration of the MPZ surrounding the keyway include

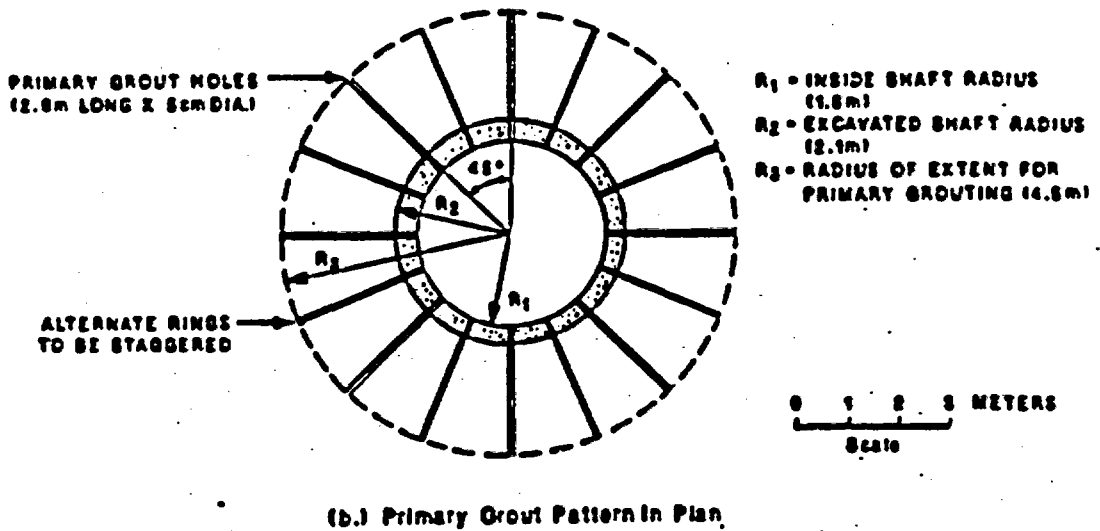
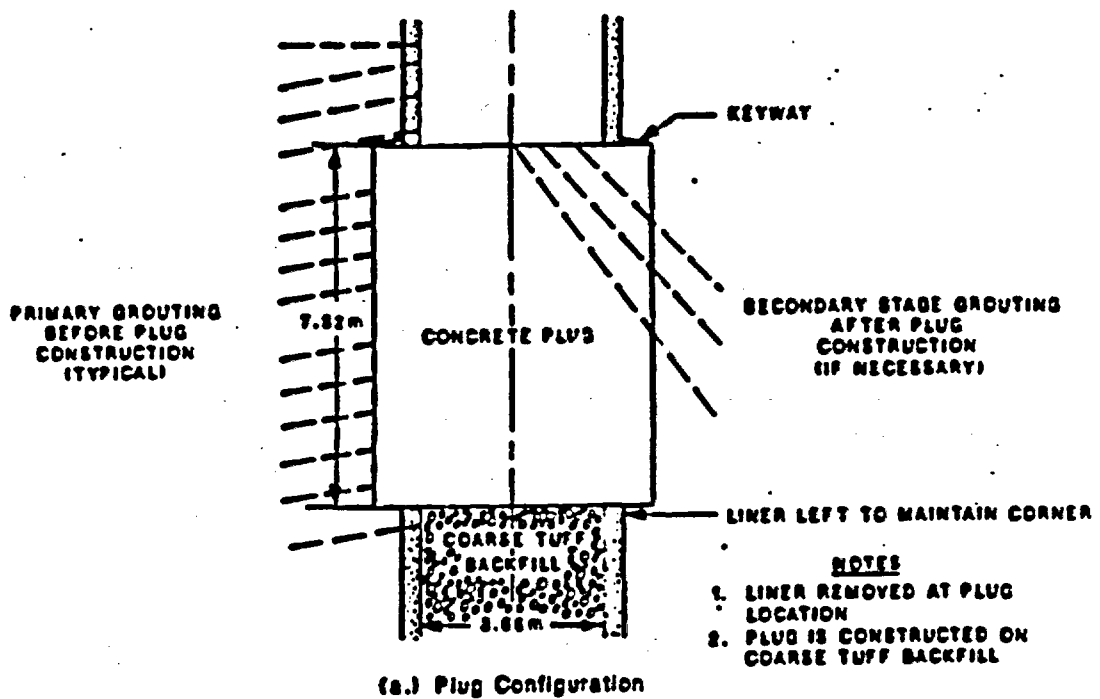


Figure 3-45. Schematic of MPZ Restoration and Shaft Seal Emplacement

- o the use of an expansive concrete and temperature control to develop interface stress and close fractures in the MPZ, and
- o primary and secondary grouting of the MPZ.

3.5.1 Restoration of the MPZ by Grouting

Emplacing grout in fractures is expected to reduce permeability in the MPZ. Grouting will reduce permeability in both the blast-induced and stress-induced fractures, irrespective of whether the rock deformed elastically or inelastically. However, grouting is not likely to increase rock mass strength significantly or increase structural stability. If grouting is needed, selection of the grout type and the method of grout application will be made based on the characteristic of the fractures defined during exploratory shafts testing.

Grouting might be performed either before or after liner removal and plug emplacement (primary) or after liner removal and plug emplacement (secondary). There are advantages to pregrouting the plug location before removal of the liner. After liner removal, there would be a gap of approximately 0.6 m or more between the work stage and the shaft walls. It is easier to locate grout pipes on the smooth surface of the concrete liner. The grouting pattern might consist of a series of eight holes with alternate rings staggered. This pattern would result in a hole spacing of approximately 1.5 m near the shaft and 3.5 m at a distance of 4.5 m from the shaft excavation (see Figure 3-45). Note that the distance would depend on the size of the MPZ at the plug location. At the ends of the holes, only the open fracture zones would have continuity of grout between holes. By redrilling holes several times and grouting, a nearby impermeable barrier would be formed by a "laced" grout structure similar to the pattern proposed by Kelsall et al. (1982, p. 122) for drilled cutoffs.

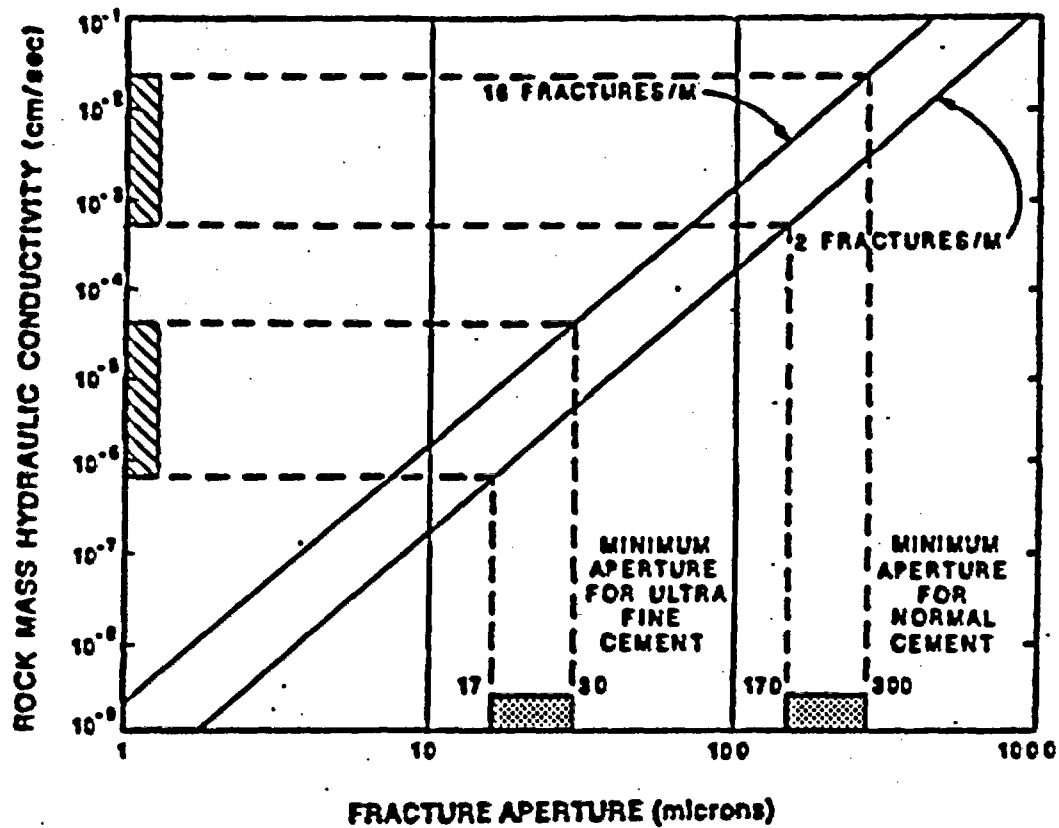
Primary and secondary grouting might be effective in reducing permeability of the MPZ. A series of holes is drilled to intercept conductive fractures either before (primary) or after (secondary) plug emplacement. The grout is selected to have a small particle size and low viscosity to penetrate under pressure into the thin fracture zones. Tests by Waterways

Experiment Station, (Kelsall et al., 1982, p. 113) showed that the ratio of crack thickness to grout particle size should be at least 1.7 and preferably 3.0 or more for adequate penetration. For ordinary cements, the maximum particle size is about 100 μm , but this can be reduced to 10 μm using ultrafine cement. Therefore, the minimum size of aperture that could be grouted is 17 to 30 μm . The relationship of rock mass hydraulic conductivity to fracture aperture over a range of fracture spacing (Langkopf and Gnirk, 1986) is shown in Figure 3-46. Over the expected range of bulk rock, saturated hydraulic conductivities for welded tuff of 10^{-5} to 10^{-2} cm/s (Fernandez et al., 1987), grouting is feasible using either a normal cement for a welded tuff conductivity of from 10^{-3} to 10^{-2} cm/s or an ultrafine cement from 10^{-5} to 10^{-6} cm/s.

While there is precedence for pressure grouting of shafts and tunnels under a variety of conditions (Dietz, 1982, pp. 602-608), there are a number of operational factors to be considered in constructing a grout curtain. These include the distance and time for transporting the grout, the required injection pressure, frictional losses through pipes, and grout setting time. At shallow depths, the use of packers may suffice to seal off sections of the injection hole; at greater depths, steel grout pipes may be required since greater injection pressures would be used. These factors increase the complexity of the design prior to field operations and require sampling the grout for physical properties during grouting.

3.5.2 Restoration of the MPZ Using Expansive Concrete

The use of an expansive concrete has been proposed elsewhere (Case et al., 1984). In this method, a concrete is selected that forms the expansive agent ettringite during cement hydration, resulting in volumetric expansion. The volumetric expansion in turn results in the development of interface stress, which will close fractures in the adjacent MPZ and thereby reduce the permeability in the MPZ. The degree to which volumetric expansion is effective depends on a number of factors: the temperature and moisture environment, evolution of the thermomechanical properties, and the degree of external restraint. Placement temperatures affect volumetric expansion of the concrete. A lower placement temperature results in elimination or reduction of the heating/cooling cycle and the development



LEGEND



MINIMUM CONDUCTIVITY THAT MAY BE GROUTED USING ULTRA FINE OR NORMAL CEMENT



MINIMUM APERTURE THAT MAY BE GROUTED USING ULTRA FINE OR NORMAL CEMENT

Figure 3-46. Minimum Conductivity for Grouting

of higher interface stress. In using an expansive concrete, it is desirable to pour the plug (250 m³) in one operation to avoid potential leakage paths through construction joints. Auld (1983, pp. 209-211) describes methods of cooling aggregates and mixing water to eliminate undesirable thermal effects. An alternative is to provide pipes filled with circulating water during cement hydration that are subsequently grouted.

The use of an expansive concrete to apply stress to the surrounding MPZ is most efficient where the stress-induced disturbance is caused by elastic deformation. If deformations are elastic, then the reapplication of stress would result in closure of open fractures. If deformations are inelastic, then stress reapplication might not result in the closure of fractures and restoration of permeability. The use of an expansive concrete would result in increased rigidity and increased confining stress in the plug and surrounding rock. The structural stability of the plug, when subjected to backfill, thermal, and seismic loads, would be enhanced. There would be less tendency for shear failure at the plug rock interface when the plug is subjected to combined loading.

The constructibility of the plug may be a key issue in the use of expansive concrete because use of an expansive concrete to restore an MPZ has not been demonstrated. As mentioned previously, the success of the method will be dependent on environmental control of moisture and temperature. Sampling of concrete and monitoring of temperature and other performance parameters may be required during and following construction of the plug. For these reasons use of an expansive concrete alone to restore the MPZ is not recommended.

3.5.3 Conclusions

From the preceding discussion, it is concluded that grouting in welded tuff is feasible and the currently preferred method for restoring the MPZ. This method is preferred because drilling smooth-walled, grout holes allows an examination of fractures in the modified permeability zone. Also, at present, it is not certain how large an interface stress can be developed through the use of only an expansive concrete or how effective such stress development would be in closing fractures.

Grouting the MPZ, however, does incur a greater cost. In Appendix D, the costs for liner removal in the vicinity of the plug and the construction of the plug are given. The estimated costs of primary and contact grouting add \$145,000 to the \$380,000 for plug construction. At this stage of the design process, these costs are intended to be used only in a comparative way.

This page is for page number only

4.0 INFLUENCE OF THE SHAFT LINER ON THE PERFORMANCE OF THE YMGDS

In this chapter, the influence of the shaft liner on the performance of the YMGDS is evaluated. When a concrete liner is placed in the ESs, it will alter the ground-water chemistry and in turn be altered by the ground water. The expected changes are the result of leaching alkaline species from the cement. The concrete will become more permeable as minerals dissolve. Similarly, the ground water, coming in contact with the concrete liner, will become unstable when its pH is increased, and precipitates will form in the ground water. These precipitates will then lodge in pore spaces within the shaft fill and in the MPZ. The potential for changing the hydraulic conductivity of the liner is evaluated in Section 4.1 and the effect of precipitate formation is evaluated in Section 4.2.

4.1 Changes in the Hydraulic Conductivity of the Liner

It is anticipated that the concrete liner will be formed with conventional materials including aggregate, sand, and cement. For these formulations, the aggregate and sand portions of the concrete are essentially inert, and all chemical interactions occur with the cement phase. Also, the hydraulic conductivity of concrete is dependent almost completely on the hydraulic conductivity of the cement phase.

When ground water comes into contact with a cement, naturally occurring aqueous carbonate reacts with alkali and excess portlandite to modify the cement structure. Carbonate minerals are deposited within the pore structure of the cement, so that the natural tendency of the cement to shrink and crack will be partially offset by the deposition of new minerals.

In assessing how the hydraulic conductivity of the concrete liner may change due to chemical alterations, it is first important to know the initial hydraulic conductivity. The range of typical hydraulic conductivities for concrete is 10^{-8} to 10^{-6} cm/s, although hydraulic conductivities less than 10^{-10} cm/s are achievable (Mather, 1967). Values for saturated conductivities obtained through laboratory testing of a

grout, mortar, and a concrete, determined as part of the NNWSI Repository Sealing Program, varied from 1.6×10^{-10} to 9.5×10^{-10} cm/s (Fernandez et al., 1987, Appendix G).

Because the waste emplaced in the repository can elevate the rock temperature surrounding the waste disposal area, it is important to know how the elevated temperatures could affect sealing components. Hydro-thermal experiments were performed at Pennsylvania State University (PSU) (Licastro et al., in preparation) to determine the effect of temperature and moisture on selected seal materials. Two of the materials (grouts and mortars) had the same composition as the grout and mortar reported in Fernandez et al. (1987, Appendix G). The hydraulic conductivity of these materials was evaluated after the materials were exposed to water having a composition of J-13* water at 38°, 60°, and 90°C. Initial conductivities in all PSU cases ranged between 10^{-10} and 10^{-11} cm/s. These initial conductivities are at the low end of the conductivity spectrum for grouts. For all of the materials evaluated, no increase in hydraulic conductivity was observed at 38°C over a 1-year period. At 60°C, one cement sample showed a small increase in conductivity after 1 month, with no other changes noted after that. Finally, at 90°C, one sample showed a small increase in conductivity after 90 days. It is recognized that the application of short-term, high-temperature experiments to long-term performance may require further evaluation.

Using the results of Blanford reported in Morales (1985), the temperature field at different portions of the liner can be approximated. We estimate that the top 220 m of the shaft will always be less than 38°C and all but the 40 m above and below the repository horizon always less than 60°C. Because alteration of the shaft liner at 38°C and possibly 60°C will probably be limited, as indicated by the laboratory experiments cited above, surface-water infiltration through the shaft liner will be significantly impeded by the shaft liner.

*Water from well J-13 has been selected as the reference water for experimental studies in the NNWSI project (DOE, 1988, pp. 4-39 and 7-10).

From the discussion above, the potential for significant changes in the hydraulic conductivity of the concrete liner is expected to be low. Therefore, surface-water infiltration through the shaft liner will be impeded by the liner. Certainly, the assumption that the hydraulic conductivity of the shaft liner is 10^{-2} cm/s* assumed in Chapter 3.0 is extremely conservative. This assumption implies that the hydraulic conductivity of the concrete liner would have to change from a range of 10^{-6} to 10^{-10} cm/s to 10^{-2} cm/s over the entire length of the shaft liner.

If the liner at the base of the shaft behaves in a similar way, water within the shaft fill would be impeded from draining into the surrounding rock. This discussion suggests that if restriction of surface-water flow is desired, leaving the concrete liner in place above the repository horizon, particularly in the upper portion of the shaft where the temperature field is lower, would be prudent. If water drainage from the base of the shaft is desired, removal of the liner below the repository horizon would probably be necessary.

4.2 Effect of Ground-Water Chemistry on the Hydraulic Conductivity of the Exploratory Shaft Fill and Modified Permeability Zone

In addition to modification in the hydraulic conductivity of the shaft liner, the liner itself may cause minor modifications to the ground water. These water chemistry changes may cause the ground water to become super-saturated with some minerals, and precipitation, following leaching of species from the liner (see Section 4.2.1), could then occur. The amount of these precipitates as well as their eventual destinations is projected in Section 4.2.3.

Water entering the ES could have a range of possible concentrations depending upon the source of the water. The primary source of water could have a variety of compositions. It could be rainwater, water equilibrated with alluvium, water equilibrated with tuff, or any of a variety of ground waters. In this paper, we have assumed that the starting water composition is that of J-13 water (Ogard and Kerrisk, 1984, pp. 9-12). In future work,

*This value is representative of a silty sand.

we will consider the other possible choices through the use of the computer code EQ3/6 (Wolery, 1979).

Further, we have assumed that local equilibrium will apply throughout the ES. In actuality, there are several rate phenomena that are operative. The leaching of minerals from the cement is governed by the diffusion of ionic species in the pore spaces of the cement and by the diffusion and dispersion of those same chemical species in the rock backfill and MPZ. Lastly, there are chemical kinetic rate processes to be considered. The above-mentioned rate processes will tend to limit pH increase of the ground water and the amount of precipitate released. Hence, the assumption of local equilibrium is a conservative one that leads to the maximum calculable change in the ground-water chemistry.

~~Leaching~~ Leaching of Alkaline Species From the Concrete Liner

A typical Portland cement is composed of three major hydrated phases: calcium silicate hydrate, tricalcium aluminate hydrate, and tetracalcium aluminoferrite hydrate. In the presence of sulphate, we also have an ettringite phase. In addition to these major phases, minor amounts of unreacted portlandite, Ca(OH)_2 , and sodium and potassium alkalis are present. A typical portland cement will contain between 0.05% and 0.15% of dissolvable alkali (Glasser et al., 1984). It is these alkalis that are primarily responsible for increasing the pH of any water that contacts cement. As will be seen in Section 4.2.2 these alkalis are the primary cause of ground-water instability. Further, the cement pore fluid will contain increased concentrations of H_2SiO_4 , Na^+ , K^+ , OH^- , and perhaps SO_4^- . The actual concentration of these species in the ground water contacting cement will depend on the water flow rate, where higher concentrations are expected at lower flow rates. Barnes (1983, p. 298) gives the pore fluid concentration of alkali after 7 days of hydration as 0.75 M. This corresponds to a pH of 13.88 for the pore fluid. After this initial small percentage of alkali has been leached from the cement, the pH of the pore fluid is dominated by the Ca(OH)_2 equilibrium (Glasser et al., 1984), and the pH of the pore fluid is expected to drop to 12.5 (Lea, 1971, p. 185).

Leaching of cement is represented by the diffusion of Na^+ , K^+ , OH^- , and possibly SO_4^{2-} through the pore spaces of the cement. All other ionic species are not expected to be present in significantly increased concentrations. In related experimentation at PSU, B. E. Sheetz and D. M. Roy (in preparation) have considered the leaching of a particular ettringite bearing concrete, formulation 82-022,* by J-13 ground water, where the water-to-solid mass ratio was 10:1 and the test was an immersion test at 90°C for 3 months. Results of this experimentation are shown in Table 4-1.

As may be seen in the table, only ions Na^+ , K^+ , SO_4^{2-} , and OH^- are significantly greater than the J-13 composition. All other species, are no more than 1 mg/l greater than their starting composition. Of these species, OH^- is potentially the most important in affecting the performance of the ES, as will be discussed in 4.2.2.

A diffusion model of the cement liner is postulated to estimate the concentration of ions that reach the ground water. The cement liner is considered to be a slab 30.5 cm thick, where the cement pore fluid assumes an equilibrium value and the surface of the liner has a concentration assumed to be zero. Under this assumption the maximum flux of any ionic species may be determined through an adaptation of Example 11.1-2 in Bird et al. (1960, p. 354). Using the analog between heat and mass transport and differentiating analogous expression for concentration versus distance, the flux may be calculated. As a result of the model, the maximum ionic flow occurs initially and is expressed as

$$\text{Flux} = \frac{2D_e (C_o - C_{\text{initial}})}{L} \quad (4-1)$$

where $C_o - C_{\text{initial}}$ is the concentration in excess of the ground-water concentration of any ionic specie within the cement pore fluid, L is the half thickness of the cement slab, and D_e is related to (Smith, 1970, p. 416) the cement void fraction, ϵ , and the molecular diffusivity D_{AB} by

$$D_e = D_{AB}\epsilon^2 \quad (4-2)$$

*Formulation 82-022 is one of several cementitious mixtures evaluated in the NNWSI Repository Sealing Program.

Table 4-1. Chemical Analyses of Water Before and After Contact With PSU 82-022 Concrete

Specie	J-13 (1) Concentration, mM (mg/l)	J-13 (2) Concentration mM (mg/l)	Concentration After 4 mo. (2) With PSU 82-022 Concrete mM (mg/l)
Al	.0010 (0.03)	<.007 (<.2)	0.008 (0.22)
Ca	0.29 (11.5)	.30-.41 (12.0-16.3)	0.181 (7.25)
Fe	0.0008 (0.04)	<0.0004 (<0.02)	0.006† (0.34)
K	0.136 (5.3)	0.13-0.24 (5.1-9.5)	1.48 (57.9)
Mg	0.072 (1.76)	0.079-0.086 (1.93-2.1)	0.013 (0.32)
Na	1.96 (45)	1.56-1.78 (36-41)	5.70 (131)
Si	1.07 (30.0)	0.93-1.18 (26-33)	2.14 (60.1)
NO ₃	0.16 (10.1)	-	0.15 (9.3)
SO ₄	0.19 (18.1)	0.20-0.24 (19-23)	0.54 (52.0)
HCO ₃	2.34 (142)	-	1.85* (113)
.....			
pH	6.9	7.7-8.13	9.9

†Data taken after 3 months
 ‡Data taken after 2 months
 (1) Data from Ogard and Kerrisk, 1984, p. 9-12
 (2) Data from Sheetz and Roy, in preparation

The concentration of species in the ground water passing below the shaft liner is then estimated by

$$C = C_{\text{initial}} + \frac{(C_o - C_{\text{initial}}) 2D_e A_{\text{shaft}}}{L Q} \quad (4-3)$$

where A_{shaft} is the shaft liner surface area and Q is the volumetric flow rate through the shaft and the MPZ. In Equation 4-3, the following values are used to determine the concentration:

$$\begin{aligned} A_{\text{shaft}} &= 4.17 \times 10^7 \text{ cm}^2, \\ c &= 0.28, \\ D_e &= 10^{-5} \text{ cm}^2/\text{s} (0.28)^2 = 7.84 \times 10^{-7} \text{ cm}^2/\text{s}, \text{ and} \\ L &= 15.24 \text{ cm}. \end{aligned}$$

Focusing our attention on the concentration of hydroxide, for an initial pH of 6.9, the initial molar concentration is 7.94×10^{-8} M. The concentration of hydroxide in the cement pores, C_o , is 0.75 M (Barnes, 1983, p. 298). To evaluate the concentration of hydroxide in the ground water after contact with cement, the flow rate through both the shaft and the MPZ must be estimated. Flow in the shaft fill and the MPZ will be unsaturated most if not all of the time. We have, however, allowed for the possibility of saturated flow in these zones; and during saturated flow periods, the flow rate is governed by the hydraulic conductivity of the shaft fill and of the MPZ. The concentration of hydroxide, expressed as pH, as a function of flow rate is shown in Figure 4-1. The concentration of other ionic species will follow the pH curve shown in Figure 4-1.

4.2.2 Chemical Equilibrium Model of Ground-Water Reactions

When ionic species are leached from the cement, these ions will interact with ground water. As a consequence, some precipitation is expected. These precipitates may then lodge in existing pores to reduce the hydraulic conductivity of both the MPZ and the shaft fill.

For the present analysis, we only estimate the nature and quantity of the precipitates formed from the interaction of ground water with a

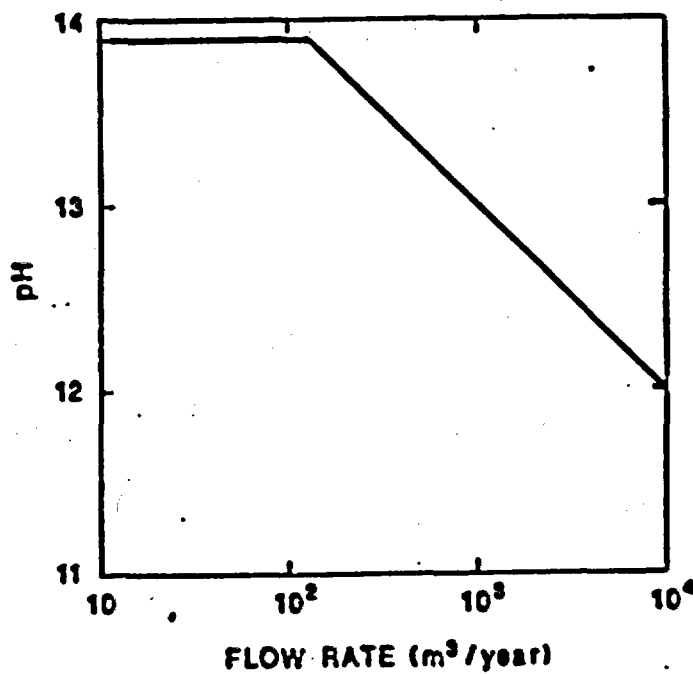


Figure 4-1. Plot of pH of Water From Below the Shaft Liner as a Function of the Volumetric Flow Rate of Water Through the Shaft or MPZ

concrete liner. We leave, as a necessary adjunct to the present work, a detailed analysis of the interaction between ground water, tuff, and cement as a function of temperature. The estimates provided here, however, do provide an indication of the likely consequences of having a cement liner contact ground water.

A consideration of a single equilibrium, that of CaCO_3 , will show that at least one species is likely to precipitate as the pH of the ground water is increased. In Table 4-1, the concentration of Ca^{++} in solution is reduced after coming into contact with cement. This reduction in Ca^{++} concentration is verified by calculations of chemical equilibrium when the pH of the water is increased. The chemical equilibrium between HCO_3^- , CO_3^{--} , and Ca^{++} is expressed in the following equations:



When OH^- is added to ground water according to Equation 4-4, more CO_3^{--} is formed. This CO_3^{--} may then react with Ca^{++} according to Equation 4-5; and if the solubility product of CaCO_3 is exceeded, then CaCO_3 will form to reduce the solution concentration of Ca^{++} . Using the equilibrium constants at 25°C for Equations 4-4 and 4-5, precipitation first occurs when a pH of 9 is reached.

A consideration of a single equilibrium, such as that illustrated in Equations 4-4 and 4-5, however, dramatically oversimplifies the interactions that occur when a cement liner is allowed to contact ground water. In actuality there are hundreds of these equilibria that should be considered simultaneously. Also, the effects of interaction with tuff, cement, and ground water, are dependent upon the order of contact as well as the temperature of the environment. While we do plan a more detailed study of this problem, we have examined the equilibrium of J-13 water after several changes have been superimposed on the water chemistry. The base case was J-13 water using the water analysis presented in Ogard and Kerrisk (1984). Variations on this base case are increasing the pH to 9.5,

increasing the temperature to 100°C, and increasing the Na^+ , K^+ , SO_4^- , and SiO_2 concentrations, each by an order of magnitude. These studies were performed using a water chemistry equilibrium code, WATEQ, developed by Truesdell and Jones (1974).

For the base case, the J-13 water pH was taken to be 6.9, the water temperature 25°C, and the Eh -0.256 volts. WATEQ includes more than 100 equilibria and displays both ion activity products and equilibrium constants. When the ion activity product was greater than the equilibrium constant, a mineral would have a tendency to precipitate. In the base case 22 minerals had already exceeded their equilibrium solubility products. In every case, however, these minerals were aluminum bearing, with the least soluble of these being clay minerals. Further, the concentration of Al in J-13 water was reported to be 0.03 mg/l. By varying the aluminum concentration in J-13 water, it was determined that the maximum concentration of soluble aluminum was 1% of 0.03 mg/l; or by implication, practically all of the aluminum in J-13 water is present in microscopic clay particles carried along with the water. It is assumed that these clay particles are so small that they would probably have no tendency to clog pores within the MPZ or the shaft fill.

Next we consider the effects of increasing the pH of the water to 9.5. In this case, WATEQ shows 12 new minerals as exceeding their solubility products. These minerals were aragonite (CaCO_3), calcite (CaCO_3), diopside ($\text{CaMgSi}_2\text{O}_6$), hematite (Fe_2O_3), maghenite (Fe_2O_3), magnetite (Fe_3O_4), goethite ($\text{FeO}(\text{OH})$), siderite (FeCO_3), clinoenstatite (MgSiO_3), talc ($\text{Mg}_3\text{Si}_4\text{O}_{10}(\text{OH})_2$), sepiolite ($\text{Mg}_2\text{Si}_3\text{O}_7.5\text{OH}\cdot 3\text{H}_2\text{O}$) and chrysotile ($\text{Mg}_3\text{Si}_2\text{O}_5(\text{OH})_4$). The least soluble of these minerals, as determined by increasing the pH in small steps, is the iron mineral hematite, followed by the magnesium and calcium minerals, talc and calcite. If we assume that the iron, magnesium, and calcium are all deposited as their least soluble mineral, then 37.9 mg/l of precipitate will form as a consequence of raising the pH of the J-13 ground water. Equivalently, the total volume of this precipitate formed per volume of solution is 1.394×10^{-5} , to be referred to as v in the following text.

Other possible changes to the ground water were also considered in addition to raising the pH. We raised the temperature to 100°C, and increased the concentration of Na^+ , K^+ , SO_4^- , and SiO_2 by one order of magnitude in each case. These additional changes cause some variation in the solubilities of the various minerals, but are considered to be small. For example, when the temperature is increased, calcite is actually less soluble than at lower temperature. Thus, the mineral that accounts for the most precipitate will tend not to redissolve as the temperature is raised. Increasing the concentrations of Na^+ , K^+ , SO_4^- , and SiO_2 similarly appear to have small additional effects, and detailed analysis of their effects is postponed until a later date.

4.2.2.1 Migration of Precipitates

The precipitation of minerals from a supersaturated solution is a rate-controlled process. When considering the formation of calcite, solid calcite is found to precipitate at nucleation sites on existent solid surfaces rather than homogeneously (Berner, 1980). The rate at which further precipitate forms on existing nucleation sites is governed by diffusional rate processes. In a quiescent fluid where the bulk of the fluid is supersaturated, excess ions will migrate to the solid surfaces and then precipitate to cause the concretion to grow. When fluid is moving through pores or fractures, the process of solid deposition is controlled by the diffusion of ions from the bulk of the fluid to the pore or fracture wall. Where pores or fractures are narrowed by ongoing precipitation, further precipitation is favored because of the reduced diffusional path length (Figure 4-2).

This local restriction in the fluid pathway will result in spreading the precipitate out over a thin shell to reduce fluid motion and hydraulic conductivity. Moreover, the precipitate will tend to seal off the MPZ and the shaft fill so that high conductivities will be locally reduced provided sufficient quantities of water enter the shaft fill and MPZ and reacts with the liner.

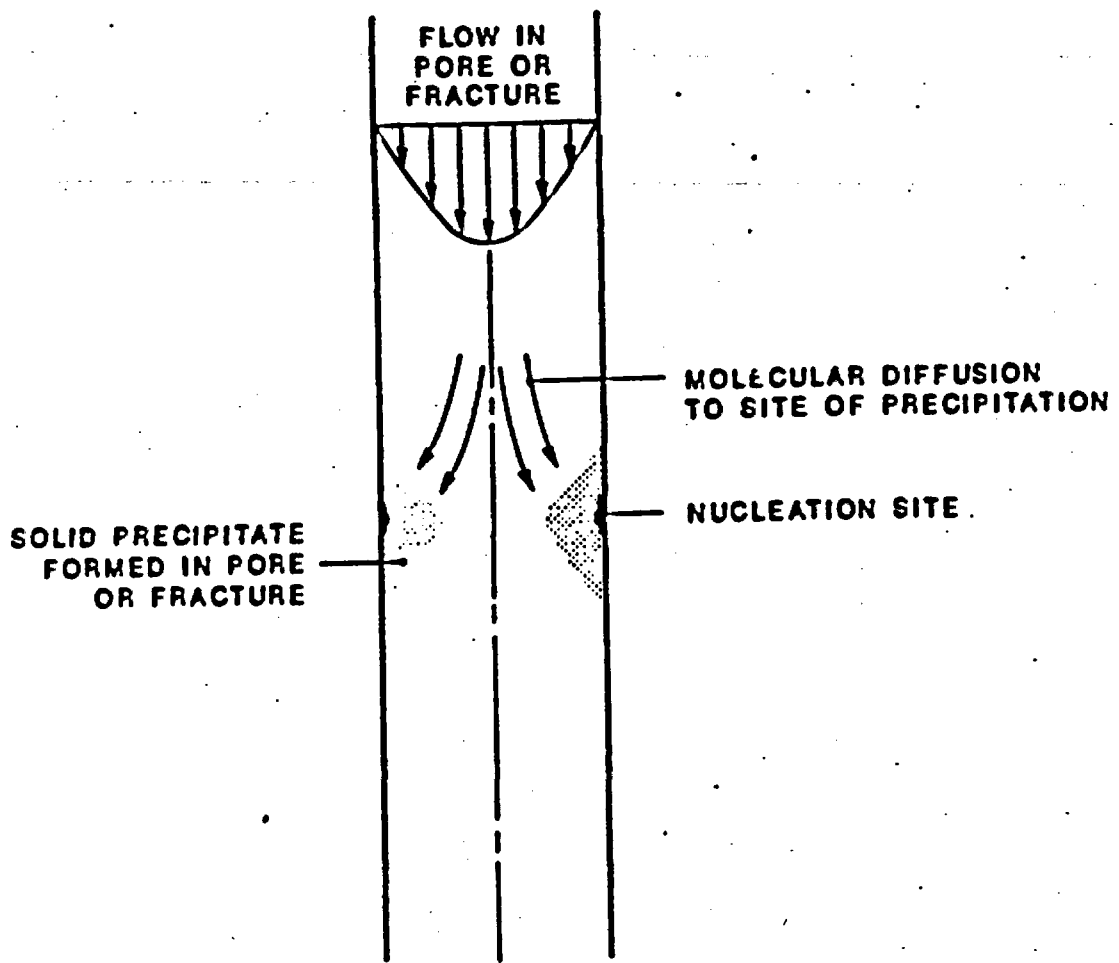


Figure 4-2. Schematic of Deposition of Precipitate

To estimate how rapidly this shell will form, consider the time required for ions in the center of a pore to migrate to a pore wall. If we make use of the conservative Einstein relationship to describe diffusion, then

$$t = \frac{x^2}{D} \quad (4-6)$$

where t = the time for a molecule to migrate in a random way through a distance, x , and

D = the fluid diffusion coefficient.

The aperture assumed is 50 μm . Therefore, the value of x used in Equation 4-6 is 25 μm . Using a representative liquid diffusivity of $10^{-5} \text{ cm}^2/\text{s}$, the time for ions to migrate from the stream centerline to the wall is given by Equation 4-6 to be 0.6 s. In the more likely case, where flow occurs primarily within the matrix, the pore diameters are inferred from matrix hydraulic conductivities to be 0.05 μm . In this instance, the migration time is 0.5 μs . Hence, we conclude that supersaturated solutions will not persist and precipitate deposition will be almost instantaneous.

4.2.2.2 Model for Precipitate Deposition

A model describing the rate of buildup of solid precipitate in porous media flow has been proposed by Berner (1980). In this model, a front of solid precipitate progresses through the porous media, where the void spaces behind the front are assumed to be completely filled. A small residual permeability is allowed so that the deposition process may continue. Beyond the front, the water is saturated so that no further deposition is assumed. Berner describes the frontal velocity, U_F , as

$$U_F = \frac{\nu Q}{A(\phi_U - \phi_d)} \quad (4-7)$$

where ν = the volume of precipitate per unit volume of water,
Q = the volumetric water flow rate,
A = the cross-sectional area for flow,
 ϕ_U = the undisturbed porosity, and
 ϕ_d = the porosity behind the deposition front.

After Berner we assume that ϕ_d is zero. Equation 4-7 may be applied to two regions: the shaft fill and the MPZ. Equation 4-7 is also applied for the modeled, anticipated flow rate of $44.2 \text{ m}^3/\text{year}$ and for flooding events where the fractures are saturated. This latter type of flow will be very transient in nature (flow for less than 1/2 year per event) and is expected to occur only infrequently over the lifetime of the repository.

4.2.3 Results

For normal annual water passage through the MPZ and the shaft fill, flow will occur in an unsaturated manner. Within the MPZ unsaturated flow will most likely occur within the matrix where the undisturbed porosity is 0.11. Within the shaft fill the porosity is assumed to be 0.3. The total flow of $44.2 \text{ m}^3/\text{year}$ is partitioned between the MPZ and shaft fill in proportion to the relative conductivities and areas. The frontal velocities in each case are then calculated from Equation 4-7 to be

$$U_{F \text{ MPZ}} = 0.1 \mu\text{m}/1000 \text{ yr and}$$

$$U_{F \text{ shaft fill}} = 0.2 \text{ m}/1000 \text{ yr} .$$

In the anticipated water passage case, we conclude that no significant migration of precipitate occurs because the frontal velocities in both cases are small.

At the other extreme of the water flow spectrum is the PMF scenario. In this case, we assume that water flow fills the fractures and saturated flow results. Up to $20,000 \text{ m}^3$ may enter the shaft in a single event. The hydraulic conductivity of the backfill is assumed to be 10^{-2} cm/s , while that of the MPZ may vary between 60×10^{-2} and $20 \times 10^{-5} \text{ cm/s}$. The porosity of the MPZ for flow in fractures is assumed to vary between 0.001 and 0.0001, estimates for natural fractures (Erickson and Waddell, 1985.

p. 1). The frontal advance in the MPZ behind the shaft liner is shown in Figure 4-3. Within the shaft fill, the frontal advance is never greater than 0.08 m for any of the above cases.

While the advance of the precipitation front (Figure 4-3) may become as large as 60 m for a maximum flooding event, this advance rate is appropriate only for flow behind the shaft liner. Once the flow advances beyond the base of the liner the appropriate porosity is no longer the very small value assigned for fracture flow in the MPZ. Here, because of the intimate communication between the shaft fill and the MPZ, the porosity of the backfill allows the interstitial flow rate to decrease. As a result, the maximum frontal advance below the shaft liner is predicted to be 0.016 m/event. Flow between the MPZ and the shaft fill can also occur periodically along the length of the shaft due to the horizontal joints occurring in the liner. We have not taken credit for this communication in the above analysis which would further reduce precipitate advance.

4.2.4 Conclusions

The deposition of solids from the interaction of the shaft liner with ground water will therefore most likely be a localized phenomenon, even considering highly improbable amounts of water, because

- o precipitation occurs rapidly after ground water contacts the shaft liner.
- o precipitation occurs as a progressively advancing front, and
- o the frontal advance is limited to regions near the shaft liner.

4.3 Remedial Measures to Remove the Liners From the Exploratory Shafts

The removal of the shaft liner will require breaking the concrete over some portion of the shaft and removal of the chunks of concrete to the surface. Liner removal techniques are discussed in Section 4.3.1 and muck removal is discussed in Section 4.3.2.

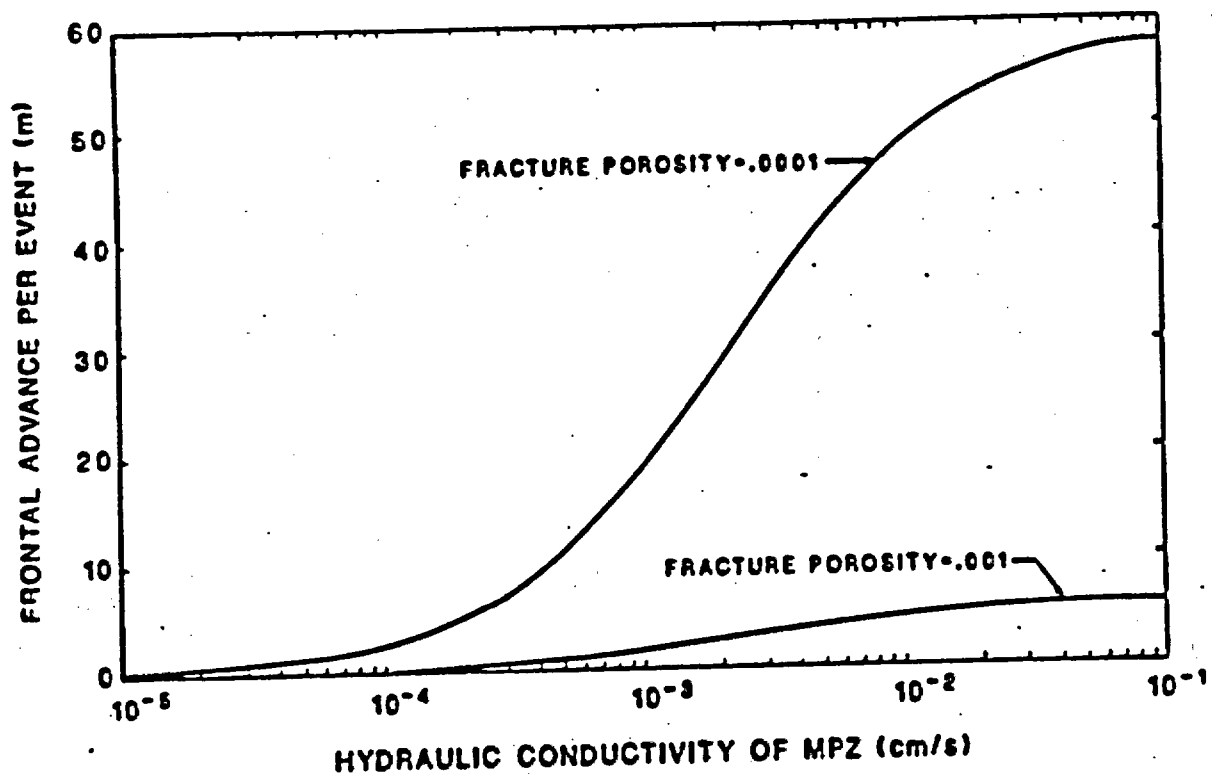


Figure 4-3. Frontal Advance of the Precipitation Front in the MPZ

4.3.1 Liner Removal

Six methods were identified for concrete breakage (liner removal):

- o Hand-held pneumatic breakers
- o Drill and blast
- o Drill and the use of a hydraulic splitter
- o Drill and the use of a nonexplosive demolition agent
- o Impact breaker
- o Roadheader boom

In the first four methods it is assumed that several operations (drilling and breakage, liner removal, and backfilling) would be performed from a single stage retreated out of the repository (Figure 4-4). In the production cycle, the concrete lining is removed upward, and the backfill is placed below the working stage (the length of unsupported rock sides would be approximately 10 m). It may be necessary to install occasional temporary support to facilitate muck removal and reduce the unsupported length in weaker zones. In the last two methods, the impact breaker or the roadheader boom (Figure 4-5) would be mounted on the base of one stage with mucking and backfilling occurring from a second stage.

Hand-held pneumatic breakers have been used to break high-strength concrete. In one unpublished experience, i.e., at Blue Mesa Dam between Montrose and Gunnison, Colorado, they were used to remove a 0.5-m, tunnel, spillway lining of 25-year old concrete with unconfined compressive strength ranging from 28 to 55 MPa. In this method, it is essential to maintain support for the breaker point; otherwise, when the liner fractures, the support is lost, and the breaker drops suddenly. To avoid this problem, the liner could be removed over 10 m in a downward direction or the breakers could be suspended by chains or other adjustable supports that would allow liner removal in the upward direction. In this method, it is estimated that horizontal drill holes spaced approximately on 0.3-m centers would be required to break out the concrete.

The drill and blast method would require that horizontal drill holes with a horizontal spacing of 0.5 m, and vertical spacing of 0.3 m be loaded with plastic explosive and detonated. Drilling and loading operations are

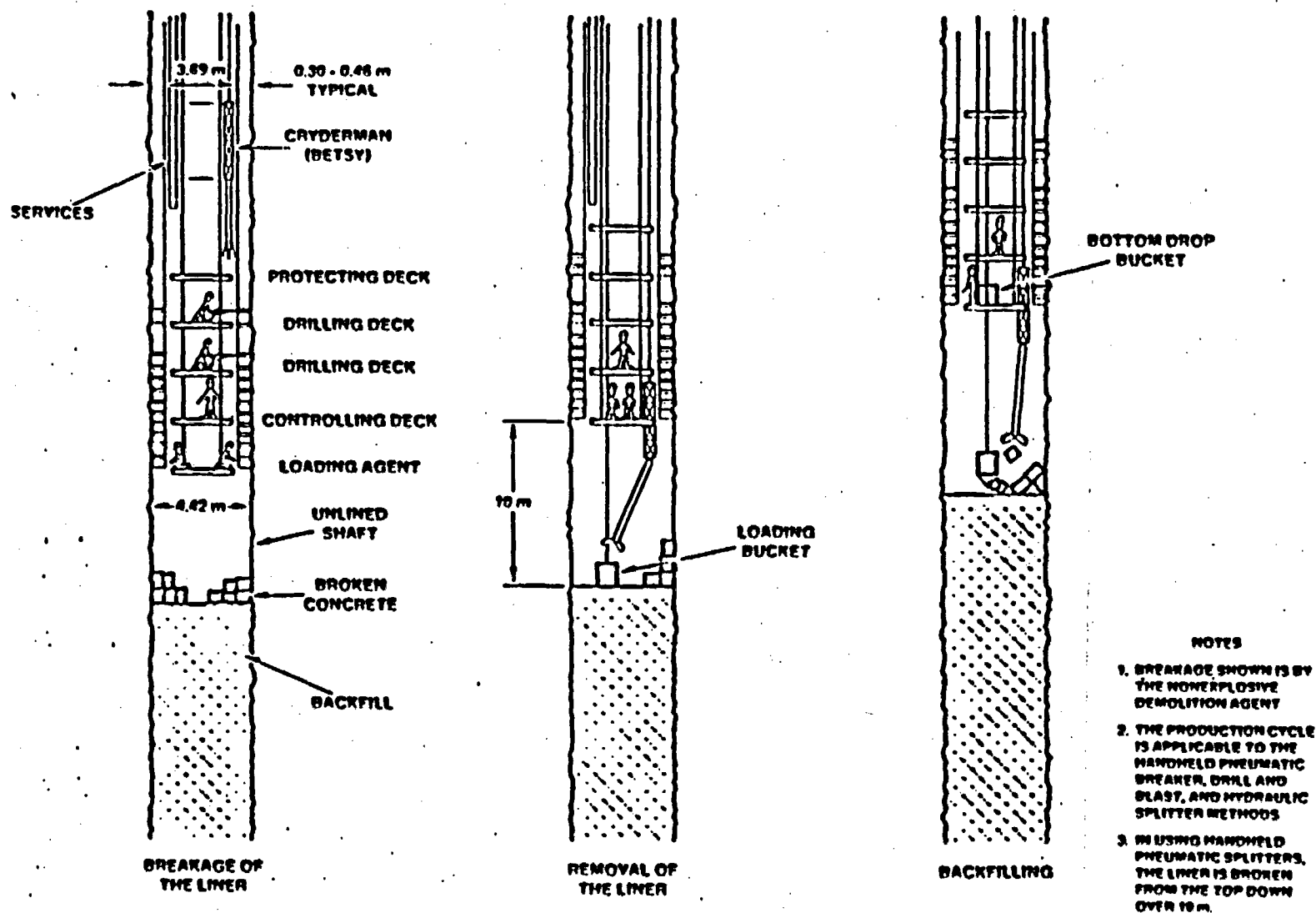


Figure 4-4. Production Cycle for Breaking and Removing the Liner and Placement of Backfill

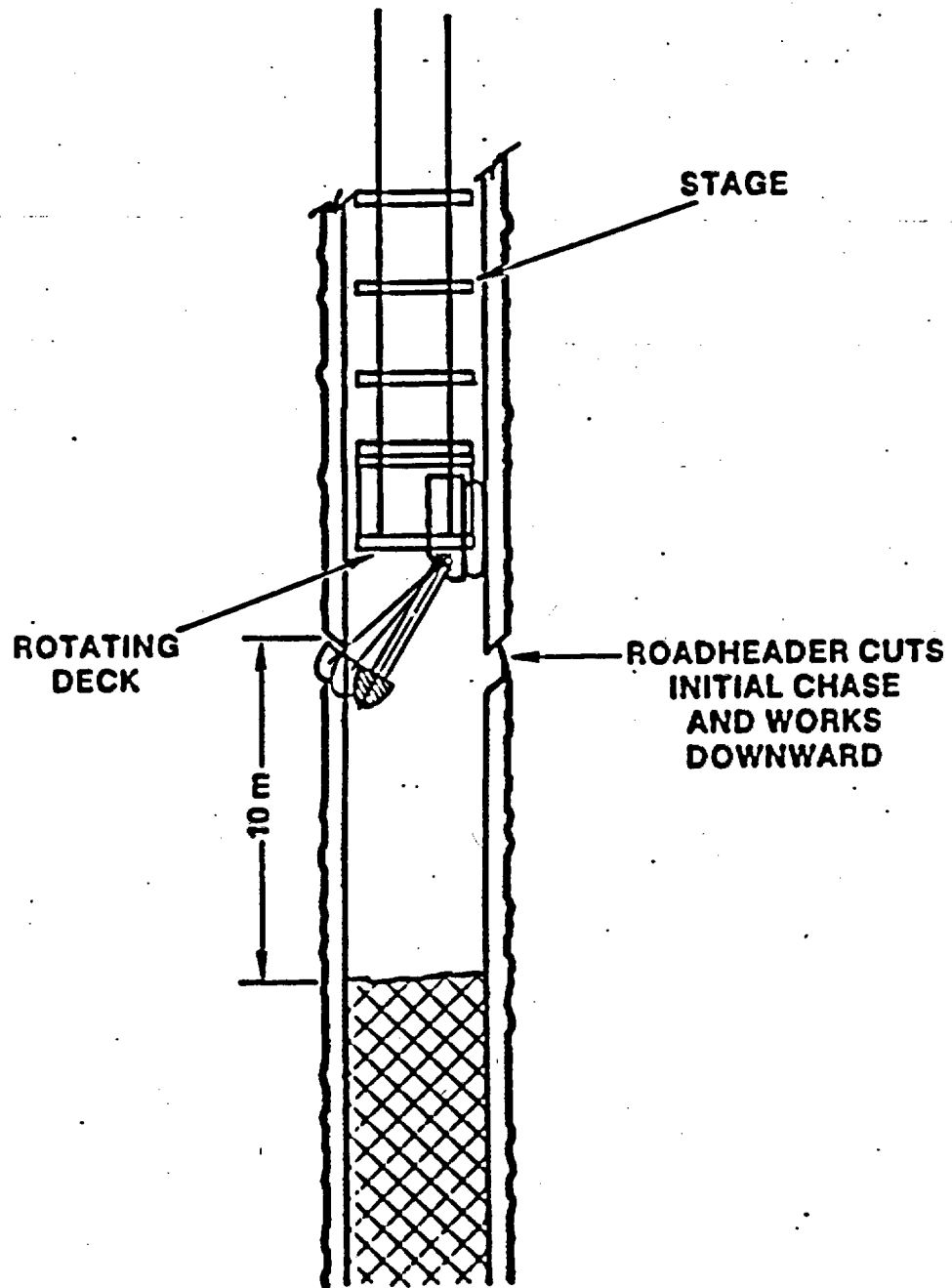


Figure 4-5. Conceptual Illustration of Liner Breakage by the Roadheader Method

performed in series. During blasting, the stage would be raised and personnel would be kept clear for about 30 minutes following each blast. Hole lengths would penetrate the surrounding rock. The method would be suitable where removal of the liner is performed to enhance drainage as discussed previously.

The drill and hydraulic splitter operate on the "plug-and-feather" principle. In a series of holes penetrating the liner, wedge pairs inserted into the drillhole series are forced apart, resulting in tension and splitting. It is estimated that twice as many holes would be required as in the drill-and-blast method. To retrieve the splitters from the broken concrete, it is necessary to suspend them on chains. Hydraulic splitting is accomplished at the lower platform of the stage with drilling operations performed on the higher platforms.

The drill and nonexplosive demolition agent method consists of drilling holes and loading them with an expansive agent. The technique has been described by Dowding and Labuz (1982, pp. 1289-1299), who describe a series of tests to fracture rock and concrete in a series of case histories that include fracturing of plain concrete. These authors, and subsequent investigators (Ingraffea and Beech, 1983, pp. 1205-1208), have interpreted tests on the basis of linear elastic fracture mechanics. It is estimated that a similar number of holes would be required as with the hydraulic splitter method. The fracturing of the liner would take place 24 to 48 hours after placement of the agent.

The impact breaker is mounted on a hydraulically operated boom below the stage and is suspended on ropes. Impact breakers mounted on rubber-tired base units have been successful in breaking concrete in surface operations. The unit breaks at a high rate and would have to be supported in a similar fashion to the hand-held breaker. Using this method, it would be necessary to break out a chase about every 10 m to allow breaking out the liner in the downward direction. Because of space restrictions, it would not be possible to muck out the broken liner and backfill unless the stage was removed after every 10-m lift.

Roadheader booms are used extensively in underground mining operations. The single head or two cutting heads are capable of excavating medium-hard rock (D'Appolonia, 1976, pp. 2-62 through 2-66) and would be suitable for concrete liner removal. In this method, the roadheader boom is mounted below the base platform of the stage and would be capable of reaching the liner from a single support point. It is best suited for cutting downward. It has the advantage over the impact breaker that it can cut as it is being swung into the concrete lining so that it can readily cut the starting chase to allow downward excavation. The use of hanging rods in the concrete liner could complicate the removal of the liner using this technique.

The advantages, disadvantages, and equipment/material costs for the several methods for liner removal are summarized in Table 4-2. This study places emphasis on conventional methods and gives preference to the use of "off-the-shelf" equipment. The impact breaker and roadheader methods are not as practical for removing concrete from the muck pile; either the impact breaker or the roadheader boom would have to be retreated from the shaft for removal of concrete and placement of backfill. It is noted that if the entire liner were to be removed, the initial fixed costs for stage modifications might be offset by the higher production rates of these two methods.

Further comparisons of production cycle times and costs for the remaining four methods are presented in Tables 4-3 and 4-4, respectively. These costs apply to complete removal of the liner from the base of the shaft to near the repository horizon. This cost comparison would suggest that the drill and hydraulic splitter method is the most economical, although when off-site preparation, on-site preparation, and other costs are factored in (Appendix D), the differences in adopting any single method are not significant.

4.3.2 Muck Removal

Two methods are identified for muck removal that would be suitable for any of the liner removal methods. These are

Table 4-2. Summary of Advantages, Disadvantages, and Cost of Liner Removal Methods^(a)

Removal Method	Advantages	Disadvantages	Equipment and Material Costs
1. Hand-held pneumatic breakers	There is experience in removing concrete liners.	The method is labor intensive and requires more production time. The method poses a potential safety problem if the breaker dropped suddenly.	The cost of 8 breakers and 4 drills is approximately \$15,000. Drilling equipment spares cost \$120,000. ^(b)
2. Drill and blast	The method is well known.	An overbreak zone may form. Drilling and loading operations cannot be performed simultaneously. Blasting would require raising the stage and clearing the area after each detonation.	The cost of 6 drills and 4 breakers is \$15,000; the cost of drilling equipment spares is \$57,000. The cost of explosives and caps is \$51,000.
3. Drill and hydraulically split	Drilling and splitting may occur simultaneously. The method is clean and does not leave chemical residue.	It is not as efficient as drilling and blasting. The method may need to be supplemented with hand methods such as the hand-held pneumatic breakers. The splitters must be suspended to avoid being dropped into broken concrete.	The cost of 6 drills and 4 breakers is \$15,000. Drilling equipment spares cost \$102,000. Rental costs for the splitters are estimated at \$54,000.

^(a)Note that the costs apply to complete removal of the liner.

^(b)Drills are required to expedite liner removal and increase productivity.

Table 4-2. Summary of Advantages, Disadvantages, and Cost of Liner Removal Methods (Continued)

Removal Method	Advantages	Disadvantages	Equipment and Material Costs
4. Drill and use a nonexplosive demolition agent	<p>Drilling and splitting may occur simultaneously.</p> <p>Experience in fracturing plain concrete (Dowling and Labuz, 1982, p. 1297)</p>	<p>Operations must be carefully planned since a period of 24 to 48 hours is required for liner fracturing.</p> <p>The chemical agent could not be recovered from the muck pile.</p>	<p>The cost for 6 drills and 4 breakers is \$15,000. Drilling equipment spares cost \$102,000. The cost of the expansive agent is \$306,000.</p>
5. Impact breaker		<p>Mucking and backfilling operations must be performed from a second stage.</p> <p>The breaker point must be supported.</p>	<p>The initial costs of power and stage modifications are \$16,000 and \$8,000, respectively. A suitable unit with equipment spares may be rented at a rate of \$100.00/hour, or an estimated cost of \$300,000.</p>
6. Roadheader boom	<p>No drilling is necessary and the production rate is high.</p> <p>It can cut as it is being swung into the concrete lining so that it can readily cut the starting chase to allow downward excavation.</p>	<p>Mucking and backfilling operations must be performed from a second stage.</p> <p>Little experience in shaft operations.</p>	<p>The initial costs of power and stage modifications are \$18,000 and \$8,000, respectively. A suitable unit with equipment spares may be purchased for \$125,000.</p>

Table 4-3. Comparison of Production Cycle Times For Various Methods Used to Remove Concrete Liners^(a)

<u>Hand-Held Pneumatic Breakers</u>	
<u>Activity</u>	<u>No. of Shifts</u>
Pneumatic removal of liner	15.0
Muck out broken ₃ liner, 62 m ³	1.5
Backfill, 160 m ³	1.5
Remove 9 m of service lines	0.5
Allow for other hoist runs, movement of stage	0.5
Total	19.0
<u>Drill and Blast</u>	
<u>Activity</u>	<u>No. of Shifts</u>
Drill approximately 800 holes 0.6 m deep	2.0
Load 60% of the holes and blast	3.0
Muck out broken ₃ liner, 62 m ³	1.5
Backfill, 160 m ³	1.5
Remove 9 m of service lines	0.5
Allow for other hoist runs, movement of stage	0.5
Total	9.0
<u>Drill and Hydraulic Splitter</u>	
<u>Activity</u>	<u>No. of Shifts</u>
Drill 1,700 holes 0.6 m deep	4.0
Simultaneously use splitter ₃ in 25% of the holes	1.5
Muck out broken ₃ liner, 62 m ³	1.5
Backfill, 160 m ³	0.5
Remove 9 m of service lines	0.5
Allow for other hoist runs, movement of stage	0.5
Total	8.0
<u>Drill and Nonexplosive Expansive Demolition Agent (NEDA)</u>	
<u>Activity</u>	<u>No. of Shifts</u>
Drill 1,700 holes 0.6 m deep	4.0
Simultaneously load 25% of the holes with NEDA	1.5
Muck out broken ₃ liner, 62 m ³	1.5
Backfill, 160 m ³	0.5
Remove 9 m of service lines	0.5
Allow for other runs, movement of stage	0.5
Total	8.0

(a) Cycle times are calculated for a 9-m length.

Table 4-4. Comparison of Costs For Breaking Out the Concrete Lining and Rock^(a) (\$ Thousands)

Cost Item	Hand-Held Pneumatic Breakers	Drill & Blast	Drill & Hydraulic Splitter	Drill & NEDA
1) Time-Related	3,447	1,149	912	912
2) Equipment-Related				
Drilling	15	15	15	15
Blasting Winch Rental		2		
Blasting Cable		17		
Firing Switch, etc.		2		
3) Consumables-Related				
Drilling	120	57	102	102
Explosives & Caps		51		
Rental of Splitters		6	54	
Bristar				306
Total	3,582	1,299	1,083	1,335
Weeks	42.6	14.2	11.2	11.3

(a) Includes only costs directly related to breaking out the concrete liner from the shaft.

- o Cryderman mucker (The Betsy) and
- o Remote controlled, orange-peel-type grab.

The smallest size Cryderman mucker would suit the small, 3.66-m. finished diameter of the exploratory shafts. This unit is normally suspended on a winch from the surface and held against the side of the shaft excavation or concrete lining by a frame-and-bolt arrangement. The unit is pneumatically operated and may be hoisted out of the shaft stage area while drilling and breakage operations are in progress. During mucking operations, the unit would remove broken concrete and place it in a conventional bucket hoisted through a trap door to the surface. During backfilling operations, the conventional bucket is replaced by a bottom drop bucket.

The other mucking method is the orange peel type grab unit that operates below the stage (Figure 4-6). This unit is raised and lowered by a hoisting winch that operates from the bottom of the shaft stage. The broken concrete liner is loaded into a bucket that may be hoisted to the surface.

An alternative method of removing the broken liner when using hydraulic splitters or pneumatic breakers is to transfer the broken liner directly into a hoist bucket. This bucket could be positioned on a platform below the working level. In this arrangement broken pieces of material would be pushed to retractable chutes that empty directly into a central hoist bucket. The size of the concrete pieces could be controlled by making breakline cuts with circular saws equipped with diamond or high-strength, carbon-steel blades.

4.3.3 Conclusions

Evaluation of the advantages and disadvantages for liner removal techniques suggests that the hydraulic splitter method is the favored approach for liner removal although the other approaches are technically feasible. Conventional equipment with the slight modification of suspending the splitters from chains may be used in employing the hydraulic splitter method. It is also possible that drilling and splitting patterns

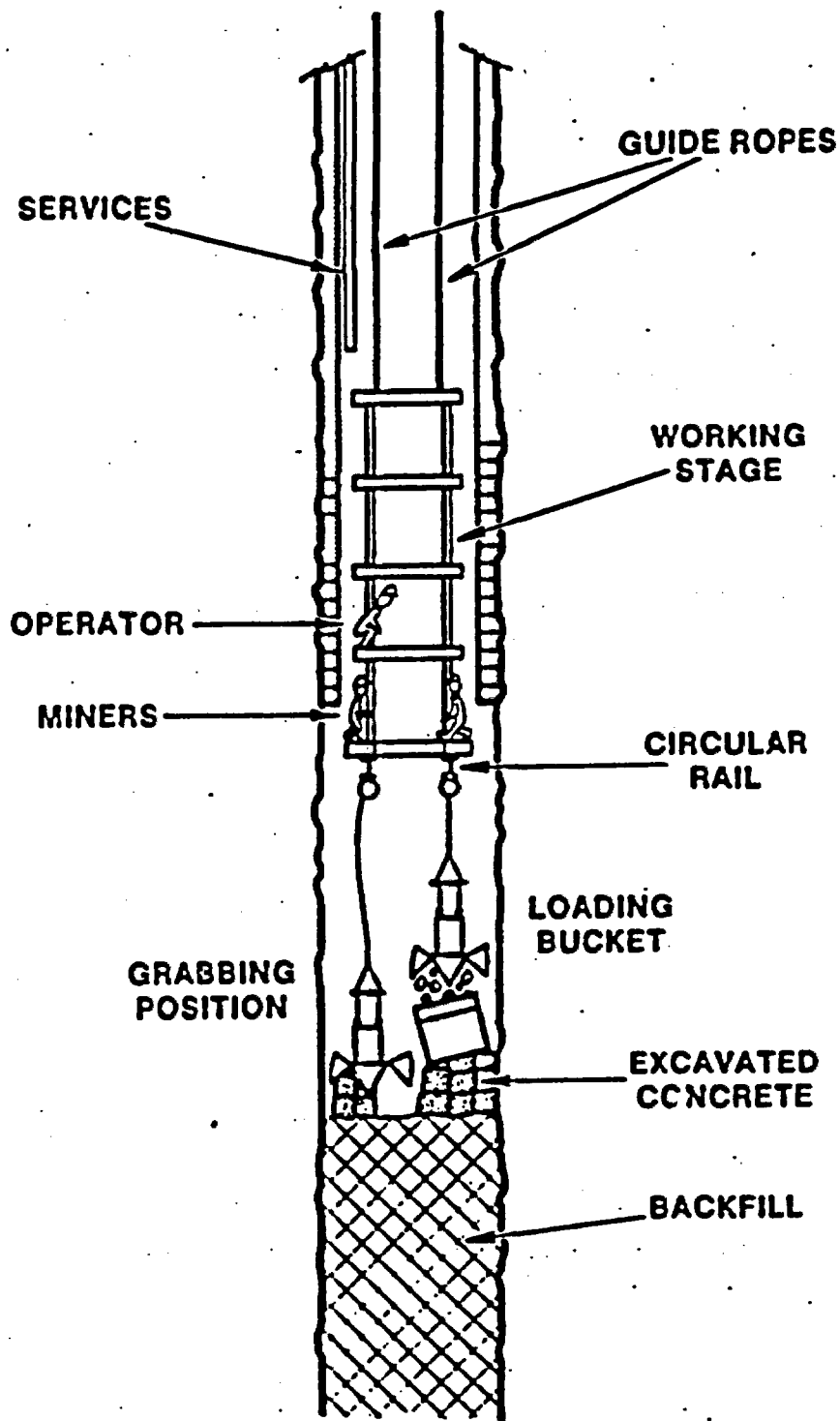


Figure 4-6. Removal of Concrete Using the Orange Peel Grab

could be optimized through analysis of superposition effects from an array of splitters. The method does not leave undesirable chemical residue. While supplemental hand methods may be required, this is not considered a significant disadvantage. Either of the two muck removal techniques are acceptable. It is recognized that additional efforts may be required during liner removal and backfilling operations to insure safety. For example, in areas where additional stability is required, i.e., where the liner has been removed and where no lateral support from the backfill is provided, additional shoring of the existing liner may be required.

5.0 INFLUENCE OF THE ES PENETRATION INTO THE CALICO HILLS UNIT

5.1 Changes in the Sorptivity of the Calico Hills Unit Due to Elevated Ground-Water Temperature

Ground water entering the exploratory shaft will experience some heating as it descends the shaft and MPZ to the elevation of the repository. From there it will continue downward to eventually cooler regions in the Calico Hills. As will be shown in Section 5.1.1, the temperature of this water will approximate the temperature of the rock surrounding the exploratory shaft. Hence, the first consideration will be given to determine the rock temperature in the vicinity of the exploratory shaft. With this rock temperature profile and assumed phase condition within the shaft and MPZ, we next estimate the fluid temperature as it enters the top of the Calico Hills unit. The fluid temperature is then compared to the temperature required to maintain mineralogical stability of Calico Hills zeolites.

5.1.1 Temperature Elevation of Water Entering the Shaft

The temperature of the ground water passing through the exploratory shaft will increase globally due to the presence of the repository. Far-field calculations have been carried out by M. L. Blanford (Morales, 1985, pp. 36-39), assuming a thermal load by the repository of 57 kW/acre (MacDougall et al., 1987, Appendix D, p. 532). At a location approximating the ES at the edge of the repository these calculations indicate that the temperature expected at the top of the Calico Hills unit at 500 years after emplacement will be 47°C and that the maximum temperature will be 52°C. These temperatures are calculated assuming that conduction of heat is the primary heat transfer mechanism. Further, these calculations assume no barrier pillar around the shafts. Such a nonwaste emplacement area will tend to lower the temperature of the rock mass around the shaft. Indeed, more recent results (Richardson, in preparation, Appendix B) which account for the presence of the barrier pillar show that the maximum temperature at the top of the Calico Hills will be less than 40°C assuming a thermal loading at the repository horizon of 57 kW/acre.

To address the thermal impact of the exploratory shaft on water that might enter the Calico Hills, a separate analysis (see Appendix E) was conducted assuming various water flow rates downward through the shaft fill and the MPZ around the ES. These calculations were directed at determining the maximum water temperature at the base of the ES, entering the Calico Hills unit. Conservative assumptions were involved in all cases to reveal that the fluid temperature never deviated greatly from the formation temperature. Under normal expected water flow conditions where the temperature at the top of the Calico Hills unit was 52°C, the water temperature increase was 0.01°C. Increasing the water flow rate to its maximum permissible value, i.e., the maximum hydraulic conductivity of the modified permeability zone, increased the water temperature by 0.8°C. Moreover, increasing the water flow rate through the shaft and MPZ by three orders of magnitude increases the temperature of water reaching the base of the ES-1 by 0.8°C. Hence, the formation temperature computed assuming conduction alone accurately approximates fluid temperatures within the ES, and the ES has little additional impact on the ground-water temperature.

5.1.2. Impact of Increased Ground-Water Temperature on the Sorptivity of the Calico Hills Unit

Within the Calico Hills unit, the principal zeolite phases are clinoptilolite, mordenite, and analcime. Of these, clinoptilolite is the most important sorptive phase (Daniels et al., 1982, p. 92 and Smyth, 1982, p. 195). Moreover, the sorptivity of the Calico Hills at elevated temperature depends on two factors: the dependence of the distribution coefficient (e.g., K_d^*) on temperature, and the hydrothermal stability of the mineral phase, clinoptilolite. Also, as has been shown above, the upper limit of temperature computed in this discussion is approximately 52.8°C. The concern at the upper margin of the Calico Hills does not involve

*The distribution coefficient is a parameter commonly used to describe the sorption behavior of radionuclides in geologic systems. K_d is defined as "the concentration per gram of a species on a solid phase divided by its concentration per milliliter in the liquid phase at equilibrium" (Wolfsberg et al., 1979, p. 4). The higher the K_d value, the higher the sorption potential of the material being evaluated.

extreme temperatures but rather represents the potential impact of more moderate temperatures on the sorptivity.

The dependence of the distribution coefficient, e.g., K_d , on temperature has been addressed in several studies (Wolfsberg et al., 1979; Daniels et al., 1982; and Ogard et al., 1983). In these studies, increases in K_d with temperature are reported in every case for temperature increases of up to 85°C. Hence, it may be stated that the distribution coefficients of the Calico Hills minerals improve as temperature increases.

The second phenomenon to be addressed is the hydrothermal stability of the zeolite phases within the Calico Hills unit. Smyth (1981 and 1982) reports on two types of stability. These are dehydration stability and mineralogical stability. Dehydration reactions occurring up to 200°C are found to be reversible and will not be considered further. However, irreversible, deleterious, mineralogical reaction is also observed. Clinoptilolite is a thermally sensitive mineral and undergoes transformations to mordenite and analcime. While the consequence of these transformations has not been investigated, it is assumed that the sorptivity will decrease. The exact transition temperature is dependent on sodium concentration and pH. For conditions found at Yucca Mountain, Smyth predicts a transition temperature of 105°C; at extreme sodium concentration levels, this transition temperature may drop to 95°C. Other investigators* at Los Alamos National Laboratory feel that cristobalite may also influence the stability of clinoptilolite and that the irreversible mineralogical transition temperatures of Smyth may be inappropriate and will probably be higher. In any case, data gathered to date indicate that the actual temperature of any part of the Calico Hills unit will be less than that required to cause any significant reaction of clinoptilolite.

5.2 Changes in the Thickness of the Calico Hills Unit Above the Ground-Water Table

An additional consideration associated with the ES-1 is its penetration into the zeolitic Calico Hills unit. Such a penetration can reduce

*C. J. Duffy, 1987, personal communication.

the effective thickness of the Calico unit used in performance assessment calculations. The current NNSI Project position is that any penetration associated with the ESF including the ES-1 should not reduce the effective thickness of the Calico Hills to a thickness less than its minimum thickness occurring anywhere within the repository boundary. Figures 5-1a and 5-1b illustrate this point.

The Calico Hills unit can be divided into a nonzeolitic portion and a zeolitic portion. In the new ES-1 location, the Calico Hills unit above the prevalent zeolites is zero. The thickness of the zeolitic portion of the Calico Hills unit (Figure 5-1b) is approximately 100 m at ES-1. Because the proposed penetration into the zeolitic portion of the Calico Hills unit is 15 m, the total thickness of the Calico Hills unit will be about 85 m. This thickness is above the minimum thickness of 70 m for the total thickness of the Calico Hills unit. The total thickness of the Calico Hills Unit at the exploratory shaft locations can be obtained by adding the thicknesses of the vitric and zeolitic portions of the Calico Hills as shown by both Figures 5-1a and 5-1b.

5.3 Conclusions

The impact of episodic water percolating through the shaft fill and MPZ on the sorptivity of the Calico Hills unit has been found to be negligible. This conclusion is reached because of the following:

- o First, water passing through the ES will be completely separated from waste stored in the repository and will not constitute a preferred pathway.
- o Second, the minimum thickness of the Calico Hills unit will be preserved, while allowing much valuable information to be gained by sinking the ES into the upper margin of the Calico Hills.
- o Third, the elevation of the temperature of the ground water percolating through the shaft fill is computed to be a maximum of 52.8°C at the top of the Calico Hills unit. This value is less than the minimum value of 95°C (Smyth, 1982, p. 195) observed to cause mineralogical transition of zeolites.

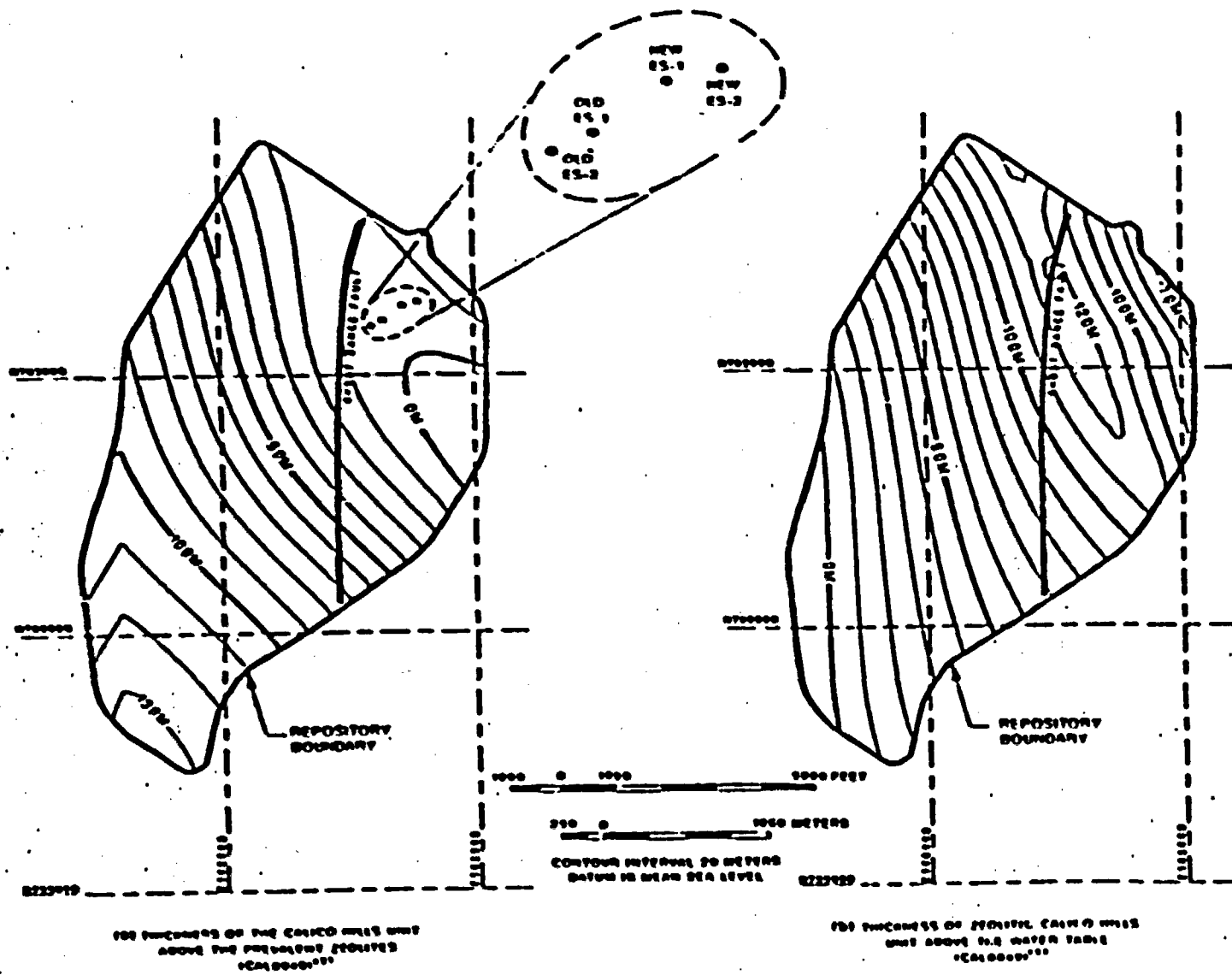


Figure 5-1. Contours of the Thickness of the Unsaturated Portion of the Calico Hills Unit
 Beneath the Repository

This page is for page number only

6.0 CONCLUSIONS AND RECOMMENDATIONS

The analyses in the report support the conclusion that the design and construction of the ESs, as currently planned, is not expected to significantly influence the performance of the potential nuclear waste repository at Yucca Mountain. This conclusion is reached for the following reasons:

- o Even when a highly improbable flooding scenario (and possibly an incredible scenario at the new ES locations) is considered at the new ES locations, any water entry past the repository station seals is predicted to be contained within the ESF (Section 3.2.5.4 and 3.2.5.5). Therefore, these waters entering the exploratory shaft do not reach the waste emplacement area, contact the waste, and enhance radionuclide release.
- o The more realistic scenario presented in Section 3.2.5.3 and 3.2.5.5, postulated shaft inflows associated with a PMF to be 10 to 100 m³. These volumes can be contained within the sump of ES-1 even if no drainage from the sump is assumed. These volumes are considerably less than those volumes estimated to enter the shaft considering the highly improbable flooding scenario, considered above.
- o Considering convectively driven air movement from the repository, the exploratory shafts (including shaft fill and MPZ) are not likely to be preferential pathways for gaseous radionuclide releases if the air conductivity of the shaft fill is less than about 3×10^{-4} m/min (Section 3.3.5). This air conductivity value is predicted to restrict air flows out of the exploratory shafts to 2.5% of the total air flow out of the repository. This value of 2.5% is one order of magnitude less than the airborne performance goal established for the shafts.
- o From the barometric air flow analyses presented in Section 3.4.4, it is concluded that the exploratory shafts (including shaft fill and the MPZ) are not likely to be preferential pathways for gaseous

radionuclide releases if the air conductivity of the shaft fill is less than about 10^{-1} m/min. This conclusion is reached because the volume of air in the exploratory shafts is not fully displaced during the occurrence of a broad range of meteorological conditions.

- o From the discussion in Section 4.1, the potential for significant changes in the hydraulic conductivity of the concrete liner due to thermochemical effects is expected to be low. Therefore, surface-water infiltration through the shaft liner is expected to be less than that which occurs through the shaft fill.
- o The deposition of solids from the interaction of the shaft liner with ground water will most likely be a localized phenomenon, even considering highly improbable amounts of water. Therefore, the effectiveness of the exploratory shaft sumps to drain should not be reduced significantly (Section 4.2.4).
- o The impact of episodic water percolating through the shaft fill and MPZ on the sorptivity of the Calico Hills unit has been found to be negligible (Section 5.1). Therefore, if water containing radionuclides reaches the base of ES-1, the effectiveness of the Calico Hills unit in sorbing radionuclide would not be reduced.
- o In the event that future analyses suggest that liner removal and/or MPZ restoration is required, a variety of construction techniques exist to remove the shaft liner, to emplace backfill, to emplace a shaft seal and to restore the modified permeability zone (Section 3.5 and 4.3).
- o The current performance analyses assume that the MPZ is not greater than 20 to 60 times the undisturbed rock mass hydraulic conductivity over a distance one radius from the edge of the liner. We believe that this model is reasonably conservative, and excavation of the shaft liner is not expected to create a condition more severe than that estimated by the MPZ model.

While it is concluded that the design and construction of the ESs are not expected to significantly influence the performance of the repository, recommended actions can be taken in constructing the ESs to enhance performance of the repository. These recommendations are:

- o The proposed construction method should not preclude nor unnecessarily complicate the removal of the concrete liner associated with the exploratory shafts. This is particularly true but not limited to that portion of the liner below the repository station. Furthermore, if the hanger rods used to secure the concrete forms used to place the shaft liner are not necessary to provide structural support for the liner, consideration should be given to using removable hanger rods. Removal of these hanger rods could facilitate removal of the liner.
- o The paste portion of the concrete liner placed in the lower portion of the shaft, i.e., the sump, should not infiltrate the fractures of the rock mass to the point where it could not be removed.
- o Overbreak that occurs while excavating the ESs should be recorded as a qualitative indicator of the quality of the rock to assure that adequate records are available for sealing the shaft. We recommend that the overbreak be recorded every foot in the upper 100 ft of the Tiva Canyon Member. In the remainder of the shaft, overbreak at any point greater than 0.5 ft should be recorded as well as depth from the surface and azimuth.
- o It is preferred that no grout injection for ground stabilization or water control occur behind the shaft liner. If future analyses indicate that grouting is necessary or desirable to achieve enhanced repository performance, it is possible that a previously grouted zone could not meet future, long-term performance objectives. Not grouting in water-producing fracture zones would simplify any grouting action that might be required for long-term performance. It is recognized, however, that some grouting may be desirable to satisfy operational or testing concerns.

This page is for page number only

APPENDIX A

Perspective into Radionuclide Transport

The purpose of this appendix is to provide a perspective into the potential for radionuclide transport due to the presence of the ESs. To achieve this perspective, descriptions of several mechanisms that can potentially enhance radionuclide releases from the underground facility are given. These descriptions are supplemented by simple calculations that compute the travel distance and/or travel time of the transporting medium. The authors recognize that these mechanisms do not represent a comprehensive evaluation of all conceivable mechanisms and processes, e.g., effects of the presence of organics and microbial organisms are not considered. However, the mechanisms do represent some of the more commonly thought of mechanisms that could affect radionuclide transport due to the presence of shafts. The mechanisms considered include:

- o downward water movement through the shafts,
- o downward water movement in fractures from the repository horizon to the base of the ES-1,
- o upward movement of water in the sumps of shafts,
- o transport of radioactive solids through shafts,
- o gaseous transport through drifts and shafts due to gaseous diffusion,
- o gaseous transport through drifts and shafts due to convective forces, and
- o gaseous transport through shafts due to barometric forces.

A.1 Downward Water Movement Through Shafts

Shafts are pathways to the underground facility that could potentially increase the amount of water that could enter into the waste disposal

areas. The analyses presented below illustrate the time required to saturate shaft fill to a 300 m depth assuming a constant supply of water at the upper portion of the shaft. It is presumed in the analysis that if water does not reach the repository horizon over a substantial period of time, there is no potential for water to reach the waste disposal areas and this mechanism should not be considered further.

The approach used was to compute the downward infiltration of water through the shaft fill which is assumed to be initially dry. The Green and Ampt solution (Hillel, 1971, pp. 140-143) was used to calculate the saturated vertical infiltration into the initially dry shaft fill. The discussion of how the Green and Ampt solution is applied is provided in Fernandez et al. (1987). The results illustrating the time to saturate 300 m of backfill is given in Figure A-1. This figure suggests there is a time delay for a fully saturated front to reach the repository horizon. Depending on the hydraulic conductivity of the shaft fill, this time delay can vary over many orders of magnitude. Figure A-1 also illustrates that if a coarse material is placed in the shaft, water from the surface is transmitted to the repository level over a short time. Because there is some potential for water to be transmitted down to the repository horizon (depending on the condition encountered at the surface), this mechanism is considered further in Chapter 3 of this report.

A.2 Downward Water Movement in Fractures From the Repository Horizon to the Base of the ES-1

In this section, the potential for the exploratory shaft (ES-1) to act as a preferred pathway in releasing radionuclides is discussed. The ES-1 is considered here because it extends below the repository horizon and slightly into the Calico Hills unit. The mechanism considered here is the preferential release of radionuclides transported by water from the waste disposal area to the sump of the exploratory shaft through the fracture system. The geometric relationship between the waste disposal area and the ES-1 is shown in Figure A-2. Because waste is stored at a minimum distance of about 200 m, an effective barrier of rock results. The effectiveness of this barrier is further enhanced because: (1) fracture flow from the repository to the ES-1 is not anticipated based on current knowledge of flow conditions and (2) even if fracture flow occurs, the dip for the

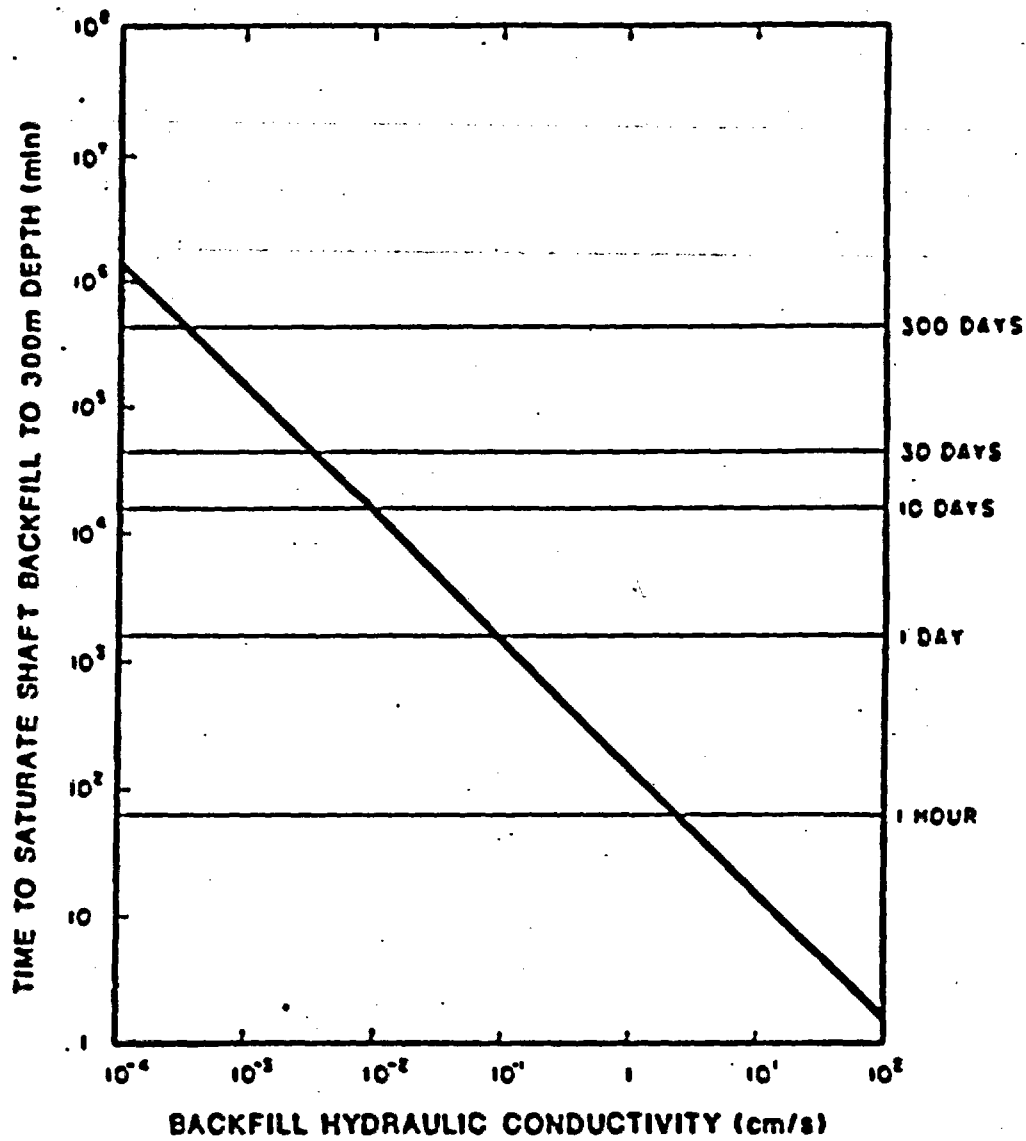


Figure A-1. Results From Green and Ampt Solution for Transient Flow Through Shaft Backfill

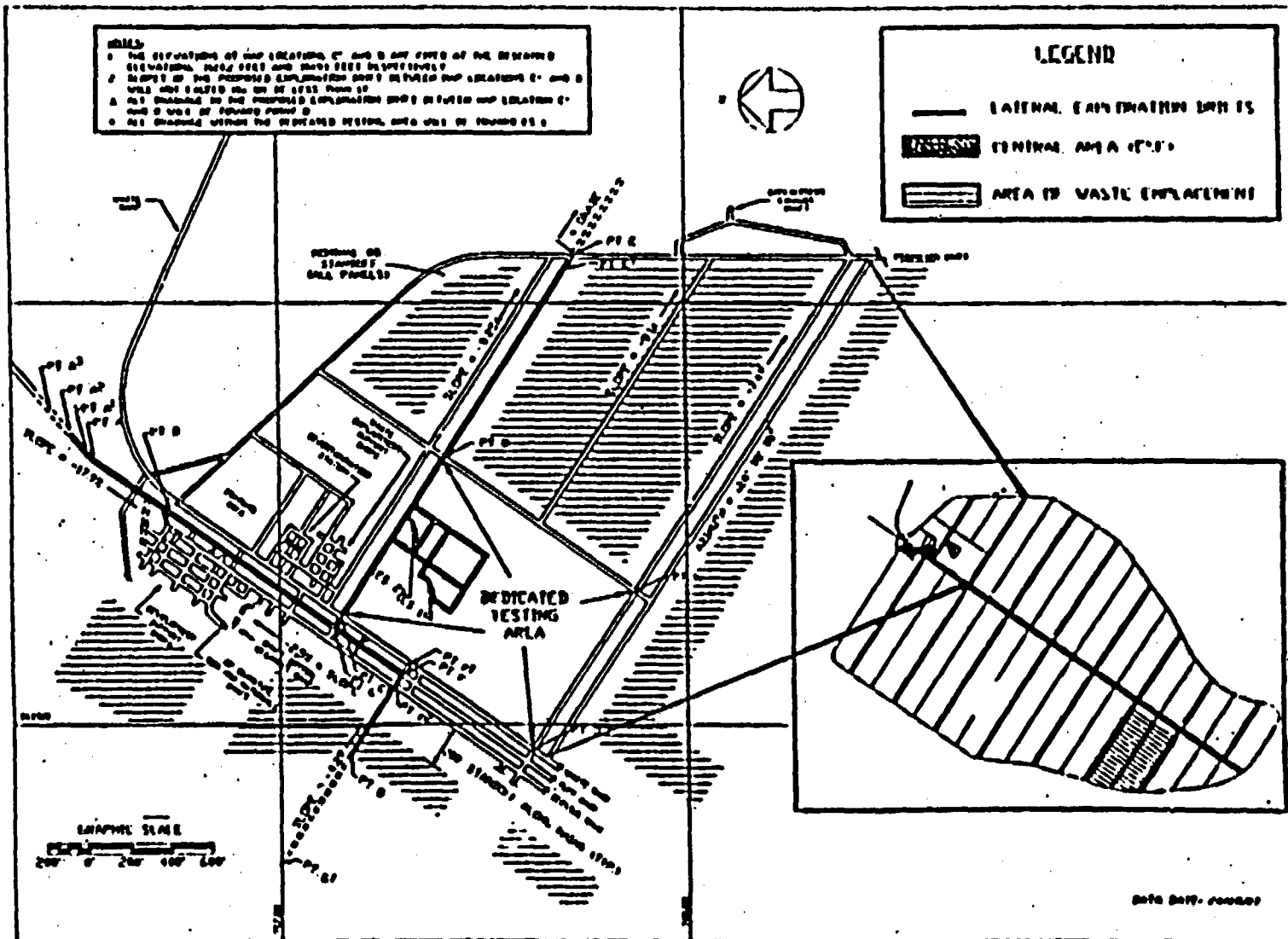


Figure A-2. Detailed Repository Layout in Vicinity of the Exploratory Shaft Facility (from DOE, 1988, p. 8.4-17)

majority of fractures is greater than 35°. Because the angle from the base of the ES-1 to the edge of the waste disposal area with the ground surface is approximately 35°, the majority of flow will not intercept the ES-1 if it is assumed that the majority of flow is controlled by fractures whose dip is greater than 35°.

If, however, we postulate saturated conditions occur in the waste disposal area which induces fracture flow, then it is reasonable to assume that a portion of this flow would be distributed uniformly in the rock mass below the repository. A portion of this distributed flow could potentially cross the ES-1 due to the fractured system. Therefore, if fracture flow occurs, together with uniform dispersion due to the presence of the fractures, then the fraction of flow down the ES-1 would occur roughly in direct proportion of the cross-sectional area of the ES-1 to the area of the whole repository. If the cross-sectional area of the ES-1 and its associated MPZ (61.4 m³) were compared with the cross-sectional area of the entire repository area (5.7 x 10⁶ m², MacDougall et al., 1988, Appendix M), the proportion of flow down the ES-1 and its MPZ would be 1.1 x 10⁻⁵ of the total flow through fractures. Therefore it is concluded that the ES-1 will not become a preferential pathway following the occurrence of an unanticipated event or scenario that would create fracture flow at the repository horizon.

A.3 Upward Movement of Water in the Sumps of Shafts

The mechanism discussed in this section involves the transport of standing water at the base of a shaft upward due to fracture and matrix capillary forces. This mechanism assumes that standing water occurs and radionuclides are in solution at the base of the shaft implying transport of contaminated water to the shaft. This assumption of transport of contaminated water to the shaft, in itself, may totally negate the feasibility of this mechanism to occur because one constraint placed on the drift grades in the underground facility is to establish a drainage pattern for the access and emplacement drifts so that no drainage occurs from these drifts into ES-1. This constraint, therefore, significantly reduces the possibility of radionuclides to reach ES-1. The following discussion nevertheless, presents discussions and calculations evaluating the effect of this mechanism.

Because the sump at the base of ES-1 is located predominantly in welded tuff which is highly fractured, the capillary forces in the modified permeability zone is controlled by the fractures. Therefore, upward transport of water in fractures due to capillarity was computed using the formula

$$h = 2\sigma \cos \theta / \rho g b$$

(Lozman, 1972, p. 2)

where h = height of water in a fracture, m,
 σ = surface tension of water against air, newton/m,
 θ = contact angle between the water in the fracture and the tuff
(assumed to be zero degrees),
 ρ = density of water, kg/m³,
 b = fracture aperture, m, and
 g = acceleration due to gravity, m/s².

This situation could be applied to fractures penetrating saturated zones such as the water table or a shaft containing water at the base. For fractures having aperture widths of 71 μm (Sinnock et al., 1984, p. 12) and 25 μm , the rise of water in the fracture was computed to be approximately 0.21 and 0.58 m, respectively. The temperature of the water was assumed to be 30°C. At 52°C, (see Section 5.1.1 of the text) the rise of water in fractures having apertures of 71 and 25 μm would be 0.20 and 0.56 m respectively. Because of the limited extent to which capillary forces within a fracture can transport water upward, radionuclide transport upward in a fracture is considered insignificant.

If standing water occurs within the shaft fill portion of the shaft sump, movement of water upward in the shaft fill by capillary forces is possible. The rise of water above the fully saturated level or the phreatic surface is termed the capillary rise. The extent of capillary rise depends on the pore sizes of the shaft fill. For example, capillary rise in a material that has larger pore sizes, such as a coarse sand, would be low (2-5 cm). For a shaft fill having small pore sizes such as a clay, the capillary rise could range from 200 to 400 cm (Bear, 1976, p. 481). Under either case, i.e., a shaft fill that is representative of a coarse

sand or clay, the capillary rise would be a function of the total length of the shaft. Therefore, because (1) capillary forces within the shaft fill can transport water over a limited extent, (2) transport of radionuclides to the shaft sump is unlikely, and (3) duration of ponding of water, if it occurs at all, is anticipated to be short because it is postulated that water can be effectively drained through the base of the shaft, radionuclide transport upward due to capillary forces in the shaft fill is considered insignificant.

A.4 Transport Due to Solid-Solid Diffusion

Using a one-dimensional solution to Fick's second law, the time for solid diffusion of radionuclides can be computed. The formula used to compute the time for radionuclide migration, for the specified conditions, is:

$$\frac{C_A}{C_{A_0}} = \text{erfc} \frac{X}{\sqrt{4\phi_{AB} t}} \quad (\text{A-1})$$

(Freeze and Cherry, 1979, p. 393)

where

- C_A = concentration of A at point X, moles/l.
- C_{A_0} = concentration of A at point of origin, moles/l.
- X = distance from original point of diffusion, m.
- ϕ_{AB} = binary diffusivity for system A-B, m^2/s , and
- t = time over which diffusion occurs.

The most significant unknown in this formula is the diffusion coefficient for uranium through welded tuff. The diffusion coefficient used below is $10^{-15} \text{ cm}^2/\text{s}$, which is believed to be extremely conservative because it is at the higher end of the diffusion coefficients of some solid-solid diffusion coefficients given in Bird, Stewart, and Lightfoot (1960, p. 505). Using this diffusion coefficient and evaluating the condition where the solid portion of the radioactive waste migrates 0.1 m and its concentration is 99% of its original concentration, a transport time of about 10^{13} years is computed. However, the diffusion coefficient of uranium or uranium oxide because of its molecular size would probably be less than the value

of 10^{-15} cm^2/s used above. A diffusion coefficient of 10^{-30} cm^2/s yields a transport time of 10^{28} years. Because of these long transport times, the potential for radionuclide release by solid-solid diffusion is considered to be insignificant.

A.5 Gaseous Transport Due to Diffusion

Some radionuclides can be released in a gaseous form and therefore the potential significance of binary-gaseous diffusion is considered here. Some potential gaseous species (Xe isotopes, Rn, Kr-85, and H-3) can be eliminated from concern because of their short half-lives, assuming the containment period to be 300 to 1000 years. The radionuclides that could potentially enter the repository in a gaseous state are C-14 and I-129 (Van Koynenburg et al., 1984, p. 1). Equation A-1 is used to compute the relative concentration-versus-time curves for I-129 and C-14. However, in order to apply Equation A-1, the diffusivity values for the gaseous forms of I-129 and C-14 are needed. It is assumed that I-129 occurs as I_2 and C-14 occurs as CO_2 . Using an approach described in Reid et al. (1977, pp. 548-550) for binary-gas diffusion coefficients and in Smith (1970, p. 406) for Knudsen diffusion coefficients, diffusivities are computed for air-iodine and air-carbon dioxide systems. The computed binary diffusion coefficients for these two systems are $0.081 \text{ cm}^2/\text{s}$ for the air-iodine system and $0.156 \text{ cm}^2/\text{s}$ for the air-carbon dioxide system. The computed Knudsen diffusion coefficients are $10.6 \text{ cm}^2/\text{s}$ for iodine and $25.3 \text{ cm}^2/\text{s}$ for carbon dioxide. These diffusivities are combined by the method described in Mason and Evans (1969, p. 362) to give overall gaseous diffusion coefficients of $0.080 \text{ cm}^2/\text{s}$ for the air-iodine system and $0.155 \text{ cm}^2/\text{s}$ for the air-carbon dioxide system. These diffusivity values assume open drifts and shafts. If backfill is emplaced, a partial restriction of the migration of the gas occurs. To compute the magnitude of this restriction, an effective diffusivity can be computed. It is a function of the porosity of the material through which the gas is diffusing, and the tortuosity. The following equation is used to compute the effective diffusivity:

$$D_e = \frac{\epsilon}{\tau} D \quad (\text{Froment and Bischoff, 1979, p. 167}) \quad (\text{A-2})$$

where D_e = effective diffusivity, cm^2/s .
 ϵ = porosity of material through which diffusion occurs
 τ = tortuosity, and
 D = diffusion coefficient, assuming no restriction to diffusion, cm^2/s .

The porosity assumed for the drift and shaft fill is 0.3. The value for tortuosity is assumed to be 3 which corresponds to loose random pore structure (Froment and Bischoff, 1979, p. 167).

Figure A-3 illustrates the relationship between the relative concentration of the gas under consideration versus time for a distance of 600 m from the waste disposal area. This distance represents an approximation of the distance from the waste disposal area to the surface entry point of ES-1 or ES-2.

Two sets of curves are presented. The first set assumes no backfilling of the shafts and drift. The second set assumes the drifts and shafts are backfilled with a material that is emplaced loosely. Figure A-3 illustrates that if only binary diffusion occurs, considerable time, 10^5 to 10^6 years, is required to release I_2 or CO_2 at a concentration of -99% of the original concentration in the waste disposal areas. Lesser concentrations are released at much shorter times following release of the gas at the disposal area. Also, a substantial reduction in the concentration exiting the shaft can be achieved by emplacing loose shaft and drift fill. Emplacement of consolidated shaft fill or a single-shaft or drift seal can further reduce the release through the shaft. Because binary gaseous diffusion is a slow process as indicated by Figure A-3 and because travel times can be reduced substantially by simple backfill, binary-gaseous diffusion is not considered to be a significant release mechanism.

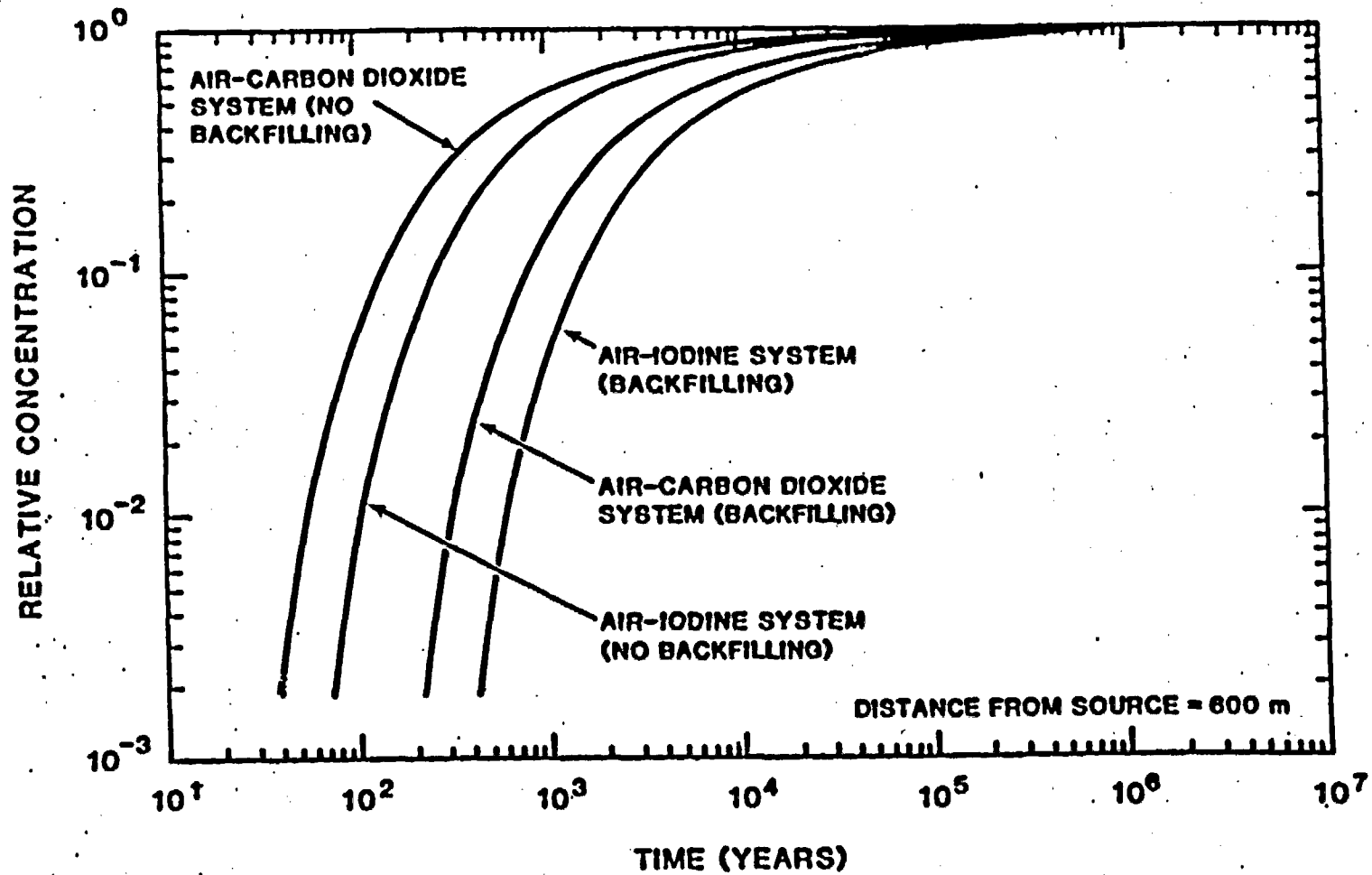


Figure A-3. Concentration of Two Gaseous Systems Due to Binary Gaseous Diffusion (600 m From Point of Release and at Various Times Following Release)

A.6 Gaseous Transport Due to Convective Forces

For a repository located above the water table, there is the possibility of release of radionuclides by air flow out of the repository through the shafts or through the host rock. Air flow may develop as a convective circulation in response to the thermal gradient.

After the emplacement of waste canisters, heat is initially transferred by conduction from the waste canisters to the surrounding rock. Vertical temperature gradients will develop from the repository horizon and potentially affect air and water density. If sufficient energy in the form of heat is imparted to the air or water vapor, convective transport is established.

Two potential convective air flow mechanisms are illustrated in Figure 3-19. Mechanism A assumes that no upward flow occurs through the host rock relative to flow through the shafts, ramps, and drifts. The Exploratory Shaft (ES-1) and adjacent Exploratory Shaft (ES-2) are within the repository boundary, and the temperature is relatively high near the repository horizon. The men-and-materials shaft, the emplacement exhaust shaft, and the ramps are located outside or just inside the repository perimeter, and the temperature gradients are lower. In response to these gradients, air will tend to rise in ES-1 and ES-2 and air will be drawn in through the other entries. This mechanism may occur if the shafts and drifts are open or if the backfill is relatively permeable compared to the host rock. In Mechanism B, convective air circulation is also assumed to occur through the host rock. The waste disposal areas are relatively hot and the heated air tends to rise vertically through the rock as well as through ES-1 and ES-2. Because temperature rises in the rock are expected and it is uncertain what the effects of this temperature rise will be, this mechanism is considered further in the text.

A.7 Gaseous Transport Due to Barometric Forces

Another potential flow mechanism for the transport of radionuclides is the development of a differential air pressure between the repository and

the ground surface. A weather front moving suddenly across the repository site might result in a reduction of barometric pressure, producing a pressure gradient between the repository and the surface. Pressure gradients may also develop more gradually in response to changing seasons. Changes in barometric pressure are cyclical or periodic in nature, so that air would eventually move back into the repository. The ease with which air moves in and out of the repository will depend upon the properties of the backfill placed in the shafts and ramps and the surrounding rock. Conceptually, large volumes of air may move through shafts and ramps containing a high-conductivity, coarse backfill. Smaller volumes of air might move through shafts and ramps containing a fine, low-conductivity backfill, although a proportionally greater amount of flow might occur through the MPZ around the shafts and ramps. In addition, a low conductivity backfill will isolate the repository from pressure variations at the surface, while a high conductivity backfill will result in a more significant pressure response within the repository. Because barometric fluctuations will occur at the surface and it is uncertain what the effect of these fluctuations are, this mechanism is considered further in the text.

APPENDIX B

Explanation of Water Inflows to ES-1

The purpose of this appendix is to describe the shape of the curves in Figure 3-7 of Section 3.2.1 of this report. For ease in explaining the shape of these curves, a single curve is selected for the discussion, i.e., the lines associated with the Tiva Canyon having a hydraulic conductivity of 10^{-2} cm/s (Figure B-1). The features discussed in Figure B-1 are labeled A through E on Figure B-1.

To explain these features of this curve, Figure B-2 is shown below. This curve shows the flow rates for the four flows considered in the model in Section 3.2.1, i.e., alluvial flow, Tiva Canyon flow, Dupuit (or radial) flow, and MPZ model flow. The curves in Figure B-2 represent the Tiva Canyon and the MPZ model flow rate components used in the calculation of flow into ES-1. When the saturated alluvial hydraulic conductivity is less than the saturated hydraulic conductivity of the underlying Tiva Canyon member, it is assumed that the rate of vertical infiltration into the Tiva Canyon member is equal to the vertical infiltration rate of water leaving the alluvium. When the hydraulic conductivity of the Tiva Canyon is less than the hydraulic conductivity of the alluvium, the vertical infiltration into the Tiva Canyon is controlled by the saturated, hydraulic conductivity of the Tiva Canyon Member. (In both instances the gradient of flow vertically downward in the alluvium and the Tiva Canyon member is conservatively assumed equal to one.)

The flow through the MPZ and the shaft fill is assumed to be dependent on the saturated, hydraulic conductivity of the Tiva Canyon member. Therefore, the MPZ model flow rate is constant for a single value of Tiva Canyon hydraulic conductivity.

The alluvial flow was described in Section 3.2.1 as being parallel or near-parallel to the bedrock-alluvium interface. The alluvial flow rate as computed in this report is dependent on the hydraulic conductivity of the

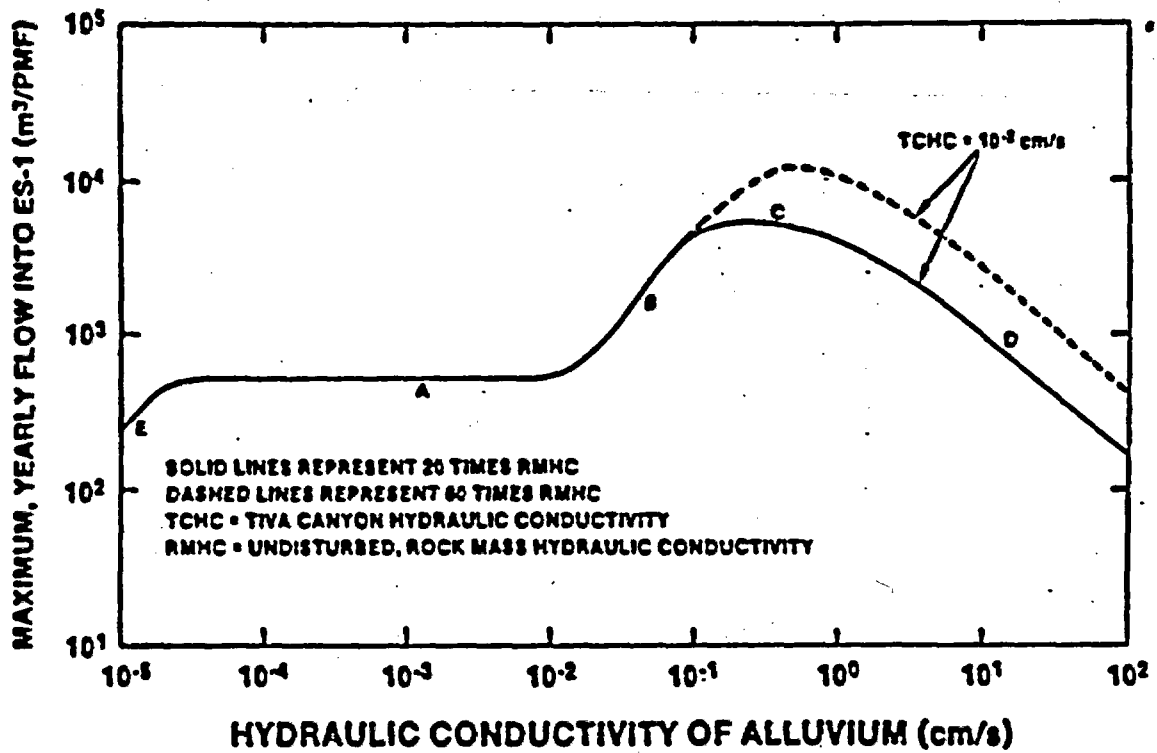


Figure B-1. Estimated Volumes of Water Entering ES-1 (PMF, Shaft Fill. Conductivity = 10^{-2} cm/s, Excavated Shaft Diameter 4.42 m, Tiva Canyon Hydraulic Conductivity = 10^{-2} cm/s)

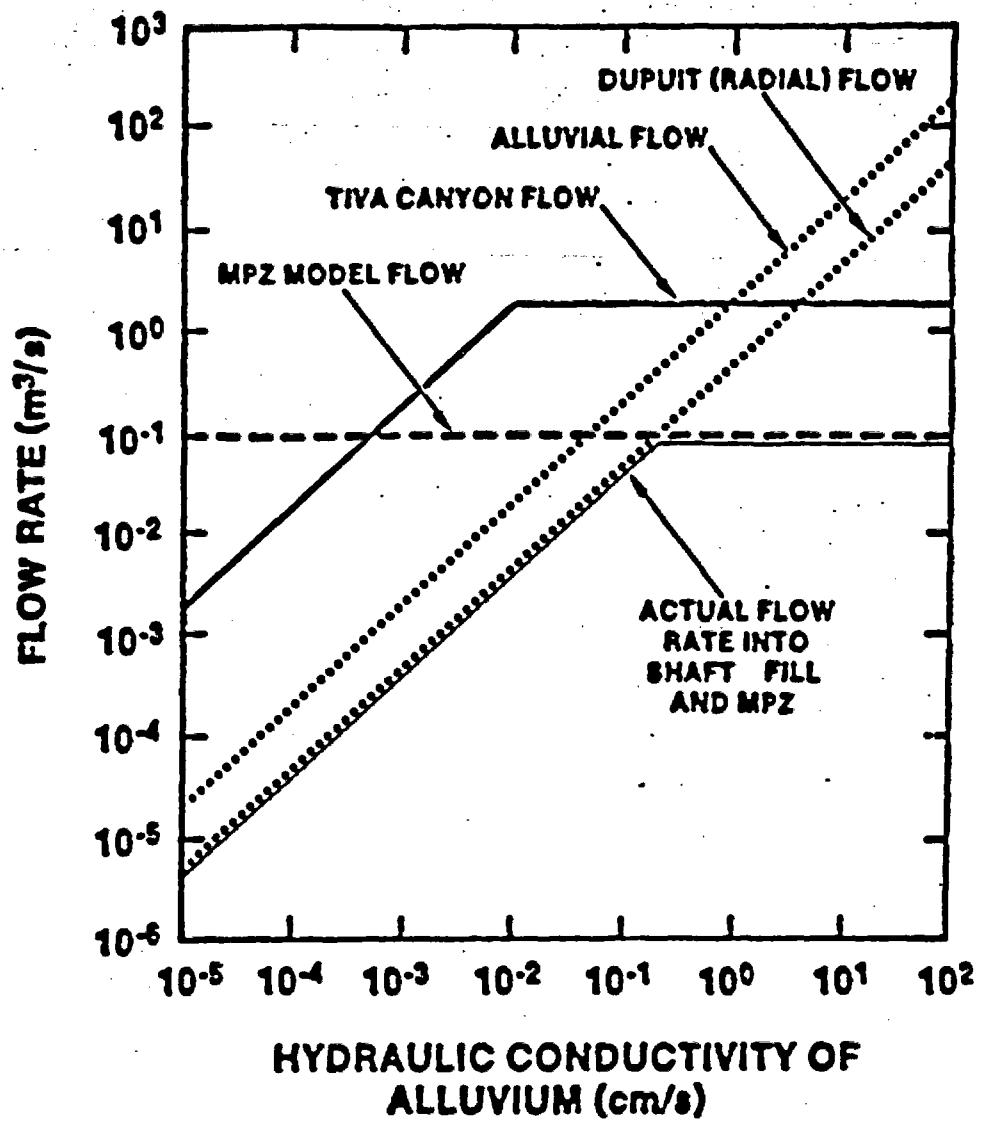


Figure B-2. Approximation of Flow Rates for Flows Used in the Model Presented in Section 3.2 (Saturated, Hydraulic Conductivity of the Tiva Canyon Member and the Shaft Fill = $10^{-2} cm/s$)

alluvium as well as the area of the alluvium that is fully saturated. The radial (Dupuit) flow rate towards the shaft is dependent on the hydraulic conductivity of the alluvium and the height of alluvium above the bedrock alluvium contact that is saturated at any given time. Because the area through which the alluvial flow occurs and the height of saturated alluvium above the bedrock-alluvium contact vary with time, a representative area for alluvial flow and a representative height of saturated alluvium are selected to illustrate how the alluvial flow rate and the radial (Dupuit) flow rate vary with the saturated hydraulic conductivity of the alluvium.

In Figure B-1, the segment of the curve defined as "A" can be explained as follows. The alluvial and Tiva Canyon flows represent flows that do not enter the shaft and MPZ. Therefore, in the "A" portion of Figure B-1, the flow into the shaft and MPZ model is the lesser of the two flows, i.e., the radial (Dupuit) flow and the MPZ model flow (see Section 3.2.1). The nonshaft and MPZ flow is comprised of the Tiva Canyon and the alluvial flow.

The relationship between these various flows and the total flood volume can be described by the following water balance equation:

(substituting the equations presented in Section 3.2.1)

$$V_{PMF} = V_s + V_{tc} + V_a \quad (B-1)$$

where V_{PMF} = cumulative flow for the PMF.
 V_s = cumulative flow down the shaft,
 V_{tc} = cumulative infiltration in the Tiva Canyon formation, and
 V_a = cumulative alluvial flow.

If the shaft flow is assumed to be governed by the radial Dupuit flow then:

$$V_{PMF} = \frac{\pi K_{all} (H - H_o)^2}{ln \frac{R}{r}} \cdot t + K_{tc} A_{tc} \cdot t + K_{all} i A_{all} \cdot t \quad (B-2)$$

where K_{tc} = Tiva Canyon hydraulic conductivity,
 K_{all} = alluvial hydraulic conductivity,
 t = time,
 i = alluvial gradient,
 R = outer radius,
 r = inner radius,
 A_{all} = alluvial area, and
 A_{tc} = Tiva Canyon area.

Therefore, if it is assumed that the Tiva Canyon has a saturated hydraulic conductivity value of 10^{-2} cm/s, and the range of alluvial hydraulic conductivity is from 10^{-5} to 10^{-2} cm/s for (segment A) of Figure B-1, then the Tiva Canyon flow will be controlled by the rate of flow vertically through the alluvium. Equation B-3 can then be written as ($10^{-5} \leq K_{all} \leq 10^{-2}$):

$$V_{PMF} = \frac{\pi K_{all} (H - H_o)^2}{\ln \frac{R}{r}} \cdot t + K_{all} A_{tc} t + K_{all} i A_{all} t \quad (B-3)$$

Assuming constant geometry, Equation B-3 can be simplified further to several constant values:

$$C_1 = C_2 t K_{all} + C_3 K_{all} t + C_4 K_{all} t \quad (B-4)$$

where $C_1 = V_{PMF}$,
 $C_2 = \frac{\pi (H - H_o)^2}{\ln \left(\frac{R}{r}\right)}$,
 $C_3 = A_{tc}$, and
 $C_4 = i A_{all}$.

Because all flows are occurring over the same time period, this equation can be further simplified as:

$$C_1 = C_2 t K_{all} + K_{all} t C_5 \text{ and} \quad (B-5)$$

$$C_1 = K_{all} t (C_2 + C_5) \quad (B-6)$$

where $C_5 = C_3 + C_4$ and $10^{-5} \leq K_{all} \leq 10^{-2}$.

The term $C_2 \pm K_{all}$ represents shaft plus MPZ flow and the term $K_{all} \pm C_5$ represents nonshaft flow. In the equation, there are only two variables, " K_{all} " and " t ." For this relation to be correct, " K_{all} " and " t " are inversely proportional to each other. Further, for any " K_{all} " and " t " combination, the flow into the shaft and MPZ and the nonshaft flow will also be constant. Therefore, the maximum, yearly flows into ES-1 between hydraulic conductivity values of 10^{-5} cm/s to 10^{-2} cm/s for the alluvium (Figure B-1) is constant. The reason for the lower flow in the range of 10^{-5} to 2×10^{-5} cm/s in Figure B-1 is the fact that when the alluvium has a low saturated hydraulic conductivity the time to drain the water from the modelled area is greater than one year. The values plotted on Figure B-1 are yearly inflows.

As the saturated hydraulic conductivity becomes greater than 10^{-2} cm/s the flow rate into the Tiva Canyon can be no greater than the product of the hydraulic conductivity of the Tiva Canyon Member (K_{tc}) or (K_{all}), whichever is lower and the cross-sectional area (A_{tc}). The term in Equation B-4 " $C_3 K_{all} t$ " that describes the Tiva Canyon flow rate no longer applies. The Tiva Canyon flow rate is constant and equal to " $C_3 K_{tc} t$." As the hydraulic conductivity of the alluvium increases between 10^{-2} cm/s to about 2×10^{-1} cm/s on Figure B-1 (Segment B), the Dupuit and alluvial flows will increase but the Tiva Canyon flow remains constant. Therefore, the combined nonshaft plus MPZ flow is constant during a greater and greater proportion as compared to the flow entering the shaft and MPZ. This explains the constantly increasing slope over segment B.

Once the peak "C" is reached on Figure B-1, there is a new factor to consider. The Dupuit flow will no longer dominate the flow into the shaft and MPZ. Rather, the flow rate described by the MPZ model controls flow. This flow rate is constant from 2×10^{-1} cm/s to 100 cm/s as indicated in Figure B-2. However because the nonshaft plus MPZ flow is increasing (due to the increasing alluvial flow) and subsequently the flow nonshaft plus MPZ flow is also increasing, the proportion of total flow going into the shaft and MPZ flow is proportionally decreasing. This phenomena describes

the decreasing flow into the shaft and MPZ, or Segment D of Figure B-1. An additional consideration that contributes to the decreasing flow in Segment D is the fact that the time to drain the PMF volume becomes less and less as the alluvial hydraulic conductivity becomes greater and hence the alluvial flow becomes greater. This effect is very noticeable when the alluvial flow becomes greater than the Tiva Canyon flow, i.e., at about 7×10^{-1} cm/s (alluvial conductivity).

APPENDIX C

The Density Method as Applied to Flow Through a Porous Media

This appendix provides detailed assumptions used in the convective air transport analysis. The assumptions are used to develop a formula for the convective flux rate which may be compared with flux rate relationships for convective transport through a porous media. A discussion of the development of thermal instability and convective air transport is also presented.

In developing the model the following assumptions are made:

1. Darcy's law is valid

The resistance to air flow through open or backfilled drifts may be characterized as either laminar or turbulent. In turbulent flow, resistance is nonlinearly related to potential. In laminar flow, resistance is linearly related to potential, and flow may be calculated using Darcy's law.

The results of the analyses were used to check the validity of Darcy's law by calculating the Reynolds number from the air velocity or specific discharge, air kinematic viscosity, and characteristic dimension. For laminar flow through backfill, the characteristic dimension is the mean grain diameter, and Darcy's law is valid as long as the Reynolds number does not exceed a value between 1 and 10 (Freeze and Cherry, 1979, p. 73). The calculated Reynolds number was within the specified limits and the assumption of head loss varying linearly with flow rate was found to be justified.

2. Air temperatures in the shaft are the same as in the adjacent rock
Convective air flow through a heated repository will involve a complex coupling of heat transfer from the rock to the air, which will tend to drive air flow, and cooling of the rock by passage of the air, which will tend to reduce the driving mechanism. In the modeling which follows, the effects of cooling of the rock are ignored. The air is assumed to be at the same temperature as the

adjacent rock at all points in the repository, including the shafts.

Intuitively, this simplified approach is most valid for the case of a backfilled repository in which air flows relatively slowly and temperatures are able to equilibrate. The faster the air flow, the greater the volume of air moving through the repository, and it is more likely that the rock will be cooled to the extent that convection slows down. A converse effect to rapid air flow could occur if the air flow is not sufficient to cool the rock in the repository significantly. Flow through the repository would be greater than that calculated using our simplified approach if air in the exit shafts (or rock) is not cooled by heat transfer to the rock. In this case, there is a potential for the repository to act as a heat engine. The driving pressure could then be about three times higher than that calculated with the assumption of equilibrated temperatures. This higher driving pressure occurs, however, because air is expelled at the ground surface at the same temperature as the temperature of the repository rooms, a condition which is intuitively over-conservative.

3. Air flow is incompressible and the air is dry

Since convective transport evolves from air buoyancy effects dependent on temperatures, thermal properties such as air density and air viscosity will change through the circuit. In reality, flow is compressible with the actual resistance to mass flow rate dependent on density and viscosity. In the analyses presented in this report, air compressibility effects on fluid flow are ignored for reasons of simplification. This assumption is considered to be reasonable given that the pressures involved are small (i.e., <0.1 psi). According to Hartman (1982, p. 160), compressibility effects may be ignored for mine static head pressure drops of less than 5 kPa (0.72 psi) or where differences in elevation are less than 430 m.

Convective transport can, in general, involve both the transport of air and water vapor. The development of high temperatures at the repository horizon will result in drying of the host rock and subsequently lowering the moisture content of the rock. It is thus assumed that the air may be dry at the time at which peak temperatures are reached. This assumption is conservative because the effect of adding moisture to the convective flow will be to increase the work required to lift the air to the surface and to thus reduce flow rates.

4. Air circulation occurs along specified paths

The model assumes that a particular path for air circulation (Mechanism A or B, Figure 3-19) is established and that flow is one-dimensional through either shaft or ramp backfill, open drifts, or through damaged or undamaged tuff. The model ignores the development of secondary circulation currents that might develop in the host rock above or below the repository away from the waste containers.

The assumptions presented above may be used to derive an expression for flux rate due to convective circulation.

The draft pressure may be calculated by the density method for the circuit (Hartman, 1982):

$$\Delta p = (\gamma_i - \gamma_o)L \quad (C-1)$$

where γ_i = mean air density of an inlet shaft, pcf,

γ_o = mean air density of an outlet shaft, pcf, and

L = height of the shaft, ft.

If it is assumed that the mean temperatures T_i and T_o correspond to the densities γ_i and γ_o respectively, then the following relationship may be used to express volumetric thermal expansion effects (Bear, 1976, p. 655):

$$\gamma_i = \gamma_o [1 - \beta(T_o - T_i)] \quad (C-2)$$

where β = coefficient of volumetric thermal expansion, $^{\circ}\text{C}^{-1}$,

T_1 = mean temperature at density γ_1 , $^{\circ}\text{C}$, and

T_0 = mean temperature at density γ_0 , $^{\circ}\text{C}$.

Substituting Equation (C-2) into Equation (C-1), the draft pressure differential is

$$\Delta p = -\beta (T_0 - T_1) L \gamma_0 \quad (\text{C-3})$$

Expressing the above reaction as a potential difference, the following expression is obtained:

$$\Delta h = \frac{\Delta p}{\gamma_0} = -\beta (T_0 - T_1) L \quad (\text{C-4})$$

Substitution of the change in potential (head loss) into Darcy's Law is used to calculate the flux rate. If it is assumed that the resistance to flow occurs in backfilled shafts with the underground repository drifts open, then:

$$V = -K_e' \cdot \frac{\Delta h}{2L} = \frac{-K_e' (T_0 - T_1) \beta}{2} \quad (\text{C-5})$$

where K_e' equals the air conductivity and V equals the Darcy flux rate.

The actual velocities through the backfilled shafts are (Freeze and Cherry, 1979, p. 71):

$$V_a = \frac{V}{n} = \frac{-K_e' (T_0 - T_1) \beta}{2n} \quad (\text{C-6})$$

where V_a = actual velocity and
 n = porosity.

The air conductivity, K_e' , may be expressed as (Freeze and Cherry, 1979, p. 27):

$$K_e = \frac{\rho g}{\mu} k \quad (C-7)$$

where k = intrinsic permeability,
 ρ = mass density,
 g = acceleration constant, and
 μ = absolute viscosity.

Substituting Equation (C-8) into Equation (C-7), the following relationship is obtained:

$$v_a = \frac{-\rho g k \beta (T_o - T_i)}{2r\mu} \quad (C-8)$$

This page is for page number only

APPENDIX D

Estimated Construction Schedule and Costs

This appendix presents estimated construction costs and schedule for the complete removal of the liner from the ES and the construction of a single anchor to bedrock plug/seal. The estimated schedule, with a duration of 44 weeks, is presented in Figure D-1. The liner is assumed to be broken by a nonexplosive expansive demolition agent. As discussed in Section 4.3, it is estimated that the use of hydraulic splitters or drilling and blasting would require a similar amount of time, while the use of hand-held pneumatic splitters would require more time. The estimated overall site costs are presented in Table D-1 and assume no existing shaft services at the time of liner removal. It is estimated that \$3.5 million is required for all activities, with approximately 60% of these costs incurred for liner removal and backfilling. The estimated costs for pre-grouting and plug construction are \$134,000 and \$380,000, respectively.

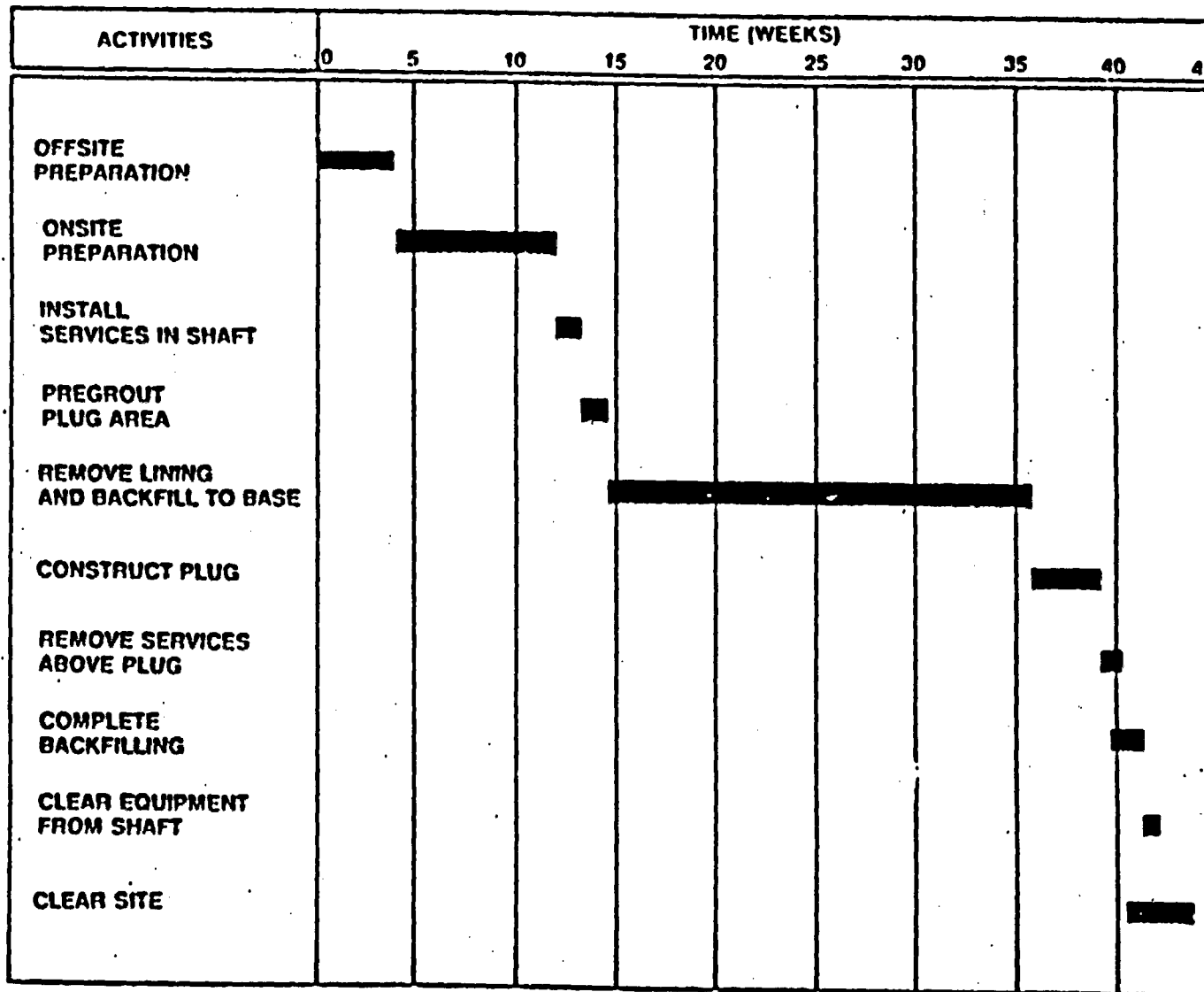


Figure D-1. Estimated Schedule for Liner Removal and Seal Installation

Table D-1. Overall Site Cost Estimate

WEEKS	Offsite ^(a) 4.0	Onsite ^(b) 8.0	Shaft Services 1.0	PregROUT Plug 1.5	Remove Lining and Backfill 22.5	Construct Plug 3.5	Shaft Services 0.5	Clear Shaft Top 1.0	Clear Site 2.5	Follow-up Reports 6.0	Total
LABOR	56,800	223,600	52,500	78,800	1,437,000	241,800	14,600	29,100	82,800	46,200	2,263,200
EQUIPMENT											
Common ^(c)	1,000	177,200	48,600	13,600	57,000	30,500	5,100	7,900	16,200		357,100
Grouting				23,400		10,700					34,100
Drilling				1,900	8,700	4,400					15,000
Mucking					6,500	3,500					10,000
Subtotal	1,000	177,200	48,600	38,900	72,200	49,100	5,100	7,900	16,200		416,200
MATERIALS											
Concrete		10,600				32,500					43,100
Grouting				2,200		300					2,500
Subtotal		10,600		2,200		32,800					45,600
CONSUMABLES											
Common ^(d)	7,400	26,200	6,600	9,900	182,900	30,400	1,800	3,600	9,000	6,000	283,800
Grouting				900	87,200	4,900					93,000
Drilling					8,400	400					8,800
Mucking											
Subtotal	7,400	26,200	6,600	10,800	278,500	35,700	1,800	3,600	9,000	6,000	385,600

(a) Offsite costs include necessary administrative costs for procurement and the mobilization costs associated with loading of equipment onto trucks.

(b) Onsite costs include placement of trailers, establishment of a power supply, and erection of the shaft head frame.

(c) Common costs for equipment include a trailer at the site, vehicles used by field personnel, and large equipment such as front end loader.

(d) Common costs for consumables include such items as protective clothing, general oil and greases, diesel fuel, pipe fittings, safety equipment necessary for construction activities, and tools.

Table D-1. Overall Site Cost Estimate (Continued)

	Offsite ^(a)	Onsite ^(b)	Shaft Services	Progrout Plug	Remove Lining and Backfill	Construct Plug	Shaft Services	Clear Shaft Top	Clear Site	Follow-up Reports	Total
WEEKS	4.0	8.0	1.0	1.5	22.5	3.5	0.5	1.0	2.5	6.0	
POWER											
Diesel		3,200	400	600	8,400	1,400	200	400	1,000		15,600
Electrical											
Bristar					306,000	12,000					318,000
Explosives											
Hydraulic Breaker											
Subtotal		3,200	400	600	314,400	13,400	200	400	1,000		333,600
OTHER											
Office	1,700	6,100	1,500	2,300	14,100	7,100	400	800	2,100	1,400	37,400
Freight		35,000							25,000		60,000
Subtotal	1,700	41,100	1,500	2,300	14,100	7,100	400	800	27,100	1,400	97,500
TOTAL	66,900	481,900	109,600	133,600	2,116,200	379,900	22,100	41,800	136,100		3,541,700

(a) Offsite costs include necessary administrative costs for procurement and the mobilization costs associated with loading of equipment onto trucks.

(b) Onsite costs include placement of trailers, establishment of a power supply, and erection of the shaft dead frame.

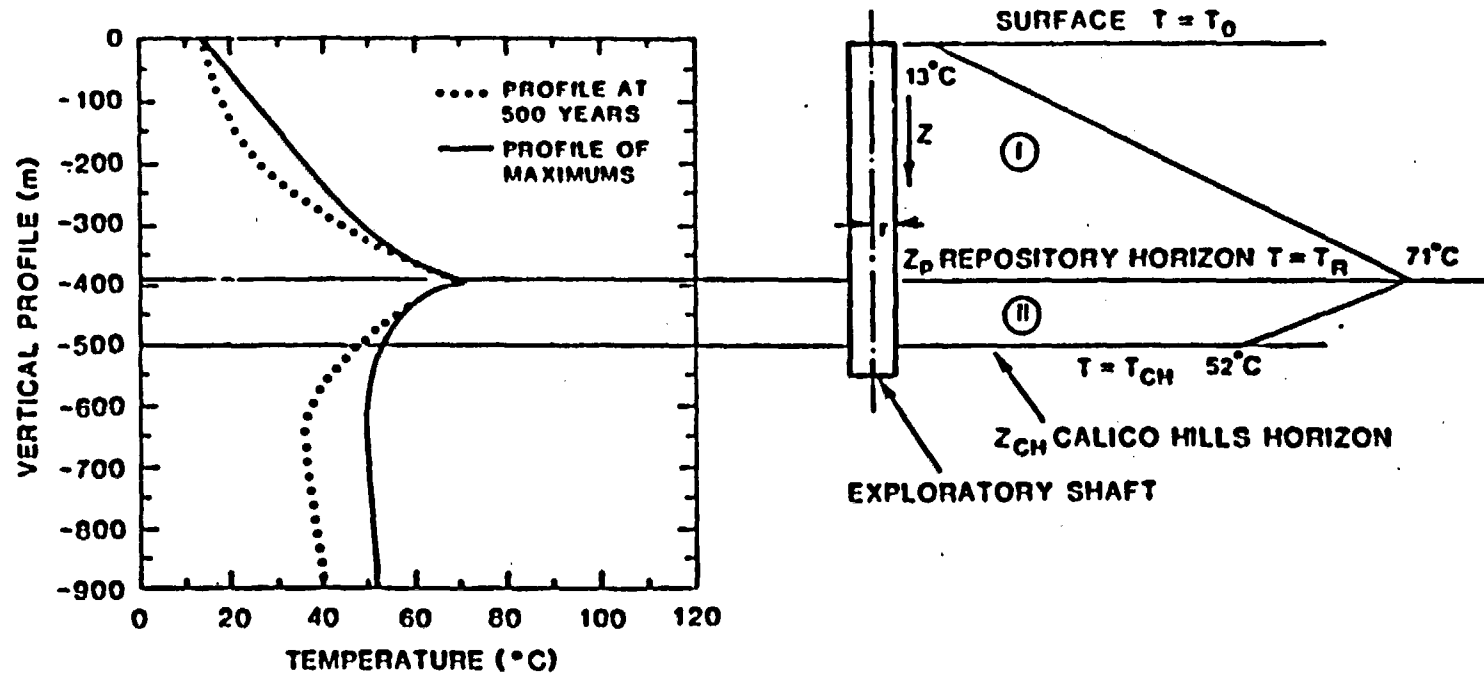
APPENDIX E

Calculation of Temperature of Water From the Base of the Exploratory Shafts

In Chapter 5 changes in the sorptivity of the Calico Hills unit due to elevated ground water temperature were addressed. The prevalent zeolites in the Calico Hills unit are known to be stable at temperatures of less than 95°C. Hence, the purpose of this appendix is to show that the expected temperature of the water entering the Calico Hills unit through the exploratory shaft is less than 95°C.

To predict the temperature of water passing through the ES and its MPZ we assume that water flow is modeled by the flow of water vertically downward through a cylinder with the surface temperature varies to model the maximum global temperature field as calculated by Blanford [A. R. Morales, 1985]. Consistent with the bounding nature of these calculations, no local cooling of the cylinder surface (as modeling the formation) is considered so that maximum effluent temperatures are obtained. As water passes through this cylinder, we model the temperature changes caused by the radial conduction of heat to the downward moving water. For a linear change in formation temperature with depth, an analytical solution to the thermal field is obtained.

Two separate water flow scenarios have been considered. These are the anticipated yearly influx of 44.2 m³/year and the PMF scenario of 20,000 m³/year at the top of the shaft. Because the 500-year flood is less severe than the PMF and the PMF results in very small temperature increases, the 500-year flood is not considered here. For these calculations, we assume that the rock mass temperature near the ES and hence the cylinder surface temperature increases in a linear fashion from 13°C (average ground-water temperature) to 71°C (average formation temperature at the repository horizon). Below the repository, we assume that the temperature decreases linearly to 52°C at the top margin of the Calico Hills unit. This model is illustrated in Figure E-1. As seen in Figure E-1, the linear approximation to the profile of maximums is always greater than the maximum temperature so that the model assumptions are again conservative.



(FROM BLANFORD IN MORALES, 1985, PP. 36-39)

Figure E-1. Model Used to Calculate Water Temperature Elevation of Water Entering Shaft

The thermal response of water flowing through the ES is described by the conservation-of-energy equation, which takes the form

$$u_z \frac{\partial T}{\partial z} = \alpha \frac{1}{r} \frac{\partial}{\partial r} \left(r \frac{\partial T}{\partial r} \right) \quad (\text{E-1})$$

where α = the thermal diffusivity of the combination of water and rock within the ES and the MPZ,

u_z = the average flow velocity,

T = the temperature,

r = the radial distance from the shaft centerline, and

z = vertical distance downward as shown in Figure E-1.

This equation is solved in two regions, I and II, where region I is the zone above the repository and region II is the zone below the repository. The boundary conditions for region I are

$$\begin{aligned} z_I = 0 & & T_I = T_o \\ r_I = R_o & \quad z_I > 0 & T_I = T_o + (T_R - T_o) \frac{z_I}{z_R} \end{aligned} \quad (\text{E-2})$$

and for region II are

$$\begin{aligned} z_{II} = z_R & & T_{II} = T_R \text{ for all } r \\ \text{and } r_{II} = R_o, z_{II} > z_R & & T_{II} = T_R + (T_{CH} - T_R) \frac{(z_{II} - z_R)}{(z_{CH} - z_R)} \end{aligned} \quad (\text{E-3})$$

These equations may be nondimensionalized, where $\theta_I = \frac{T_I - T_o}{T_R - T_o}$

$r_I = r_I R_o$, $z_I = z_I z_R$ and $K_I = \frac{\alpha z_R}{u_z R_o^2}$ in region I to give

$$\frac{\partial \theta_I}{\partial z_I} = \frac{K_I}{r_I} \frac{\partial}{\partial r_I} \left(r_I \frac{\partial \theta_I}{\partial r_I} \right) \quad (\text{E-4})$$

$$z_I = 0 \quad \theta_I = 0$$

$$r_I = 1 \quad \theta_I = z_I$$

In region II, we similarly nondimensionalize, where $\theta_{II} = \frac{T_{II} - T_R}{T_{CH} - T_R}$.

$r_{II} = r_{II}' R_0$, $z_{II} = z_{II}' (z_{CH} - z_R) + z_R$ and $K_{II} = \frac{a}{U_2} \frac{(z_{CH} - z_R)}{R_0^2}$, to give

$$\frac{\partial \theta_{II}}{\partial z_{II}'} = \frac{K_{II}}{r_{II}'} \frac{a}{\partial r_{II}'} (r_{II}' \frac{\partial \theta_{II}}{\partial r_{II}'}) \quad (E-5)$$

$$\begin{aligned} z_{II}' = 0 & & \theta_{II} = 0 \\ r_{II}' = 1 & & \theta_{II} = z' \end{aligned}$$

Equations E-4 and E-5 are identical except that the nondimensional diffusivities are slightly different. Equations E-4 and E-5 are solved analytically in (Carslaw and Jaeger, 1959, p. 201), and involve a series of Bessel functions that converge very rapidly to their solution.

The solution is

$$\theta = \left(z' - \frac{1-r'^2}{4K} \right) + \frac{2}{K} \sum_{n=1}^{\infty} e^{(-K\alpha_n^2 z')} \frac{J_0(r'\alpha_n)}{\alpha_n^3 J_1(\alpha_n)} \quad (E-6)$$

where α_n are the nonzero roots of $J_0(\alpha) = 0$.

To solve this equation for the average fluid temperature entering the Calico Hills, we should apply Equation E-6 in both regions I and II. The solution obtained in region I would then be used as a starting temperature for region II. However, since our problem is to estimate the maximum fluid temperature entering the Calico Hills, a convenient simplification is to assume that the fluid temperature exiting region I and entering region II is in thermal equilibrium with the formation at the repository horizon. If lower temperature water were to enter region II, then the water temperature exiting region II would be correspondingly reduced. Hence, we now consider the solution in region II with the assumption that T_R is the rock temperature computed by Blanford. Hence, T_R is taken to be 71°C and T_{CH} is 52°C.

The solution to Equation E-6 for region II is a function of r' , Z' , and K . At the entrance to the Calico Hills, where Z' is 1, we are interested in the average fluid temperature, which is

$$\theta_{AVG} = \frac{\int_0^1 \theta(r') 2\pi r' dr'}{\int_0^1 2\pi r' dr'} = 2 \int_0^1 \theta(r') r' dr' \quad (E-7)$$

The variation in dimensionless fluid temperature with radius is shown in Figure E-2 for K varying between 0.5 and 10.

The fluid temperature profile more closely approaches the formation temperature as the dimensionless thermal diffusivity increases (Figure E-3). Hence, the average fluid temperature at the upper margin of the Calico Hills may be represented solely as a function of K (Figure E-3).

In this figure, the average dimensionless fluid temperature increases as the dimensionless thermal diffusivity increases and the average dimensionless fluid temperature is greater than 0.9 for values of K exceeding 1. When θ_{AVG} is equal to 0.9, the actual fluid temperature is 53.9°C.

In the estimation of the dimensionless thermal diffusivity,

$$K = \frac{\alpha}{U_z} \frac{(Z_{CH} - Z_R)}{R_o^2} \quad (E-8)$$

a range of values are considered for α and U_z , while R_o , and $Z_{CH} - Z_R$ are defined by the design of the ES. The values of these parameters for two extreme conditions are presented in Table E-1.

For both of these cases, the shaft radius is assumed to encompass the MPZ. By selecting this larger radius, the value of K assumes a conservatively smaller value. In addition, the permeability of the MPZ is assumed to be 60 times the conductivity of the Tiva Canyon. The fluid velocity for the expected flow condition corresponds to 44.2 m³/year, while the maximum fluid velocity is taken to be equivalent to the worst-case hydraulic conductivity assumed for the MPZ. The thermal diffusivity is

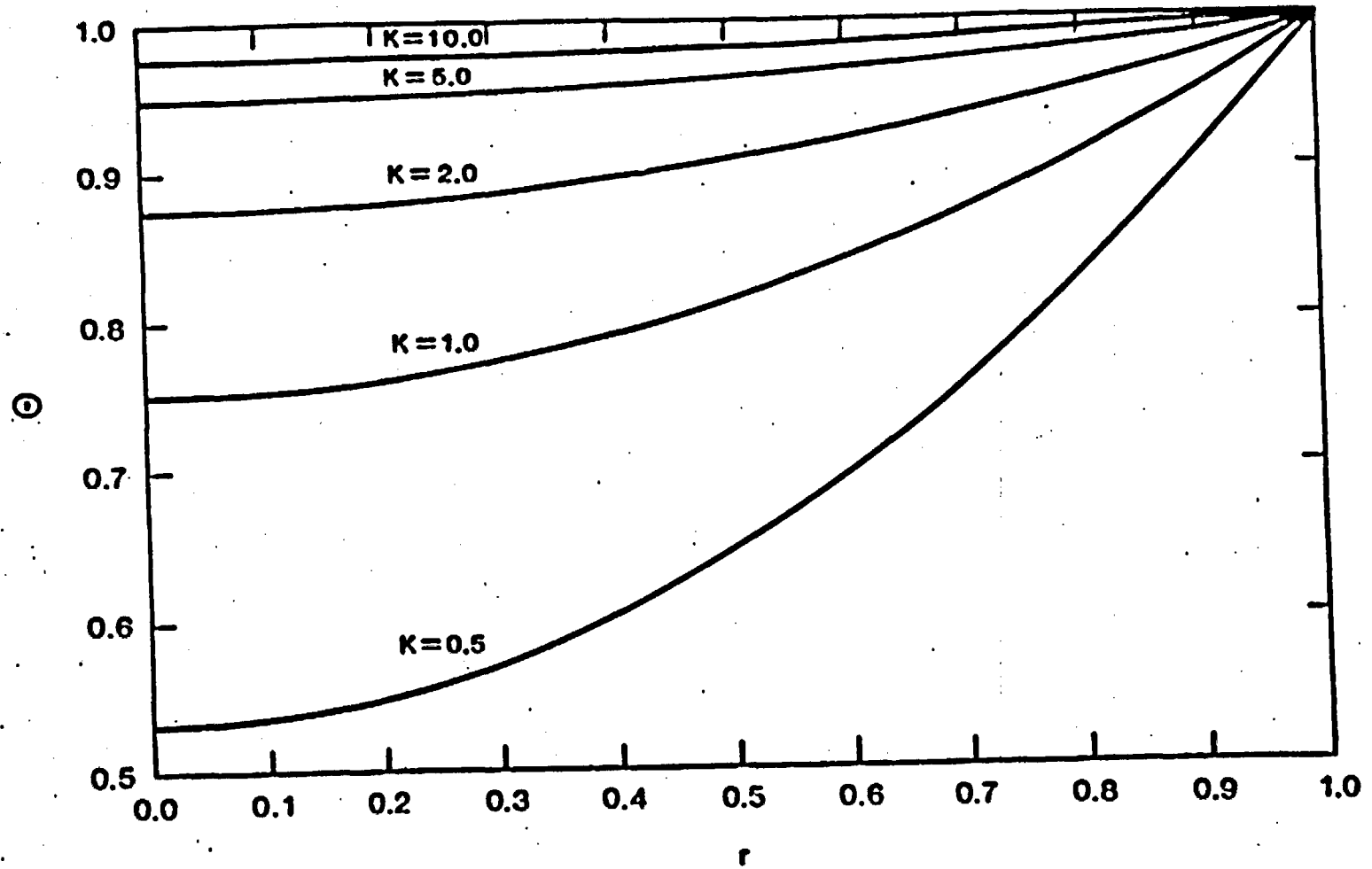


Figure B-2. Dimensionless Temperature (θ) Versus Radius (r) for Different Dimensionless Thermal Diffusivities (K)

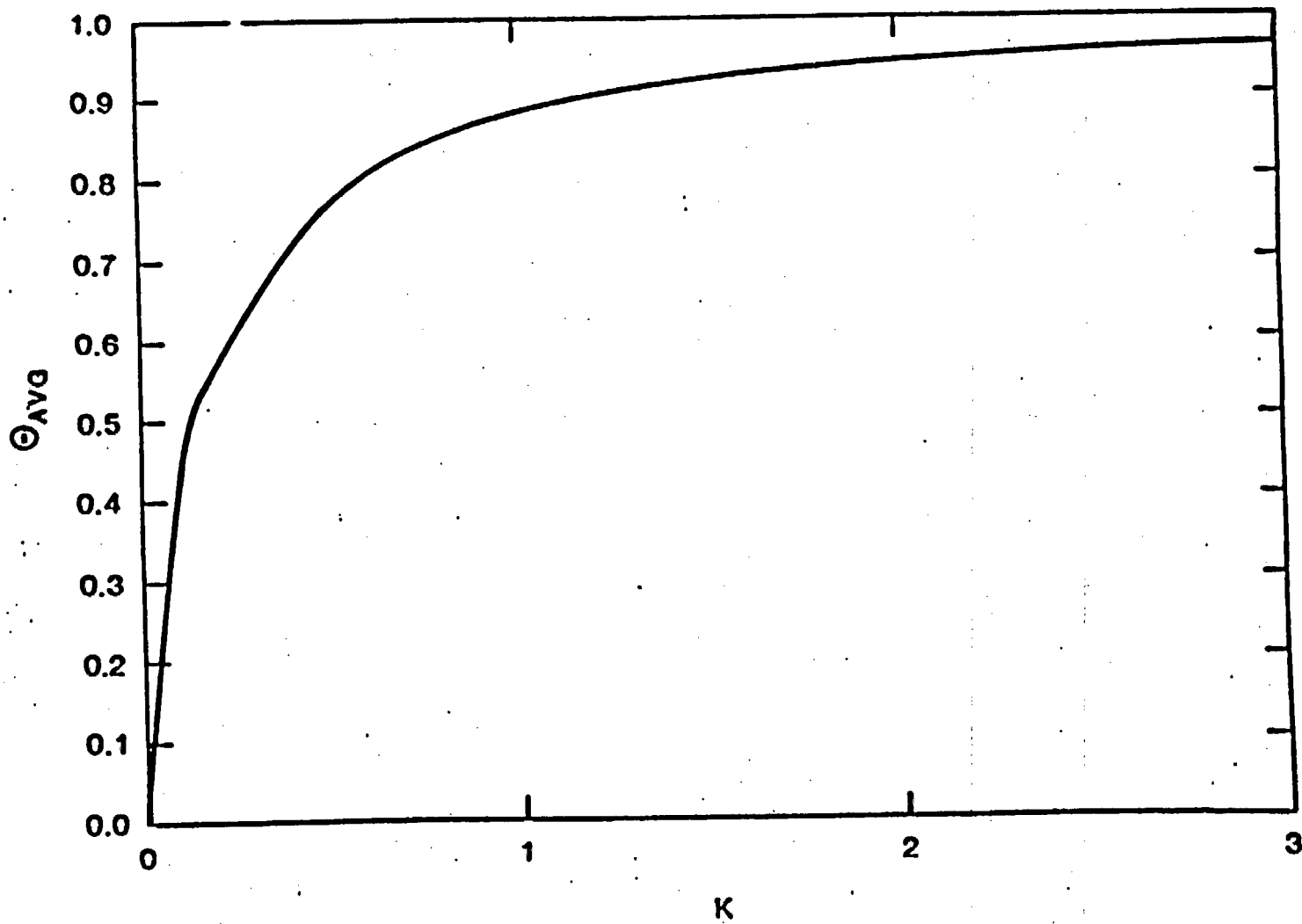


Figure E-3. Average Dimensionless Temperature (Θ_{AVG}) Versus Dimensionless Thermal Diffusivity (K)

Table E-1. Values of Parameters Used to Estimate the Dimensionless Thermal Diffusivity and Resultant Average Dimensionless Temperatures

Case	$Z_{CH} - Z_R$ (m)	R_o (m)	U_2 (cm/s)	α (cm ² /s)	K	θ_{AVG}
Expected flow	116.7(383 ft)	4.42(14.5 ft)	2.4×10^{-6}	.0078	192	1.00
Probable maximum flooding	116.7(383 ft)	4.42(14.5 ft)	6×10^{-1}	30	3	.96

computed by one of two possible methods. When the fluid velocity is very low, as in the expected flow case, a volumetric average of the thermal diffusivity of the rock and of the intergranular water is computed. At large fluid velocities, the thermal diffusivity is determined by convection processes and is computed by

$$\alpha = \frac{2U_2 d_p}{t} \quad [\text{Levenspiel, 1972, p. 282}] \quad (\text{E-9})$$

where d_p is the effective distance between fractures, and other terms are as defined previously. We assume 16 fractures/meter to give the smallest possible d_p within the MPZ.

As may be seen in Table E-1, the value of K even in the highest flow case of the PMF is large enough so that the average dimensionless temperature is 0.96. In actual temperature units, the maximum fluid temperature is expected to be 52.8°C, while the more normal expected flow condition results in a fluid temperature of 52.01°C.

APPENDIX F

Comparison of Data Used in This Report With the
Reference Information Base (RIB)*

The following notes are used throughout this appendix:

- (A) No section found in RIB applicable to these parameters.
- (B) Section identified in the RIB, but values not found.

*The April 1986 version of the RIB was used for comparison purposes because all analyses were completed or initiated before the issuance of the May 1, 1987 version 02.001.

Appendix F-1. Comparison of Data Used in This Report With the Reference Information Base (RIB)

PARAMETER	PAGE #	REPORT VALUE	RIB VALUE	RIB SECTION	EXPLANATION
MEN AND MATERIALS SHAFT SUMP	25	24 m	NONE	2.2.7	(B)
EMPLACEMENT EXHAUST SHAFT SUMP	25	3 m	NONE	2.2.7	(B)
EXPLORATORY SHAFT SUMP	25	140 m	NONE	2.2.7	(B)
LOCATIONS OF ES-1 AND ES-2	28	FIGURE 2-2	NONE	2.2.7	(B)
EXCAVATED DIAMETERS OF ES-1 AND ES-2	29	4.3 m AND 4.3 m	14 ft AND 8 ft	2.2.6	EXCAVATED DIAMETER FOR ES-2 CHANGED FROM 8 ft TO 14 ft TO REFLECT RECENT PROJECT GUIDANCE.
FINISHED DIAMETERS OF ES-1 AND ES-2	29	3.7 m AND 3.7 m	3.7 m AND 1.8 m	2.2.6	FINISHED DIAMETER OF ES-2 RECENTLY CHANGED FROM 1.83 m TO 3.7 m
THICKNESS OF ES-1 AND ES-2 LINERS	29	0.3 m AND 0.3 m	1 ft AND 1 ft	2.2.6	
FRACTURE SPACING IN NONWELDED TUFF	34	80 cm to 200 cm	NONE	1.3.2.4.2.3	(B)
MINIMUM FRACTURE SPACING IN DENSELY, WELDED TUFF	34	6 cm	NONE	1.3.2.4.2.3	(B)
BLAST-DAMAGE ZONE EXTENT INTO ROCK FROM EDGE OF SHAFT	37	0.5 m TO 1.0	NONE	2.3	(B)
EXPECTED ENHANCEMENT OF PERMEABILITY OF ROCK MASS AROUND SHAFT	40	70 TIMES THE PERMEABILITY OF UNDISTURBED ROCK MASS.	NONE	2.3	(B)

(A) NO SECTION FOUND IN RIB APPLICABLE TO THESE PARAMETERS.
 (B) SECTION IDENTIFIED IN THE RIB, BUT VALUES NOT FOUND.

Appendix F-1. Comparison of Data Used in This Report With the Reference Information Base (RIB) (Continued)

PARAMETER	PAGE #	REPORT VALUE	RIB VALUE	RIB SECTION	EXPLANATION
UPPER BOUND ENHANCEMENT OF PERMEABILITY OF ROCK MASS AROUND SHAFT	40	40 TO 80 TIMES THE PERMEABILITY OF UNDISTURBED ROCK MASS.	NONE	2.3	(B)
SATURATED, HYDRAULIC CONDUCTIVITY OF SHAFT FILL	43	10^{-2} cm/s	NONE	2.3	(B)
PROBABLE MAXIMUM FLOOD (PMF) CLEAR WATER VOLUME	41	159,000 m ³	NONE	1.17.1	(B)
EXCAVATED DIAMETER ASSUMED IN MPZ MODEL	51	4.4 m	4.27 m	2.2.6	SLIGHT OVERBREAK ASSUMED IN MPZ MODEL.
RANGE OF THE SATURATED, HYDRAULIC CONDUCTIVITY FOR ALLUVIUM	51	10^{-3} TO 10^2 cm/s	NONE	--	(A)
RANGE OF THE SATURATED, HYDRAULIC CONDUCTIVITY OF THE BULK ROCK - TIVA CANYON MEMBER	51	10^{-3} TO 10^{-2} cm/s	3.65×10^3 mm/yr OR 1.2×10^{-3} cm/s	1.1.4.3	SINGLE VALUE GIVEN IN THE RIB
AVERAGE GRADE OF THE WATERCOURSE IN COYOTE WASH	51	0.16	NONE	--	(A)
POROSITY OF ALLUVIUM	51	0.30	NONE	--	(A)
BULK, SATURATED HYDRAULIC CONDUCTIVITY OF TOPOPAH SPRING MEMBER AND TUFFACEOUS BEDS OF CALICO HILLS	65	1.2×10^{-3} cm/s	1.2×10^{-3} cm/s (OR 3.65×10^3 mm/yr) [TOPOPAH SPRING]	1.1.4.3	
	65	2.4×10^{-6} AND 10^{-3} cm/s	2.4×10^{-6} cm/s (OR 3.5×10^6 mm/yr) [CALICO HILLS]	1.1.4.3	

(A) NO SECTION FOUND IN RIB APPLICABLE TO THESE PARAMETERS.
 (B) SECTION IDENTIFIED IN THE RIB, BUT VALUES NOT FOUND.

Appendix P-1. Comparison of Data Used in This Report With the Reference Information Base (RIB) (Continued)

PARAMETER	PAGE #	REPORT VALUE	RIB VALUE	RIB SECTION	EXPLANATION
MANNING'S ROUGHNESS COEFFICIENT	73	0.060	NONE	--	(A)
PEAK TEMPERATURE AT THE REPOSITORY HORIZON	85	115°C	115°C	3.1.1.2	
TEMPERATURE AT THE INLET SHAFTS	85	13°C	54.9°F (OR 13°C)	1.11.1	
TOTAL CROSS-SECTIONAL ROOF AREA OF REPOSITORY (WASTE ROOMS, SUBMAINS, AND MAINS)	86	983,700 m ² (VERTICAL EMPLACEMENT) 486,000 m ² (HORIZONTAL EMPLACEMENT)	NONE	--	(A)
TOTAL THICKNESS OF WELDED UNITS ABOVE THE REPOSITORY	86	260 m	NONE	1.3.1.1.1	(B) VALUES OBTAINED FROM CALMA SYSTEM
TOTAL THICKNESS OF NONWELDED UNITS ABOVE THE REPOSITORY	86	40 m	NONE	1.3.1.1.1	(B) VALUES OBTAINED FROM CALMA SYSTEM
ASSUMED AIR CONDUCTIVITY OF NONWELDED PAINTBRUSH TUFF UNIT	86	3×10^{-7} to 3×10^{-5} m/min.	NONE	--	(A)
ASSUMED AIR CONDUCTIVITY OF TOPOPAH SPRING AND TIVA CANYON MEMBERS	88	3×10^{-7} to 3×10^{-6} m/min.	NONE	--	(A)
INTERNAL AREA OF RAMP/SHAFTS - WASTE RAMP (HORIZONTAL EMBLACEMENT)	87	28.3 m ²	28.3 m ² (19-ft DIAMETER)	2.2.1.7 AND 2.2.8	CALCULATED FROM DATA IN RIB

(A) NO SECTION FOUND IN RIB APPLICABLE TO THESE PARAMETERS.
 (B) SECTION IDENTIFIED IN THE RIB, BUT VALUES NOT FOUND.

Appendix F-1. Comparison of Data Used in This Report With the Reference Information Base (RIB) (Continued)

PARAMETER	PAGE #	REPORT VALUE	RIB VALUE	RIB SECTION	EXPLANATION
• TUFF RAMP (HORIZONTAL EMPLACEMENT)	87	30.1 m ²	30.1 m ² (20-ft DIAMETER)	2.2.1.7 AND 2.2.8	CALCULATED FROM DATA IN RIB
• WASTE RAMP (HORIZONTAL EMPLACEMENT)	87	34.2 m ²	34.2 m ² (22-ft DIAMETER)	2.2.2.7 AND 2.2.8	CALCULATED FROM DATA IN RIB
• TUFF RAMP (VERTICAL EMPLACEMENT)	87	42.8 m ²	42.8 m ² (24-ft DIAMETER)	2.2.2.7 AND 2.2.8	CALCULATED FROM DATA IN RIB
• MEN-AND-MATERIALS SHAFT	87	29.2 m ²	29.2 m ² (20-ft DIAMETER)	2.2.8	CALCULATED FROM DATA IN RIB
• EMPLACEMENT EXHAUST SHAFT	87	29.2 m ²	(20-ft DIAMETER)	2.2.8	CALCULATED FROM DATA IN RIB
• ES-1	87	10.5 m ²	(12-ft DIAMETER)	2.2.8	CALCULATED FROM DATA IN RIB
• ES-2	87	10.5 m ²	(6-ft DIAMETER)	2.2.8	CALCULATED FROM DATA IN RIB
LENGTH OF RAMP/SHAFTS TO REPOSITORY HORIZON					
• WASTE RAMP	87	2012 m	6603 ft (OR 2012 m)	2.2.8	..
• TUFF RAMP	87	1410 m	4627 ft (OR 1410 m)	2.2.8	..
• MEN-AND-MATERIALS SHAFT	87	314 m	1030 ft (OR 314 m)	2.2.8	..

(A) NO SECTION FOUND IN RIB APPLICABLE TO THESE PARAMETERS.
(B) SECTION IDENTIFIED IN THE RIB, BUT VALUES NOT FOUND.

Appendix F-1. Comparison of Data Used in This Report With the Reference Information Base (RIB) (Continued)

PARAMETER	PAGE #	REPORT VALUE	RIB VALUE	RIB SECTION	EXPLANATION
- ENPLACEMENT EXHAUST SHAFT	87	314 m	1030 ft (OR 314 m)	2.2.8	..
- ES-1	87	311 m	1020 ft (OR 311 m)	2.2.8	..
- ES-2	87	311 m	1020 ft (OR 311 m)	2.2.8	..
HYDRAULIC CONDUCTIVITY OF SHAFT FILL	88	10 ⁻⁶ TO 100 cm/s	NONE	..	(A)
THUNDERSTORM	102				
- AMPLITUDE		20 mbar	18.96 mbar (MAXIMUM VALUE)	1.11.4	VALUE INFERRED FROM DATA PRESENTED IN RIB
- PERIOD		5 days	NONE		(A)
TORNADO	102				
- AMPLITUDE		135 mbar	NONE	..	(A)
- PERIOD		1 minute	NONE	..	(A)
SEASONAL FLUCTUATION	102				
- AMPLITUDE		3 mbar	3 mbar	1.11.4	..
- PERIOD		365 days	365 days	1.11.4	..
POROSITY OF SHAFT FILL	104	30%	NONE	2.3	(B)
UNSATURATED; ROCK POROSITY IN MPZ	104	0.042	NONE	1.1.3.1 AND 1.3.1.2	(B) VALUE OBTAINED AS- SUMING AMBIENT SATURA- TION OF 0.65 AND MATRIX POROSITY OF 12 %

(A) NO SECTION FOUND IN RIB APPLICABLE TO THESE PARAMETERS.

(B) SECTION IDENTIFIED IN THE RIB, BUT VALUES NOT FOUND.

Appendix F-1. Comparison of Data Used in This Report With the Reference Information Base (RIB) (Continued)

PARAMETER	PAGE #	REPORT VALUE	RIB VALUE	RIB SECTION	EXPLANATION
MAXIMUM PARTICLE SIZE FOR ORDINARY CEMENTS	117	100 microns	NONE	--	(A)
PARTICLE SIZE FOR ULTRAFINE CEMENT	117	10 microns	NONE	--	(A)
HYDRAULIC CONDUCTIVITY OF ORDINARY PORTLAND CONCRETE	121	10^{-8} - 10^{-9} cm/s	NONE	2.3	(B)
HYDRAULIC CONDUCTIVITY OF GROUT, MORTAR, AND CONCRETE DETERMINED BY MMSI SEALING PROGRAM	121	1.6×10^{-10} - 9.5×10^{-10} cm/s	NONE	2.3	(B)
CEMENT COMPOSITION - ALKALI CONTENT OF ORDINARY PORTLAND CEMENT	124	0.05 - 0.15 %	NONE	2.3	(B)
CEMENT COMPOSITION - pH OF ORDINARY PORTLAND CEMENT PORE FLUID	124	13.88	NONE	2.3	(B)
ES CONCRETE LINER THICKNESS	125	30.5 cm	30.5 cm	2.2.5.2	--
J-13 WATER COMPOSITION	126	TABLE 4-1	NONE	1.2.3.2	(B)
SHAFT LINER SURFACE AREA	127	4.17×10^7 cm ²	COMPUTED VALUE CONSISTENT WITH RIB	2.2.5.2	--
CONCRETE LINER VOID FRACTION	127	0.28	NONE	--	(A)

(A) NO SECTION FOUND IN RIB APPLICABLE TO THESE PARAMETERS.
 (B) SECTION IDENTIFIED IN THE RIB, BUT VALUES NOT FOUND.

Appendix F-1. Comparison of Data Used in This Report With the Reference Information Base (RIB) (Continued)

PARAMETER	PAGE #	REPORT VALUE	RIB VALUE	RIB SECTION	EXPLANATION
FRACTURE APERTURE IN MODIFIED PERMEABILITY ZONE	133	50 microns	NONE	1.3.2.4.2.3	(B)
POROSITY OF TSW2 MATRIX	134	.11	.1062	1.1.8.1	--
FRACTURE POROSITY IN MODIFIED PERMEABILITY ZONE	134	0.0001 - 0.001	NONE	1.3.2.4.2	(B)
THICKNESS OF CALICO HILLS UNIT (ZEOLITIC) AT ES-1	152	100 m	100 m	1.3.1.1.2	IN CALMA SYSTEM
PENETRATION OF ES-1 INTO CALICO HILLS	152	15 m	NONE	--	(A)
FRACTURE APERTURE	164	71 microns and 25 microns	NONE	1.3.4.2	(B)
CONTACT ANGLE BETWEEN WATER IN FRACTURES AND TUFF	164	0	NONE	--	(A)
DIFFUSION COEFFICIENT FOR SOLID-SOLID DIFFUSION	165 166	10^{-15} cm ² /s and 10^{-20} cm ² /s	NONE	--	(A)
BINARY-GAS DIFFUSION COEFFICIENT FOR					
o AIR-IODINE SYSTEM	166	0.081 cm ² /s	NONE	--	(A)
o AIR-CARBON DIOXIDE SYSTEM	166	0.156 cm ² /s	NONE	--	(A)
KNUDSEN DIFFUSION COEFFICIENT FOR					
o IODINE	166	10.6 cm ² /s	NONE	--	(A)
o CARBON DIOXIDE	166	25.3 cm ² /s	NONE	--	(A)

(A) NO SECTION FOUND IN RIB APPLICABLE TO THESE PARAMETERS.
 (B) SECTION IDENTIFIED IN THE RIB, BUT VALUES NOT FOUND.

Appendix P-1. Comparison of Data Used in This Report With the Reference Information Base (RIB) (Continued)

PARAMETER	PAGE #	REPORT VALUE	RIB VALUE	RIB SECTION	EXPLANATION
POROSITY OF DRIFT AND SHAFT FILL	167	0.3	NONE	2.3	(B)
TORTUOSITY OF SHAFT FILL	167	3	NONE	--	(A)

(A) NO SECTION FOUND IN RIB APPLICABLE TO THESE PARAMETERS.
 (B) SECTION IDENTIFIED IN THE RIB, BUT VALUES NOT FOUND.

APPENDIX C

Data Recommended for Inclusion Into the Site and
Engineering Properties Data Base (SEPDB)
and Information Proposed for the Inclusion Into the
Reference Information Base (RIB)

No data or information contained in this report is recommended for inclusion into the RIB. No data or information is currently recommended for inclusion into the SEPDB. However, the data or information in this report may be reviewed in the future, if necessary for inclusion into the SEPDB.

This page is for page number only

REFERENCES

- Auld, F. A., 1983, "Design of Underground Plugs," International Journal of Mining Engineering, Chapman and Hall Ltd., London, Vol. 1, pp. 189-228.
- Barnes, P., 1983, Structure and Performance of Cements, Applied Science Publishers, London.
- Bear, J., Dynamics of Fluids in Porous Media, 1976, American Elsevier, New York, 763 pp.
- Berner, R. A., 1980, Early Diagenesis, Princeton University Press, Princeton, NJ., pp. 118-124.
- Bird, R. B., W. E. Stewart, and E. N. Lightfoot, 1960, Transport Phenomena, John Wiley and Sons, Inc., New York.
- Brady, B. H. G., and E. T. Brown, 1985, Rock Mechanics for Underground Mining, George Allen and Unwin Ltd., London, England.
- Bullard, K. L., 1986, PMF (Probable Maximum Flood) Study for Nevada Nuclear Waste Storage Investigations Project, GR-87-8, U.S. Department of the Interior, Bureau of Reclamation, Denver, CO.
- Carlsaw, H. S., and J. C. Jaeger, 1959, Conduction of Heat in Solids, Clarendon Press, Oxford.
- Case, J. B., and P. C. Kelsall, 1987, Modification of Rock Mass Permeability in the Zone Surrounding a Shaft in Fractured, Welded Tuff, SAND86-7001, Sandia National Laboratories, Albuquerque, NM, 79 pp.
- Case, J. B., P. C. Kelsall, and J. F. Holland, 1984, "The Development of Interface Stress in a Concrete Plug During Cement Hydration," Symposium on Concrete and Cementitious Materials for Radioactive Waste Management, November 1, 1984, American Concrete Institute, New York, NY.
- Chow, Ven Te, 1964, Handbook of Applied Hydrology, McGraw Hill, New York, 29 chapters.
- Church, H., 1987, Personal Communication.
- Daniels, W. R., K. Wolfsberg, R. S. Rundberg, A. E. Ogard, J. F. Kerrisk, and C. J. Duffy, et al., 1982, Summary Report on the Geochemistry of Yucca Mountain and Environs, LA-9328-MS, Los Alamos National Laboratory Report, Los Alamos, NM.
- D'Appolonia, 1976, Preliminary State-of-the-Art Survey: Mining Techniques for Salt and Other Rock Types, Office of Waste Isolation, Union Carbide Corporation, Nuclear Division, Oak Ridge, TN.

- Dietz, H. K. O., 1982, "Grouting Technique Used in Deep South African Mines." Proc. of Conference on Grouting in Geotechnical Engineering. American Society of Civil Engineers, New York, NY, pp. 606-620.
- Dowding, C. H., and J. F. Labuz, 1982, "Fracturing of Rock with Expansive Cement." Journal of the Geotechnical Engineering Division, Vol. 108, No. GT10, American Society of Civil Engineers, New York, NY, pp. 1288-1299.
- Duffy, C., 1987, Personal Communication.
- Erickson, J. R., and R. K. Waddell, 1985, Identification and Characterization of Hydrologic Properties of Fractured Tuff Using Hydraulic and Tracer Tests--Test Well USW H-4, Yucca Mountain, Nye County, Nevada, 85-4066, U.S. Geological Survey, Denver, CO.
- Fernandez, J. A., P. C. Kelsall, J. B. Case, D. Meyer, 1987, Technical Basis for Performance Goals, Design Requirements, and Material Recommendations for the NNSI Repository Sealing Program, SAND84-1895, Sandia National Laboratories, Albuquerque, NM.
- Freeze, R. A., and J. A. Cherry, 1979, Groundwater. Prentice-Hall, Inc., Englewood Cliffs, NJ.
- Froment, G. F., and K. B. Bischoff, 1979, Chemical Reactor Analysis and Design. John Wiley and Sons, New York, NY.
- Glasser, F. P., M. J. Angus, C. E. McCulloch, D. MacPhee, and A. A. Rahman, 1984, "The Chemical Environment in Cement," Proceedings of the Materials Research Society Symposium, Vol. 44, p. 849
- Hartman, H. L., 1982, Mine Ventilation and Air Conditioning. John Wiley and Sons, New York, NY.
- Hillel, D., 1971, Soil and Water. Academic Press, New York, NY, 288 pp.
- Hoek, E., and E. T. Brown, 1980, Underground Excavations in Rock. Institution of Mining and Metallurgy, London, England, 527 pp.
- Holmberg, R., and P. A. Persson, 1980, "Design of Tunnel Perimeter Blast-hole Patterns to Prevent Rock Damage." Transactions of the Institution of Mining and Metallurgy, London, England, 89:A37-A40.
- Ingraffea, A. R., and J. F. Beech, 1983, "Discussion on Fracturing of Rock with Expansive Cement." Journal of Geotechnical Engineering, Vol. 109, No. 9, American Society of Civil Engineers, New York, NY, pp. 1205-1208.
- Kelsall, P. C., J. B. Case, and C. R. Chabannes, 1982, A Preliminary Evaluation of the Rock Mass Disturbance Resulting from Shaft, Tunnel or Borehole Excavation. ONWI-411, Office of Nuclear Waste Isolation, Battelle Memorial Institute, Columbus, OH.

- Klavetter, E. A., and R. R. Peters, 1986, Fluid Flow in a Fractured Rock Mass. SAND85-0855, Sandia National Laboratories, Albuquerque, NM.
- Langefors, U., and B. Kihlstrom, 1978, Rock Blasting. John Wiley and Sons, New York, NY, 438 pp.
- Langkopf, B. S., and P. R. Gnirk, 1986, Rock Mass Classification of Candidate Repository Units at Yucca Mountain, Nye County, Nevada. SAND82-2034, Sandia National Laboratories, Albuquerque, NM.
- Lea, F. M., 1971, The Chemistry of Cement and Concrete. Chemical Publishing Co., New York, NY.
- Levenspiel, O., 1972, Chemical Reaction Engineering. John Wiley and Sons, New York, NY.
- Licastro, P. H., D. M. Roy, and J. A. Fernandez, in preparation, Mechanical Compatibility Between Selected Cementitious Materials and Topopah Spring Member Tuff. SAND86-0558, Sandia National Laboratories, Albuquerque, NM.
- Lohman, S. W., ed. 1972, Definitions of Selected Ground Water Terms - Revisions and Conceptual Refinements. U.S. Geol. Surv. Water Supply Paper 1988, 21 pp.
- MacDougall, H. R., L. W. Scully, and J. R. Tillerson (editors), 1988, Site Characterization Plan - Repository Conceptual Design. SAND84-2641. Sandia National Laboratories, Albuquerque, NM.
- Mason, E. A., and R. B. Evans III, 1969, "Graham's Laws: Simple Demonstrations of Gases in Motion," J. of Chemical Education, 46, pp. 358-364.
- Mather, B., 1967, Cement Performance in Concrete. US-CE-C No. 6-787, U.S. Army Engineer Waterways Experiment Station, Corps of Engineers, Vicksburg, Mississippi, 34 pp.
- Morales, A. R., 1985, Technical Correspondence in Support of the Final Environmental Assessment. SAND85-2509, Sandia National Laboratories, Albuquerque, NM.
- Ogard, A. E., K. Wolfsberg, D. T. Vaniman, 1983, Research and Development Related to the Nevada Nuclear Waste Storage Investigation, April 1 through June 30, 1983. LA-9846-PR, Los Alamos National Laboratories, Los Alamos, NM.
- Ogard, A. E., and J. F. Kerrisk, 1984 Ground-Water Chemistry Along Flow Paths Between a Proposed Repository Site and the Accessible Environment. LA-10188-MS, Los Alamos National Laboratories, Los Alamos, NM.
- Peters, R. R., E. A. Klavetter, I. J. Hall, S. C. Blair, P. R. Heller, G. W. Gee, 1984, Fracture and Matrix Hydrologic Characteristics of Tuffaceous Materials from Yucca Mountain, Nye County, Nevada. SAND84-1471, Sandia National Laboratories, Albuquerque, NM.
- Reid, R. C., J. M. Prausnitz, and T. K. Sherwood, 1977, The Properties of Gases and Liquids. McGraw-Hill Book Company, New York, NY.

- Richardson, A. M., in preparation, Preliminary Shaft Liner Design Criteria and Methodology Guide (Working-Draft; Revision B), SAND86-7052, Sandia National Laboratories, Albuquerque, NM.
- Scott, R. B., and J. Bonk, 1984, Preliminary Geologic Map of Yucca Mountain, Nye County, Nevada with Geologic Sections, Open-Site Report 84-494, U.S. Geological Survey, Denver, CO.
- Scott, R. B., R. W. Spengler, S. Diehl, A. R. Lappin, and M. P. Chornack, 1983, "Geologic Character of Tuffs in the Unsaturated Zone at Yucca Mountain, Southern Nevada, Role of the Unsaturated Zone in Radioactive and Hazardous Waste Disposal, J. Mercer, ed., Ann Arbor, MI, pp. 285-335.
- Sheetz, B. E., and D. M. Roy, in preparation, Preliminary Survey of the Stability of Silica-Rich Cementitious Mortars 82-22 and 84-12 with Tuff, Los Alamos National Laboratory, Los Alamos, NM.
- Sinnock, S., Y. T. Lin, and J. P. Brannen, 1984, Preliminary Bounds on the Expected Postclosure of the Yucca Mountain Repository Site, Southern Nevada, SAND84-1492, Sandia National Laboratories, Albuquerque, NM.
- Smith, J. M., 1970, Chemical Engineering Kinetics, McGraw-Hill, New York, NY.
- Smyth, J. R., 1982, Zeolite Stability Constraints on Radioactive Waste Isolation in Zeolite-Bearing Volcanic Rocks, Journal of Geol., Vol. 90, p. 195.
- Smyth, J. R., and F. A. Caporuscio, 1981, Review of the Thermal Stability and Cation Exchange Properties of the Zeolite Minerals Clinoptilolite, Mordenite, and Analcime: Application to Radioactive Waste Isolation in Silicic Tuff, LA-8841-MS, Los Alamos National Laboratory, Los Alamos, NM.
- Squires, R. R., and R. L. Young, 1984, Flood Potential of Fortymile Wash and Its Principle Southeastern Tributaries, Nevada Test Site, Southern Nevada, Water Resources Investigations Report 83-4001, U. S. Geological Survey, Denver, CO.
- Stephens, D. B., and S. P. Neuman, 1982, "Vadose Zone Permeability Tests: Steady State Results," Journal of the Hydraulics Division, Proceedings of the American Society of Civil Engineers, Vol. 108, No. HY5, pp. 640-659.
- Terzaghi, K., and R. Peck, 1967, Soil Mechanics in Engineering Practice, John Wiley and Sons, Inc., New York, NY.
- Truesdell, A. H., and B. F. Jones, 1974, WATEQ A Computer Program for Calculating Chemical Equilibrium of Natural Waters, Jour. Research U.S. Geol. Survey, Vol. 2, No. 2, p. 233.

- U.S. Department of Energy (DOE), 1986. Environmental Assessment, Yucca Mountain Site, Nevada Research and Development Area, Nevada. DOE/RW-0073. U.S. Department of Energy, Office of Civilian Radioactive Waste Management, Washington, D.C.
- U.S. Department of Energy (DOE), 1988. Consultative Draft - Site Characterization Plan, Yucca Mountain Site, Nevada Research and Development Area, Nevada. U.S. Department of Energy, Office of Civilian Radioactive Waste Management, Washington, D.C.
- U.S. Department of Energy, Nevada Operations Office (DOE-NVO), 1987. Exploratory Shaft Facility, Subsystem Design Requirements Document, NVO-309. U.S. Department of Energy, Nevada Operations Office, Las Vegas, NV.
- Valley, 1986. Handbook of Geophysics and Space Environment.
- Van Koyneburg, R. A., C. F. Smith, H. W. Culham, and C. H. Otto, Jr., 1984. "Behavior of Carbon-14 in Waste Packages for Spent Fuel in a Repository in Tuff." UCRL-90855, Materials Research Society Symposia Proceedings on the Scientific Basis for Nuclear Waste Management VIII. Boston, MA, Vol. 44, Materials Research Society, Pittsburgh, PA. pp. 405-412.
- Wang, J. S. Y., and T. N. Narasimhan, 1985. Hydrologic Mechanisms Governing Fluid Flow in Partially Saturated, Fractured, Porous Tuff at Yucca Mountain. LBL-18473, Lawrence Berkeley Laboratory, Berkeley, CA.
- West, K. A. in preparation, Exploratory Shaft Facility Fluids and Materials Evaluation. Los Alamos National Laboratory, Los Alamos, NM.
- Wolery, T. J., 1979. Calculations of Chemical Equilibrium Between Aqueous Solution and Minerals: The EQ 3/6 Software Package. UCRL-52658, Lawrence Livermore Laboratory, Livermore, CA.
- Wolfsberg, K., B. P. Bayhurst, E. M. Crowe, W. R. Daniels, E. R. Erdal, F. O. Lawrence, A. E. Norris, J. R. Smyth, 1979. Sorption - Desorption Studies on Tuff I. Initial Studies with Samples from the J-13 Drill Site Jackass Flats, Nevada. LA-7480-MS, Los Alamos National Laboratory, Los Alamos, NM.
- Zienkiewicz, O. C., 1977. The Finite Element Method. McGraw-Hill Book Company, NY, 787 pp.

This page is for page number only

DISTRIBUTION LIST

C. E. Kay, Acting Director (RW-1)
Office of Civilian Radioactive
Waste Management
U.S. Department of Energy
Forrestal Bldg.
Washington, D.C. 20585

Ralph Stein (RW-23)
Office of Civilian Radioactive
Waste Management
U.S. Department of Energy
Forrestal Bldg.
Washington, D.C. 20585

J. J. Fiore (RW-221)
Office of Civilian Radioactive
Waste Management
U.S. Department of Energy
Forrestal Bldg.
Washington, D.C. 20585

H. V. Frei (RW-231)
Office of Civilian Radioactive
Waste Management
U.S. Department of Energy
Forrestal Bldg.
Washington, D.C. 20585

B. G. Gale (RW-223)
Office of Civilian Radioactive
Waste Management
U.S. Department of Energy
Forrestal Bldg.
Washington, D.C. 20585

J. D. Saltzman (RW-40)
Office of Civilian Radioactive
Waste Management
U.S. Department of Energy
Forrestal Bldg.
Washington, D.C. 20585

S. J. Brocoun (RW-233)
Office of Civilian Radioactive
Waste Management
U.S. Department of Energy
Forrestal Building
Washington, D.C. 20585

V. J. Cassella (RW-222)
Office of Civilian Radioactive
Waste Management
U.S. Department of Energy
Forrestal Bldg.
Washington, D.C. 20585

S. H. Kale (RW-20)
Office of Civilian Radioactive
Waste Management
U.S. Department of Energy
Forrestal Bldg.
Washington, D.C. 20585

T. H. Isaacs (RW-20)
Office of Civilian Radioactive
Waste Management
U.S. Department of Energy
Forrestal Bldg.
Washington, D.C. 20585

D. H. Alexander (RW-232)
Office of Civilian Radioactive
Waste Management
U.S. Department of Energy
Forrestal Bldg.
Washington, D.C. 20585

C. Bresee (RW-22)
Office of Civilian Radioactive
Waste Management
U.S. Department of Energy
Forrestal Bldg.
Washington, D.C. 20585

Gerald Parker (RW-241)
Office of Civilian Radioactive
Waste Management
U.S. Department of Energy
Forrestal Bldg.
Washington, D.C. 20585

J. P. Knight (RW-24)
Office of Civilian Radioactive
Waste Management
U.S. Department of Energy
Forrestal Bldg.
Washington, D.C. 20585

Allen Jelacic (RW-233)
Office of Civilian Radioactive
Waste Management
U.S. Department of Energy
Forrestal Bldg.
Washington, D.C. 20585

Chief, Repository Projects Branch
Division of Waste Management
U.S. Nuclear Regulatory Commission
Washington, D.C. 20555

WTS Section Leader
Repository Project Branch
Division of Waste Management
U.S. Nuclear Regulatory Commission
Washington, D.C. 20555

Document Control Center
Division of Waste Management
U.S. Nuclear Regulatory Commission
Washington, D.C. 20555

Carl P. Gertz, Project Manager (6)
Waste Management Project Office
U.S. Department of Energy
Nevada Operations Office
P.O. Box 98518
Mail Stop 523
Las Vegas, NV 89193-8518

J. L. Fogg (12)
Technical Information office
Nevada Operations Office
U. S. Department of Energy
P.O. Box 98518
Las Vegas, NV 89193-8518

C. L. West, Director
Office of External Affairs
U.S. Department of Energy
Nevada Operations Office
P.O. Box 98518
Las Vegas, NV 89193-8518

W. M. Hewitt, Program Manager
Roy F. Weston, Inc.
955 L'Enfant Plaza, Southwest
Suite 800
Washington, D.C. 20024

Technical Information Center
Roy F. Weston, Inc.
955 L'Enfant Plaza, Southwest
Suite 800
Washington, D.C. 20024

L. D. Ranspott (3)
Technical Project Officer for NRS:
Lawrence Livermore National
Laboratory
P.O. Box 808
Mail Stop L-204
Livermore, CA 94550

M. E. Spaeth
Technical Project Officer for NRS:
Science Applications International
Corp.
101 Convention Center Dr.
Suite 407
Las Vegas, NV 89109

D. T. Oakley (4)
Technical Project Officer for NRS:
Los Alamos National Laboratory
P.O. Box 1663
N-5, Mail Stop J521
Los Alamos, NM 87545

L. R. Hayes (6)
Technical Project Officer for NRS:
U.S. Geological Survey
P.O. Box 25046
421 Federal Center
Denver, CO 80225

R. L. Bullock
Technical Project Officer for NRS:
Fenix & Scisson, Inc.
P.O. Box 93265
Mail Stop 514
Las Vegas, NV 89193-3265

James C. Calovini
Technical Project Officer for NRS:
Holmes & Narver, Inc.
101 Convention Center Dr.
Suite 860
Las Vegas, NV 89109

M. D. Voegele
Science Applications International
Corp.
101 Convention Center Dr.
Suite 407
Las Vegas, NV 89109

J. A. Cross, Manager
Las Vegas Branch
Fenix & Scisson, Inc.
P.O. Box 93265
Mail Stop 514
Las Vegas, NV 89193-3265

P. T. Prestholt
NRC Site Representative
1050 East Flamingo Road
Suite 319
Las Vegas, NV 89109

A. E. Currola, General Manager
Energy Support Division
Holmes & Narver, Inc.
P.O. Box 93838
Mail Stop 580
Las Vegas, NV 89193-3838

B. L. Fraser, General Manager
Reynolds Electrical & Engineering Co.
P.O. Box 98521
Mail Stop 555
Las Vegas, NV 89193-8521

P. K. Fitzsimmons, Director
Health Physics & Environmental
Division
Nevada Operations Office
U.S. Department of Energy
P.O. Box 98518
Las Vegas, NV 89193-8518

Robert F. Pritchett
Technical Project Officer for NNVSI
Reynolds Electrical & Engineering Co.
P.O. Box 98521
Mail Stop 615
Las Vegas, NV 89193-8521

Elaine Ezra
NNVSI GIS Project Manager
EG&C Energy Measurements, Inc.
P.O. Box 1912
Mail Stop H-02
Las Vegas, NV 89125

SAIC-T&M'S Library (2)
Science Applications International
Corp.
101 Convention Center Dr.
Suite 407
Las Vegas, NV 89109

Dr. Martin Hifflin
Desert Research Institute
Water Resources Center
2505 Chandler Avenue
Suite 1
Las Vegas, NV 89120

E. P. Binnall
Field Systems Group Leader
Building 50B/4235
Lawrence Berkeley Laboratory
Berkeley, CA 94720

T. G. Barbour
Science Applications International
Corp.
1626 Cole Blvd., Suite 270
Golden, CO 80401

V. M. Glanzman
U.S. Geological Survey
P.O. Box 25046
913 Federal Center
Denver, CO 80225

W. S. Tvenhofel, Consultant
Science Applications International
Corp.
820 Estes Street
Lakewood, CO 89215

S. A. Mann, Manager
Crystalline Rock Project Office
U.S. Department of Energy
9800 South Cass Avenue
Argonne, IL 60439

C. H. Johnson
Technical Program Manager
Nuclear Waste Project Office
State of Nevada
Evergreen Center, Suite 252
1802 North Carson Street
Carson City, NV 89701

T. Hay, Executive Assistant
Office of the Governor
State of Nevada
Capitol Complex
Carson City, NV 89710

R. R. Loux, Jr., (3)
Executive Director
Nuclear Waste Project Office
State of Nevada
Evergreen Center, Suite 252
1802 North Carson Street
Carson City, NV 89701

John Fordham
Desert Research Institute
Water Resources Center
P.O. Box 60220
Reno, NV 89506

Prof. S. W. Dickson
Department of Geological Sciences
Mackay School of Mines
University of Nevada
Reno, NV 89557

J. R. Rollo
Deputy Assistant Director for
Engineering Geology
U.S. Geological Survey
106 National Center
12201 Sunrise Valley Dr.
Reston, VA 22092

Eric Anderson
Mountain West Research-Southwest
Inc.
Phoenix Gateway Center
432 North 44 Street
Suite 400
Phoenix, AZ 85008-6572

Judy Foremaster (S)
City of Caliente
P.O. Box 158
Caliente, NV 89008

A. T. Tamura
Science and Technology Division
Office of Scientific and Technical
Information
U.S. Department of Energy
P.O. Box 62
Oak Ridge, TN 37831

L. Jardine
Project Manager
Bechtel National Inc.
P.O. Box 3965
San Francisco, CA 94119

R. Harig
Parsons Brinckerhoff Quade &
Douglas
1625 Van Ness Ave.
San Francisco, CA 94109-3679

Dr. Roger Kasperson
CENTED
Clark University
950 Main Street
Worcester, MA 01610

Robert E. Cummings
Engineers International, Inc.
P.O. Box 43817
Tucson, AZ 85733-3817

Dr. Jaak Daemen
Department of Mining and
Geotechnical Engineering
University of Arizona
Tucson, AZ 85721

Department of Comprehensive Planning
Clark County
225 Bridger Avenue, 7th Floor
Las Vegas, NV 89155

Economic Development Department
City of Las Vegas
600 East Stewart Avenue
Las Vegas, NV 89109

Planning Department
Nye County
P.O. Box 153
Tonopah, NV 89049

Director of Community Planning
City of Boulder City
P.O. Box 367
Boulder City, NV 89005

Commission of the European
Communities
200 Rue de la Loi
B-1049 Brussels
Belgium

Lincoln County Commission
Lincoln County
P.O. Box 90
Pioche, NV 89043

Community Planning & Development
City of North Las Vegas
P.O. Box 4086
North Las Vegas, NV 89030

City Manager
City of Henderson
Henderson, NV 89015

ONWT Library
Battelle Columbus Laboratory
Office of Nuclear Waste Isolation
505 King Avenue
Columbus, OH 43201

Librarian
Los Alamos Technical
Associates, Inc.
P.O. Box 410
Los Alamos, NM 87544

6300 R. W. Lynch
6310 T. O. Hunter
6310 60/124233/1.1/Q2
6310 NEWSICF
6311 A. L. Stevens
6311 C. Horne (2)
6311 C. Mora
6312 F. W. Bingham
6312 R. R. Peters
6312 A. C. Peterson
6312 M. Tierney
6313 T. E. Blejwas
6313 E. A. Klavetter
6314 J. R. Tillerson
6314 J. A. Fernandez (20)
6314 T. E. Hinkebein (5)
6314 R. E. Stinebaugh
6315 S. Sinnock
6316 R. B. Pope
6316 J. F. Schelling
6332 WMT Library (20)
6410 K. R. Ortiz
3141 S. A. Landenberger (5)
3151 W. L. Garner (5)
8024 P. W. Dean
3154-3 C. H. Dalin (8)
for DOE/OSTI

The following number is for Office of
Civilian Radioactive Waste Management
purposes only and should not be used
when ordering this publication:

Accession Number: NN1.880914.0005